

Temporal and spatial dynamics of Arctic coastal changes and the resulting impacts: Yukon Territory, Canada

**Anna Maria Irrgang
(geb. Konopczak)**

Dissertation

zur Erlangung des akademischen Grades

"doctor rerum naturalium"

(Dr. rer. nat.)

in der Wissenschaftsdisziplin "Geomorphologie"

**eingereicht in Form einer kumulativen Arbeit an der
Mathematisch-Naturwissenschaftlichen Fakultät
der Universität Potsdam
angefertigt**

**am Alfred-Wegener Institut
Helmholtz Zentrum für Polar- und Meeresforschung**

**Potsdam,
September 2017**

Temporal and spatial dynamics of Arctic coastal changes and the resulting impacts: Yukon Territory, Canada

**Anna Maria Irrgang
(geb. Konopczak)**

Dissertation

zur Erlangung des akademischen Grades

"doctor rerum naturalium"

(Dr. rer. nat.)

in der Wissenschaftsdisziplin "Geomorphologie"

**eingereicht in Form einer kumulativen Arbeit an der
Mathematisch-Naturwissenschaftlichen Fakultät
der Universität Potsdam
angefertigt**

**am Alfred-Wegener Institut
Helmholtz Zentrum für Polar- und Meeresforschung**

Ort und Tag der Disputation: Universität Potsdam, Golm, 19.04.2018

Hauptbetreuer: Prof. Dr. Hugues Lantuit

weitere Gutachter: Prof. Dr. Hans-Wolfgang Hubberten, Prof. Dr. Aart Kroon

Dla mojej rodziny

To my family

You stand at a sandy beach with your feet in the water – a wave comes, you close your eyes. Your feet get soaked and you feel the pull of the water when it gets sucked back into the ocean. It does not matter how small the wave is, by the time you open your eyes the World around you is never as it was before – it is relentlessly changing. Realizing this as a little kid with my feet in the Baltic Sea, this is how my fascination for the coast began.

Abstract

In the Arctic, temperatures are rising twice as fast as the global mean. Since most of the terrestrial Arctic is underlain by permafrost it is particularly vulnerable to rising air temperatures. Permafrost holds vast amounts of carbon which upon release can considerably impact the Earth climate system. Studying processes which lead to permafrost degradation and carbon mobilization is thus important for quantifying this impact. The erosion of permafrost coasts is one of these processes and results in the mobilization of previously frozen carbon from the cliff, as well as from the hinterland. Since 34% of the World's coasts are characterized by the presence of permafrost, the net effect is substantial and leads to the release of large amounts of organic matter. Yet, little data on rates of shoreline change and fluxes of organic matter are available for the Arctic. This thesis fills a gap by providing new baseline data on the temporal and spatial variability of shoreline changes along the ice-rich Yukon coast in the western Canadian Arctic, as well as on subsequent impacts on the natural and human environment.

Shoreline change rates were obtained from geocoded aerial images from the 1950s, 1970s and 1990s, as well as from satellite images from 2011. Differential global positioning system (DGPS) measurements of shore zone and cliff profiles along seven field sites were analyzed. Based on this data, shoreline changes were estimated for several time periods. Even though acceleration in shoreline retreat was not reflected in the mean shoreline change rates for the whole coast, analyses along six shorter sections of the coast revealed that coastal erosion is accelerating since the mid-1990s. DGPS field site measurements also indicate a rapid acceleration in shoreline retreat since 2006.

Based on the shoreline change rates, sediment and soil organic carbon (SOC) fluxes to the Beaufort Sea were quantified. The SOC fluxes were calculated accounting for ground ice, which reduced the total flux rates by 19%. Sampling of the entire cliff, instead of just the upper meter, allowed the inclusion of SOC fluxes from the whole soil column, which increased the total SOC flux rate by 46%. Annually, 35.0×10^6 kg of SOC are mobilized by shoreline retreat from the Yukon coast, which is 131 kg SOC per metre of coast. These new

estimations of SOC fluxes are nearly three times as high as the fluxes which were previously used for the region in organic carbon budgets.

Retrogressive thaw slumps (RTSs) are a thermokarst landform, which occurs frequently along the Yukon coast. Analyses of geocoded aerial images from the 1950s and 1970s and satellite images from 2011 revealed that even though RTSs occur only along 28 km of the 238 km long shoreline, they occupy an area of 402 ha and deliver large amounts of sediment and carbon from the hinterland. For a better understanding of the initiation and activity of RTSs, univariate regression tree models were fed with 16 environmental variables, including shoreline change rates. Ground ice characteristics (volume and thickness) and terrain characteristics (terrain height and slope) appeared to be the most influencing factors for RTS initiation and activity. However, coastal erosion is considered to play a crucial role in setting the preconditions for RTS initiation and activity by removing the insulating layer from the massive ice body and eroding the outflow materials. The currently observed enhanced RTS activity along the Yukon coast is therefore considered to be linked to intensified coastal erosion processes.

This thesis also investigated present and potential future impacts of coastal dynamics on man-made structures and cultural heritage along the Yukon coast. A cultural features database was created and the positions of these features were analyzed with respect to two projected shoreline positions for the year 2100. The analyses reveal that more than 50% of all known cultural features will be lost to the ocean due to coastal erosion by 2100. Further, the usage of the two only landings strips located along the coast will be very restricted. Travelling along the traditional boating routes is expected to become more challenging due to increasing sediment supply and dynamics.

This thesis contributes to an enhanced understanding of past, present and potential future coastal changes and the resulting impacts on the natural and human environment along the Yukon coast. It shows that coastal changes are occurring at an accelerating pace and lead to impacts much greater than previously thought both in terms of net impact on the ecosystem and on infrastructure and cultural heritage.

Zusammenfassung

In der Arktis steigen die Temperaturen doppelt so schnell, wie im globalen Mittel. Da der größte Teil der terrestrischen Arktis aus Permafrost aufgebaut ist, ist die Arktis besonders empfindlich gegenüber diesem Temperaturanstieg. Permafrost beinhaltet große Mengen an Kohlenstoff, dessen Freisetzung das Potenzial hat, das globale Klimasystem erheblich zu beeinflussen. Für die Quantifizierung dieses Einflusses ist es wichtig, die Prozesse zu verstehen, welche zu der Degradierung von Permafrostböden und der miteinhergehenden Kohlenstoffmobilisierung führen. Die Erosion von Permafrostküsten ist ein solcher Prozess, welcher die Mobilisierung des, im Kliff wie auch im Hinterland, gefrorenen Kohlenstoffs hervorruft. Da 34% aller Küsten weltweit aus Permafrost aufgebaut sind, führt dieser Prozess zu der Mobilisierung von großen Mengen an organischem Material. Der Fokus dieser Arbeit liegt auf der Untersuchung der zeitlichen und räumlichen Variabilität der Küstendynamik entlang der eisreichen Yukon Küste in der westlichen kanadischen Arktis und auf den Auswirkungen dieser Veränderungen auf die natürliche und menschliche Umwelt.

Positionsveränderungen der Küstenlinie wurden aus georeferenzierten Luftbildaufnahmen der 1950er, 1970er und 1990er Jahre, und Satellitenbildern von 2011, entnommen. Des Weiteren wurden differenzielle globale Positionssystem (DGPS) Messungen von Küstenprofilen an sieben Messorten erhoben und ausgewertet. Basierend auf diesen Daten, wurden Positionsveränderungen der Küstenlinie für mehrere Zeitspannen analysiert. Eine Beschleunigung der Küstenerosion wurde in den mittleren Veränderungsdaten nicht verzeichnet. Jedoch zeigten zeitlich höher aufgelöste Analysen, welche entlang von sechs kurzen Küstenabschnitten durchgeführt wurden, dass sich die Küstenerosion seit den 1990er Jahren beschleunigt. Diese Untersuchungsergebnisse wurden durch die DGPS Analysen bestätigt, in welchen eine Beschleunigung seit 2006 zu erkennen ist.

Basierend auf diesen Untersuchungsergebnissen, wurde berechnet, wie viel Sediment und im Boden gebundener organischer Kohlenstoff (SOC) durch Küstenerosion freigesetzt werden. Bei den Berechnungen wurde das Volumen des im Festland enthaltenen Bodeneises miteinberechnet, was die SOC Freisetzung um 19% reduzierte. Der Einbezug des SOC aus der ganzen Sedimentsäule, führte zu der Erhöhung der SOC Flüsse um 46%. Jährlich ergibt

sich ein SOC Fluss von 35.0×10^6 kg entlang der Yukon Küste, was 131 kg SOC pro Meter Küsten entspricht. Diese neuen Abschätzungen sind fast dreimal so hoch, wie die bisher für diese Region in Kohlenstoffbilanzen verwendeten Werte.

Rückschreitende Auftaurutschungen (RTSs) sind Thermokarst-Landformen, welche charakteristisch für weite Teile der Yukon Küste sind. Eine Analyse georeferenzierter Luftbildaufnahmen aus den 1950er und 1970er Jahren und von Satellitenbildaufnahmen von 2011 hat ergeben, dass RTSs 28 km der Küstenlinie direkt beeinflussen, wobei sie SOC und Sedimentflüsse von 402 ha Land an die Küste transportieren. Um besser zu verstehen, welche Faktoren ausschlaggebend für die Initiierung und Aufrechterhaltung der Aktivität von RTSs wichtig sind, wurden univariate Regressionsbaummodelle mit 16 Variablen, unter anderem Positionsveränderungsraten der Küstenlinie, verwendet. Die Analysen ergaben, dass Grundeis-Charakteristika (Volumen und Mächtigkeit) und Gelände-Charakteristika (Geländehöhe und Neigungswinkel zur Küste) die wichtigsten Faktoren für die Initiierung und Aktivität der RTSs sind. Der Küstenerosion wird eine wichtige indirekte Rolle für die Initiierung und Aktivität von RTSs zugeschrieben. Durch die Entfernung der isolierenden Bodenschicht wird durch Küstenerosion die nötige Voraussetzung für die RTS Initiierung geschaffen. Durch den Abtransport des Ausflussmaterials durch Küstenerosion wird zudem der Neigungswinkel aufrechterhalten, welcher wichtig für die Aktivität des RTS ist. Die derzeit beobachtete erhöhte RTS Aktivität entlang der Yukon Küste wird somit der sich beschleunigten Küstenerosion zugeschrieben.

Des Weiteren, wurden heutige und zukünftige Auswirkungen von Küstendynamiken auf das Leben der Menschen, und auf die Bedrohung dortiger Kulturstätten, untersucht. Es wurde eine Datenbank erstellt, in welcher alle entlang der Yukon Küste gelegenen und bekannten Kulturgegenstände eingetragen wurden. Die Lage der einzelnen Objekte wurde mit zwei projizierten Küstenlinien für das Jahr 2100 verglichen. Laut der Analysen werden über 50% aller bekannten Objekte bis zum Jahr 2100 durch Küstenerosion zerstört sein. Ferner wird die Nutzung der beiden an der Küste liegenden Landebahnen erheblich beeinträchtigt werden. Der Gebrauch von traditionellen Bootsrouten wird durch den, durch Küstenerosion verursachten, zunehmenden Sedimenteintrag behindert.

Diese Arbeit trägt zu einem besseren Verständnis von vergangenen, gegenwärtigen und potenziellen zukünftigen Küstenveränderungen und den daraus entstehenden Auswirkungen auf die natürliche und menschliche Umwelt entlang der Yukon Küste bei. Es wird gezeigt, dass sich die Küste zunehmend schnell verändert, was zu größeren Auswirkungen hat, als bislang angenommen wurde.

Table of contents

Abstract	I
Zusammenfassung	III
1 Motivation	1
2 Introduction	3
2.1 Arctic climate changes and their impacts on coastal processes.....	3
2.2 Shoreline retreat along Arctic coasts	5
2.3 Impacts of coastal erosion	7
2.3.1 Material fluxes.....	7
2.3.2 Retrogressive thaw slumps	9
2.3.3 Socio-economic impacts	10
2.4 Objectives	12
2.5 Study area	12
2.6 Thesis structure.....	17
2.7 Authors' contributions.....	17
3 Variability in rates of coastal change along the Yukon coast, 1951 to 2015 ...	19
3.1 Introduction	20
3.2 Study Area	21
3.3 Data and Methods	23
3.3.1 Remote sensing data.....	23
3.3.2 Field survey data	27
3.3.3 Classification of shoreline	28
3.3.4 Transect-wise analyses of shoreline movements through time	29
3.4 Results	30
3.4.1 Temporal variations in shoreline change rates	30
3.4.2 Alongshore rates of change	32
3.4.3 Shoreline dynamics along field sites	35
3.4.4 Dynamics of lagoons, barrier islands and spits (gravel features).....	37
3.4.5 Yukon Territory land loss	38

3.5	Discussion.....	38
3.5.1	Temporal variations in shoreline change rates.....	38
3.5.2	Alongshore rates of change.....	40
3.5.3	Dynamics of lagoons, barrier islands, and spits (gravel features).....	42
3.5.4	Expected shoreline changes as a consequence of future climate warming.....	43
3.6	Conclusions.....	44
	Context.....	47
4	Coastal erosion of permafrost soils along the Yukon Coastal Plain and fluxes of organic carbon to the Canadian Beaufort Sea.....	49
4.1	Introduction.....	50
4.2	Study Area.....	52
4.3	Methods.....	54
4.3.1	Sample collection and laboratory analyses.....	54
4.3.2	Soil organic carbon determinations.....	55
4.3.3	Flux of organic soil carbon and sediments.....	57
4.3.4	Fate of the eroded soil organic carbon.....	58
4.4	Results.....	59
4.4.1	Ground Ice.....	59
4.4.2	Organic carbon contents.....	59
4.4.3	Material fluxes.....	64
4.5	Discussion.....	67
4.5.1	Ground Ice.....	67
4.5.2	Organic carbon contents.....	68
4.5.3	Material fluxes.....	69
4.5.4	Organic carbon in nearshore sediments.....	70
4.6	Conclusion.....	72
	Context.....	75
5	Terrain controls on the occurrence of coastal retrogressive thaw slumps along the Yukon Coast, Canada.....	77
5.1	Introduction.....	78
5.2	Study Area.....	80
5.3	Methods.....	82
5.3.1	Mapping of RTSs and landform classification.....	82
5.3.2	Environmental variables.....	85

5.3.3	Univariate regression trees	87
5.4	Results	88
5.4.1	Characteristics of RTS along the coast	88
5.4.2	Density and areal coverage of RTSs along the Yukon Coast.....	90
5.5	Discussion.....	96
5.5.1	Characteristics and distribution of RTSs along the Yukon Coast.....	96
5.5.2	Terrain factors explaining RTS occurrence	96
5.5.3	Coastal processes.....	97
5.6	Conclusions	99
Context	101
6 Impacts of past and future coastal changes on the Yukon coast - threats for cultural sites, infrastructure and travel routes	103
6.1	Introduction	104
6.2	Study Area	105
6.3	Methods	107
6.3.1	Data for shoreline projections	107
6.3.2	Shoreline projection for the conservative scenario (S1)	108
6.3.3	Shoreline Projection for the dynamic scenario (S2).....	108
6.3.4	Positioning and characterizing of cultural sites.....	109
6.3.5	Calculation of losses under the S1 and S2 scenarios	110
6.3.6	Estimation of future dynamics in very dynamic areas	111
6.4	Results and discussion	111
6.4.1	Past and future shoreline change rates	111
6.4.2	Cultural sites.....	112
6.4.3	Infrastructure and travel routes	119
6.5	Conclusions	121
7 Discussion	123
7.1	The importance of understanding climatic drivers of coastal changes.....	123
7.2	The influence of shoreline change rates on retrogressive thaw slump activity	124
7.3	On the calculation of carbon fluxes from coastal erosion along the Yukon coast ..	126
7.4	Impacts of present and future coastal erosion on the natural and human environment	127
7.5	Synthesis.....	128
8 Summary and Conclusions	131

Bibliography	135
Supporting Material	i
Data Set ds01.....	i
Table S1.....	i
Table S3.....	ix
Abbreviations and Nomenclature	xi
Acknowledgements	xiii
Eidesstaatliche Erklärung	xv

Motivation

In the Arctic, global warming is twice as high as the global mean [Winton, 2006; Richter-Menge *et al.*, 2016a]. Rising atmospheric temperatures are causing sea ice and snow to melt earlier and freeze-up later on, which in turn diminishes the extent of areas which reflect incoming energy back to the atmosphere. This leads to the absorption of more solar energy and thus further warming – a process which is known as Arctic Amplification [Winton, 2006; Serreze and Barry, 2011].

The smaller the temperature difference between the polar and the mid-northern latitudes is, the weaker is the polar jet stream, which facilitates its meandering and deflection [Francis and Vavrus, 2012; Cohen *et al.*, 2014; Overland *et al.*, 2015]. When the polar jet stream gets blocked further south it can influence mid-latitude weather patterns, such as wintertime cold spells, record snow falls, but also summer heatwaves, droughts and floods [Francis and Vavrus, 2012; Cohen *et al.*, 2014; Overland *et al.*, 2016a]. This is only one of many examples why Arctic climate change is of global relevance and how it can affect the daily life of people beyond the Arctic.

However, warming of the Arctic has even further implications. Most of the terrestrial Arctic is built out of permafrost – soil which remains frozen for at least two consecutive years [Brown and Kupsch, 1974]. Due to the short summers and very long and cold winters, a large portion of the produced biomass (fauna and flora) is not, or only partially, decomposed. Thus, permafrost soils are one of the major global carbon sinks, storing organic matter which can be up to thousands of years old [Vonk *et al.*, 2012]. With rising temperatures, organic matter is made available for microbial decay, which results in the release of carbon dioxide and methane [Schuur *et al.*, 2015]. These gases, in turn, reinforce global warming, a feedback loop which is known as permafrost carbon feedback [Koven *et al.*, 2011; Schaefer *et al.*, 2014;

Schuur et al., 2015]. So far, the focus in investigating the permafrost carbon feedback was laid on vertical fluxes to and from the atmosphere [*Schuur et al.*, 2008, 2015; *McGuire et al.*, 2009; *Koven et al.*, 2011; *Elberling et al.*, 2013; *Knoblauch et al.*, 2013; *Schaefer et al.*, 2014]. Lateral transport processes did not receive much attention.

Coastal erosion is one of these processes and leads to the mobilization of organic matter which is transferred to the Arctic Ocean (to the nearshore zone, or off-shelf), or to the atmosphere [*Fritz et al.*, 2017]. One third of the Earth's coasts are made out of permafrost, most of them being exposed to coastal erosion [*Lantuit et al.*, 2012b]. However, the contribution of coastal erosion to the mobilization of carbon stored in organic matter on the regional to global scale remains uncertain. This is due to a lack of coastal erosion data, as well as the scarce availability of sediment and carbon content data. Yet, these estimations are urgently needed since the erosion of permafrost coasts is expected to increase [*Forbes*, 2011]. Indeed, the ice-free period during which Arctic coasts are exposed to coastal processes is elongating because of the decrease in sea ice [*Barnhart et al.*, 2014b]. Coastal erosion is already increasing among many coasts in the Arctic [*Jones et al.*, 2009a; *Günther et al.*, 2015].

The study of coastal processes in the Arctic is also needed to understand their impact on the socio-economic framework in the Arctic. Arctic coasts are an important locus of human activity and play a vital role for indigenous people to pursue their traditional lifestyle, as well as for the development of the economy. The rapid retreat of these coasts poses a serious threat to local communities and infrastructure and are challenging people to continuously adapt to a fast changing environment [*Jones et al.*, 2008; *Forbes*, 2011]. Understanding past and projecting future shoreline changes will help to plan adaptation of coastal infrastructure and to undertake preservation efforts for historical artifacts along the coast. These artifacts are part of the living history of Arctic coastal residents and are also being threatened by erosion.

Introduction

2.1 Arctic climate changes and their impacts on coastal processes

In the Arctic, global climate change occurs at a greater rate than elsewhere on Earth [Serreze and Barry, 2011]. The rise of air, sea surface and soil temperatures is measured to be 3.5 °C [Overland *et al.*, 2016b], up to 5 °C [Timmermans, 2016], and up to 2 °C, [AMAP, 2011] respectively. These increasing temperatures are facilitating arctic coastal retreat in many different ways, especially along coasts with high ground ice contents [Aré, 1988; Dallimore *et al.*, 1996; Lantuit and Pollard, 2008; Günther *et al.*, 2015]. Consequently, Arctic coasts are one of the fastest eroding coasts on Earth [Reimnitz *et al.*, 1988; Jorgenson and Brown, 2005]. The Yukon coast, where the focus of this thesis lies is known to be ice-rich and to erode at a fast pace [Lantuit *et al.*, 2012b].

Over the last 30 years, the sea ice melt season lengthened by 5 to 9 days per decade, shortening the time in which sea ice is protecting the coast [Markus *et al.*, 2009; Stroeve *et al.*, 2014]. The September sea ice extent has decreased by 40% since 1979 [Kwok and Rothrock, 2009], sea ice thickness has decreased by approximately 1.8 m and its volume by approximately 75-80% [Overland *et al.*, 2013]. The changes in sea ice physiology and extent lead to longer fetches and easier sea ice break up [Stroeve *et al.*, 2007, 2011, 2014; Kwok and Rothrock, 2009; Serreze *et al.*, 2009]. This favours the formation of higher energetic waves which can act upon the coast for longer periods of time [Overeem *et al.*, 2011; Barnhart *et al.*, 2014b; Thomson and Rogers, 2014] (Figure 2.1). Current estimations predict that the ocean will be ice-free during the summers by the middle of the 21st century [Wang and Overland, 2009]. However, there is considerable uncertainty regarding the timing of total sea ice loss during the summer [Jahn *et al.*, 2016]. A higher frequency of severe storms, especially in the freeze up season, and warmer water temperatures are additionally contributing to intensified mechanical and thermal erosion of frozen sediments [Kobayashi *et al.*, 1999; Solomon, 2005;

Aré et al., 2008; *Barnhart et al.*, 2014a]. Relative sea-level rise, especially in combination with a deepening of the nearshore profile through processes like submarine permafrost thaw or ice gouging further contribute to an intensification of coastal erosion [*Héquette and Barnes*, 1990; *Wolfe et al.*, 1998] (Figure 2.1).

On land, an increase in the thawing depth of permafrost has been observed over the past 30 years [*AMAP*, 2011]. Consequently, the sediments lose cohesion and are non-resistive even against low energetic waves, which facilitates their erosion and transport away from the coast [*Serreze et al.*, 2000; *Jorgenson and Brown*, 2005; *Dupeyrat et al.*, 2011]. Thus, some parts of Arctic coasts are observed to be rather “melting away” than being actively eroded by waves [*Harper*, 1990]. Further, the increase in precipitation, as it is predicted for example in the Yukon, as well as enhanced melting of ice in the active layer may lead to increased slope destabilization, again favoring coastal retreat [*Bird* 2009, *Kroon*, 2014; *Streicker*, 2016].

Climate projections estimate that in the Arctic climate change is expected to intensify in the range of 1 °C (RCP 2.6) to 8 °C (RCP 8.5) over land by 2100 [*IPCC*, 2013]. This gives reason to expect that coastal erosion will further intensify in the future. A comparison of coastal studies across all Arctic coasts came to the conclusion that current data cannot detect spatial and temporal changes in coastal processes sufficiently, showing that there is a need for more detailed studies on arctic coastal dynamics [*Overduin et al.*, 2014]. It is one of this thesis’ objectives to fill this gap by providing high resolution high quality datasets on recent trends in erosion for the Yukon coast.

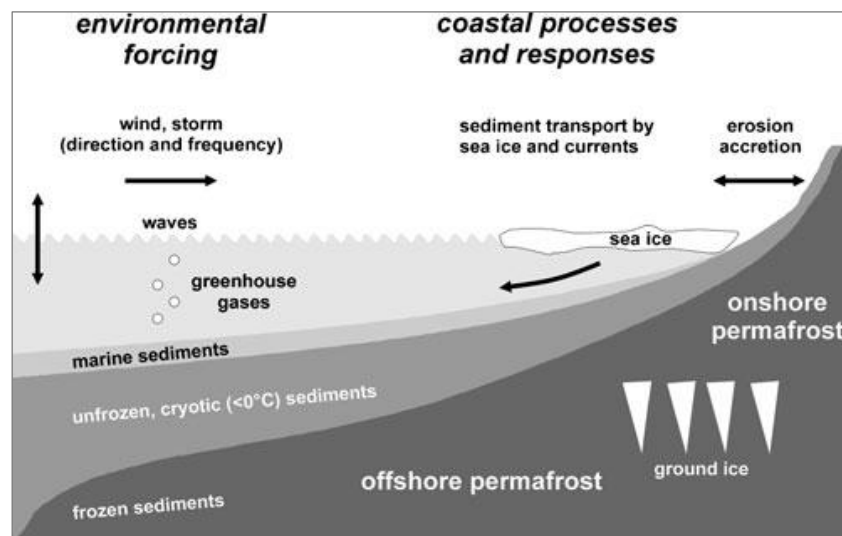


Figure 2.1: Arctic coastal processes and responses to climatic changes. Figure from Lantuit et al., [2012b], after Rachold et al., [2004a].

2.2 Shoreline retreat along Arctic coasts

In 2012, Lantuit et al. [2012b] published the first circum-Arctic coastal change map (Figure 2.2) and Wegener et al. [2015] calculated resulting mean annual carbon fluxes (Figure 2.3). Their study was based on the efforts of the Arctic Coastal Dynamics (ACD) project, which unified coastal change data from numerous different field sites across the coasts of all Arctic seas [Rachold et al., 2004; Lantuit et al., 2012; ACD, 2016]. According to these findings, the American Beaufort Sea coast, Canadian Beaufort Sea coast and East Siberian Sea coast are eroding particularly fast, with annual mean rates of -1.15 m a^{-1} , -1.12 m a^{-1} and -0.87 m a^{-1} , respectively [Lantuit et al., 2012b]. Over the past two decades, high coastal erosion rates were reported for the Alaskan Beaufort Sea coast [Brown et al., 2003; Mars and Houseknecht, 2007; Jones et al., 2008, 2009a; Arp et al., 2010; Tweedie et al., 2012; Barnhart et al., 2014a; Gibbs and Richmond, 2015], with short-term erosion rates higher than 10 m a^{-1} in the Drew Point area [Jones et al., 2009a; Arp et al., 2010; Barnhart et al., 2014a], and an overall mean rate of change of -1.7 m a^{-1} [Gibbs and Richmond, 2015]. High erosion rates were also reported for the East Siberian coast high [Lantuit et al., 2011; Günther et al., 2013, 2015; Maslakov and Kraev, 2016], with short-term erosion rates of up to -10.2 m a^{-1} along the coasts of Muostakh Island [Günther et al., 2015].



Figure 2.2: Circum-Arctic map of shoreline change rates. Figure from Lantuit et al. [2012b].

In addition to its high mean erosion rate, the Canadian Beaufort coast is the region with the highest ground ice contents throughout the Arctic, thus, making it particularly prone to climate warming [Lantuit *et al.*, 2012b]. In the context of this thesis, the Yukon coast was taken as the study area, in order to assess the magnitude and impacts of climatic change on coastal changes.

By comparing site descriptions from the early explorations of Franklin, Amundsen and Stefansson with own field observations and data from official reports, Mackay (1963) first pointed out the fast eroding nature of the Yukon coast [Mackay, 1963]. In the 1970s to 1990s, regional to local reconnaissance studies along the Yukon coast driven by governmental and industrial needs such as the Distant Early Warning (DEW) line station clean-up, the assessment of hazards for cultural and archaeological sites, or offshore hydrocarbon exploration added to the body of knowledge on the coast in the area [McDonald and Lewis, 1973; Lewis and Forbes, 1974; Pinchin *et al.*, 1985; Solomon *et al.*, 1994; Forbes *et al.*, 1995; Forbes, 1997; Solomon, 1998]. All of the work was published in governmental reports and most of it was carried out under the Northern Oil and Gas Action Plan, which was sought to assess potential effects of hydrocarbon development and production along the Canadian Arctic coast [INAC, 2017a]. For these studies, different data sources were used for the quantification of shoreline changes, such as aerial imagery (available for the Yukon coast since 1951), oblique airborne videos, and geodetic field site measurements. All studies focused on selected locations rather than quantifying rates of shoreline change along the whole Yukon coast. The only study which provided rates of shoreline change for the whole Yukon coast was performed by Harper *et al.* [1985], who used coastal videos from 1980, 1981 and 1984, as well as aerial photographs from 1950 and 1970. Mean rates of coastal erosion were considerably high at Stokes Point, Kay Point and King Point with -5.33 m a^{-1} , -3.39 m a^{-1} , and -3.13 m a^{-1} , respectively [Harper *et al.*, 1985]. The highest accumulation rates were measured along Simpson Point, in Ptarmigan Bay, and near Niakolik with 2.89 m a^{-1} , 2.83 m a^{-1} and 3.65 m a^{-1} , respectively [Harper *et al.*, 1985].

Over the past 10 years, advances in computing power and better software enabled a more consistent determination of shoreline change rates over large areas. By using the Digital Shoreline Analysis System (DSAS), an Esri ArcMap software extension, rates of shoreline changes can now be obtained consistently and uniformly from remotely sensed images [Thieler *et al.*, 2009]. Since the 2000s, the usage of satellite images has widely replaced air photos and is extending the time series to recent times.

Lantuit and Pollard [2008] calculated mean annual coastal change data for Herschel Island for the time periods of 1952-1970 and 1970-2000. The mean values were -0.61 m a^{-1} and -0.45 m a^{-1} [Lantuit and Pollard, 2008]. The results suggested that there was a slight deceleration in coastal erosion since 1970. Konopczak et al. [2014] calculated rates of coastal change for a 35 km long stretch of coast between Komakuk Beach and the Canadian – U.S. American border for the time periods 1951-1972 and 1972-2009 of -1.4 m a^{-1} and -1.2 m a^{-1} , respectively [Konopczak et al., 2014]. Again, an acceleration of coastal erosion was not detectable. A study done by Obu et al. [2016a] was the first one which detected an acceleration of coastal retreat along Herschel Island by more than 50% from 2000 to 2011 in comparison to rates of change from 1970 to 2000.

So far, these studies mainly focused on very short stretches of coast, or considered only one time period, prohibiting the detection of temporal changes of shoreline dynamics. Even though the observed changes in the Arctic climate should lead to higher erosion rates along the ice-rich Yukon coast, a consistent investigation of the whole coast including recent data is missing. Thus, there is a need for assessing shoreline changes along the entire Yukon coast over longer time periods to assess recent trends in erosion and accumulation.

2.3 Impacts of coastal erosion

2.3.1 Material fluxes

Permafrost soils store $1035 \pm 150 \times 10^{15} \text{ g}$ of soil organic carbon within the upper three metres of soils [Hugelius et al., 2014], or $1672 \times 10^{15} \text{ g}$ when including deeper soil layers [Tarnocai et al., 2009]. This corresponds to approximately half of the carbon which is estimated to be stored in soils, worldwide [Tarnocai et al., 2009]. Several geomorphological processes disturb these carbon pools, which leads to the mobilisation of carbon, as well as other nutrients and sediments. Coastal erosion is such a process. It transfers sediments, carbon and nutrients from the terrestrial into the aquatic system [Dunton et al., 2006; Gustafsson et al., 2017]. Depending on their particle size, the sediments either stay in suspension, or settle on the sea bottom [Hjulström, 1932]. Thereby, strong sediment fluxes can change the water turbidity in the nearshore zone and the corresponding light availability, which is crucial for primary production [Neff and Asner, 2001; Dittmar and Kattner, 2003]. When carbon enters the nearshore zone, it is observed to take four major paths [Fritz et al., 2017]. Part of the carbon settles on the sea floor in the nearshore zone. Since the nearshore zone is a very dynamic area, carbon can be re-mobilized by wave action, bottom fast sea ice pick-up, or ice gauging [Aré et al., 2008; Vonk et al., 2012; Macdonald et al., 2015]. Further, carbon can be transported

beyond the nearshore zone and settle in deeper shelf areas or even off shelf [Vonk, 2014; Gustafsson *et al.*, 2017]. However, a considerable fraction of the carbon does not settle on the ground. Instead, it is mineralized by microbes, whereby a portion of the carbon is outgassed [Dunton *et al.*, 2006; Battin *et al.*, 2009; Gustafsson *et al.*, 2017]. Further, the increased concentration of carbon and of other limited nutrients has the potential to enhance primary production in the ocean, upon which all organisms rely. Very high primary production can, in turn, lead to algae blooms and oxygen depletion, which can have massive effects on nearshore ecosystems [Fritz *et al.*, 2017].

Rivers and coastal erosion are the two main sources of sediment and carbon fluxes into the Arctic Ocean [Rachold *et al.*, 2004b]. However, the separate contributions of both delivery sources vary regionally. Along the Beaufort Sea, rivers, especially the Mackenzie River, are considered to deliver the bulk part of the carbon (0.89×10^{12} g a⁻¹ by coastal erosion, 4.43×10^{12} g a⁻¹ by rivers). Circum-Arctic estimations show that rivers supply approximately 30.04 to 34.04×10^{12} g a⁻¹ of carbon per year [Rachold *et al.*, 2004b; Holmes *et al.*, 2012], whereas estimations on carbon fluxes derived from coastal erosion vary between 4.9 to 14×10^{12} g a⁻¹ [Wegner *et al.*, 2015 and references therein].

For the Yukon coast in particular, Harper and Penland [1982] published the first estimates of material fluxes, yielding 1.5×10^6 m³ a⁻¹ of sediment. Using estimated cliff heights from video records and erosion rates from McDonald and Lewis [1973], this was a first rough estimation of how much material is annually released into the Beaufort Sea. A subsequent study conducted by Hill *et al.* [1991b] estimated a mean annual sediment flux of 7.12×10^{12} g a⁻¹. By using an average total organic carbon concentration in coastal sediments of 5%, Macdonald *et al.* [1998] calculated a mean annual flux of total organic carbon of 0.06×10^6 m³ a⁻¹ from the Yukon coast into the Beaufort Sea [Macdonald *et al.*, 1998]. This value is used until present for the calculation of carbon fluxes to the Yukon coast [Rachold *et al.*, 2000, 2004b].

A more accurate estimation of mobilized sediments and carbon is the initial step to assess the potential impacts these fluxes have on the aquatic system and which role they are playing in the general carbon and sediment cycle.

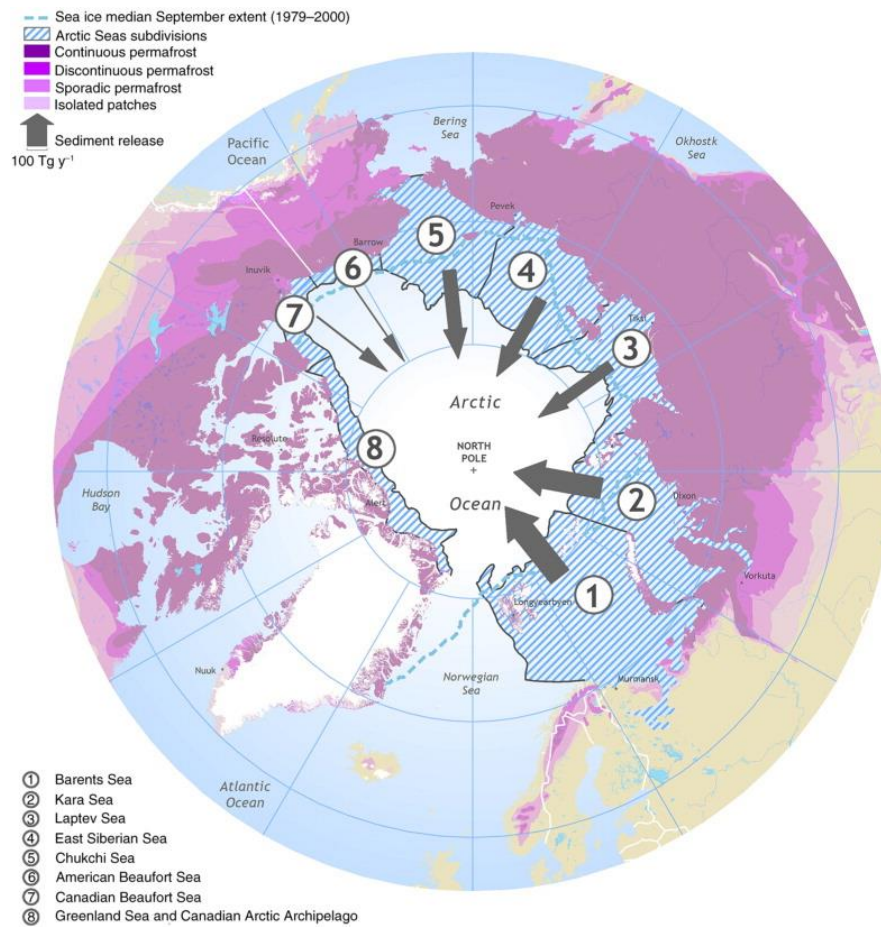


Figure 2.3: Modern sediment contribution (Tg a^{-1}) from coastal erosion into the Arctic Ocean. Figure from Wegner et al. [2015].

2.3.2 Retrogressive thaw slumps

Retrogressive thaw slumps are unique permafrost landscapes which are found along many Arctic coasts and rivers. They are back-wasting thermokarst features which can develop when a previously buried massive ice body gets exposed due to a disruption process, such as an active layer detachment or coastal erosion [Burn and Lewkowicz, 1990; Lantuit et al., 2012a; Kokelj and Jorgenson, 2013]. When the massive ice body gets exposed to solar radiation, the ice melts or ablates and releases the previously frozen sediments and carbon therein. When the melting process of the massive ice body causes it to retreat faster than coastal processes are eroding the cliff, a retrogressive thaw slump occurs [Lewkowicz, 1987a]. A retrogressive thaw slump consists of a headwall, a slump floor and a slump lobe [Burn and Lewkowicz, 1990] (Figure 2.4). The headwall is comprised of the upper soil layer and the massive ice body. They are reported to recede up to 10 m a^{-1} along the Yukon coast [Lantuit and Pollard, 2005]. The slump floor, which is fronting the headwall, contains part of the released material. The material is transported from the mud pool downslope towards the ocean, and creates a

slump lobe. The removal of the sediments at the base of the retrogressive thaw slump by waves maintains a steep shore gradient, which is important for the material transport. If material does not get transported shoreward any longer, it will accumulate in front of the headwall, causing its insolation [Lantuit and Pollard, 2005]. In this case, the development of the retrogressive thaw slump decelerates or even stops. A re-exposure of the ice-body by thermokarst processes or coastal erosion leads to the re-activation of parts of the initial retrogressive thaw slump. Many retrogressive thaw slumps are observed to have such a polycyclic nature [Wolfe *et al.*, 2001; Lantuit and Pollard, 2005, 2008; Lantuit *et al.*, 2012a]. Along the Canadian Beaufort Coast, a phase of enhanced retrogressive thaw slump initiation and re-activation is observed within the last 20 years [Lantz and Kokelj, 2008; Lantuit *et al.*, 2012a; Segal *et al.*, 2016].

Depending on their size, retrogressive thaw slumps release considerable amounts of sediments, carbon and nutrients to the nearshore [Lantuit and Pollard, 2005; Obu *et al.*, 2017; Tanski *et al.*, 2017]. Hence, it is important to consider these landforms for estimations of material fluxes into the sea. The main challenge relates to the association between retrogressive thaw slump occurrence and terrain characteristics, such as substrate, relief or ground ice contents. A comprehensive statistical and empirical assessment of the relation between slumps and terrain is needed to understand the main drivers of slump initiation.

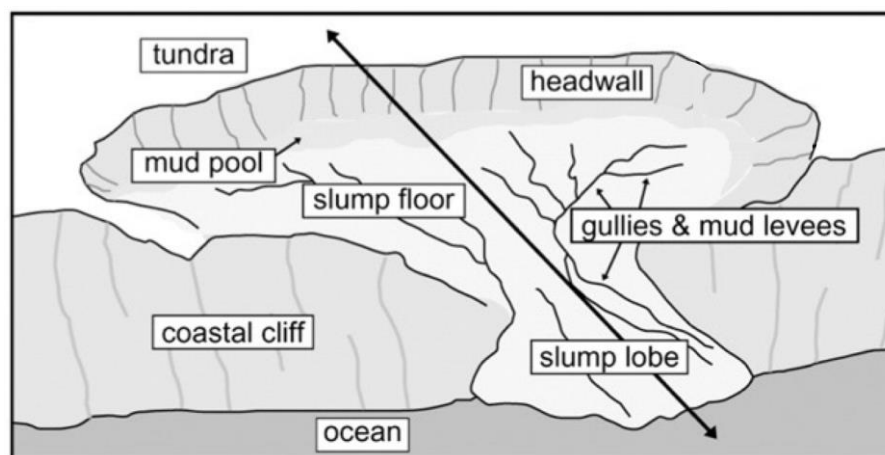


Figure 2.4: Morphology of a retrogressive thaw slump, modified after Lantuit and Pollard [2005].

2.3.3 Socio-economic impacts

Over the last decades much work has focused on the biogeochemical processes induced by arctic coastal erosion (Chpt. 2.3.1). However, it is the pictures of collapsing houses and eroding roads which are illustrating the importance of studying arctic coastal erosion processes best. Climatic warming in the Arctic is both a threat and an opportunity. It is a

threat for coastal infrastructure, such as the former DEW line stations along the US-American and Canadian Arctic coasts [Jones *et al.*, 2008]. It is also threatening industry infrastructure such as the Varandei oil terminal at the Pechora Sea coast [Ogorodov *et al.*, 2016]. It directly threatens settlements, such as Tuktoyaktuk at the Northwest Territories Beaufort coast [Johnson *et al.*, 2003; Forbes *et al.*, 2013] as well as cultural and archaeological sites [Jones *et al.*, 2008; Kroon *et al.*, 2010; Radosavljevic *et al.*, 2015; O'Rourke, 2017]. On the other hand, it is an opportunity for the shipping industry to establish new Arctic-Pacific shipping routes [Smith and Stephenson, 2013; Stephenson and Smith, 2015], for the oil and gas industry to explore new offshore plays [Zöckler *et al.*, 2011], and for the tourism sector to open new destinations [Olsen *et al.*, 2011].

There are no permanent settlements along the Yukon coast at present times. However, the coastal area is still crucial for the Inuvialuit to pursue their traditional lifestyle, as well as for other indigenous and non-indigenous peoples for subsistence harvesting, recreation and transportation [Alunik *et al.*, 2003; Hacquebord, 2011; Zöckler *et al.*, 2011]. The Yukon coast has a long settlement history [Friesen, 2015; Arnold, 2016; Jensen, 2016]. The region is preserving valuable information about human history in the North in form of numerous cultural and archaeological heritage sites. These are containing remains from the Thule Inuit in the Washout Site at Herschel Island [Friesen and Arnold, 2008], are documenting the life of the Inuvialuit [Adams, 2004; Lyons, 2004], and are reporting on the arrival and activities of the Europeans [Bockstoce, 1986; Saxberg, 1993]. The recognition of the cultural and natural richness of the Ivvavik National Park and Herschel Island made this region a candidate for UNESCO World Heritage Site status [UNESCO, 2004].

In the late 1990s, a comprehensive study of all cultural and archaeological heritage sites within the Ivvavik National Park (Figure 2.5) was carried out by Thomson *et al.* [1998], who systematically inventoried each site and the corresponding artifacts. This study was accompanied by shoreline change studies in 1996 and 1997 along five main heritage sites [Solomon, 1996; Forbes, 1997]. Further, a detailed investigation of potential erosion and flood hazards of a former whaling settlement at Simpson Point, Herschel Island was carried out, and showed that sea-level rise, together with an intensification in storms, is substantially increasing the flood risk potential [Radosavljevic *et al.*, 2015]. Despite this increasing hazard potential and its impact on cultural heritage sites along the Yukon coast, no comprehensive study of the future risk of coastal processes for cultural heritage exists. The potential impact of erosion on important infrastructure such as the DEW line airstrips, and on highly

frequented travel routes, are also unknown. Thus, there is a drastic need to assess the effects coastal processes have on the human component in the Arctic system.

2.4 Objectives

The following research objectives are driving the work performed in this thesis:

- 1) To investigate the spatial and temporal variability of arctic coastal changes along the ice-rich Yukon coast.
- 2) To quantify the amount of sediment and carbon being mobilized due to coastal erosion, accounting for ground ice.
- 3) To analyze the role of coastal erosion for the initiation of landforms (i.e., retrogressive thaw slumps) which are known to mobilize large amounts of sediments and organic material.
- 4) To project the position of future shorelines under different scenarios.
- 5) To discuss, which consequences future coastal dynamics might have for living along the coast.

The overall goal of this PhD thesis is to contribute to an improved understanding of the role coastal dynamics are playing for material flows and landscape evolution and which impacts they have on infrastructure, travel routes and cultural sites at the present and in the future along the Yukon coast.

2.5 Study area

The Yukon Coast is situated within the Yukon Coastal Plain, a gently sloping surface which comprises the emergent part of the Beaufort continental shelf (Figure 2.4). The shelf break is at a water depth of approximately 80 m and is 40 km to 150 km from the coast [Hill *et al.*, 1991b]. The Yukon Coastal Plain is about 10 km to 40 km wide and is bordered to the north by the Beaufort Sea and to the south by the British, Barn and Richardson Mountains [Rampton, 1982]. The Buckland glaciation was the last and furthest advance of the Wisconsin glaciation and represents the maximum limit of the Laurentide ice sheet [Hill *et al.*, 1991a and references therein]. Advancing from the current location of the Mackenzie River, an extension tongue of the ice sheet reached westwards approximately as far as the Firth River [Mackay, 1959; Rampton, 1982]. Parts of the former push moraine were separated from the land between 1600 and 650 years ago, creating Herschel Island and the Workboat Passage which constitutes a major sediment sink along the coast [Burn, 2009, 2016] (Figure 2.4). The

Mackenzie Trough, a glacially eroded valley [Hill, 1990] and Herschel Basin, a shelf depression, are subsea remains of the Wisconsin glaciation.

Several hundreds of metres thick, continuous permafrost is underlying the whole Yukon Coastal Plain, except beneath large thermokarst lakes and river beds [Rampton, 1982]. Active layer depths on Herschel Island are on average 0.55 m, which is 30 to 50% deeper than in 1985 [Burn and Zhang, 2009]. The glaciation history is characterizing the surficial geology of the Yukon Coastal Plain and is dividing it into a formerly glaciated and a formerly unglaciated area.

In the formerly unglaciated area the terrain is very even and slopes gently towards the coast. It is mainly comprised of fine-grained lacustrine and alluvial sediments [Hughes, 1972; Rampton, 1982]. Ground ice contents reach as high as 66 vol% in the region of Komakuk but are generally lower than in the formerly glaciated area [Couture and Pollard, 2017]. Coastal elevations are highest in the area of the Canadian – U.S. American border (6 m) and lower to 1 m east of Komakuk. The Malcom River and Firth Rivers build together an approximately 40 km long delta, which is fronted by a well-developed barrier spit and barrier island system, called Nunaluk Spit. According to Harper *et al.* [1985], there is no evident sediment transportation from the deltas to the spit system, so that ice-push, besides longshore drift, is suggested to be the dominant process of sediment supply. Ice push ridges provide evidence that beaches along the Yukon coast are subject to intensive rework by sea ice during winter (Figure 2.5 inset b). The combined impact of wave induced mechanical and thermal erosion and thermal denudation lead to rapid retreat of the ice-rich coastal cliffs of the formerly unglaciated area (Figure 2.5, inset a).

Nunaluk Spit together with Herschel Island and the Workboat Passage, comprise one of Canada's Important Bird Area, which is particularly known because it comprises the only black guillemot nesting area along the Yukon coast [Eckert *et al.*, 2005; Environment Canada, 2015; IBA 2017b].

The formerly glaciated area is mainly comprised of rolling moraines with coarse grained tills, as well as fine-grained lacustrine and outwash plains [Hughes, 1972; Rampton, 1982; Harry *et al.*, 1988]. The whole formerly glaciated area is hilly and contains numerous thermokarst lakes. It bears high ground ice contents, which are reaching values of 74 vol% in the area south east of King Point [Couture and Pollard, 2017]. Ground ice is present in many different forms, including of non-massive ice, ice wedges, and extensive massive ice bodies which are partly composed of buried glacier and snow ice [Mackay, 1959; Harry *et al.*, 1988]. Coastal elevations reach more than 60 m between Kay Point and King Point and more than 70 m

along the northern coast of Herschel Island. The high ice contents determine coastal morphology along many sections of the coast. Between King Point and Kay Point, very high ice contents and steep shore gradients are favoring the development of retrogressive thaw slumps (Chpt. 2.3.2) and gully formation along cliffs (Figure 2.5, inset f). Along the exposed tip of Kay Point, block failures are present (Figure 2.5, inset e). Block failures occur, when waves undercut the cliff in a polygonal tundra terrain. When the niche is deep enough to destabilize the tundra polygon, it fails, usually separating along an ice wedge [Hoque and Pollard, 2009; Wobus *et al.*, 2011]. The sediments of the tundra block are cohesive enough to make the block fall towards the sea in one piece. Wave-induced thermal and mechanical erosion is capable of degrading the block within a few days [Barnhart *et al.*, 2014a]. When waves undercut the cliff of a terrain with less developed polygonal tundra, notching of the cliff can cause the overlying vegetation to break off (Figure 2.5, inset d).

The main river which enters the Beaufort Sea in the previously glaciated area is the Babbage River. The Babbage River delta and its adjacent region with its sheltered bays and wetlands is a further Important Bird Areas [IBA, 2017a]. However, the low elevation of this terrain renders it susceptible to flooding and inundation, as a result of the combined effects of thaw settlement and storm surges and/or sea-level rise (Figure 2.5, inset c).

The open water season during which sea ice is absent and the coast is exposed to waves is starting in late June and ending in the beginning of October [Galley *et al.*, 2016]. However, fetch is limited by sea ice throughout the open water season. During the open water season, winds along the Yukon coast are bimodal. Winds come most frequently from the northwest to southeast, however northwesterly winds create positive storm surges which can reach as high as 3 m and cause large scale flooding [Reimnitz and Maurer, 1979; Harper *et al.*, 1988, Environment Canada, 2016]. Storms from the southeast generate negative storm surges and are thus less effective in eroding the coast [Henry, 1975; Harper and Penland, 1982]. Storm frequency increases from late August on, with the stormiest period being usually during ice freeze-up in October [Hudak and Young, 2002; Atkinson, 2005]. The major headlands of Kay Point and Herschel Island significantly influence the local wave climate by sheltering the bordering easterly coasts. Relative sea-level rise along the Yukon coast is on average $3.5 \pm 1.1 \text{ mm a}^{-1}$ [Manson *et al.*, 2005]. Astronomical tides are semidiurnal and in the microtidal range of 0.3 to 0.5 m [Héquette *et al.*, 1995].

The Yukon Coastal Plain has a subarctic climate which is dominated by continental air in the winter, but is influenced by maritime air during the summer [Rampton, 1982]. The average annual temperatures of the two weather stations at the DEW line sites of Komakuk Beach and

Shingle Point amount to -11 °C and -9.9 °C, respectively, with July average temperatures of 7.8 °C and 11.2 °C, respectively (averages for 1971 to 2000 [*Environment Canada*, 2016]). Approximately half of the annual precipitation falls as snow and half as rain. Annual average precipitation values are in between 161.3 mm to 253.9 mm (averages for 1971 to 2000 [*Environment Canada*, 2016]). Vegetation along the Yukon Coastal Plain is dominated by erect dwarf shrubs, sedges and mosses [*Walker et al.*, 2005]. The treeline is south and east of the Yukon Coastal Plain.

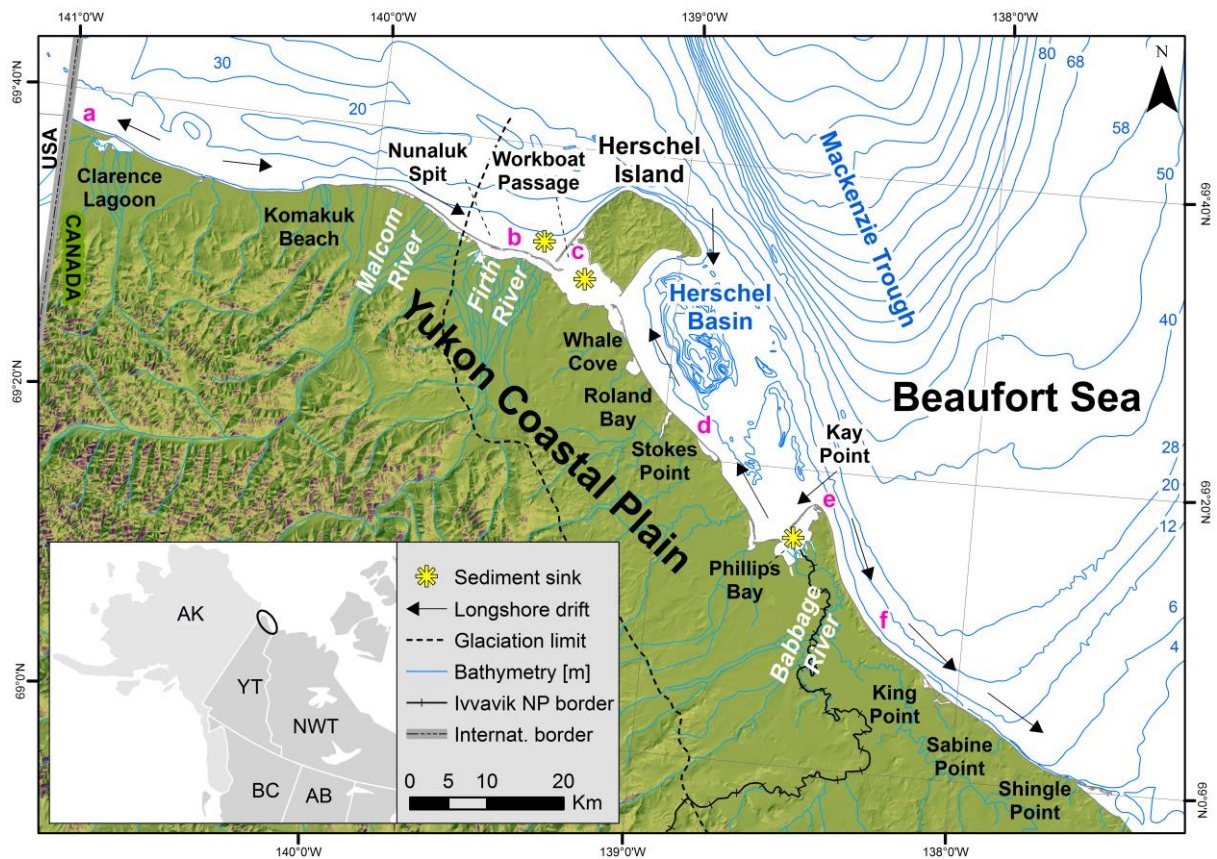


Figure 2.5: Map of the study area with insets showing examples of coastal geomorphology. **Inset a)** Thermal denudation and erosion of ice rich cliffs, Canadian – U.S. American border, photo by G. Tanski, 2015, **Inset b)** ice push ridges along Nunaluk Spit, photo by A. Irrgang, 2015, **Inset c)** Inundating tundra as a result of thaw settlement and sea level rise, Orca Cove, Herschel Island, photo by A. Irrgang, 2015, **Inset d)** collapsed vegetation mats in front of massive ice cliff, Stokes Point West, photo by D. Forbes, 2012, **Inset e)** Block failures as a result of wave undercutting at cliff toe, Kay Point, photo by A. Irrgang, 2012, **Inset f)** Retrogressive thaw slumps on rolling moraine, between Kay Point and King Point, photo by A. Irrgang, 2015. Bathymetry information is based on Canadian Hydrographic Survey Navigational Charts improved by local surveys performed in the 1980s [Thompson, 1994]. Basemap: 30m Yukon DEM, interpolated from the digital 1:50 000 Canadian Topographic Database [Yukon Department of Environment, 2016]. Sediment sink and longshore drift information were derived from Environmental Atlas of the Beaufort Coastlines [Pelletier and Medioli, 2014].

2.6 Thesis structure

The introductory chapters (one and two) provide background information, the state of the art and, research objectives of this thesis. The subsequent chapters (three to six) contain four separate studies which are either in review or published in international peer-reviewed journals. The study in chapter three, “Variability in rates of coastal change along the Yukon coast, 1951 to 2015”, is focusing on the temporal and spatial variability of coastal change rates along the Yukon mainland coast. The comparison of rates of change from several time periods made it possible to not just quantify rates of shoreline change, but also to detect acceleration and deceleration in coastal change rates. The study in chapter four, “Coastal erosion of permafrost soils along the Yukon Coastal Plain and fluxes of organic carbon to the Canadian Beaufort Sea”, gives an example of the consequences of coastal erosion. In this study, the amount of sediments and carbon which are released due to coastal erosion is quantified for the entire Yukon coast. It is accounted for ground ice, which is taking up considerable parts of the volume of the coast, thus making the quantifications of annual sediment and carbon fluxes more accurate. The study in the fifth chapter, “Terrain controls on the occurrence of coastal retrogressive thaw slumps along the Yukon Coast, Canada”, is dealing with the factors which are favoring the occurrence of retrogressive thaw slumps, unique arctic landforms which are mainly appearing along coasts or river beds. Since retrogressive thaw slumps are generally triggered by rapid mass movements, it is hypothesized that coastal erosion is the driving factor for their initiation. The sixth chapter, “Impacts of past and future coastal changes on the Yukon coast – threats for cultural sites, infrastructure and travel routes”, is focusing on the human component. By investigating shoreline changes since the 1950s and projecting shorelines for the year 2100, effects of past and future shoreline dynamics on the peoples are discussed. In chapter seven, an overarching discussion of all four studies highlights the links between the results of the individual studies and puts them into a greater scientific context. Chapter eight gives a summary and conclusions of this thesis.

2.7 Authors’ contributions

Chapter 3: Variability in rates of coastal change along the Yukon coast, 1951 to 2015

Authors: Irrgang, A.M., Lantuit, H., Manson, G.K., Günther, F., Grosse, G., and P.P. Overduin

A. Irrgang and H. Lantuit designed the study. A. Irrgang and G. Manson coordinated and carried out field work. A. Irrgang geo-coded all aerial photographs. A. Irrgang drew all

shorelines, classified the coast, carried out all statistical analyses, interpreted the dataset, made all figures and tables, and wrote the manuscript. Input from all co-authors was received through scientific discussions and proof reading of all manuscript drafts.

Chapter 4: Coastal erosion of permafrost soils along the Yukon Coastal Plain and fluxes of organic carbon to the Canadian Beaufort Sea

Authors: Couture, N., Irrgang, A.M., Pollard, W., Lantuit, H. and M. Fritz

N. Couture and W. Pollard designed the study. N. Couture, W. Pollard, and H. Lantuit carried out field work. N. Couture did all laboratory work. M. Fritz provided additional carbon contents data, which he obtained from separate field work and data processing. A. Irrgang digitized all shorelines, calculated all rates of shoreline change, all areal changes and all mean terrain heights. N. Couture and A. Irrgang calculated all sediment and carbon fluxes and wrote the manuscript. N. Couture made all figures and tables, except for Table 4.3 which was done by N. Couture and A. Irrgang, and Figure 4.1 which was done by A. Irrgang. Input from all co-authors was received through scientific discussions.

Chapter 5: Terrain controls on the occurrence of coastal retrogressive thaw slumps along the Yukon Coast, Canada

Authors: Ramage, J., Irrgang, A.M., Herzsuh, U., Morgenstern, A., Couture, N. and H. Lantuit

J. Ramage and H. Lantuit designed the study. A. Irrgang geo-coded all historical images and digitized the shorelines. J. Ramage digitized all retrogressive thaw slumps and made all statistical analyses. A. Irrgang calculated all mean rates of change, which were used as input parameters for the regression tree models. J. Ramage made all figures and tables and wrote the manuscript. A. Irrgang contributed to the manuscript by editing all versions of the manuscript. Input from all co-authors was received through scientific discussions.

Chapter 6: Impacts of past and future coastal changes on the Yukon coast – threats for cultural sites, infrastructure and travel routes

Authors: Irrgang, A.M., Lantuit, H., Gordon, R., Piskor, A. and G.K. Manson

A. Irrgang, H. Lantuit and R. Gordon designed the study. A. Irrgang projected the shorelines, carried out all statistical analyses, interpreted the dataset, made all figures and tables, and wrote the manuscript. R. Gordon and A. Piskor provided information about the Thule and the Inuvialuit, as well as the European settlers' history and helped to interpret the data. Input from all co-authors was received through scientific discussions and proof reading of all manuscript drafts.

Variability in rates of coastal change along the Yukon coast, 1951 to 2015

ABSTRACT

The Arctic is warming, but the impacts on its coasts are sparsely documented. To better understand the reaction of Arctic coasts to increasing environmental pressure, shoreline position changes along a 210 km length of the Yukon Territory mainland coast in north-west Canada were investigated for the time period from 1951 to 2015. Shoreline positions were extracted from georeferenced aerial images from 1951, 1953, 1954, 1972, 1976, 1992, 1994, and 1996, and from WorldView-2 and GeoEye-1 satellite images from 2011. Shoreline change was then analyzed using the Digital Shoreline Analysis System (DSAS) extension for ESRI ArcGIS. Additionally, differential GPS (DGPS) measurements of shoreline positions from seven field sites were used to analyze coastal dynamics from 1996 to 2015 at higher spatial resolution. The mean shoreline change rate was -0.5 m a^{-1} between the 1970s and 1990s. This was followed by a significant increase in coastal erosion to -1.3 m a^{-1} in the 1990s to 2011 time period. This acceleration is confirmed by the DGPS measurements which indicate increased erosion rates at unprecedented local rates up to -8.9 m a^{-1} since 2006. Ground surveys and observations, with remote sensing data indicate that the current rate of coastal retreat along the Yukon coast is higher than at any time before in the 64 year long observation record. This in turn might favor the buildup of gravel beaches, which have been growing in extent throughout the last six decades.

A manuscript with equal content is in review in the Journal: *Journal of Geophysical Research: Earth Surface*.

Irrgang, A.M., H. Lantuit, G. K. Manson, F. Günther, G. Grosse, and P.P. Overduin (in review). Variability in rates of coastal change along the Yukon coast, 1951 to 2015. *Journal of Geophysical Research: Earth Surface*.

3.1 Introduction

Permafrost coasts are highly dynamic landscapes in the Arctic. Approximately 65% of all Arctic coasts are un-lithified but bonded by permafrost. Upon thaw, these coasts are affected by high erosion rates [Lantuit *et al.*, 2012b; Jones *et al.*, 2013; Günther *et al.*, 2015]. Erosion has large impacts on the ecological and socio-economical coastal systems. Since large quantities of organic carbon are stored in permafrost, released fluxes from coastal erosion could form a significant contribution to the Arctic carbon cycle [McGuire *et al.*, 1995; Zhang and Chen, 2005; Callaghan *et al.*, 2011; Vonk *et al.*, 2012; Hugelius *et al.*, 2013; Fritz *et al.*, 2017; Tanski *et al.*, 2017]. Coastal erosion is also threatening infrastructure, settlements and archaeological sites along many Arctic coasts [Forbes, 2011; Ogorodov *et al.*, 2016].

In the Arctic, air temperatures are expected to increase by 1 °C (RCP 2.6) to 8 °C (RCP 8.5) by the year 2100 [IPCC, 2013]. This increase in air temperature leads to higher permafrost and water temperatures [Smith *et al.*, 2010; AMAP, 2011; Overland *et al.*, 2015; Proshutinsky *et al.*, 2015], decreasing sea ice extent and thickness [Stroeve *et al.*, 2007, 2011, 2014; Serreze *et al.*, 2009] and longer open water seasons [Markus *et al.*, 2009; Stroeve *et al.*, 2014], higher frequency of more severe storms [Atkinson, 2005; Manson *et al.*, 2005], rising sea-level [Manson and Solomon, 2007] and deeper thawing depths of soils [Hinzman *et al.*, 2005; Grosse *et al.*, 2016]. All these changes have the potential to enhance coastal erosion, especially along coasts with high ground ice contents [Aré, 1988; Dallimore *et al.*, 1996; Lantuit and Pollard, 2008; Kizyakov *et al.*, 2013; Günther *et al.*, 2015]. Yet, the intensity at which Arctic coasts are responding to these changes is not well known, since baseline erosion datasets covering multiple time periods are very scarce.

Increasing erosion rates have been reported from several locations along the Arctic coast, but no Arctic-wide increase in erosion rates has yet been substantiated, because of the lack of suitable data and the scarce coverage of these studies [Overduin *et al.*, 2014]. High coastal erosion rates have been described along the Siberian coast [Vasiliev *et al.*, 2005; Lantuit *et al.*, 2011; Günther *et al.*, 2013, 2015; Maslakov and Kraev, 2016], as well as along the Alaskan coast [Brown *et al.*, 2003; Mars and Houseknecht, 2007; Jones *et al.*, 2008, 2009a, 2009b; Ping *et al.*, 2011; Tweedie *et al.*, 2012; Gibbs and Richmond, 2015]. However, despite the fact that the Yukon coast is one of the most ice-rich and fastest eroding coasts in the Arctic [Lantuit *et al.*, 2012b], little is known about the spatial and temporal variability of erosion along this coast. The only study systematically investigating the whole Yukon coast by means of aerial imagery analyses from the 1950s and 1970s was published in 1985 and reported average retreat rates of -0.5 m a^{-1} with local rates up to -5.3 m a^{-1} [Harper *et al.*, 1985].

Further studies concentrated on shorter parts of the Yukon coast [McDonald and Lewis, 1973; Forbes, 1997; Solomon, 1998; Lantuit and Pollard, 2008; Konopczak et al., 2014; Radosavljevic et al., 2015], or on much shorter time scales [Obu et al., 2017 a].

In this paper, the previous studies are complemented and significantly expanded by 1) quantifying shoreline position changes along 210 km of the Yukon mainland coast over a 64-year period (1951-2015), and 2) investigating the temporal and spatial variability of these shoreline changes.

3.2 Study Area

The Yukon coast is the northern limit of the Yukon Coastal Plain, which is the emergent part of the Beaufort continental shelf (Figure 3.1). The Yukon Coastal Plain is 10 to 40 km wide and extends from the Alaskan border to the Mackenzie Delta [Rampton, 1982]. The region was partially glaciated by an extension tongue of the Laurentide Ice Sheet flowing from the south east during the Wisconsin glaciation. During glacial advance the ice sheet deformed sediments and left extensive morainic deposits behind after retreat. The progression stopped at what is today the fan of the Firth River. The Yukon coast region is therefore characterized by two distinct physiographic areas located within and beyond this glacial limit [Rampton, 1982; Fritz et al., 2012] (Figure 3.1).

The coast west of the Firth River delta is characterized by a gently sloping backshore composed of fine-grained lacustrine and alluvial sediments [Rampton, 1982]. Coastal cliffs are higher near the Canada – U.S. American border (6 m) and decrease in height towards Komakuk Beach (3 m). Very high ground ice volumes in this section of coast (up to 66%, [Couture and Pollard, 2017]), lead to the occurrence of thermo-erosional processes which alter the landscape. The river deltas of the Malcom and Firth rivers are fronted by a 40 km long system of barrier spits and barrier islands termed Nunaluk Spit, which protects the delta coast (Figure 3.1).

The formerly glaciated part of the coast, east of the two river deltas, is composed of fine-grained lacustrine and outwash plains, as well as rolling moraines which contain coarse grained tills [Bouchard, 1974; Rampton, 1982]. The morphology of this section of coast is much more diverse than the western part. From the Workboat Passage to the Babbage River delta, cliff heights vary between 2 to 3 m (towards the west) to 15 m high ice-rich cliffs (towards the east). From Kay Point to Shingle Point, the coast rises up to 60 m high and is mainly characterized by steep cliffs made of till deposits, often with very high ground ice contents including massive ground ice [Harry et al., 1988]. Processes like retrogressive thaw

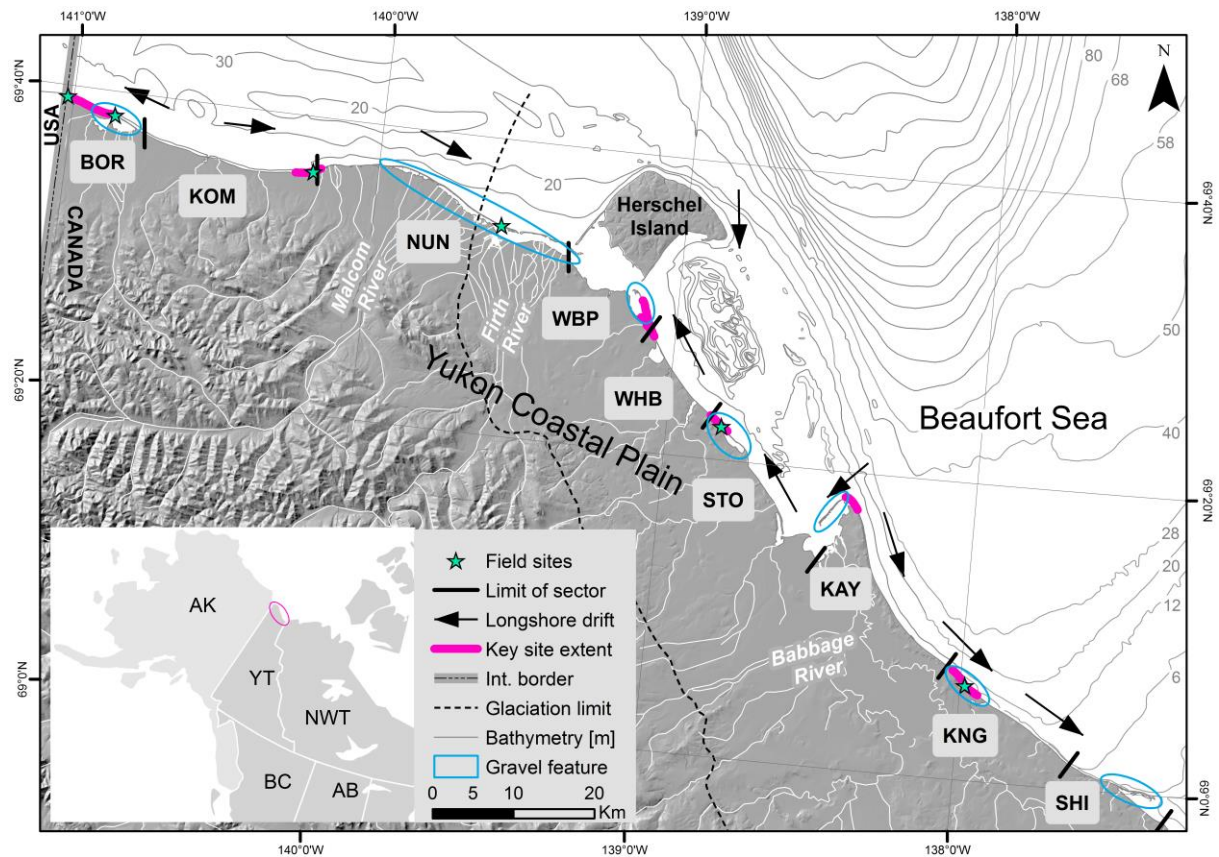


Figure 3.1: Yukon coast with marked sections used for spatial differentiation of shoreline change rates: 1. BOR (Border), 2. KOM (Komakuk Beach), 3. NUN (Nunaluk Spit), 4. WBP (Workboat Passage), 5. WHB (Whale Bay), 6. STO (Stokes Point), 7. KAY (Kay Point), 8. KNG (King Point), and 9. SHI (Shingle Point). The stars are marking the field sites, along which DGPS measurements were taken. The purple bars mark the key site extents. These key sites are additionally covered by aerial images from the 1990s. Blue circles indicate the seven main gravel features along the mainland coast which were assessed to analyze land change dynamics. They are from west to east: Clarence Lagoon, Nunaluk Spit, Catton Spit, Stokes Lagoon, Phillips Spit, King Point Lagoon and Shingle Point spit. Longshore drift information was obtained from the Environmental Atlas of the Beaufort Coastlines 2016. Bathymetry information is based on Canadian Hydrographic Survey Navigational Charts improved by local surveys performed in the 1980s [Thompson, 1994]. Basemap: 30m Yukon DEM, interpolated from the digital 1:50 000 Canadian Topographic Database [Yukon Department of Environment, 2016].

slumping and cliff face gulying are characteristic for this region, as well as block failure along the coast as a consequence of thermal abrasion at the cliff toe [Wolfe *et al.*, 2001].

The Canadian Beaufort shelf fronting the Yukon Coastal Plain is 40 to 150 km wide and is gently sloping towards the shelf break located approximately at the 80 m isobath [Hill *et al.*, 1991b]. The period when sea ice is absent and liquid water and waves affect the shoreface is limited to about 3.5 months from late June to early October [Galley *et al.*, 2016]. Relative sea-level rise in this region is on average about $3.5 \pm 1.1 \text{ mm a}^{-1}$ [Manson *et al.*, 2005]. Astronomical tides are semidiurnal and in the micro-tidal (0.3 to 0.5 m) range [Héquette *et al.*, 1995]. However, storm surges can raise water levels up to 3 m and can cause large scale flooding [Reimnitz and Maurer, 1979; Harper *et al.*, 1988]. The prevailing wind directions are from the south-east and north-west, though most storms come from the north-west [Hill *et al.*, 1991b; Hudak and Young, 2002]. Storms from north-east generate negative surges and are

thus less effective in eroding the coast [Henry, 1975; Harper and Penland, 1982]. Storm occurrences usually peak within the last month before sea ice freeze-up in October [Hudak and Young, 2002; Atkinson, 2005].

The mean annual temperature for Komakuk Beach is $-11.0\text{ }^{\circ}\text{C}$, with a July maximum of $7.8\text{ }^{\circ}\text{C}$ (1971-2000) [Environment Canada, 2016]. Continuous permafrost is underlying the whole Yukon Coastal Plain, except beneath large thermokarst lakes and riverbeds [Rampton, 1982]. Permafrost temperature has been warming by up to $2.6\text{ }^{\circ}\text{C}$ since 1905 [Burn and Zhang, 2009]. This increase is linked to a warming of air temperatures, which are $2.8\text{ }^{\circ}\text{C}$ higher than the ones of the early twentieth century [Richter-Menge and Mathis, 2016].

3.3 Data and Methods

In order to understand how the shoreline changed along the Yukon coast, a 210 km length of coast from the Canadian – U.S. American border in the west to Shingle Point in the east was investigated using remote sensing and field survey data.

3.3.1 Remote sensing data

A combination of aerial images and satellite images was used to map shoreline positions. A series of scanned aerial black and white images was obtained from the Canadian National Air Photo Library [NRCan, 2016a] for the 1950s (i.e., 1951, 1952, 1953, 1954), the 1970s (i.e., 1972, 1976) and the 1990s (i.e., 1992, 1994, 1996). No one year in the 1950s or 1970s had full observational coverage of the study domain so photos from multiple years within a decade needed to be combined to get full coverage for the respective decade. Additionally, seven short shoreline sections (key sites) were digitized in the 1990s. The 2011 shoreline position was mapped using satellite images [Digital Globe 2014, 2016]. In the rest of the paper, all aerial images from 1951, 1952, 1953 and 1954 will be referred to as the 1950s aerial images series. The aerial images from 1972 and 1976 will be referred to as the 1970s aerial image series and the ones from 1992, 1994 and 1996 as the 1990s aerial image series.

3.3.1.1 Geo-coding

Orthorectification of all aerial images was performed by geo-coding all images to the 2011 satellite images using PCI Geomatic's Geomatica Orthoengine© software (2014). The software accounts for camera tilt, lens distortion, radial distortion, Earth curvature and refraction when orthorectifying aerial images. Digital elevation datasets were used to reduce displacement caused by terrain relief. These included the Yukon Digital Elevation Model (DEM) (30.0 m ground resolution) [Environment Yukon, 2016], airplane-based LiDAR (Light

Detection and Ranging) elevation data (1.0 m ground resolution) [Obu *et al.*, 2016b], and the TanDEM-X intermediate DEM (12.0 m ground resolution) [Huber *et al.*, 2012]. Each image was orthorectified to the average height of the digitized shoreline position. Aerial images from the 1950s and 1970s have a ground resolution of 3.5 m and 3.0 m, respectively. This means that the smallest distinguishable objects are 3.5 m, or 3.0 m apart. The aerial images from the 1950s were taken in four consecutive years (i.e., 1951, 1952, 1953, 1954). The aerial images from the 1970s were all taken in 1972, except for one in 1976. Assuming that landscape changes which occurred between the overflights from 1951 to 1954 and from 1972 to 1976 are within the range of the ground resolution, aerial images from the 1950s and 1970s were treated as two series. The 1990s were treated differently because the ground resolution of the aerial images was higher (0.3 m). Aerial images taken within one year in the 1990s each display a single site which was spatially separated from pictures from other years. A total number of 520, 261 and 202 ground control points (GCP) was used to orthorectify the 1950s, 1970s and 1990s images, respectively. The average root mean square positional errors (RMS) for the orthorectified aerial images were 5.45 m, 9.81 m and 4.38 m for the 1950s, the 1970s and the 1990s images, respectively (Table 3.1).

Table 3.1: Metadata and accuracy for all used images. E_{GR} is ground resolution, GCP stands for ground control point, TP for tie point, RMS for the average root mean squared error of all Orthoengine© projects for one decade, LOA for loss of accuracy and U for shoreline uncertainty for the given year.

Date dd.mm. yyyy	Number of images	Type of image	Scale 1:	Ground resolution (E_{GRa}) [m]	GCPs (TPs)	RMS [m]	LOA [m]	U [m]
18.07.2011 20.07.2011 31.08.2011 13.09.2011	5	GeoEye-1 (multispectral pansharpened)	/	0.4	Base image	/	2	2.06
31.08.2011 13.09.2011	2	WorldView-2 (multispectral pansharpened)	/	0.5	Base image			
25.07.1996 13.07.1994 08.06.1992	11 11 21	panchromatic airphotos	6 000	0.3	520 (159)	4.38	2	4.85
07.07.1976 08.07.1972 09.07.1972 31.07.1972 14.08.1972	1 19	panchromatic air photos	60 000	3.0	261 (56)	9.81	4	11.02
22.08.1954 27.07.1953 20.07.1952 14.07.1951	8 3 3 3	panchromatic air photos	70 000	3.5	202 (80)	5.45	7	9.55

3.3.1.2 Shoreline digitalization

The shoreline was digitized manually at a scale of 1:1 000. Because of the wide range of landforms associated with the shoreline in the study area, a set of shoreline proxies such as the cliff top line or the water line was used to digitize the shoreline (Figure 3.2). Delta shorelines were excluded. If the geomorphological setting changed throughout the years, for example from an active to an inactive cliff, the same indicator was used nevertheless. In this case, the indicator which could be distinguished best in both images was selected. The same approach was used when a shoreline indicator could not be distinguished in an image because of terrain shadows or cloud cover.

For computation of shoreline change rates, the shoreline was digitized in two different images taken at the beginning and the end of a time step. The uncertainty of the shoreline position (U) for each time step was calculated as shown in Equation 3.1:

$$U = \sqrt{(E_{GR\ aerial\ image}^2 + E_{GR\ satellite\ image}^2 + RMS^2 + LOA^2)} \quad , \quad (3.1)$$

where $E_{GR\ satellite\ image}$ is the ground resolution of the satellite images, $E_{GR\ aerial\ image}$ represents the ground resolution of the aerial images from a particular year, RMS is the root mean squared error associated with the geo-coding of aerial images from a particular year, and LOA is the estimated loss of accuracy for a particular year (Table 3.1) (modified after *Hapke and Reid*, [2007]). The LOA accounts for the digitizing error and was determined by calculating the variance associated with repeated shoreline digitization of the same extent of shoreline. For consistency, all shorelines were digitized by the same operator.

3.3.1.3 Calculation of shoreline position change rates

Shoreline change rates were calculated using the Esri ArcGIS extension Digital Shoreline Analysis System (DSAS) version 4.3 [*Thieler et al.*, 2009]. The rates were computed along transects perpendicular to the shoreline, with a transect spacing of 100 m. For each transect and each time step, the total shoreline movement as well as yearly shoreline change rates were extracted. DSAS analyses were conducted for the time step from the 1950s to the 1970s, the 1970s to 2011 and for the 1950s to 2011 for the whole study area. For the conduction of DSAS analyses the date of the 16 Aug. 1953 was used for the 1950s (average date of all aerial images from the 1950s), the 17 Jul. 1972 was used for the 1970s (average date of all aerial images from 1972) and the 16 Aug. 2011 (average date of all satellite images from 2011) was used for the 2011 shoreline. Additionally, shoreline change rates were calculated for the time steps from the 1970s to the 1990s and from the 1990s to 2011 for the areas for which shoreline position data from the 1990s was available. The picture extent of the 1990s images

covers a total shoreline length of 27 km, which accounts for 12.9% of the whole shoreline. Since the seven sites are spatially separated from each other, the actual shoreline dates were used for DSAS (06 Aug. 1992, 13 Jul. 1994, 25 Jul. 1996). In the following sections, these segments of coast which are covered in all image series, including the 1990s, are referred to as key sites.

An indicator for the accuracy of the calculated shoreline change rate is the dilution of accuracy (DOA). The DOA was calculated as is shown in Equation 3.2:

$$DOA = \frac{\sqrt{U_1^2 + U_2^2}}{\Delta t}, \quad (3.2)$$

where U_1 is the uncertainty of the shoreline position from the first point in time, U_2 is the uncertainty of the shoreline position from the second point in time and Δt is the amount of years covering the analyzed time span (modified after *Foster et al.*, [1989]). Table 3.2 displays the DOAs for all analyzed time periods.

Table 3.2: Dilution of Accuracy (DOA) for all considered time periods.

Time period	DOA [m a^{-1}]
1950-1970	0.81
1970-1990	0.55
1990-2011	0.31
1970-2011	0.29
1950-2011	0.17

3.3.1.4 Methods of change detection along lagoons, barrier islands and spits (gravel features)

For the purpose of this study, erosion is defined as a landward movement and accretion as a seaward movement of the shoreline. This definition can be misleading if it comes to shoreline dynamics along lagoons, barrier islands and spits since a landward movement of these geomorphological forms indicates land shift, but not necessarily land loss. In order to capture land loss and land gain more adequately along these features, which will be referred to as gravel features, their areal extent was digitized for the 1950s, 1970s and 2011 at a scale of 1:1 000. Then, the areas of the generated vector polygon shapefiles were compared. Due to a lack of aerial image coverage, no area calculations could be performed for the 1990s. This analysis was done for the seven largest gravel features which occur along the mainland coast; Clarence Lagoon, Nunaluk Spit, Catton Point Spit, Stokes Point Lagoon, Phillips Bay Spit, King Point Lagoon and Shingle Point Spit (Figure 3.1).

3.3.2 Field survey data

Field site measurements were used to capture local scale (0.1 to 2 km) coastal changes at high temporal resolution. For the purpose of this study, data from seven field sites were analyzed for the period from 1991 to 2015. Multi-year data collection was conducted from 1991 to 1995 using theodolite-based geodetic surveys and since then with a Differential Global Positioning System (DGPS). The theodolite measurements and the DGPS measurements reach a position accuracy of ≤ 5 cm [NRCan, 2013]. At most field sites, the DGPS base station was set upon a geodetic benchmark with a known absolute position. Position accuracy of the collected survey information was enhanced by Precise Point Positioning (PPP) in 2012, using the Canadian Spatial Reference System (CSRS)-PPP online tool [NRCan, 2016b]. Table 3.3 gives the length of shoreline encompassed by transects at each site, as well as the years of measurement and the number of transects. For comparison to remote sensing data, additional transects were created in DSAS that were coincident with the field transects and separate statistics were calculated.

Table 3.3: Description of the field sites. Site positions are shown in Figure 3.1. Revisiting of the sites occurred irregularly, with a one to eight years break between two consecutive visits.

Site name	Survey years	Shoreline length [m]	Number of cross-shore transects
Border	1991, 1999, 2006, 2012, 2015	120	3
Clarence	1997, 2006, 2015	100	3
Lagoon			
Komakuk	1997, 2000, 2006, 2012, 2014, 2015	570	9
Beach			
Nunaluk Spit	1995, 1996, 1997, 2000, 2003, 2006, 2012, 2014, 2015	100	4
Catton Point	1996, 2006, 2012, 2014, 2015	420	2
Stokes Point	1995, 1996, 1997, 1999, 2006, 2007, 2012, 2014, 2015,	330	5
King Point	2012, 2014, 2015	1700	3

3.3.2.1 Calculation of shoreline position change rates

The field sites were first established in different years and were surveyed in irregular time steps. Since the sites were established to serve a variety of purposes (e.g. characterizing representative coastal cliff features, monitoring of archaeological sites, Defense Early Warning (DEW) line station monitoring), they also have different spatial extents (Table 3.3). Coastal monitoring was conducted in the form of point measurements along designated cross-

shore profiles and along-shore measurements at the water line, at the cliff toe, and at the cliff top. For the calculation of shoreline position change rates the cliff top was chosen as main shoreline indicator. The average annual rate of change (R_{ave}) in metres per year was calculated by dividing the cliff edge position differences (Δx and Δy) by the number of years in between two consecutive measurements (Δt):

$$R_{ave} = \frac{\sqrt{(\Delta x)^2 + (\Delta y)^2}}{\Delta t} . \quad (3.3)$$

3.3.3 Classification of shoreline

To classify the variety and distribution of coastal landforms along the Yukon coast, a coastal classification scheme was established based on *Harper* [1985] and *Couture et al.* [2015a]. This classification scheme was applied to the shoreline at a scale of 1:1 000. Figure 3.2 shows examples for each of the five established classes, being: 1. *beach, barrier island, spit*, 2. *inundated tundra*, 3. *tundra flats*, 4. *tundra slopes* and 5. *active tundra cliff*. Table 3.4 contains the definition of each class. The coastal classification information was assigned to the rate of change for each DSAS transect for the time step from the 1950s to 2011.

Table 3.4: Coastal landform classification

Coastal landform class	Definition	Shoreline proxy
Beach, barrier island, spit	Subaerial sand and gravel beaches which are surrounded by water from both sites, such as spit extensions from the mainland, barrier islands fronting the mainland, lagoons and river inlets	Wet-dry line
Inundated tundra	Tundra inundated due to thaw subsidence and/or coastal flooding as an effect of sea-level rise. This class includes wetlands and tidal flats.	Vegetation line
Tundra flats	low lying tundra with no evident active cliff or inactive cliff	Vegetation line
Tundra slopes	Inactive cliffs and inactive retrogressive thaw slumps which are flattened and vegetated due to the absence of coastal erosion	Cliff toe
Active tundra cliff	Cliffs and bluffs which are actively eroding	Cliff top

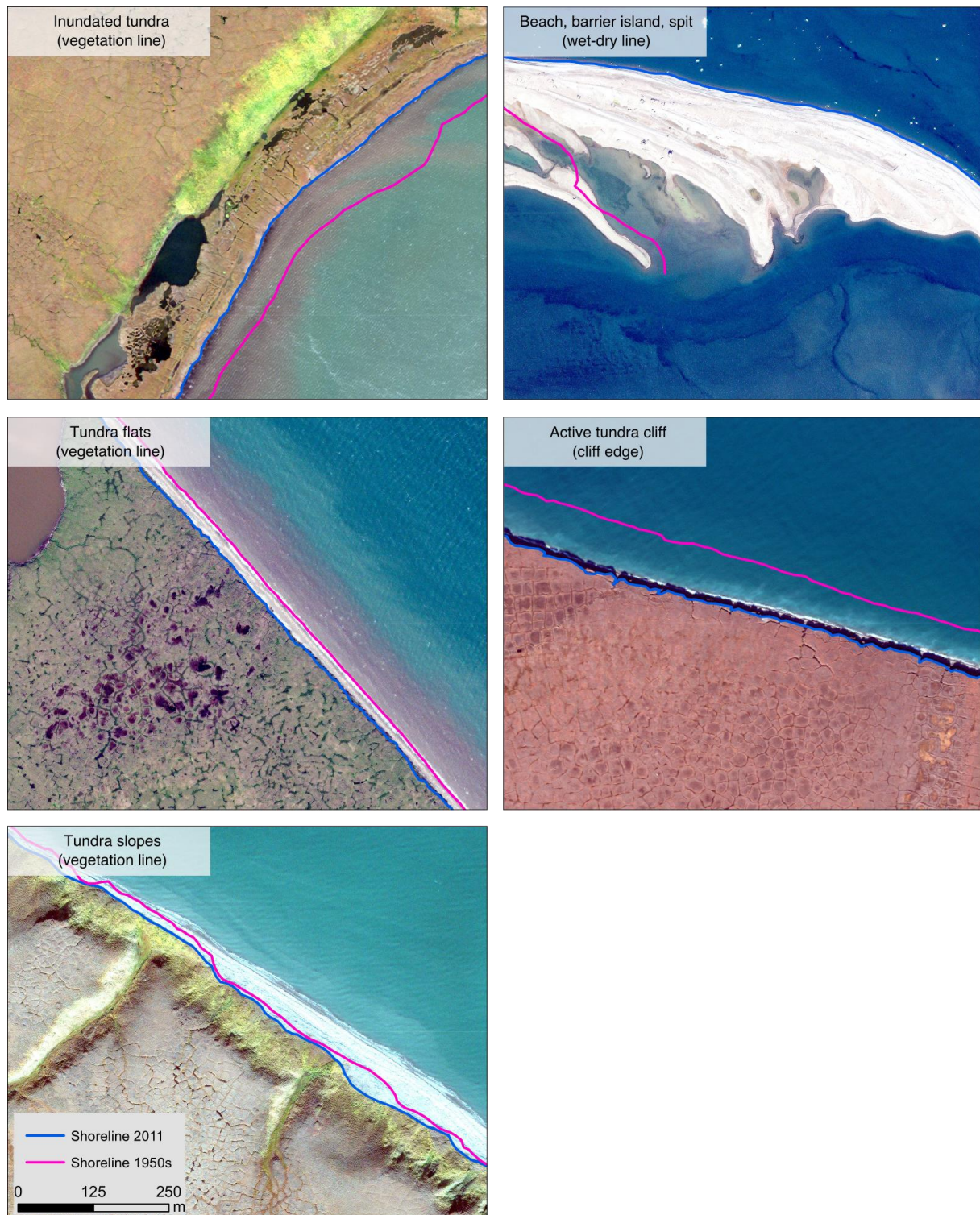


Figure 3.2: Examples of coastal landforms associated with the five coastal landform classes used to describe the shoreline (for definitions see Table 3.4). The indicators used to digitize the shoreline are provided between brackets.

3.3.4 Transect-wise analyses of shoreline movements through time

In order to better understand the evolution of the shoreline between the different time periods, a detailed analysis of the movement of the shoreline at each DSAS transect was performed. Transects were categorized based on whether shoreline change rates showed increasing or

decreasing erosion, increasing or decreasing accumulation, whether accumulation changed to erosion, or vice versa. This transect-wise analysis was performed to compare two consecutive time periods, over the whole length of coast and to compare three consecutive time periods for the key sites extent. Therefore, three distinct analyses were conducted: 1) the shoreline change rates of the 1950s to 1970s time period were compared with the 1970s to 2011 time period, 2) the shoreline change rates of the 1950s to 1970s time period were compared with the 1970s to 1990s time period and 3) the shoreline change rates from the 1970s to 1990s time period were compared with the 1990s to 2011 time period.

3.4 Results

The results provide shoreline change rates along 210 km length of the Yukon coast for the time between 1951 and 2015. The mean coastal change for the whole length of coast was -0.7 m a^{-1} . Thirteen percent of the coast was either accumulating or stable while 87% of the coast was eroding. The dataset comprising all DSAS analysis results for all time periods is published in the data archive PANGAEA [Irrgang *et al.*, 2017].

3.4.1 Temporal variations in shoreline change rates

Temporal changes in shoreline positions were analyzed using five observation time periods, based on images from the 1950s, 1970s, 1990s, and 2011 (Table 3.5). Throughout all time periods, the mean shoreline change of the whole coast remained stable. However, after a substantial deceleration in erosion from the 1970s to the 1990s, a strong acceleration in erosion since the 1990s was measured along the key sites which was as high as for the 1950s to 1970s time period.

For the whole coast, the mean rate of change of -0.7 m a^{-1} varied only marginally over time (1950s-1970s: -0.72 m a^{-1} , 1970s-2011: -0.71 m a^{-1} , Table 3.5) and did not change significantly (level of significance $\alpha = 0.05$). Along the key sites, a mean rate of change of approximately -1.3 m a^{-1} was measured for the 1950s to 1970s. In the 1970s to 1990s time period, the mean rate of change decelerated significantly to -0.5 m a^{-1} . The mean shoreline change rate of the 1990s to 2011 time period at the key sites was significantly higher (-1.3 m a^{-1}) than during all previous time periods ($\alpha = 0.05$) and nearly twice as high as the mean rate of change for the whole coast.

Transect-wise analyses performed along the whole coast show that the number of transects recording erosion increased since the 1970s (Figure 3.3, inset A). However, along most of these transects shoreline change rates decreased from the 1950s to 1970s time period to the

1970s to 2011 time period (Figure 3.3, inset A). The amount of transects along which shoreline change rates of more than -5 m a^{-1} were recorded increased in the 1970s to 2011 time period.

Transect-wise analyses performed at the key sites show a deceleration in erosion to the 1990s, followed by a strong shift towards a highly erosive regime. The comparison of rates of change of the 1950s to 1970s time period with the 1970s to 1990s time period shows that coastal erosion decelerated along 51% of the key sites transects (Figure 3.3, inset B). Over the same period of time, 15% of the key sites transects shifted from erosion to accumulation. In the following time period, from the 1990s to 2011 a strong acceleration in erosion was measured along 54% of all key site transects (Figure 3.3, inset C). This latter time period (1990s – 2011) also has the largest number of eroding key site transects (Figure 3.3, inset B and inset C). In summary, the key sites showed a shift towards an increase in the percentage of eroding transects and an acceleration of erosion since the 1990s.

Table 3.5: Rate of change statistics for all analysed time steps for the whole study area and for the key sites. The key sites have additional information because of the use of 1990s aerial images. The 1990s aerial images cover 27 km of the whole study area and rate of change statistics were compiled specifically for their spatial extent. ER stands for erosion, AC stands for accumulation.

	Time period	Mean rate of change [m a ⁻¹]	Median rate of change [m a ⁻¹]	ER [% of all measurements]	ER ≤ -1 m a ⁻¹ [% of all measurements]	AC [% of all measurements]	AC ≥ 1 m a ⁻¹ [% of all measurements]
Whole coast	1950s-1970s	-0.72	-0.54	77	34	23	4
	1970s-2011	-0.71	-0.47	84	29	16	2
	1950s-2011	-0.72	-0.51	87	30	13	2
Key sites	1950s-1970s	-1.26	-1.16	86	53	14	2
	1970s-1990s	-0.54	-0.62	78	32	22	6
	1990s-2011	-1.30	-1.18	85	55	15	4
	1950s-2011	-1.02	-1.04	87	53	13	1

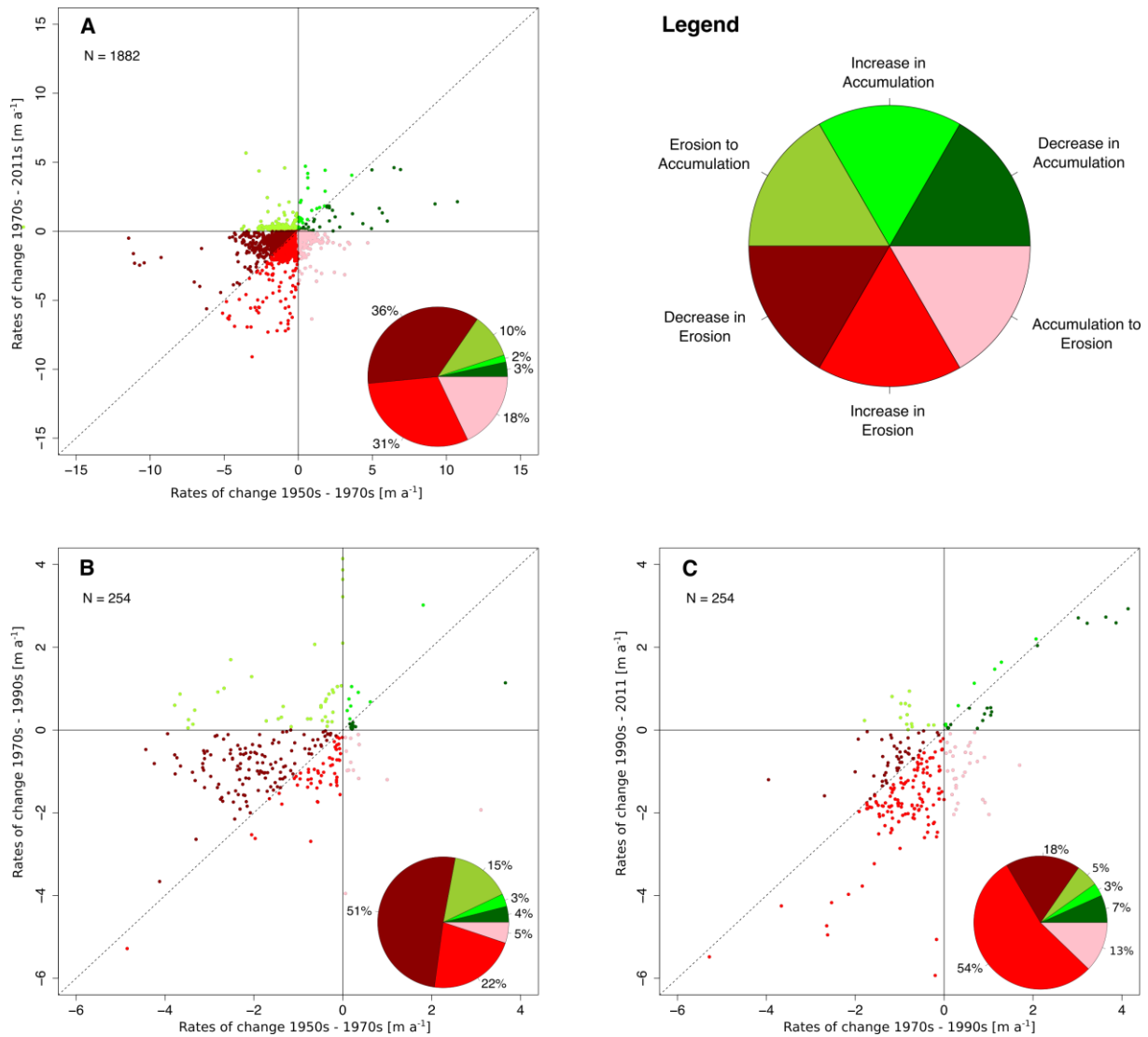


Figure 3.3: Transect-wise analyses of shoreline movements for the whole coast (inset A) and for the key sites (insets B and C). Each point in the scatter plot stands for measurements of rates of shoreline change along one DSAS transect in two consecutive time periods. The colours in the pie charts correspond to the colours in the graphs.

3.4.2 Alongshore rates of change

The study area was subdivided into nine sections to characterize the spatial variability of erosion along the Yukon coast (Table 3.6, Figure 3.4). The subdivision was made on the basis of different physiographic units.

Over the 1950s to 2011 time period, the western Yukon coast (west of Herschel Island) experienced higher mean annual rates of erosion than did the eastern Yukon coast. Change occurred at the Border, Komakuk Beach and Nunaluk Spit sections at mean rates of -1.4 m a^{-1} , -1.3 m a^{-1} , and -0.9 m a^{-1} , respectively. With mean change rates of -0.1 m a^{-1} to

-0.5 m a^{-1} , the sections south and east of Herschel Island were closer to the overall mean rate of change of -0.7 m a^{-1} along the whole coast.

Table 3.6: Rate of change statistics for coastal sections arranged from west to east (Figure 3.1) over the 1950s to 2011 time period. AC stands for accumulation, ER for erosion. BOR stands for Border, KOM for Komakuk Beach, NUN for Nunaluk Spit, WBP for Workboat Passage, WHB for Whale Bay, STO for Stokes Point, KAY for Kay Point, KNG for King Point and SHI for Shingle Point.

Section	Coverage [km] (%)	Max. ER Rate [m a ⁻¹]	Mean rate of change [m a ⁻¹]	Median rate of change [m a ⁻¹]	Max. AC rate [m a ⁻¹]	ER along section [%](ER ≤ - 1 m a ⁻¹)	AC along section [%] (AC > 1 m a ⁻¹)	ER along coast [%] (ER ≤ -1 m a ⁻¹)	AC along coast [%] (AC > 1 m a ⁻¹)
BOR	11.7 (5.6)	-2.1	-1.4	-1.3	0.0	99.1 (71.8)	0.9 (0.0)	5.5 (4.0)	0.1 (0.0)
KOM	24.5 (11.5)	-2.0	-1.3	-1.3	-0.3	100.0(77.1)	0.0 (0.0)	11.5 (8.9)	0.0 (0.0)
NUN	29.1 (13.9)	-7.2	-0.9	-1.1	5.0	95.2 (39.9)	4.8 (2.6)	13.2 (5.5)	0.7 (0.4)
WBP	23.2 (11.0)	-2.5	-0.3	-0.4	0.6	86.2 (12.4)	13.8 (0.0)	9.5 (1.4)	1.5 (0.0)
WHB	14.3 (6.8)	-1.5	-0.5	-0.5	0.2	93.3 (13.4)	6.7 (0.0)	6.4 (0.9)	0.5 (0.0)
STO	31.9 (15.2)	-6.2	-0.5	-0.9	2.9	79.9 (31.4)	20.1 (3.0)	12.2 (4.8)	3.1 (0.5)
KAY	33.6 (16.0)	-5.8	-0.2	-0.5	0.9	83.8 (9.5)	16.2 (0.0)	13.4 (1.5)	2.6 (0.0)
KNG	20.6 (9.8)	-2.5	-0.5	-0.6	2.5	95.3 (20.7)	4.7 (1.6)	9.4 (2.0)	0.5 (0.2)
SHI	21.2 (10.1)	-1.8	-0.1	0.1	5.3	63.3 (4.5)	36.7 (8.0)	6.4 (0.5)	3.7 (0.8)

The highest erosion rates were measured in the Nunaluk Spit (-7.2 m a^{-1}) and Stokes Point (-6.2 m a^{-1}) sections and were associated with the *beach, barrier island, spit* class. In the Kay Point section, very high erosion rates were also measured at -5.8 m a^{-1} and -5.7 m a^{-1} . These were associated with the *inundated tundra* class in the wave sheltered area behind the Phillips Bay Spit and with the *active tundra cliff* class at the very tip of King Point. Along 30.5% of all transects, erosion rates of more than -1 m a^{-1} were recorded. The sections of Komakuk Beach, Nunaluk Spit and Stokes Point had the largest amounts of these high erosion rates, with 8.9%, 5.5% and 4.8%, respectively. Most of these high erosion rates were associated with the *active tundra cliff* class (14.4%) and to a lesser extent with the *beach, barrier island, spit* class (10.8%). These two classes not only contain the highest rates of erosion, they also cover the longest stretches of the coast.

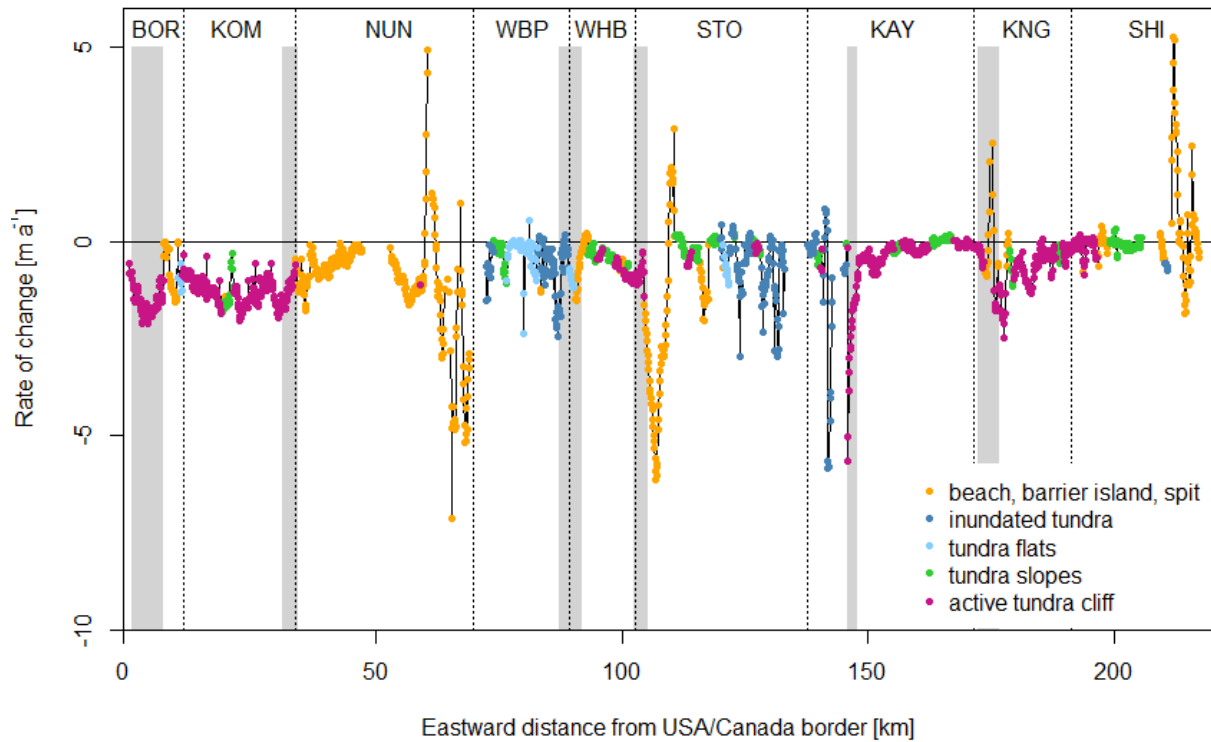


Figure 3.4: Rates of change along the coast for the time period 1950s-2011 with corresponding coastal landform classes (coloured dots) and key site extents (grey bars). Negative rates of change indicate erosion, positive rates of change indicate accumulation. The respective sections are indexed on top, BOR stands for Border, KOM for Komakuk Beach, NUN for Nunaluk Spit, WBP for Workboat Passage, WHB for Whale Bay, STO for Stokes Point, KAY for Kay Point, KNG for King Point and SHI for Shingle Point. The gap in the NUN section is due to a lack of aerial image coverage in the 1950s and subsequently missing rate of shoreline change analyses.

The highest accumulation rates were measured in the Shingle Point (5.3 m a^{-1}), Nunaluk Spit (5.0 m a^{-1}) and Stokes Point (2.9 m a^{-1}) sections and were associated with the *beach, barrier island, spit* class (Figure 3.4). Along 1.9% of all transects, accumulation rates of more than 1.0 m a^{-1} were recorded. The sections of Shingle Point, Stokes Point and Nunaluk Spit had the largest amount of these high accumulation rates, with 0.8%, 0.5% and 0.4%, respectively. Most accumulation rates were associated with the *beach, barrier island, spit* class and the *tundra slopes* class.

In summary, the sections of Nunaluk Spit and Stokes Point showed the highest variability in shoreline change rates, whereas the sections of Komakuk Beach and Border had the most uniformly changing (i.e., eroding) shorelines (Figure 3.4). The classes of *beach, bar spit* showed the highest variability in shoreline change rates, whereas the shoreline in the *tundra slopes* class changed the least (Figure 3.4).

Table 3.7: Coastal landform classes and corresponding rate of shoreline change statistics for the time period 1950s to 2011. AC stands for accumulation, ER for erosion.

Class	Coverage [km] (%)	Max. ER rate [m a ⁻¹]	Mean rate of change [m a ⁻¹]	Median rate of change [m a ⁻¹]	Max. AC rate [m a ⁻¹]	ER in class [%] (ER ≤ -1 m a ⁻¹)	AC in class [%] (AC > 1 m a ⁻¹)	ER along coast [%] (ER ≤ -1 m a ⁻¹)	AC along coast [%] (AC > 1 m a ⁻¹)
Beach, barrier island, spit	61.7 (29.4)	-7.2	-0.9	-0.7	5.3	82.4 (36.7)	17.6 (6.1)	24.2 (10.8)	5.2 (1.8)
Tundra slopes	35.2 (16.8)	-1.8	-0.2	-0.1	0.3	75.8 (6.1)	24.2 (0.0)	12.7 (1.0)	4.1 (0.0)
Inundated tundra	23.8 (11.3)	-5.8	-0.8	-0.5	0.9	85.7 (23.8)	14.3 (0.0)	9.7 (2.7)	1.6 (0.0)
Tundra flats	9.9 (4.7)	-2.4	-0.5	-0.4	0.6	95.7 (14.0)	4.3 (0.0)	4.5 (0.7)	0.2 (0.0)
Active tundra cliff	79.3 (37.8)	-5.7	-0.8	-0.8	0.2	96.2 (38.1)	3.8 (0.0)	36.3 (14.4)	1.4 (0.0)
Whole coast	210 (100.0)	-7.2	-0.7	-0.5	5.3			87.5 (30.5)	12.5 (1.9)

3.4.3 Shoreline dynamics along field sites

Results derived from the DGPS measurements and corresponding DSAS analyses along the field sites (Figure 3.5) are in good agreement with the analyses of the remotely sensed data. Since 2012, measurements along the field sites Border (Figure 3.5, BORs), Nunaluk Spit (Figure 3.5, NUNs) and Stokes Point (Figure 3.5, STOs) revealed erosion at unprecedented speeds of -3.3 m a⁻¹, -2.2 m a⁻¹ and -8.9 m a⁻¹, respectively. On the contrary, mean annual shoreline change rates along Clarence Lagoon (CLAs) and King Point (KNGs) were highest in the 1950s to 1970s time period (CLAs = 2.9 m a⁻¹, KNGs = 4.3 m a⁻¹) and decreased by 96% and 74% since then (CLAs = 0.1 m a⁻¹ in 2006-2015, KNGs = 1.1 m a⁻¹ in 2012-2015). Measurements along Catton Point show that this field site is stable - no change through time was recorded. The DGPS measurements along the Komakuk Beach field site show that erosion along this site seems to follow an inter-annual pattern, where each ten years the coast erodes faster, followed by a gradual deceleration of erosion (Figure 3.5, KOMs).

Except for the measurements along Clarence Lagoon and Catton Point, some erosion rates measured since 2006 were up to 12 times higher than the long term mean of -0.7 m a⁻¹ for the 1950s to 2011.

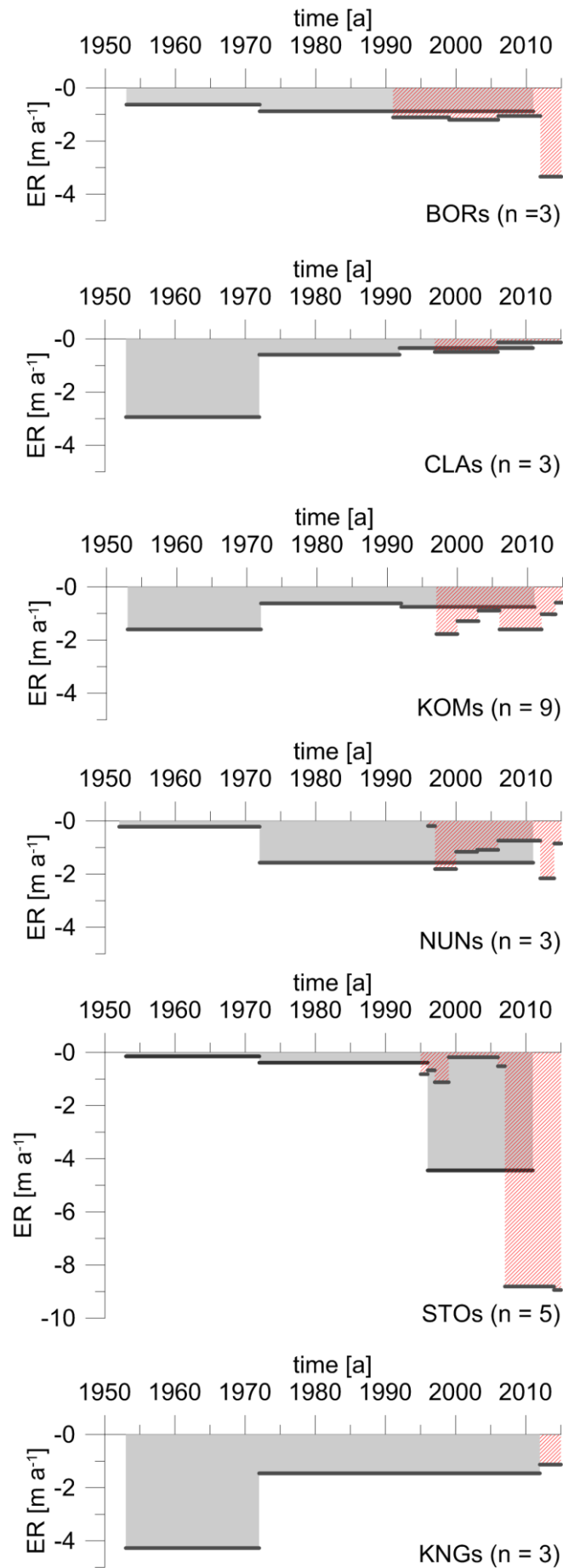


Figure 3.5: Erosion rates along the six out of seven field sites. The field site positions are indicated in Figure 3.1. Each site is named like the section in which it is located with the additional letter s which stands for short, meaning that just a short part of the sector is covered by GPS measurements. BOR_s stands for Border_{short} and so on. CLAs is short for Clarence Lagoon which is situated in the eastern part of the Border section. The n in the brackets indicates the number of transects along the respective monitoring site. Additional information about the field sites can be obtained from Table 3.3. The field site of Catton Point was neither eroding nor accumulating throughout all time periods and is thus not displayed here. The GPS measurements (red shaded bars) are shown together with the remote sensing measurements (grey bars).

3.4.4 Dynamics of lagoons, barrier islands and spits (gravel features)

Most of the gravel features analyzed along the Yukon coast expanded in area (Figure 3.6). The largest change, with an increase of 110%, was detected along the lagoon at King Point. The lagoon closed between the 1950s and the 1970s and since then the lagoon grew to an extent of approximately 366 200 m² in 2011. Since the 1950s, Phillips Bay Spit, which is situated just north of the fast eroding Kay Point tip grew by half of its size (51%). The largest gravel feature along the Yukon coast is Nunaluk Spit, with a total extent of 3 064 500 m² in 2011, 39% more than in the 1950s. The two gravel features which show smallest changes since the 1950s are closures of lagoons. In 2011, Stokes Point lagoon was 12% larger than in the 1950s. Clarence Lagoon decreased in size since the 1950s.

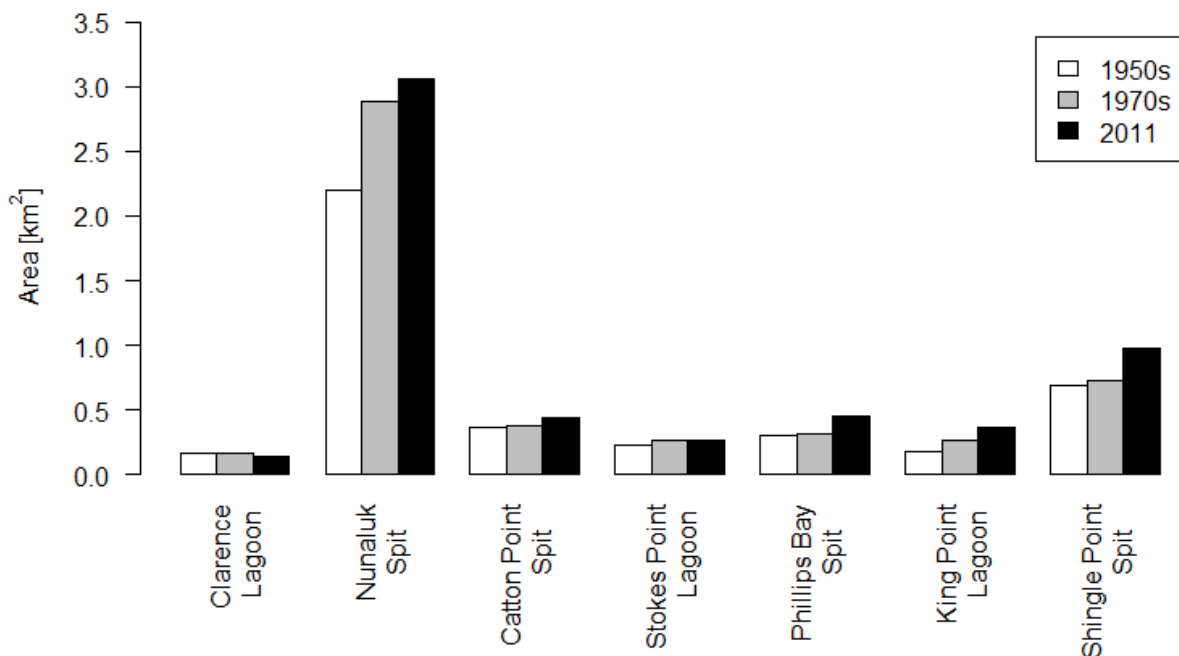


Figure 3.6: Areas of the seven largest gravel features along the Yukon coast measured in the 1950s, 1970s and 2011. The areas are displayed from west to east. For locations see Figure 3.1.

3.4.5 Yukon Territory land loss

From the 1950s to 2011, the Yukon Territory lost a total area of approximately 8 323 100 m² due to shoreline retreat, which is approximately 14 ha a⁻¹. However, the definition of coastal erosion and accretion used for this calculation does not adequately capture the full dynamics of gravel features such as barrier islands, spits, and lagoon beaches, which can be sites of sediment deposition and net accumulation despite shifting towards the mainland. The calculation was therefore performed once more, excluding gravel features. In this case, the Yukon Territory mainland lost approximately 5 985 500 m² of land due to shoreline retreat over the 1950s to 2011 period, which is approximately 10 ha a⁻¹.

3.5 Discussion

3.5.1 Temporal variations in shoreline change rates

A mean rate of shoreline change of -0.7 m a⁻¹ along the 210 km of the Yukon coast indicates long-term stability of spatially averaged rates of shoreline change from the 1950s to 2011 (Table 3.5). The overall rate is in good agreement with *Harper et al.* [1985], who calculated a mean annual shoreline change rate of -0.5 m for the time period of the early 1950s to 1970s, but is considerably lower than the mean coastal retreat rate of -1.12 m a⁻¹, published by *Lantuit et al.* [2012b] for the Canadian Beaufort coast. A potential reason for the higher erosion rates from *Lantuit et al.* [2012b] is that these comprise rates of change from the whole Beaufort sea coast, including the Mackenzie River delta and its outer islands and up to the northern end of Banks Island. These regions are oriented north-west to west and are therefore directly exposed to the most effective storms, resulting in higher mean erosion rates [*Solomon, 2005*].

Two possible explanations for the stability of the mean rate of change through time are that 1) the driving environmental factors did not change over time, or 2) that the mean retreat rate does not spatially capture the changes occurring at the coast. Observations show that environmental factors, such as sea surface, water and air temperatures and the length of the open water season are changing since decades – temperatures are getting warmer and open water seasons are getting longer [*Hinzman et al., 2005; Serreze and Barry, 2011; Parkinson and Comiso, 2013; Stroeve et al., 2014*]. These changes should lead to higher erosion rates along the coast [*Barnhart et al., 2014b*]. The average rate of change was compiled with nearly 2 000 measurements along 210 km of coast. This averaging involves an inevitable smoothing of the highly dynamic areas, as can be seen in Figure 3.4. Yet, the number of transects shifting from accumulation in the 1950s to 1970s to erosion in the 1970s to 2011 was twice as high as

the number of transects shifting, from erosion to accumulation (Figure 3.3, inset A), indicating a substantial change in the erosion vs. accumulation regime along the coast. Also, the amount of transects recording fast retreat was much higher in the most recent time period of 1990s to 2011. Thus, a change towards higher erosion is visible but not reflected in the overall mean coastal change rates.

The analysis of the key sites included the 1990s images and provided a greater temporal resolution, with three equally long time steps (1950s to 1970s, 1970s to 1990s, 1990s to 2011) (Table 3.5). This analysis suggests that shoreline retreat slowed down significantly between the 1970s and the 1990s, followed by a significant acceleration of shoreline retreat from the 1990s to 2011 (Table 3.5). Studies performed along the coast of Herschel Island, Kay Point and along the eastern Beaufort Sea coast also detected a deceleration of shoreline retreat for the time period of the mid-1950s to early 1970s [Solomon *et al.*, 1994; Solomon, 2005; Lantuit and Pollard, 2008]. Since a decrease of storm frequency was measured since the mid-1970s and throughout the 1980s, it is very likely that the deceleration in coastal erosion is linked to it [Reimnitz and Maurer, 1979; Manson *et al.*, 2005; Hansom *et al.*, 2008]. The shoreline change rates from the 1990s to 2011 were significantly more negative (higher erosion rates) than the ones from the 1950s to the 1970s, suggesting that erosion is occurring at highest speed since the beginning of measurements in the 1950s.

The GPS measurements at the field sites extend to 2015 and show that this pattern is continuing and erosion even intensified since 2006 along some field sites (Figure 3.5). The observation of an acceleration of coastal erosion since the early 1990s is in good agreement with findings from the Alaskan part of the Beaufort Sea coast and from the Siberian coast [Mars and Houseknecht, 2007; Jones *et al.*, 2009a; Ping *et al.*, 2011; Günther *et al.*, 2013; Maslakov and Kraev, 2016; Obu *et al.*, 2017a]. The latest observations of increasing erosion rates might be partly attributable to the fast declining sea-ice extent within the last years, leading to a longer exposure of the shoreline to waves and to more favorable conditions for the development of higher waves because of a longer fetch [Galley *et al.*, 2016; Overeem *et al.*, 2011; Barnhart *et al.*, 2014b]. Since the GPS rates are calculated for sub-decadal time steps, the rates of change are susceptible to weather anomalies, like for example single severe storms. Thus, rates of change averaged over short time periods are often higher and more variable than long-term averages [Dolan *et al.*, 1991; Dallimore *et al.*, 1996]. The aerial image analyses are averaging 20 to 40 year time periods so that the observed inter-annual variations have a lower influence.

In summary, temporal changes in coastal dynamics along the Yukon coast show an increase in erosion in recent years, but this is not necessarily reflected in the long-term mean shoreline change rate. These changes seem to be mainly attributable changes in the length of the open water season or the change of storm intensity and frequency. However, further analyses will be needed for an enhanced understanding of the relation of forcing factors and rates of shoreline change.

3.5.2 Alongshore rates of change

On the regional scale, the magnitude of shoreline changes along the Yukon mainland coast can be explained by coastal orientation. The regions beyond the Buckland glaciation limit west of Herschel Island (BOR, KOM, NUN) show mean rates of change of -1.4 m a^{-1} to -0.9 m a^{-1} , while the shoreline in the regions southeast of Herschel Island (WBP, WHB, STO, KAY, KNG, SHI) is changing at a mean speed of -0.5 m a^{-1} to -0.1 m a^{-1} (Table 3.6). The orientation of the mainland coast changes from a north to north-west orientation west of Herschel Island, to a north-east to east orientation, east of Herschel Island. The gradient in rates of change between the regions west and east of Herschel Island suggests that coastal erosion along the Yukon coast is linked to exposure towards storms, since the predominant direction of storms is north to north-west [Solomon *et al.*, 1994; Hudak and Young, 2002; Manson and Solomon, 2007]. The regions west of Herschel Island are directly exposed to the most effective storms. Herschel Island shields the regions to its south (WBP) and east (WHB). These findings are in good agreement with those from Solomon [2005], who observed that rates of change along the eastern Beaufort coast (Mackenzie Delta to Tuktoyaktuk) are strongly influenced by the exposure to north-west wind-driven waves and the resulting high water levels. The second most prominent direction from which storms originate along the Yukon coast is south-east to south-south east. However, these storms result in negative surges and are thus less erosive [Harper and Penland, 1982; Henry, 1975].

An increase in negative shoreline change rates (meaning an increase in erosion rates) from east to west, west of Herschel Island can also be explained by coastal orientation. The Nuneluk Spit section has the smallest mean shoreline change rate of -0.9 m a^{-1} while the Border section has the highest mean shoreline change rate of -1.4 m a^{-1} . Publications reporting on erosion from the Alaskan side of the Beaufort Sea coast show that shoreline change rates west of Herschel Island correspond well with shoreline change rates in west Alaska and that a further increase in erosion towards Point Barrow can be observed. Around Demarcation Point shoreline change rates reach approximately -1.2 m a^{-1} and increase towards the west to -13.6 m a^{-1} and -19.0 m a^{-1} around Point Barrow [Jones *et al.*, 2009b; Ping *et al.*, 2011;

Barnhart et al., 2014a; *Gibbs and Richmond*, 2015]. This, again, can be explained by the exposure of the coast towards storms. Additionally, Point Barrow, as a headland, is extremely exposed to storms coming from the west, north and east.

In wave-sheltered areas, relative sea-level rise seems to play an important role for coastal retreat. All areas which are eroding despite being sheltered from waves lay in the *inundated tundra* class, or to a minor extent in the *tundra flats* class. Bluffs in these classes are very low, usually not exceeding 2 m in height. Consequently, the inundation of coastal tundra might be attributed to relative sea-level rise, as a consequence of thaw settlement in the coastal zone. Thaw settlement can have a major impact on coastal dynamics, as can be observed in the section of Stokes Point. With a mean shoreline change rate of -8.5 m a^{-1} , the area immediately north- west of Stokes Point lagoon is one of the most rapidly retreating areas along the whole Yukon coast. These high rates of erosion are very limited in extent and are likely to be linked with local controls. In this case, ground-ice volume is probably controlling coastal evolution. Along the fast retreating cliff, large bodies of massive ice are visible, which get exposed by coastal erosion. During the summers, the massive ice in the cliff face is exposed to solar radiation, leading to fast melting. *Harper* [1990] already noticed that large parts of the Yukon coasts are rather melting away than eroding away. During the surveys performed at the field sites in 2012, 2014 and 2015, waves were notching the ice-rich cliff face despite un-stormy weather conditions, even though aerial images from 1996 showed that there was a beach fronting the cliff. This could be an indicator for a local deepening of the nearshore bathymetry. Ground settlement as a consequence of subsea permafrost or massive ice thaw or another mechanism of active submarine erosion might have caused this local deepening of the nearshore bathymetry, as was observed elsewhere along the Beaufort Sea coast [*Héquette and Barnes*, 1990; *Brown et al.*, 2003]. Thus, Stokes Point is an example for how place-bound factors, in particular the amount and state of ground ice volume in the coastal zone can substantially alter coastal dynamics. The strong control of local geomorphology on coastal dynamics along the Yukon coast was already observed by *Harper* [1990] and *Solomon* [2005]. However, analyses done by *Lantuit et al.* [2008, 2012b] suggest, that ground ice contents are only weakly correlated with coastal retreat rates, though it seems that the strength of the correlation is very dependent on the local setting.

In summary, spatial variation in coastal dynamics along the Yukon coast at the regional scale seems attributable to larger scale environmental forcing factors such as predominant storm track direction and its interaction with coastline orientation. At the local scale, coastal geomorphology (e.g., ground ice volume and exposure) may play a more important role.

3.5.3 Dynamics of lagoons, barrier islands, and spits (gravel features)

Along the Yukon coast, the highest shoreline dynamics were observed along gravel features. The *beach, barrier island, spit* class has the highest peak-to-peak variability in rates of change (-7.2 m a^{-1} to 5.3 m a^{-1} ; Figure 3.4). Coastal heights in this class do not exceed 2 m and can thaw to a depth of over 1.5 m during summers [Owens and Harper, 1977]. Thus, the sands, gravels and cobbles are reworked by waves during the ice-free season, especially during storms and on a daily basis by longshore currents [Harper, 1990]. During the sea ice freeze-up and break-up seasons, as observed along Komakuk Beach, beaches are exposed to the processes of ice-push, through ice pile-ups and ice ride-ups. This can essentially alter the beach geomorphology and is a source of sediment [Hume and Schalk, 1964; Kovacs, 1983; Harper et al., 1985; Héquette and Barnes, 1990; Reimnitz et al., 1990].

Six out of seven investigated gravel features have their largest extent in the latest measurement from 2011 (Figure 3.6). The increase in erosion since the 1990s likely increases the availability of material for the expansion of coastal gravel features such as barrier spits and barrier islands. For Nunaluk Spit, another possible source of sediment, as suggested by Harper et al. [1985], is by ice-push. During overflights in the years of 2012, 2014 and 2015, berms most likely formed by ice-push were visible at the beach of Nunaluk Spit, supporting the hypothesis raised by Harper [1990]. In contrast, smallest increase or even a decrease in extent of gravel features was measured along the beaches of Clarence Lagoon and Stokes Point Lagoon. In the updrift direction of the longshore drift which is delivering sediments to Clarence Lagoon, coastal erosion considerably decreased after 1972, thus less sediment is being delivered. Along Stokes Point, erosion remarkably intensified after 1994. A possible reason for this is the occurrence of high massive ice contents in the cliffs (Chpt. 3.5.2). Erosion of these cliffs only releases small amounts of sediments. Moreover, a deepening of the nearshore seabed as a consequence of subsea permafrost or massive ice thaw, as is suggested to have happened along Stokes Point, would result in an exposure of the beach to higher wave energy. This causes enhanced sediment mobilization in the upper part of the lagoon and deposition in the down drift direction of the lagoon which is observed towards the south.

The findings suggest that sediment supply along most parts of the Yukon coast increased through time and since the start of the observation period in 1950s is at its highest today.

3.5.4 Expected shoreline changes as a consequence of future climate warming

Further climate warming might lead to changes in the distribution of the five coastal landform classes along the Yukon coast. Sea-level projections for the Yukon coast result in a rise of 0.31 m by 2050 and of 0.76 m by 2100 [Manson and Solomon, 2007]. Together with an already observed higher frequency and severance of storms [Manson and Solomon, 2007], warmer water temperatures and longer sea ice free seasons [Stroeve *et al.*, 2014], these environmental changes have great potential to lead to increases in coastal erosion. Thus, increasing annual losses of the Yukon Territory mainland are likely.

Active tundra cliffs which are fronted by very narrow or no beaches, are exposed to a very energetic local wave regime, which is capable to transport sediments away quickly [Brown *et al.*, 1999]. Broad sections of this coastal setting, like for example along the northern part of Stokes Point or at the tip of Kay Point, already experienced an intensification of erosion within the last 64 years (Figure 3.5) and are particularly prone to experience further wave intensification. Moreover, continuous sea-level rise will change the height at which water will reach the cliff. This might be particularly important along cliffs where sea-level rise will cause water to reach material with different characteristics, like massive ice overlying permafrost, or vice versa, which in turn may alter the mechanism of coastal erosion [Reimnitz *et al.*, 1985; Kobayashi *et al.*, 1999].

Low-lying areas, like *tundra flats* and *inundated tundra* are expected to experience a further intensification of coastal erosion. Absolute sea-level rise in combination with land subsidence due to thaw settlement and isostatic adjustment renders low lying stretches of coast with low backshore elevations especially vulnerable towards coastal erosion and coastal flooding [IPCC, 2014]. This can be for example observed along the section of Workboat Passage (Figure 3.4, Table 3.6). Wetlands, which are included in the *inundated tundra* class, bare important ecosystems along the Yukon coast [Environment Canada, 2015]. Where not constrained by rising backshore elevations, wetlands will migrate inland [Bird, 2009]. Otherwise, shoreline regression will result in coastal squeeze [Bird, 2009].

Intensification in erosion of *tundra cliffs* might enhance sediment supply for the build-up of *beaches, barrier islands and spits*. The extent of these gravel features is increasing continuously since the 1950s. Nevertheless, projections of future flooding potential conducted along a wave sheltered spit at Herschel Island showed that a rise of sea level of only 10 cm will already lead to a submergence of considerable amounts of the gravel spit [Radosavljevic *et al.*, 2015]. Well fed, drift dominated beaches, such as the Nunaluk barrier spits and barrier islands, might benefit from increased sediment supply and extend towards the longshore drift

direction. However, the expected rise in storm severity renders even high gravel features susceptible towards breaching. Many swash dominated beaches, like beaches which are fronting the tundra cliffs, will most likely get narrower or totally disappear, since sea-level rise will lead to a deepening of the nearshore zone and allow larger waves approach closer to shore, resulting in enhanced wave energy transmission to the shore [Bruun, 1988; Woodroffe and Murray-Wallace, 2012].

In summary, further climate change is expected to lead to intensified coastal erosion along already eroding stretches of coast (*active tundra cliffs*) and to the activation of parts of currently stable stretches of coast (*tundra slopes*). Continuous sea-level rise and an increase in storm severity might lead to more frequent coastal flooding and enhanced erosion of low-lying areas (*tundra flats* and *inundated tundra*). An increase of erosion may, in turn, favor the nourishment of *beaches, barrier islands and spits*. This effect might be even detectable today, although volumetric analyses would be needed to assert this with certainty. An acquisition of a highly resolved digital elevation model reaching at least 500 m inland from the shoreline in combination with the setup of a tide gauge along the Yukon coast would significantly increase the ability to detect areas which are highly vulnerable to future sea-level rise and particularly prone to coastal flooding, as well as areas which gain material from enhanced erosion elsewhere. Since coastal erosion mobilizes not only gravel but also smaller sized particles, carbon and nutrients [Dunton *et al.*, 2006; Vonk *et al.*, 2012; Tanski *et al.*, 2017], it is important to further investigate coastal changes along the Yukon coast to get a better understanding of the annual rates and volumes of coastal erosion and their effect on the surrounding environment.

3.6 Conclusions

In this study, shoreline evolution over 64 years (1951 - 2015) along a 210 km length of the Yukon mainland coast was examined. The following conclusions can be drawn:

- 1) The mean rate of change for the whole coast for the 1950s to 2011 amounts to -0.7 m a^{-1} . Even though the mean rate of change stayed approximately the same through time, the total number of transects recording erosion increased through time, indicating a substantial change in the erosion vs. accumulation regime along the coast. Aerial imagery analysis and GPS observations at the key sites indicate that coastal retreat significantly increased since the 1990s along some sites.
- 2) Mean shoreline change rates for the whole coast decrease eastward, being highest at the Yukon-Alaska border with -1.4 m a^{-1} and lowest along Shingle Point with a mean

rate of -0.1 m a^{-1} . Coastal change rates at the regional scale seem to be attributable to the coastal exposure to north-west wind-driven waves and the resulting high water levels.

- 3) The areal extent of the seven main gravel features along the Yukon coast is rising since the 1950s. This might be caused by enhanced sediment availability due to enhanced shoreline retreat. Monitoring of volumetric changes along the coastal zone would enhance the understanding of sediment dynamics.
- 4) The Yukon Territory mainland (excluding gravel features) is losing approximately 10 ha of land each year due to the process of coastal erosion. With the prognosticated rise of sea level to the end of this century, along with further effects of climate warming, it is likely that the yearly territorial losses will increase in the future.
- 5) Sixteen percent of the whole coast have been classified as *inundated tundra* and *tundra flats*. In both classes, the shore is characterized by low backshore elevations and is thus prone to flooding which can be caused by further sea-level rise and by severe storms. Monitoring of the process of ground settlement along some of the subsiding terrains and the installation of a tide gauge along the Yukon coast would enhance the understanding of the processes which are leading to the fast disappearance of these regions and would contribute to a better estimation of impacts of a rising sea level along the Yukon coast in the future.

Acknowledgements

The conduction of field work would not have been possible without the support of the Polar Continental Shelf Project. Logistical support from the Aurora Research Institute in Inuvik and the support from the rangers of the Herschel Island-Qikiqtaruk Territorial Park was greatly appreciated. Donald Forbes, David Frobel, Steven Solomon, Dustin Whalen, Patrick Potter, George Tanski, Samuel Stettner, and Justine Ramage provided valuable help in the field. Atossa Pandazmapoo helped with the geo-coding of the historical aerial imagery. A. Irrgang was financed by the Deutsche Bundesstiftung Umwelt and was part of the Helmholtz Young Investigator Group “COPER” (grant VH-NG-801 to H. Lantuit). G. Grosse and F. Günther were supported by an ERC grant (project number 338335). G. Manson was funded by the Climate Change Geoscience Program of the Earth Science Section of Natural Resources Canada. The DSAS data and coastal landform classification data presented here is available through the PANGAEA data repository [Irrgang *et al.*, 2017]. Readers interested in field survey data may contact A.M. Irrgang.

Context

In the first study, shoreline change retreat for the Yukon coast was shown to have accelerated within the last two decades. This is of particular concern, because the Yukon coast is affected by permafrost, which stores large amounts of carbon. Coastal erosion mobilizes this carbon. In the next chapter, annual fluxes of sediments and soil organic carbon which are triggered by coastal erosion were estimated. Further, the amount of soil organic carbon was quantified, which was sequestered in the sediments of the nearshore zone. Since the Beaufort coast bears higher volumetric ground ice contents than other Arctic coasts [*Lantuit et al.*, 2012b], the calculations of sediment and carbon fluxes were done accounting for ground ice in the sediment column.

Coastal erosion of permafrost soils along the Yukon Coastal Plain and fluxes of organic carbon to the Canadian Beaufort Sea

ABSTRACT

Narrowing uncertainties about carbon cycling is important in the Arctic where rapid environmental changes contribute to enhanced mobilization of carbon. Here we quantify soil organic carbon (SOC) contents of permafrost soils along the Yukon Coastal Plain and determine the annual fluxes from erosion. Different terrain units are assessed based on surficial geology, morphology, and ground ice conditions. To account for the volume of wedge ice and massive ice in a unit, sample SOC contents are reduced by 19% and sediment contents by 16%. The SOC content in a 1 m² column of soil varies according to the height of the bluff, ranging from 30 to 662 kg, with a mean value of 183 kg. Forty-four per cent of the SOC is within the top 1 m of soil and values vary based on surficial materials, ranging from 30 to 53 kg C m⁻³, with a mean of 41 kg. Eighty per cent of the shoreline is retreating with a mean annual rate of change of -0.7 m a⁻¹. This results in a SOC flux per meter of shoreline of 131 kg C m⁻¹ a⁻¹, and a total flux for the entire Yukon coast of 35.0×10⁶ kg C a⁻¹ (0.035 Tg C a⁻¹). The mean flux of sediment per meter of shoreline is 5.3×10³ kg m⁻¹ a⁻¹, with a total flux of 1 801.2×10⁶ kg a⁻¹ (1.801 Tg a⁻¹). Sedimentation rates indicate that approximately 13% of the eroded carbon is sequestered in nearshore sediments, where the overwhelming majority of organic carbon is of terrestrial origin.

A manuscript with equal content is in review in the Journal: *Journal of Geophysical Research: Biogeosciences*.

Couture, N., A.M. Irrgang, W. Pollard, H. Lantuit, and M. Fritz (in review): Coastal erosion of permafrost soils along the Yukon Coastal Plain and fluxes of organic carbon to the Canadian Beaufort Sea. *Journal of Geophysical Research: Biogeosciences*.

4.1 Introduction

It is estimated that 1035 ± 150 Pg (10^{15} g) of soil organic carbon (SOC) are stored in permafrost [Hugelius *et al.*, 2014], which is approximately 20% more carbon than is currently circulating in the atmosphere [Houghton, 2007]. Because permafrost is such an important global carbon sink, quantifying the carbon fluxes which result from its disturbance is crucial for understanding carbon cycling from local to global scales and for refining projections of future climatic changes [Fritz *et al.*, 2017]. Thirty four per cent of the Earth's coasts consist of permafrost [Lantuit *et al.*, 2012b] and these coasts have a mean shoreline change rate of -0.5 m a⁻¹ [Lantuit *et al.*, 2012b], with local coastal retreat rates as high as 30 m a⁻¹ [Wobus *et al.*, 2011]. Consequently, coastal erosion is an important process for mobilizing organic carbon in permafrost regions, releasing an estimated 14.0 Tg (10^{12} g) of particulate organic carbon (POC) to the nearshore zone each year [Wegner *et al.*, 2015]. This carbon flux is comparable to that contributed annually by all Arctic rivers, or to the net methane (CH₄) emissions from terrestrial permafrost [Koven *et al.*, 2011]. Terrestrially-derived organic carbon plays a crucial role in Arctic biogeochemical cycling once released into the nearshore zone, where it can be remineralized in the water column, buried on the shelf, or transported to the deep ocean [Fritz *et al.*, 2017]. Uncertainties remain about the carbon fluxes to and from the system, however, and narrowing those uncertainties is especially critical in the Arctic, where rapid environmental changes due to Arctic amplification [Serreze and Barry, 2011] are likely to increase the cycling of carbon [Schuur *et al.*, 2008; McGuire *et al.*, 2009].

Studies of the overall cycling of organic carbon in the Arctic Ocean have progressed towards elucidating the processes involved and highlighting the knowledge gaps [Stein and Macdonald, 2004; Vetrov and Romankevich, 2004]. On a volume basis, the Arctic Ocean receives higher levels of terrestrially-derived organic matter than any other ocean [Dittmar and Kattner, 2003], with inputs from both riverine and coastal sources [Rachold *et al.*, 2000, 2004b]. A major goal of the Arctic Coastal Dynamics project was to develop circum-Arctic estimates of the coastal contribution of sediment and carbon [Rachold *et al.*, 2005]. The coastal inputs of organic carbon from some regions are well constrained [Rachold *et al.*, 2004b; Jorgenson and Brown, 2005; Streletskaya *et al.*, 2009; Ping *et al.*, 2011], but uncertainty still exists for other areas. For the Canadian Beaufort Sea, inputs are largely dominated by discharge from the Mackenzie River [Macdonald *et al.*, 1998]. However, although several studies have provided estimates of material fluxes to the Beaufort Sea from coastal sources [McDonald and Lewis, 1973; Harper and Penland, 1982; Harper, 1990; Yunker *et al.*, 1990; Hill *et al.*, 1991b; Yunker *et al.*, 1991; Yunker *et al.*, 1993; MacDonald *et*

al., 1998], organic carbon inputs for this region are still not very well defined. Here, we seek to redress that by carrying out a systematic analysis to determine the sediment and carbon contents of soils along the Yukon Coastal Plain and fluxes to the Beaufort Sea.

The long-term mean shoreline change rate along the Yukon coast is -0.7 m a^{-1} , with some parts of the coast having mean shoreline change rates as high as -9 m a^{-1} [Irrgang *et al.*, in review]. This region therefore has the potential to release high amounts of organic matter. In North America, total organic carbon (TOC) contents of permafrost soils have been shown to vary considerably depending on soil type and landcover [Michaelson *et al.*, 1996; Bockheim *et al.*, 1998, 1999, 2003, 2004; Tarnocai, 1998; Tarnocai *et al.*, 2003, 2007, 2009; Bockheim and Hinkel, 2007; Ping *et al.*, 2008; Obu *et al.* 2017b], with mean values between 30 and 60 kg C m^{-3} . Most measurements of TOC in permafrost have been confined to the top 1 m of soil, although some recent studies have examined deeper deposits [Zimov *et al.*, 2006; Bockheim and Hinkel, 2007; Tarnocai *et al.*, 2009; Strauss *et al.*, 2013]. In Arctic soils in general, most soil organic matter is stored in the seasonally unfrozen active layer near the ground surface, so organic matter tends to decrease with depth. However, a considerable amount of organic matter can be transferred into the upper part of permafrost through cryoturbation [Bockheim and Tarnocai, 1998]. Along the Yukon Coastal Plain, measurements of TOC in soils have been conducted at only a few sites [Smith *et al.*, 1989; Tarnocai and Lacelle, 1996; Yunker *et al.*, 1990; Kokelj *et al.*, 2002; Fritz *et al.*, 2012; Obu *et al.*, 2017b], yielding values between 2.9 and 99.2 kg C m^{-3} .

A preliminary estimate of the flux of organic carbon, based on earlier studies of erosion, provided a value of 0.055 Tg a^{-1} (with a maximum of 0.3 Tg a^{-1}) for the entire Canadian Beaufort Sea coast [Macdonald *et al.*, 1998]. However, although that study implicitly accounted for pore ice through the use of soil bulk densities in its calculations, it did not account for other ground ice types, despite the fact that ground ice represents a significant portion of earth materials along the Yukon coast [Couture and Pollard, 2017]. Potential off-shelf transport is especially important along the Yukon coast because, with a width of 40 km and even 10 km in some places, it is very narrow in comparison to other shelves of the Arctic Ocean. Although databases exist of organic carbon in offshore sediments of the Alaska Beaufort Sea [Naidu *et al.*, 2000] and of the Mackenzie Shelf [Macdonald *et al.*, 2004], they include only a few samples from the Yukon coastal area.

Environmental changes in the Arctic such as longer open water seasons [Markus *et al.*, 2009; Stroeve *et al.*, 2014], intensified storms [Manson and Solomon, 2007], warmer air, water and

soil temperatures [AMAP, 2012; Overland *et al.*, 2015; Timmermans and Proshutinsky, 2016] and rising sea-level [Manson and Solomon, 2007] are very likely to further increase coastal erosion [Zhang *et al.*, 2004; Günther *et al.*, 2015] and thus carbon mobilization [Schuur *et al.*, 2008, 2015; Mc Guire *et al.*, 2009]. This trend is already becoming evident, with erosion rates along many parts of the Beaufort Sea coast more than doubling in recent decades [Irrgang *et al.*, in review; Jones *et al.*, 2009a]. In order to contribute to an enhanced understanding of the implications of these changes for carbon cycling in the Arctic, our objectives are, 1) to quantify the annual fluxes of sediments and organic carbon from eroding permafrost along the Yukon coast, ensuring that ground ice volumes at different depths are taken into consideration and, 2) to estimate the amount of terrestrially-derived organic matter being sequestered in shelf sediments in this region of the Beaufort Sea.

4.2 Study Area

The study area is part of the Yukon Coastal Plain, a pediment surface about 280 km long and 10-30 km wide that slopes gently from a series of inland mountain ranges to the Canadian Beaufort Sea (Figure 4.1). It was partially glaciated during the Wisconsinan Glaciation, with the Laurentide Ice Sheet extending just to the west of Herschel Island [Rampton, 1982; Fritz *et al.*, 2012]. This formerly glaciated area is characterized by a mixture of morainic deposits and coarse-grained glaciofluvial material, but low spits and fine-grained lacustrine and fluvial sediments occur as well [Bouchard, 1974; Rampton, 1982]. Cliff heights are diverse, ranging from 2-3 m on the mainland across from Herschel Island to 60 m in the eastern part of the study area. In the unglaciated region to the west of Herschel Island, sediments are of lacustrine or fluvial origin and are mostly fine-grained [Rampton, 1982]. Coastal cliffs heights are more uniform in this western region, rising gently from about 3 m high near the glaciation limit to approximately 6 m near the Yukon-Alaska border [Irrgang *et al.*, in review]. A long barrier spit and barrier island system comprised of sand and gravel beach deposits fronts the deltas of the Malcolm and Firth rivers.

Permafrost is found everywhere throughout the Yukon Coastal Plain except under large lakes and rivers [Rampton, 1982]. The mean annual temperature at Komakuk Beach is -11 °C; July is the warmest month with a mean temperature of 7.8 °C (1971-2000) [Environment Canada, 2016]. Over the last 100 years (from the period 1899-1905 to 1995-2006), mean air temperatures along the Yukon coast have increased by 2.5 °C and permafrost temperatures have increased by 2.6 °C [Burn and Zhang, 2009]. This part of Canada is one of the most ice-rich areas of the Arctic and the permafrost contains high amounts of ground ice in the

form of pore ice and thin lenses, ice wedges, and bodies of massive ice, the latter occurring primarily in the formerly glaciated area. Overall, ground ice accounts for 46% by volume of earth materials in the study area [Couture and Pollard, 2017], but it can range as high as 74% in some coastal segments. The sediments along the Yukon Coastal Plain are also rich in organic material, and a layer up to 3.5 m thick blankets many of the deposits [Rampton, 1982]. Much of this organic matter accumulated in thermokarst basins, which were formed by melting of ground ice; the accumulation is further promoted by poor drainage and the low regional slope gradients, particularly in the western part of the Yukon Coastal Plain [Rampton, 1982; Fritz *et al.*, 2012]. A considerable amount of organic material along the Yukon Coastal Plain is also found at depth in pre-glaciated floodplain and deltaic sediments, and where surface organic matter appears to have been buried by glacial deformation [Rampton, 1982]. Current active layers along the Yukon coast range in depth from approximately 0.3 to 1.5 m [Burn, 1997; Kokelj *et al.*, 2002; Fritz *et al.*, 2012]. However, during the Holocene warm period 9000 BP, active layer thicknesses in the region were up to 2.5 times present-day ones [Burn, 1997; Kokelj *et al.*, 2002; Fritz *et al.*, 2012], so organic material that originated in the paleo-active layer is found in that depth range.

Because of the high ground ice contents, thermo-erosional processes play an important role in shaping the landscape along the Yukon Coastal Plain. These processes include the development of retrogressive thaw slumps [Wolfe *et al.*, 2001; Lantuit and Pollard, 2005, 2008; Ramage *et al.*, 2017] and cliff collapse due to wave notching [Hoque and Pollard, 2009, 2015]. Sea ice is present in the region from early October to late June [Galley *et al.*, 2016], so coastal erosion and the resulting mobilization of sediment and carbon is concentrated in those 3.5 months. The most common wind directions are from the southeast and the northwest, though most effective storms come from the north-west and peak in October [Hill *et al.*, 1991b; Hudak and Young, 2002; Atkinson, 2005]. Sea level rise along the Yukon coast is on average 3.5 ± 1.1 mm [Manson and Solomon, 2007]. Astronomical tides are semidiurnal and in the micro-tidal range (0.3-0.5 m) [H  quette *et al.*, 1995].

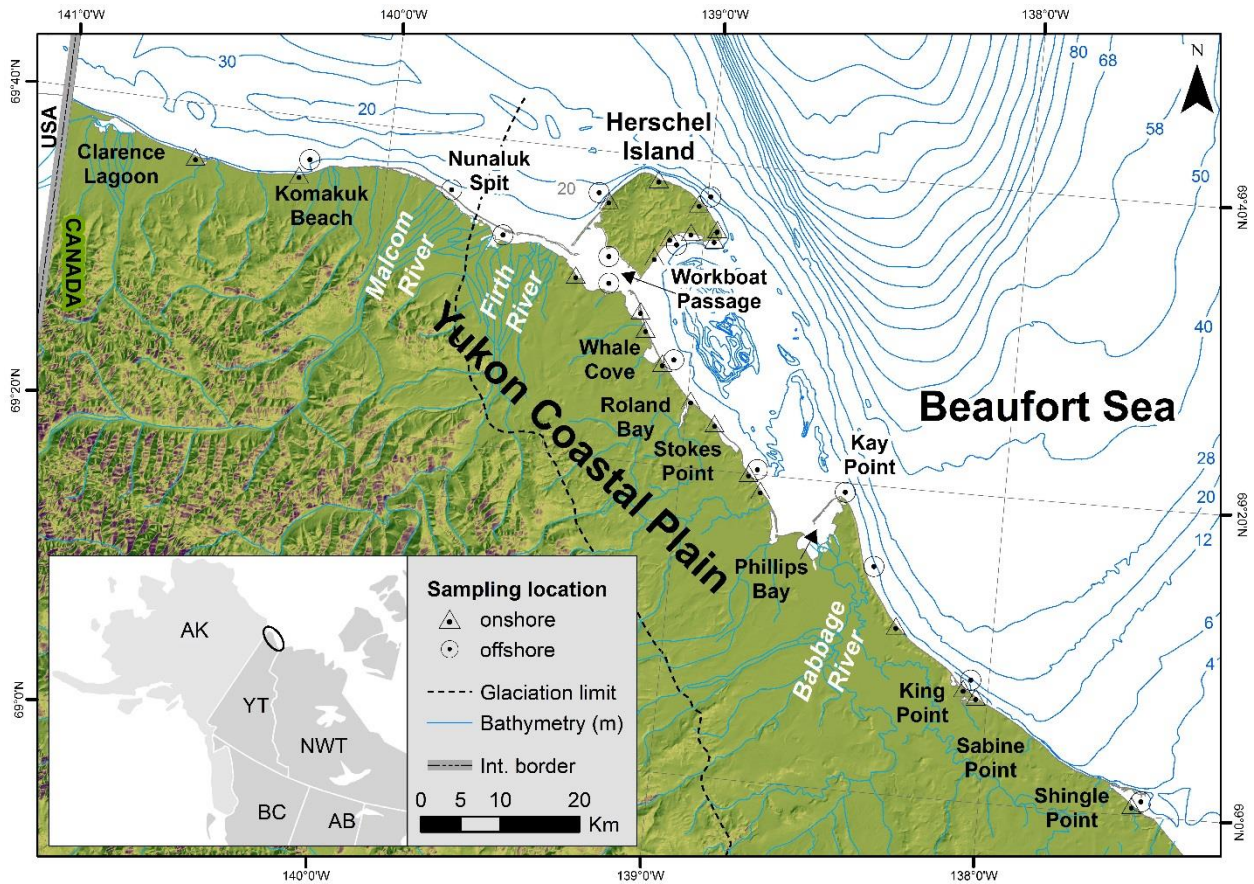


Figure 4.1: Map of the study area along the Yukon Coastal Plain, Canada. Samples of soil organic carbon (SOC) were collected at 22 onshore sites (Δ) and 14 offshore (O) sites. Bathymetry information is based on Canadian Hydrographic Survey Navigational Charts improved by local surveys performed in the 1980s [Thompson, 1994]. Basemap: 30m Yukon DEM, interpolated from the digital 1:50 000 Canadian Topographic Database [Yukon Department of Environment, 2016].

4.3 Methods

The Yukon coast was segmented into 44 different terrain units based on landforms, surficial material, permafrost conditions, and coastal processes, since each of these factors influences the amount and flux of soil organic carbon. For each of the terrain units along the Yukon Coastal Plain, the flux of soil organic carbon (SOC) was calculated from the measured total organic carbon (TOC) contents and the long-term rates of change for each terrain unit [Irrgang *et al.*, in review]. Analyses of seabed sediments allowed a quantification of the terrestrially-derived SOC being buried in the nearshore.

4.3.1 Sample collection and laboratory analyses

Onshore soil sampling was carried out at 22 locations along the coast in August 2004, 2005, 2006 and 2009 (Figure 4.1). Locations were selected to represent terrain units from different parts of the coast. Sampling west of Herschel Island was restricted by ice conditions in 2005,

and coarse-grained units are not well represented due to difficulties associated with coring in gravelly and pebbly material. Samples were collected from the side of soil pits in the unfrozen active layer. In the underlying permafrost, they were obtained using a modified CRREL corer (7.5 cm i.d.) or, in a limited number of cases (7% of samples), using a hammer or an axe to cut samples (approximately 1000 cm³) from the face of natural exposures. Active layer thicknesses ranged from 0.25 to 0.90 m. Cores began at the base of the active layer and penetrated to a maximum of 2.04 m below the ground surface. Natural exposures were sampled to a depth of 5.8 m from the surface. At two sites, samples were taken from the base of bluffs and are assumed to be representative of the entire lower portion of the bluff. The frozen cores were sub-sampled every 5 cm or where there was a distinct change in material composition. Samples were weighed in the field, then freeze-dried and re-weighed in the laboratory to determine ice content and bulk densities (based on frozen core volume or measurement of the sample block).

Offshore samples were obtained at 14 locations in July 2006 (Figure 4.1). A Ponar grab sampler was used to obtain samples from bottom sediments along profiles perpendicular to the shore. Sample size varied due to differences in substrate and water depths, but averaged about 1000 cm³. Samples were taken at distances of approximately 30 m, 50 m, 100 m, 250 m and 500 m from shore to assess how the composition of the organic carbon in the sediments changes.

Dried samples were ground to homogenize them, and then total carbon (TC), total organic carbon (TOC), and total nitrogen (TN) were measured using an Elementar Vario EL III elemental analyzer. Prior to TOC measurements, samples were treated with 10% HCl to remove carbonates. Samples were measured twice and their mean value is reported. Stable carbon isotopes were measured on carbonate-free samples using a Finnigan MAT Delta-S mass spectrometer equipped with a FLASH elemental analyzer and a CONFLO III gas mixing system. The $\delta^{13}\text{C}_{\text{org}}$ of the sample is reported in ‰ relative to VPDB. The standard deviation (1Φ) is generally better than $\delta^{13}\text{C} = \pm 0.15\text{‰}$.

4.3.2 Soil organic carbon determinations

For each terrain unit, the onshore SOC measurements were used to calculate the mass of soil organic carbon (M_c) for a 1 m² soil column equal in depth to the mean bluff height. Heights were obtained from 2013 LiDAR data (1.0 m ground resolution and vertical accuracy of 0.15 ± 0.1 m) [Kohnert *et al.*, 2014; Obu, *et al.*, 2016b; 2017a] and, using the zonal statistics tool in ESRI ArcMap, a mean value for each terrain unit was established for an area 200 m

inland of a shoreline which was digitized from 2011 satellite images [Digital Globe, 2014, 2016]. For terrain units comprised of gravel features such as barrier islands and spits, the mean terrain height was set to 1 m, except for one (Stokes Point) which was assigned a height of 1.9 m based on survey data from Forbes [1997].

Where more than one sampling site occurred in a terrain unit, TOC values of the same depth were averaged before calculating M_C . For terrain units that did not contain a sampling site, values were extrapolated from areas with similar surficial geology and permafrost conditions. A column's M_C is given by:

$$M_C = \sum_{j=1}^n \rho_b \times h \times \%OC \quad (4.1)$$

where M_C is the mass of SOC in a soil column (kg), ρ_b is the dry bulk density based on the original frozen volume (kg m^{-3}), h is the thickness of a soil layer (m), and %OC is the percentage of TOC by weight in a unit layer. The layers are summed to arrive at a value for the entire soil column. A similar procedure is followed to obtain the mass of the mineral portion of the sediment:

$$M_S = \sum_{j=1}^n (\rho_b \times h) - M_C \quad , \quad (4.2)$$

where M_S is the mass of mineral sediment (kg).

For M_C , the lowermost soil layer, which generally comprises the largest percentage of the bluff, was assigned the lowest measured value for organic carbon. In cases of high bluffs where this value did not appear representative of the lowermost layer, a default value of 0.792 TOC (%wt) was assigned. This was one of the lowest values found in the study and came from a sample at the base of the highest cliff in the study area. Where no surface layer sample was available, a 10 cm-thick organic layer was assumed, with a TOC content of 25%. These are conservative estimates based on horizon data reported by Michaelson et al. [1996] and Bockheim et al. [1999, 2003]. Sand and gravel beach deposits were assigned a TOC value of 1.8% based on measurements by Smith et al. [1989] and Lawrence et al. [1984]. For grab samples that had no volume measurements (9% of samples), bulk density was estimated from gravimetric ice contents according to the following equation:

$$\Delta_b = \frac{\text{mass of sediment}}{\text{volume of ice} + \text{volume of sediment}} = \frac{100}{\left(\frac{\theta_i}{\rho_i}\right) + \left(\frac{100}{\rho_p}\right)} \quad , \quad (4.3)$$

where θ_i is the gravimetric ice content of the sample (%wt) and the mass of the sediment is therefore assumed to be 100 g, ρ_i is the bulk density of ice (assumed to be 0.917 g cm^{-3}), and

ρ_p is the particle density of the sediment (assumed to be 2.6 g cm^{-3}). There was a strong correlation ($R^2 = 0.92$) when values estimated using this method were compared to measured values (Figure 4.2).

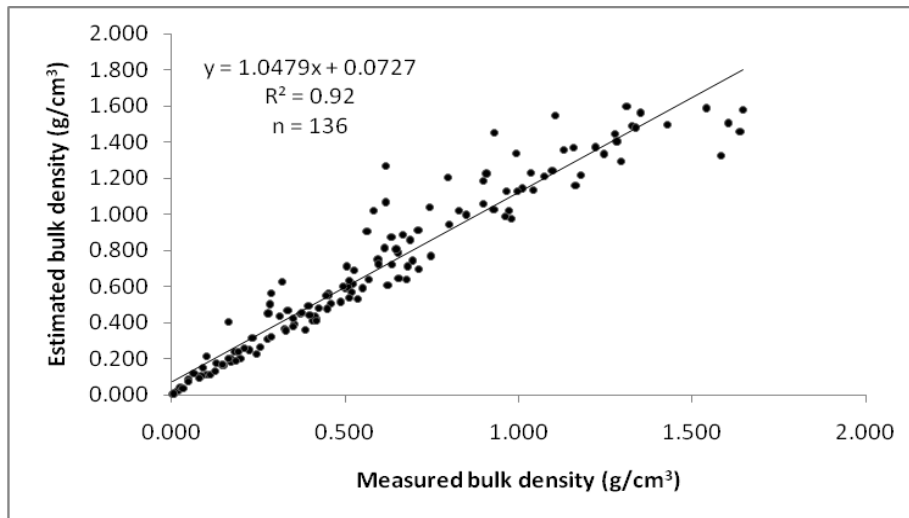


Figure 4.3: Correlation between measured bulk densities and bulk densities estimated from gravimetric ice contents.

Where gravimetric ice contents were not available (35% of samples), another method was used based on several studies that showed a significant relationship ($R^2 = 0.823$) between organic carbon concentrations and bulk densities [Bockheim *et al.*, 1998, 2003]. In those cases, bulk density was estimated according to the following empirically derived equation [Bockheim *et al.*, 1998]:

$$\Delta_b = 1.374 (10^{-0.026x}) \quad , \quad (4.4)$$

where x is the TOC (% wt).

All SOC values were corrected to account for the volume occupied by wedge ice and massive ground ice in each layer within the column. Percentages of these ice types for each terrain unit are given by Couture [2010] and Couture and Pollard [2015b]. Corrections were not applied for pore ice and thin lenses of segregated ice, since it was already accounted for by the use of dry bulk density in the mass calculations.

4.3.3 Flux of organic soil carbon and sediments

The following equation was used to calculate the annual SOC and sediment fluxes from coastal erosion for an entire terrain unit:

$$F = A \left(\frac{M}{1000} \right) , \quad (4.5)$$

where F is the annual flux of SOC or sediment from the terrain unit (10^3kg a^{-1}), A is the mean annual area eroded per terrain unit (m^2), and M is the total mass of material per soil column as defined above (Equations 4.1 and 4.2).

For the determination of flux of SOC and sediment per meter of coast, mean annual rates of change for 35 of the terrain units were calculated for the period 1953-2011 [Irrgang *et al.*, in review]. For the six terrain units on Herschel Island, mean annual rates of change were calculated following the same method, but for the period 1975-2011. Irrgang *et al.* [in review] were not able to determine rates of change for three of the terrain units (Running River, Kay Point Spit, and Malcolm River fan with barrier islands), so rates of change from Harper *et al.* [1985] were used. The mean rates of change were then multiplied by M_C and M_S in a 1m^2 column to obtain annual fluxes per meter of coast for SOC and sediment, respectively. In two of the terrain units (Shingle Point E and Stokes Point SE), mean annual rates of change were positive, indicating accumulation rather than erosion, but there was nevertheless an overall loss of sediment over the time period examined. For those two terrain units, the fluxes per meter of coast were therefore obtained by dividing the total annual flux from the unit by the shoreline length of the terrain unit.

4.3.4 Fate of the eroded soil organic carbon

In order to establish how much of SOC from the Yukon Coastal Plain is being sequestered in nearshore sediments, two bulk identifiers were examined in the seabed sediments: stable carbon isotopes ($\delta^{13}\text{C}_{\text{org}}$) and organic carbon/total nitrogen (TOC/N) ratios. The amount of terrigenous organic carbon (TerrOC) in the bottom samples was determined from a mixing model that used the following equation, which assumes linear mixing between the terrigenous and marine sources of organic matter:

$$\text{TerrOC} = 100 \left(\frac{\delta^{13}\text{C}_{\text{sample}} - \delta^{13}\text{C}_{\text{marine}}}{\delta^{13}\text{C}_{\text{terrigenous}} - \delta^{13}\text{C}_{\text{marine}}} \right) . \quad (4.6)$$

For the terrigenous end-member in Equation 4.6, $\delta^{13}\text{C}_{\text{org}}$ was measured directly in the onshore samples. The marine end-member can be quite variable in the Arctic due to phytoplankton and contributions from sea-ice algae [Stein and Macdonald, 2004 and references therein]. Here, we use a value of -20.75‰ , as this is the mean of the one proposed by Naidu *et al.* [2000] (-24‰) and that used by Belicka and Harvey [2009] (-17.5‰). The use of the TOC/N ratio helps to reduce uncertainty associated with the variability of the marine end-member.

4.4 Results

Of the 44 terrain units in the study area, TOC samples were collected directly from 17 terrain units. Results were extrapolated to a further 16 terrain units with similar characteristics, and in some cases, supplemented with stratigraphic information from previously published sources. For the marine units (i.e., beaches and spits) which we were unable to sample, TOC values reported in the literature were used.

4.4.1 Ground Ice

As noted earlier, pore ice and thin lenses of ground ice are accounted for in SOC calculations by the use of dry bulk densities, but other types of ground ice need to be considered. The amount of wedge ice decreases with depth and ranges from a high of 53% of soil volume to less than 1%. Massive ice, although not present everywhere, accounted for between 52% and 97% of the volume in soil layers where it did occur. Applying corrections for the volume taken up by wedge ice and massive ice reduces overall SOC values by a mean of 19%, and sediment values by 16%. However, in terrain units with a high proportion of ground ice, reductions can be as high as 43% for SOC and 46% for sediment. This underscores the importance of properly identifying and quantifying massive ice bodies in permafrost to accurately quantify carbon stocks and fluxes. Table 4.1 shows the specific reductions for each of the terrain units that contained wedge ice or massive ice.

4.4.2 Organic carbon contents

The SOC and sediment contents and fluxes for all units (corrected to account for ground ice) are shown in Table 4.2. Across all units, the mean SOC content in a 1 m² soil column is 183 kg. Values range from 30 to 662 kg C m⁻² and generally increase with bluff height, as the volume under consideration increases. Within the top 1 m, the mean value is 41 ± 14 kg C m⁻³. Mean values varied based on surficial materials and were highest in fluvial deposits (53 ± 15 kg C m⁻³), followed by lacustrine (47 ± 13 kg C m⁻³), glaciofluvial (44 ± 17 kg C m⁻³), morainal (40 ± 13 kg C m⁻³), and finally marine (30 ± 3 kg C m⁻³). Analysis of variance (ANOVA) shows significant differences based on material type, but further testing (Tukey-Kramer HSD) reveals that only the marine unit shows a significant difference from the fluvial and the lacustrine groups (Figure 4.3). On average, the top meter contains 43.8 ± 33.0% of the organic carbon in the entire soil column.

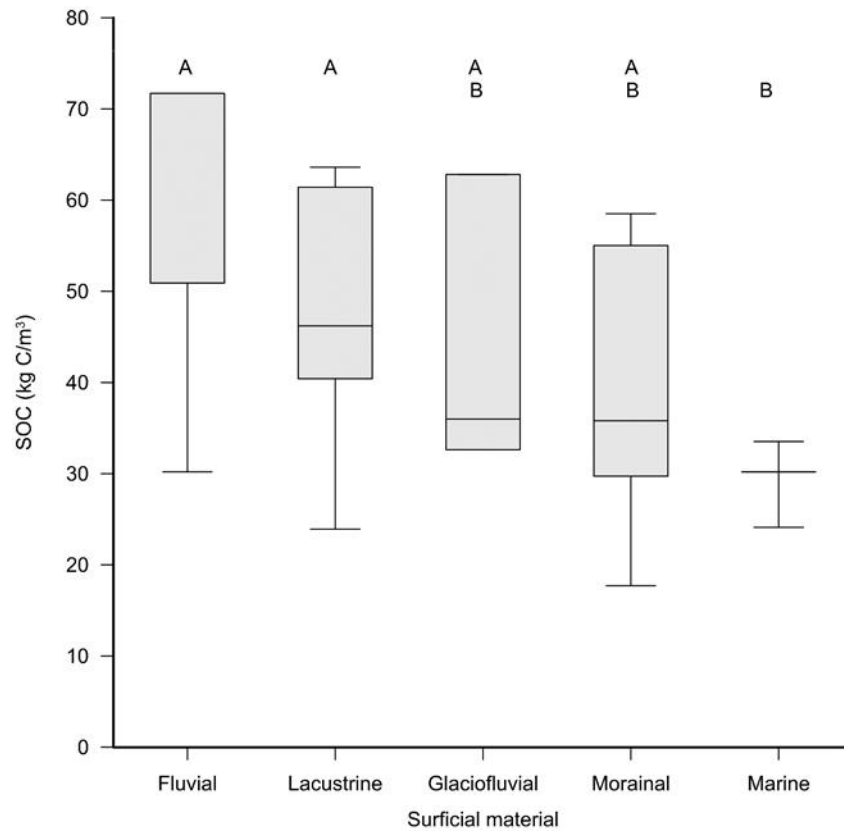


Figure 4.3: Soil organic carbon (SOC) density in the top 1 m for terrain units with different surficial geologies. The line in the middle of boxes represents the median, with lower and upper parts of the box representing 25% and 75% of the distribution, while the lower and upper whiskers represent the minimum and maximum of the distribution. Materials not sharing the same letter above the box plots are significantly different from each other based on the Tukey-Kramer HSD comparison of means ($p < 0.05$).

Table 4.1: Reduction in values of soil organic carbon and sediment due to the presence of ground ice. Note: Corrections are needed because volumes of wedge ice and massive ice were determined for the overall terrain unit, so are not accounted for within individual samples. The volume of each ice type was calculated for every sampled layer of soil and a correction applied to the measured values of SOC and sediment. The results shown here are the summed values for all layers within a 1 m² soil column.

Terrain unit	Soil organic carbon (SOC)			Mineral sediment		
	Before	After	Reduction	Before	After	Reduction
	correction	correction		correction	correction	
(kg)	(kg)	(%)	(kg)	(kg)	(%)	
Running River	578	560	3	24559	24218	1
Shingle Point E	249	212	15	16342	15169	7
Shingle Point W	443	252	43	25008	21158	15
Sabine Point E	514	321	38	6996	5566	20
Sabine Point	807	662	18	21819	12724	42
Sabine Point W	596	566	5	8544	8247	3
King Point SE	169	111	35	12680	6823	46
King Point	308	236	24	2644	2023	23
King Point NW	424	366	14	41411	34787	16
Kay Point SE	467	402	14	28673	26109	9
Kay Point	275	216	21	8890	7905	11
Phillips Bay	141	125	11	2837	2699	5
Phillips Bay NW	316	245	22	17848	13748	23
Stokes Point SE	195	161	17	6539	6352	3
Stokes Point West	301	240	20	15343	12165	21
Roland Bay East	221	210	5	10267	9825	4
Roland Bay W	203	150	26	9123	6541	28
Roland Bay NW	152	124	18	1749	1486	15
Whale Cove E	130	96	26	7579	5486	28
Whale Cove W	53	45	15	725	626	14
Workboat Passage E	68	50	26	1142	861	25
Workboat Passage W	191	147	23	2831	2188	23
Herschel Island S	157	138	12	13940	12392	11
Herschel Island E	486	312	36	25594	17422	32
Herschel Island N	401	336	16	36894	32206	13
Herschel Island W	553	444	20	33830	26595	21
Malcolm River fan	71	67	6	2058	1829	11
Komakuk Beach	187	176	6	3397	3279	3
Komakuk W1	197	140	29	3940	3332	15
Komakuk W2	233	207	11	6048	5601	7
Clarence Lagoon E	78	73	5	2421	2189	10
Clarence Lagoon W	240	138	43	6034	5297	12
Mean	294	235	19	12741	10526	16
Minimum	53	45	3	725	626	1
Maximum	807	662	43	41411	34787	46

Table 4.2: Terrain unit characteristics and material fluxes. Note: The values for the mass of soil organic carbon (M_C) and mineral sediment (M_S) shown here have been corrected for the presence of ground ice.

Terrain unit	Bluff height (m)	Change rate ($m\ yr^{-1}$)	Mean annual eroded area ($m^2\ yr^{-1}$)	Soil organic carbon (SOC)					Mineral sediment			
				M_C in 1 m^2 column (kg)	M_C in top 1 m (kg)	M_C in $M_C > 1m$ (kg)	C in top m (%)	M_C flux per m of coast ($kg\ yr^{-1}$)	M_C flux from unit ($10^3\ kg\ yr^{-1}$)	M_S in 1 m^2 column ($10^3\ kg$)	M_S flux per m of coast ($10^2\ kg\ yr^{-1}$)	M_S flux from unit ($10^3\ kg\ yr^{-1}$)
1. Running River	22.6	-0.7	2827	560	59	501	11	392	1583	24.2	17.0	68463
2. Shingle Point E	13.7	0.2	3103	212	34	178	16	40	658	15.2	0.0	47070
3. Shingle Point W	21.1	-0.2	1995	252	35	217	14	50	503	21.2	4.2	42211
4. Sabine Point E	19.0	-0.4	894	321	46	275	14	114	287	5.6	2.0	4976
5. Sabine Point	20.6	-0.8	2000	662	59	604	9	549	1324	12.7	10.6	25448
6. Sabine Point W	20.6	-0.7	1958	566	46	519	8	406	1108	8.2	5.9	16148
7. King Point SE	10.2	-1.1	4057	111	31	80	28	117	449	6.8	7.2	27682
8. King Point	7.4	-0.6	945	236	40	195	17	136	223	2.0	1.2	1912
9. King Point Lagoon	1.0	-0.3	598	30	30	0	100	9	18	1.6	0.5	984
10. King Point NW	32.7	-0.2	686	366	40	326	11	78	251	34.8	7.4	23864
11. Kay Point SE	26.1	-0.2	3863	402	29	373	7	83	1554	26.1	5.4	100860
12. Kay Point	8.5	-2.3	5972	216	63	153	29	496	1290	7.9	18.2	47210
13. Kay Point Spit	1.0	0.0	0	30	30	0	100	0	0	1.6	0.0	0
14. Babbage River Delta	3.2	-1.0	12184	159	72	88	45	152	1942	2.7	2.6	32974
15. Phillips Bay	4.7	-0.6	6545	125	47	78	38	81	815	2.7	1.7	17666
16. Phillips Bay W	1.0	-0.5	3154	34	34	0	100	17	106	1.6	0.8	5177
17. Phillips Bay NW	13.8	-0.4	1011	245	28	217	11	92	248	13.7	5.2	13899
18. Stokes Point SE	8.3	0.5	408	161	42	120	26	16	66	6.4	0.0	2592
19. Stokes Point	1.9	-3.6	16989	57	30	27	53	204	410	3.1	11.1	22356
20. Stokes Point W	12.5	-0.9	2556	240	57	183	24	212	613	12.2	10.8	31094
21. Roland Bay E	8.4	-0.7	1733	210	24	186	11	157	364	9.8	7.4	17026
22. Roland Bay W	8.4	-0.4	1209	150	55	95	37	67	181	6.5	2.9	7908
23. Roland Bay NW	5.9	-0.3	909	124	43	81	35	41	113	1.5	0.5	1351

Terrain unit	Bluff height (m)	Change rate (m yr ⁻¹)	Mean annual eroded area (m ² yr ⁻¹)	Soil organic carbon (SOC)						Mineral sediment		
				M _c in 1 m ² column (kg)	M _c in top 1 m (kg)	M _c > 1m (kg)	C in top m (%)	M _c flux per m of coast (kg yr ⁻¹)	M _c flux from unit (10 ³ kg yr ⁻¹)	M _s in 1 m ² column (10 ³ kg)	M _s flux per m of coast (10 ³ kg yr ⁻¹)	M _s flux from unit (10 ³ kg yr ⁻¹)
24. Whale Cove E	8.2	-0.2	150	96	18	78	18	17	14	5.5	1.0	823
25. Whale Cove	1.0	-0.5	1384	30	30	0	100	14	42	1.6	0.7	2277
26. Whale Cove W	1.7	-1.0	3685	45	36	9	79	45	167	0.6	0.6	2306
27. Catton Point	1.4	-0.3	2156	42	30	12	72	12	91	2.3	0.7	4965
28. Workboat Passage E	2.3	-0.4	4284	50	33	18	65	19	215	0.9	0.3	3688
29. Workboat Passage W	6.4	-0.5	857	147	42	105	28	72	126	2.2	1.1	1875
30. Herschel S	11.0	-0.3	4604	138	36	102	26	0	636	12.4	3.7	57055
31. Herschel E	21.8	-0.4	4365	312	34	278	11	125	1360	17.4	7.0	76048
32. Simpson Point	1.0	-0.5	2322	30	30	0	100	15	70	1.6	0.8	3819
33. Herschel N	36.0	-1.2	21261	336	30	306	9	403	7138	32.2	38.6	684737
34. Herschel W	27.7	-0.9	6064	444	55	389	12	400	2695	26.6	23.9	161271
35. Avadtek Spit	1.2	-0.7	5283	36	30	6	83	25	191	2.0	1.4	10428
36. Nunakuk Spit	1.0	-1.2	27180	30	24	6	80	36	819	1.6	2.0	44707
37. Malcolm River Fan with barrier islands	1.0	0.0	0	30	30	0	100	0	0	1.6	0.0	0
38. Malcolm River Fan	1.9	-0.8	7211	67	51	16	76	54	481	1.8	1.5	13189
39. Komakuk Beach	6.2	-1.3	17377	176	63	113	36	236	3058	3.3	4.4	56974
40. Komakuk W1	6.8	-1.6	2894	140	64	76	45	223	405	3.3	5.3	9642
41. Komakuk W2	6.7	-1.1	8982	207	61	146	30	237	1859	5.6	6.4	50311
42. Clarence Lagoon E	2.2	-0.9	891	73	51	22	69	65	65	2.2	1.9	1950
43. Clarence Lagoon	1.0	-0.8	2738	30	30	0	100	25	83	1.6	1.4	4504
44. Clarence Lagoon W	7.1	-1.6	9779	138	61	77	44	215	1347	5.3	8.3	51798
Mean	9.7	-0.7	4751.4	183	41	142	44	131	795	8.2	5.3	40937
Minimum	1.0	-3.6	0.0	30	18	0	7	0	0	0.6	0.0	0
Maximum	36.0	0.5	27180.0	662	72	604	100	549	7138	34.8	38.6	684737
Total flux (10³ kg yr⁻¹)									34967			1801233

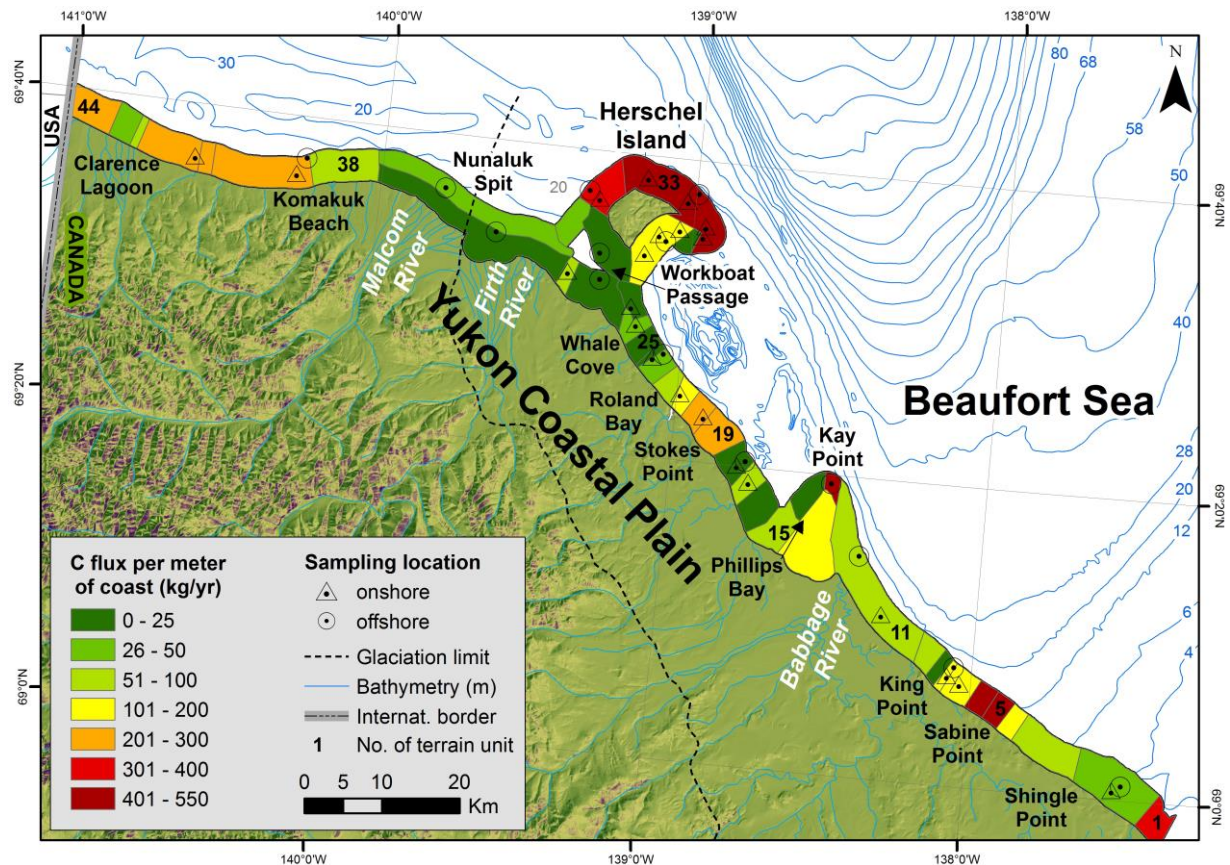


Figure 4.4: Annual flux of soil organic carbon per meter of coastline. Details on terrain unit characteristics are listed in Table 4.2.

4.4.3 Material fluxes

The mean annual rate of change for the entire Yukon Coastal Plain is 0.7 m a^{-1} . Forty of the terrain units (comprising 80% of the shoreline) are undergoing erosion, two are accreting (6%), and two are stable (13%). Although fluxes from individual terrain units are provided in Table 2, it is the flux per meter of shoreline that is important for comparison between different parts of the coast, and between the Yukon coast and other regions in the circum-Arctic. The mean flux of SOC is $131 \text{ kg C m}^{-1} \text{ a}^{-1}$, with a maximum of $549 \text{ kg C m}^{-1} \text{ a}^{-1}$ (Table 4.2, Figure 4.4). This results in a total flux of organic carbon from the Yukon coast of $35.0 \times 10^6 \text{ kg a}^{-1}$ (0.035 Tg a^{-1}). The mean flux of sediment per meter of shoreline is $5.3 \times 10^3 \text{ kg m}^{-1} \text{ a}^{-1}$, with a maximum value of $38.6 \times 10^3 \text{ kg m}^{-1} \text{ a}^{-1}$, resulting in a total flux of sediment of $1.801 \times 10^6 \text{ kg a}^{-1}$ (1.801 Tg a^{-1}).

4.4.3.1 Organic carbon in nearshore sediments

Analysis of 50 onshore samples taken from different terrain units gives a mean $\delta^{13}\text{C}_{\text{org}}$ value of $-27.12 \pm 0.77\text{‰}$. This is the value used as the terrigenous end-member in the mixing model to determine the percentage of terrigenous organic carbon in the nearshore sediments.

Samples of nearshore sediments were taken up to 500 m from shore and at water depths ranging from 0.9 to 14.5 m. Twenty-two of the nearshore samples were analyzed for $\delta^{13}\text{C}_{\text{org}} \text{‰}$. Table 3 shows the results from isotopic analyses and from the mixing model. Three samples should be viewed with caution because they showed very little decomposition visually and appeared to consist almost entirely of terrestrial organic matter, a fact corroborated by their low $\delta^{13}\text{C}$ values and simultaneously high C/N ratios (Figure 4.5); these were omitted from further calculations. Values of $\delta^{13}\text{C}$ for the nearshore samples ranged from -27.00 to -26.10‰ and C/N ratios ranged from 11.3 to 25.9. Based on results from the isotopic mixing model, the organic carbon in the nearshore sediments is overwhelmingly terrestrial, with a mean terrigenous organic carbon content of 91.3% and a marine content of 8.7%.

Table 4.3: Properties of Nearshore Sediment Samples. Note: Samples marked with * were omitted from calculation of means, maxima and minima because of unusually high terrigenous content.

Sample	Distance from shore (m)	Water depth (m)	TOC (%)	C/N ratio	$\delta^{13}\text{C}_{\text{org}}$ (‰ VPDB)	Terrigenous OC (%)
01-06	500	10.6	0.630	20.3	-26.86	95.9
03-06	100	3.7	0.979	11.9	-26.10	84.0
05-06	30	1.9	1.013	11.3	-26.21	85.7
06-06	500	14.5	0.829	18.0	-26.44	89.4
13-06	110	2.3	1.384	16.2	-26.91	96.7
15-06	500	2.7	1.375	20.1	-26.59	91.7
20-06	500	7.6	1.175	15.3	-27.00	98.1
27-06	250	1.2	1.014 *	18.6 *	-27.07 *	99.2 *
29-06	50	3.0	0.661 *	16.3 *	-27.19 *	> 100 *
30-06	30	2.0	15.317 *	45.1 *	-27.86 *	> 100 *
33-06	500	5.0	0.275	12.2	-26.69	93.2
38-06	30	3.8	0.861	13.4	-26.99	98.0
42-06	500	9.6	7.877	25.9	-26.72	93.7
45-06	250	5.2	1.142	14.0	-26.44	89.4
46-06	500	8.0	1.074	11.5	-26.52	90.5
47-06	30	2.3	1.853	13.5	-26.67	93.0
49-06	100	2.3	1.809	13.4	-26.37	88.3
51-06	500	2.5	1.944	13.1	-26.49	90.1
55-06	120	2.9	2.218	14.5	-26.58	91.4
57-06	500	2.7	1.435	15.0	-26.58	91.5
58-06	30	0.9	1.269	14.0	-26.31	87.3
62-06	500	6.7	0.801	12.4	-26.22	85.8
Mean			1.6	15.1	-26.6	91.3
Minimum		0.9	0.3	11.3	-27.0	84.0
Maximum		14.5	7.9	25.9	-26.1	98.1

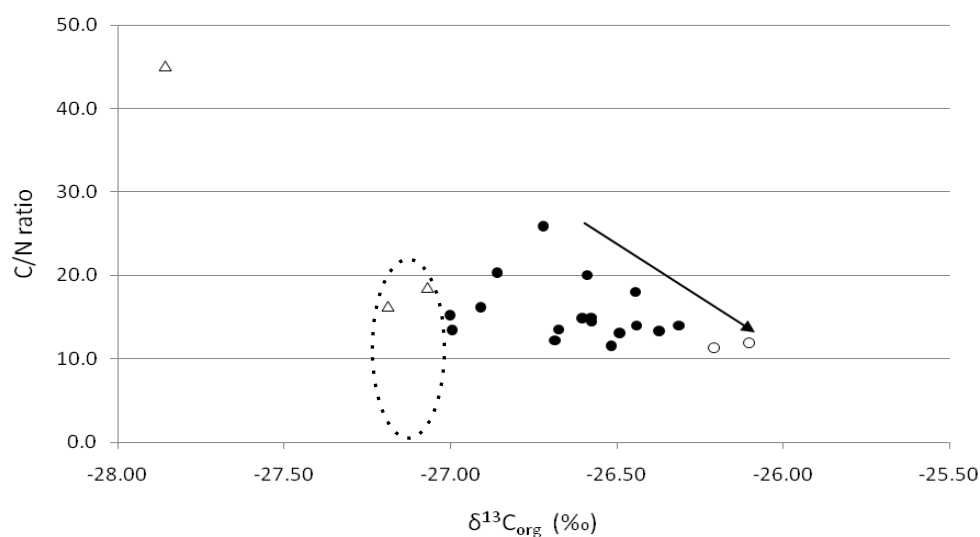


Figure 4.5: A Plot displaying the relationship between C/N ratios and $\delta^{13}\text{C}_{\text{org}}$ for seabed samples from the nearshore zone along the Yukon Coastal Plain. Open triangles represent three samples that showed very little decomposition and consist almost entirely of terrestrial organic matter. The dashed circle shows where a typical terrigenous end-member would be found, while the arrow indicates increasing marine organic matter content. The open circles are samples with the highest marine content, taken north of Herschel Island.

4.5 Discussion

4.5.1 Ground Ice

As was seen from the reduction of SOC and sediment values in Table 4.1, failing to account for ground ice can result in significant overestimates of the total amount of material contained within a terrain unit and its annual flux. Although wedge ice has been shown to account for 8% of frozen materials along the Yukon Coastal Plain [Couture & Pollard, 2017], it comprises 23% of the upper 7 m of soil. It is therefore not just the overall volume of ground ice that is important, but the stratigraphic relationship between wedge ice and organic carbon, in particular, since they both vary with depth [Couture & Pollard, 2017; Ulrich *et al.*, 2014]. Some studies, while acknowledging the importance of ground ice, do not include it in their calculations of material fluxes [i.e., Harper & Penland, 1982; Hill *et al.*, 1991]. Others consider ground ice volumes in varying degrees of detail. Our values for wedge ice are approximately twice those of Jorgenson and Brown (2005) who use a slightly cruder ice wedge geometry in their calculations of SOC contents for the Alaska Beaufort Sea coast. Brown *et al.* [2003] use a mean value of 50% for all ground ice types along the Alaskan Beaufort Sea. Rachold *et al.* [2000] use different values for different coastal types along the Laptev Sea; some are simple means, while other are based on the various types of ground ice. Dallimore *et al.* [1996] provide an in-depth evaluation of all types of ice in their calculations

of sediments fluxes from northern Richards Island in the Mackenzie Delta. In some cases, the importance of a detailed investigation depends on the geomorphology of the coast. For instance, Brown et al.'s [2003] use of a mean ground ice value of 50% does not have a significant impact on potential stratigraphic differences because the mean elevation of bluffs they are looking at is only 2.5 m, so changes in ice content or in SOC content with depth are not as important. Considering the varied elevations along the Yukon coast and the wide range of ground ice volumes with depth, our detailed approach is warranted.

4.5.2 Organic carbon contents

Given the sparseness of data on SOC for the Yukon Coastal Plain, this study contributes to a more thorough estimate of C stores in a region where carbon cycling is likely to increase with accelerating coastal erosion [*Obu, et al., 2016b; Radosavljevic et al., 2016; Irrgang et al., in review*]. In addition to nearly tripling the number of pedons for which data is available, the results provide important information about deeper stores of organic carbon. The overall mean SOC value reported here (183 kg C m^{-2}) is approximately 3 to 6 times higher than many previous estimates of TOC primarily because this study examines the entire soil column, whereas previous ones focused on the upper portions. Our values are much closer to those reported by Hugelius et al. [2014] who look at depths up to 3 m and found organic carbon contents of 150 kg C m^{-2} in the Arctic coastal lowlands. When comparing the top 1 m of soil, our mean value of 41 kg C m^{-3} is consistent with the value reported by Bockheim et al. [1999] for the Alaska coast (50 kg C m^{-3}). As noted by those authors, this is less than other inland Arctic sites (62 kg C m^{-3} reported in Michaelson et al., [1996], and 65 kg C m^{-3} in Bockheim et al., [1998]), which might be due to higher ground ice contents in the coastal regions. Our results emphasize how important it is to include deeper carbon in calculations since only 44% of the SOC in our study was stored in the upper 1 m, with 56% of it at greater depths. Bockheim and Hinkel [2007] found 64% of SOC within the upper 1 m and 36% in the 1-2 m depth range. Tarnocai et al. [2009] calculated 48% for the upper 1 m, and 52% between 1 and 3 m; when they included even deeper deposits, the ratio became 30% SOC above 1 m to 70% below. A number of different processes have contributed to the presence of organic carbon at depth in the sediments of the Yukon Coastal Plain including cryoturbation, alluvial deposition, ice-thrusting, accumulation in lacustrine basins, and possibly some aeolian deposition [*Rampton, 1982*]. Coastal erosion involves the mobilization of all the carbon in the soil column relative to the sea level, so it is essential to consider deep SOC in flux calculations. In more inland regions, processes that affect carbon cycling (such as the thaw of

the upper part of permafrost), are more likely to involve near-surface SOC only, so the consideration of carbon at greater depths may not be as critical. Several of the assumptions made in this study are conservative, particularly with regards to the 25% organic carbon content in the surface horizon and in extrapolating the values of 0.792% to the base of soil columns. In addition, the amount of carbon in some ice-thrust morainal units is likely underestimated since a minimum SOC value was used for most of the volume of the bluff, but glaciotectonic and thaw slump activity likely resulted in an interlayering of carbon-rich and carbon-poor layers.

4.5.3 Material fluxes

The results presented here provide fluxes of SOC (0.035 Tg a^{-1}) and sediment (1.801 Tg a^{-1}) from the Yukon Coastal Plain. The sediment flux is 17% more than the value given by earlier studies by Harper and Penland [1982] for the Yukon (and later used by Hill et al. [1991]). Those authors noted that their sediment flux was a first approximation only and was likely a maximum value since they were not accounting for ground ice volumes. The discrepancy with our results is partly due to the fact that their study considered less of the shoreline to be erosive (150 km vs. the approximately 280 km considered here), and partly due to probable differences in bluff height estimation. The only other study of SOC flux for the region is based on the entire shoreline of the Canadian Beaufort Sea [Macdonald et al., 1998] and provides a range of potential fluxes. Using data from Yunker et al. [1991], Macdonald et al. estimate annual flux to be 0.06 Tg a^{-1} . Their value for the Yukon coast would be 0.015 Tg a^{-1} , which is less than half of the flux found in this study. Again, they consider a shorter length of shoreline and only look at eroding peat, not other sediment contained in the coastal bluffs. Their maximum estimate for SOC flux is 0.3 Tg a^{-1} based on data from Hill et al. [1991] and a presumed SOC content for all coastal sediments of 5% by weight. The value for the Yukon portion of the coast would be 0.12 Tg a^{-1} , which is 3.5 times our result. As seen above, however, eroded volumes did not account for ground ice and so are likely too high. It is interesting to note that even though SOC values for our terrain units ranged from 1.2% to 15.6%, the value assumed by Macdonald et al. [1998] is very similar to our mean of 4.5% for all units. If our results from the Yukon Coastal Plain are applied to the other areas of peat erosion examined by Macdonald et al. [1998], the mean flux of SOC to the Canadian Beaufort Sea would be 0.17 Tg a^{-1} , which is almost three times the value used to date in Arctic Ocean budgets [Rachold et al., 2004]. This is approximately 10% of the POC input by the

Mackenzie River each year [MacDonald *et al.*, 1998; Hilton *et al.*, 2015], which has the largest carbon input of any Arctic river [Rachold *et al.*, 2004].

The flux of SOC per meter of shoreline found in this study (131 kg C m^{-1}) is intermediate to the results of studies for other Arctic Seas. Along the Alaskan Beaufort coast, estimates of the mean annual flux range from 73 kg C m^{-1} [Ping *et al.*, 2011] to 149 kg C m^{-1} [Jorgenson and Brown, 2005], while results from Streletskaia *et al.* [2009] for the Kara Sea indicate a flux of 154 kg C m^{-1} . Rachold *et al.* [2004] found a mean of 263 kg C m^{-1} for different coastal types along the Laptev Sea and 375 kg C m^{-1} for the East Siberian Sea. Sediment fluxes show similar trends for the different seas. The lower values for the Alaskan Beaufort and Kara Seas appear to be the result of lower bluffs and lower SOC contents, respectively. The higher fluxes from the Laptev and East Siberian Seas are chiefly the result of higher erosion rates [Vonk *et al.*, 2012].

Finally, it should be noted that the calculations in this study only involve sub-aerial erosion, although, over time, a significant amount of material can be eroded below the waterline [Aré, 1988; Reimnitz *et al.*, 1988; Vonk *et al.*, 2012]. This is primarily due to the paucity of data available for the nearshore along the Yukon Coastal Plain.

4.5.4 Organic carbon in nearshore sediments

Our results for carbon in nearshore sediments (91.3% terrigenous and 8.7% marine) are similar to those of Vonk *et al.* [2012] who found that marine organic carbon constituted 7% of nearshore shelf sediments in the East Siberian Sea. The influence of the value for the marine end-member in the mixing model can be seen by examining some of the values invoked in the literature. If we had we chosen a heavier value of -17.5‰ proposed by Belicka and Harvey [2009], the proportion of terrigenous carbon would have been 94%. Using the lighter value (-24.0‰) for the marine end-member suggested by Naidu *et al.* [2000] would have resulted in a mean terrigenous OC value of 82%. Belicka and Harvey [2009] compared several different methods of estimating terrestrial organic carbon, including the isotopic mixing model. Although each of the four proxy methods they examined produced different results, the mixing model despite its sensitivity to the marine end-member, produced intermediate results. Because of the variability of the marine end-member, C/N ratios are used here to help in assessing the source of organic carbon in nearshore sediments. Figure 4.5 shows a plot of these two parameters for the nearshore samples. Although most samples are heavier than the terrigenous end-member, indicating a marine influence, the high C/N ratios help to confirm the strong contribution of terrigenous carbon to these samples. Previous studies of organic

carbon in the Beaufort Sea show a progressive decrease in the terrigenous component as distance from shore increases [Naidu *et al.*, 2000; Macdonald *et al.*, 2004]. No obvious trend was seen in our data set when comparing terrigenous carbon contents with distance from shore, likely due to the fact that the maximum distance from shore was limited to 500 m. However, it is interesting to note that the two samples with the highest marine content (open circles in Figure 4.5) were taken north of Herschel Island; although this area has one of the highest fluxes of C per meter of shoreline, it is furthest from the mainland, and therefore most likely to be subject to marine influences. Several studies show an overall shift towards heavier $\delta^{13}\text{C}$ values from east to west in the Beaufort Sea due to decreased influence of the Mackenzie River and to the greater importance of marine productivity in the more nutrient-rich waters in the west [Naidu *et al.*, 2000; Dunton *et al.*, 2006]. Our data are consistent with that trend and are intermediate between values measured on the Mackenzie Shelf to the east and the Alaskan shelf to the west [Goñi *et al.*, 2000; Naidu *et al.*, 2000; Macdonald *et al.*, 2004].

Knowing how much of the OC in the nearshore sediments is of terrestrial origin provides an indication of how much of the annual flux is being sequestered in those sediments and how much may be remineralized or exported off-shelf. Following Macdonald *et al.* [1998], we estimate OC burial based on sedimentation rate and the proportion of OC in marine sediments. Sedimentation rates for the area adjacent to the Mackenzie Delta are relatively well known, but there is very little information for the shelf area to the west. Based on data from Harper and Penland [1982], rates range from 2 mm a^{-1} near the delta to less than 0.1 mm a^{-1} in more distal areas. If we use the lower value of sedimentation and assume a solid density of 2.6 g cm^{-3} and a porosity of 60% for the marine sediments, then the annual flux of material to the seafloor for the entire shelf off the Yukon coast (which covers an area of 3100 km^2 according to Macdonald *et al.* [1998]) would be 0.32 Tg a^{-1} . Of this, 1.5% is OC based on our measurements, 91.7% of which is of terrestrial origin. Therefore, 0.004 Tg or 12.7% of the OC eroded from the coastal sediments is sequestered in the nearshore sediments. This estimation requires validation based on extensive $^{210}\text{Pb}/^{137}\text{Cs}$ dating of sediment cores from the shelf, comparable to the approach used by Vonk *et al.* [2012]. The OC not sequestered in the nearshore is mineralized or transported off the shelf (de Haas *et al.*, 2002; Hedges *et al.*, 1997). There is strong support that TerrOC is involved in both processes. For instance, a considerable amount of terrigenous material has been found in sediment traps at the shelf edge [O'Brien *et al.*, 2006] and beyond [Belicka *et al.*, 2002, 2009; Stein & Macdonald, 2004a], and Dunton *et al.* [2006] demonstrate that TerrOC may constitute up to 70% of the dietary requirements of species in the nearshore along the Alaskan Beaufort Sea.

4.6 Conclusion

This study provides the first in-depth estimate of soil organic carbon (SOC) content in coastal sediments of the Yukon Coastal Plain, and the first to specifically account for the volumes taken up by ground ice in those calculations. SOC is shown to constitute a large proportion of coastal bluffs. SOC accounted for between 0.5 and 49% by weight of the sediments sampled. This resulted in a mean carbon density of 41 kg C m⁻³ in the top 1 meter of soil. Mean values differed based on terrain units, being highest in fluvial sediments (53 kg C m⁻³) and lowest in marine deposits (30 kg C m⁻³), although differences between units were not considered significant in most cases. A considerable amount of SOC was also seen at depth, with the top meter accounting for only 43.8% of the total SOC in the soil column. In coastal flux studies, the entire soil column must therefore be considered, since failing to do so can result in underestimating carbon transfer by more than half. Terrain units with the lowest overall values of SOC were high bluffs with a high mineral content, while those with the highest SOC values were low bluffs with a thick organic cover. Wedge ice and massive ground ice constitute a significant portion of coastal sediments, with wedge ice accounting for up to 53% of the volume in some cases in the upper, carbon-rich soil layers. The variation of ground ice with depth is less important in low bluffs. If ground ice is not taken into consideration, flux measurements can be overestimated by 19% for SOC and 16% for sediment. The annual flux of organic carbon from coastal erosion along the Yukon Coastal Plain is 0.035 Tg a⁻¹. Extrapolating these results to the area east of the Mackenzie Delta would result in a total coastal flux of organic carbon from the Canadian Beaufort Sea of 0.17 Tg a⁻¹. This is almost three times more than the values used to date in organic carbon budget calculations [Macdonald *et al.*, 1998; Rachold *et al.*, 2004]. The sediment flux for the Yukon part of the Beaufort Sea coast is 1.801 Tg a⁻¹, which is 17% higher than previous estimates due to differences in the length of shoreline considered and probable differences in cliff height estimates. First estimations indicate that up to 12.7% of the organic carbon contributed to the nearshore by coastal erosion is sequestered in the shelf sediments. The rest is either metabolized in the nearshore or exported off the shelf by waves or ice action.

Acknowledgements

Financial support was provided to N. Couture by the Fonds québécois de la recherche sur la nature et les technologies (FQRNT), the ArcticNet Network of Centres of Excellence of Canada, the Eben Hobson Fellowship in Arctic Studies. A.M. Irrgang was funded by a grant from the German Federal Environmental Foundation. W. Pollard received support from the National Science and Engineering

Research Council of Canada. H. Lantuit was funded through the Helmholtz Young Investigators Group “COPER” (grant #VH-NG-801). M. Fritz was supported by the Daimler and Benz Foundation (grant #32-02/15). We wish to express our thanks to the Yukon Territorial Government and the Yukon Parks (Herschel Island Qiqiktaruk Territorial Park). Fieldwork would not have been possible without support from the Polar Continental Shelf Project, the Aurora Research Institute (ARI, Inuvik), and the Northern Scientific Training Program. T. Haltigin, G. De Pascale, G. Manson, H. Meyer and L. Schirrmeister assisted in the field. Analytical support from Ute Kuschel at the Alfred Wegener Institute Helmholtz Centre for Polar and Marine Research, Potsdam is gratefully acknowledged. The georeferenced images used for analysis of the Herschel Island terrain units were provided by J. Ramage. Additional supporting data can be found in the PANGAEA depository at <https://doi.pangaea.de/PANGAEA.884689> (Couture et al., 2018). This is contribution number 20170202 of Natural Resources Canada’s Lands and Minerals Sector.

Context

Coastal erosion leads to the mobilization of considerable amounts of carbon and sediments, each year (Chpt. 4). However, the contribution of retrogressive thaw slumps (RTSs) to the sediment and carbon fluxes is not accounted for in these calculations. The previous study focused on material fluxes which were a direct consequence of shoreline retreat. Since the mobilization of organic matter in RTSs is mainly taking place along the headwall and in the slump floor, rather than directly along the shoreline, RTSs deliver considerable amounts of material to the nearshore zone, without impacting much of the shoreline. The following study was conducted in order to improve the understanding of the factors triggering RTS activity and, in particular, which role coastal erosion plays for these processes. This is the first step towards a better understanding of how enhanced coastal retreat is influencing material fluxes along the Yukon coast.

Terrain controls on the occurrence of coastal retrogressive thaw slumps along the Yukon Coast, Canada

ABSTRACT

Retrogressive thaw slumps (RTSs) are among the most active landforms in the Arctic; their number has increased significantly over the past decades. While processes initiating discrete RTSs are well defined, the major terrain controls on the development of coastal RTSs at a regional scale are not well-defined. Our research reveals the main geomorphic factors that determine the development of RTSs along a 238 km coastal segment of the Yukon Coast, Canada. We 1) show the current extent of RTSs, 2) ascertain the factors controlling their activity and initiation, and 3) explain the differences in the density and areal coverage of RTSs. We mapped and classified 287 RTSs using high-resolution satellite images acquired in 2011. We highlighted the main terrain controls over their development using univariate regression trees. Both activity and initiation of RTSs were influenced by coastal geomorphology: active RTSs and RTSs initiated after 1972 occurred primarily on terrains with slope angles greater than 3.9° and 5.9° , respectively. The density and coverage of RTSs were constrained by the volume and thickness of massive ice bodies. Differences in coastal erosion rates along the coast did not affect the model. We infer that coastal erosion rates averaged over a 39-year period are unable to reflect the complex relationship between RTSs and coastline dynamics. We emphasize the need for large-scale studies of RTSs – to evaluate their impact on the ecosystem and to measure their contribution to the global carbon budget.

A manuscript with equal content is published as:

Ramage, J., A.M. Irrgang, U. Herzschuh, A. Morgenstern, N. Couture, and H. Lantuit (2017). Terrain Controls on the Occurrence of Coastal Retrogressive Thaw Slumps along the Yukon Coast, Canada. *Journal of Geophysical Research: Earth Surface*. DOI: 10.1002/2017JF004231.

5.1 Introduction

Permafrost degradation processes are highly dynamic and profoundly reshape Arctic landscapes. Disturbances caused by ground subsidence and collapse (thermokarst and thermal erosion) induced by these processes can greatly affect the tundra ecosystem [Kokelj *et al.*, 2013; Malone *et al.*, 2013; Lantz *et al.*, 2009]. Dynamic degrading permafrost landforms represent major sources of instability, affecting biomass and hydrologic fluxes in the Arctic [Abbott *et al.*, 2016].

Thermokarst landforms develop when ice-rich permafrost thaws. Retrogressive thaw slumps (RTSs) are a type of slope failure, which are amongst the most dynamic thermokarst landforms in the Arctic. These slope failures can be initiated following active layer detachment, lateral and thermal erosion along the coast [Kokelj and Jorgenson, 2013; Kokelj *et al.*, 2009b; Lantuit *et al.*, 2012a; Burn and Lewkowicz, 1990], expansion of thermoerosional gullies [Bowden *et al.*, 2008], or wildfire [Lacelle *et al.*, 2010]. RTS morphology comprises a vertical headwall, an inclined headscarp, a floor filled with flow deposits and a lobe that conveys thawed sediments downslope [Burn and Lewkowicz, 1990].

The number of RTSs has increased considerably across the Arctic in the last decades [Brooker *et al.*, 2014; Lantuit *et al.*, 2012a; Lacelle *et al.*, 2010; Kokelj *et al.*, 2009b; Lantuit and Pollard, 2008; Lantz and Kokelj, 2008], mostly in ice-rich permafrost terrains located on the ice marginal glaciated landscapes [Kokelj *et al.*, 2017]. Studies describing the dynamics of inland RTSs, occurring on plateaus [Segal *et al.*, 2016; Lacelle *et al.*, 2015; Brooker *et al.*, 2014; Lacelle *et al.*, 2010], in deltas, and along lakeshores [Kokelj *et al.*, 2009a; Lantz and Kokelj, 2008] have shown that RTSs have increased in both size and number. Moreover, their headwalls have retreated extensively over the past decades [Lantuit *et al.*, 2005; Lewkowicz, 1987a]. These disturbances have a considerable impact on the surrounding ecosystems, strongly affecting terrestrial [Tanski *et al.*, 2016; Cray and Pollard, 2015; Cannone *et al.*, 2010; Lantz *et al.*, 2009; Lantz and Kokelj, 2008] and aquatic ecosystems [Chin *et al.*, 2016; Houben *et al.*, 2016; Chipman *et al.*, 2016; Kokelj *et al.*, 2013] by reworking sediments and mobilizing carbon, nitrogen and nutrients.

RTSs can go through several cycles of activation and stabilization. Many RTSs are polycyclic; they superimpose on surfaces previously affected by RTS activity. Polycyclic activity is associated with the destabilization of formerly stabilized surfaces, when incompletely melted massive ground ice is being re-exposed by erosional processes [Lantuit and Pollard, 2008; Burn, 2000]. In coastal settings, polycyclic activity occurs when coastal and surficial erosion or

changes in the physical properties of the sediments expose massive ice bodies to solar radiation and sensible heat [Lantuit *et al.*, 2012a, 2008].

While climatic factors influence the development of RTSs [Kokelj *et al.*, 2015b; Balser *et al.*, 2014; Lantz and Kokelj, 2008], their impact only becomes decisive in a certain geomorphic context [Kokelj *et al.*, 2017; Kokelj *et al.*, 2015b]. For example, the effect of incoming solar radiation on the permafrost greatly varies depending on slope aspect and ground ice content [Lacelle *et al.*, 2010; Lewkowicz, 1988]. Precipitation influences the activity of RTSs through its impact on the surficial flow on gently sloping scar zones: increased surficial flow allows maintaining RTSs activity and therefore contribute to the occurrence of larger RTSs [Kokelj *et al.*, 2015b].

In coastal environments, RTSs are undergoing a period of enhanced activity since the 1950s [Segal *et al.*, 2016; Kizyakov *et al.*, 2013; Lantuit *et al.*, 2012a; Lantuit and Pollard, 2005; Wolfe *et al.*, 2001]. Sixty five percent of Arctic coasts are unlithified and characterized by high ice contents [Lantuit *et al.*, 2012b], which are subject to erosion and slumping. Along the Canadian Beaufort Sea, 60% of the coast which is comprised of unconsolidated sediments is eroding [Harper, 1990]. Wave energy, through its impact on coastal erosion likely plays a major role in RTSs initiation [Lantuit *et al.*, 2011; Jones *et al.*, 2008; Mars and Houseknecht, 2007]. As it is the case for inland RTSs, coastal RTSs are rather triggered by shoreline erosional processes rather than by changes in air temperature [Lacelle *et al.*, 2010]. Therefore, the reported accelerating rates of coastal erosion in the Arctic [Barnhart *et al.*, 2014b; Overduin *et al.*, 2014; Jones *et al.*, 2009a] likely influence coastal RTS dynamics. In turn, the variability of short-term shoreline dynamics in the Arctic is partially influenced by mass-wasting processes acting along permafrost coasts since coastal RTSs greatly contribute to the release of sediments from land to the nearshore zone in the Arctic [Tanski *et al.*, 2017; Obu *et al.*, 2017a; Lantuit and Pollard, 2005].

The impact of coastal erosional processes on coastal RTSs has been reported in previous studies [Obu *et al.*, 2017a; Lantuit *et al.*, 2011]. We hypothesize that coastal erosion rates will emerge as the most decisive factor in the development of coastal RTSs. However, one must understand the impacts of coastal erosion processes on a regional scale in order to reach a conclusive insight. Using statistical analyses, our research provides new understanding of the distribution and dynamics of coastal RTSs. It highlights the main geomorphic factors influencing the development of RTSs along a 238 km coastal segment of the Yukon Coastal Plain, Canada. We 1) describe the current extent of RTSs, 2) ascertain the factors controlling their activity and initiation, and 3) explain differences in the density and areal coverage of

RTSs. Our findings will help predict the future evolution of RTSs and their potential impacts on the coastal ecosystem.

5.2 Study Area

The study area comprises a 238 km-long coastal segment of the Yukon Coastal Plain including Herschel Island, Canada (Fig. 5.1).

The Yukon Coastal Plain is an erosional surface underlain by unconsolidated glacial and glacial-marine deposits, which accumulated during the Pleistocene and Holocene [Rampton, 1982]. The study area is located at the interface between the easternmost part of Beringia (Fig. 5.1) – unglaciated during the Late Wisconsin (MIS 2) – and the westernmost margin of the Laurentide ice sheet, which reached a maximum ice extent at ca. 16 200 years BP [Fritz *et al.*, 2012]. The overall landscape reflects this history. The formerly non-glaciated part of the Yukon Coastal Plain is gently sloping and only incised by stream valleys, fluvial deltas, alluvial fans and thermokarst basins. The formerly glaciated part is underlain by ice-rich permafrost and has a heterogeneous topography, comprising areas of ice-rich permafrost of glacial origin and moraine deposits highly reworked by periglacial processes. Ice-rich cliffs constitute 35% of the coast [Harper, 1990]. Herschel Island is a moraine thrust deposited at the margin of the glaciated area, located 2 km off the Yukon mainland coast. It is one of the largest moraine deposits in the area, consisting of unconsolidated and fine-grained marine and glacial sediments [Mackay, 1959; Pollard, 1990]. On average, 30% to 60% of Herschel Island is composed of ground ice, mostly expressed as massive ice [Pollard, 1990; Rampton, 1982].

Available air temperature records (from west to east: Komakuk Beach, Herschel Island and Shingle Point) are similar across the study area throughout the year [Burn and Zhang, 2009]. The meteorological stations located at the extremities of the study area – Komakuk Beach in the west and Shingle Point in the east – recorded highly correlated air temperatures ($r^2 > 0.90$ for most months) between 1995 and 2007 [Burn and Zhang, 2009]. The mean summer air temperature (June, July and August, 1971-2000) is 6.0 °C at Komakuk and 8.7 °C at Shingle Point [Environment Canada, 2017]. Precipitation is the main climatic difference between the two stations. Komakuk Beach receives an average summer precipitation of 79.8 mm, while 112.9 mm of precipitation falls at Shingle Point (June, July, August, 1971-2000) [Environment Canada, 2017]. The influence of the Mackenzie River on seawater temperature and sea ice extent is the main forcing on the local precipitation patterns [Burn and Zhang, 2009].

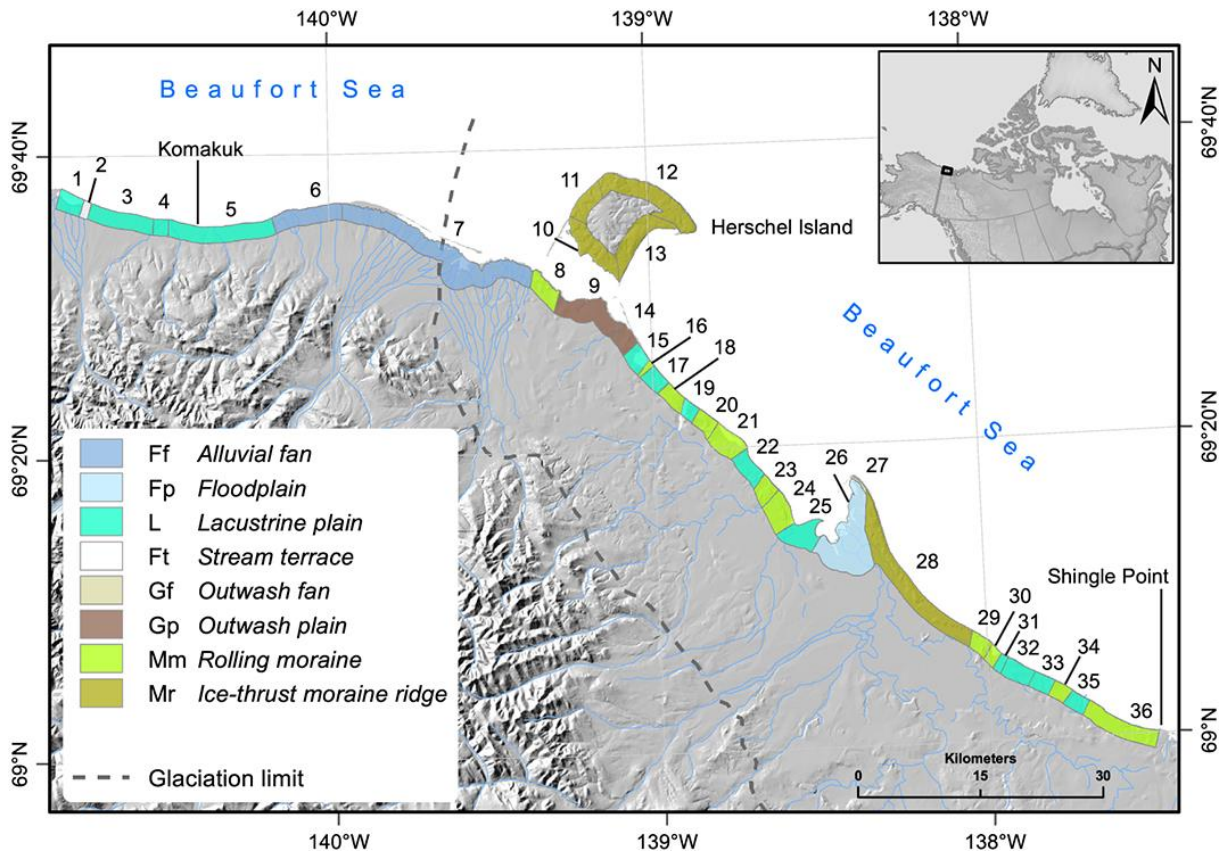


Figure 5.1: Location of the study area. The numbers represent the coastal segments stretching along the coast from west to east. The limit of the glaciation was reproduced after Dyke and Prest [1987] and the surficial sediments after Rampton [1982].

The western Yukon Coast is undergoing widespread coastal retreat [Harper, 1990]. The mean annual erosion rate between Komakuk Beach and Shingle Point was -1.2 m per year between 1951 and 2009. There is a general spatial pattern of decreasing erosion rates from west to east along the Yukon Coast [Konopczak *et al.*, 2014].

The study area is divided into 36 coastal segments (Fig. 5.1), derived from the Arctic Coastal Dynamics Database [Lantuit *et al.*, 2012b; Lantuit and Pollard, 2005] and refined by Couture [2010] to account for ground ice, surficial geology and geomorphology. Coastal heights range from 0.5 m to 27.6 m (Table S2 in the Supportive Information) and average slopes are between 0° and 22° . Ten of the segments are protected from direct wave influence by spits and barrier islands. Estimates of the volume of ground ice in the different coastal segments along the coast come from the model developed by Couture and Pollard [2017]. The model takes into account 14 input variables including soil characteristics, measured volumetric ice contents and geomorphic information. Ground ice varies between coastal segments; occurring as massive ice, pore ice and wedge ice, and ranges from 0% to 74% [Couture and Pollard, 2017]. The heterogeneity of coastal segments, including the surficial geology, is inherited from the glacial history of the area. Most of the segments fall into one of three surficial

geology units: ice-thrust moraines (30%); lacustrine plains (23%) and rolling moraines (16%). The remaining segments (30%) are underlain by alluvial fans, stream terraces, floodplains and outwash plains [Rampton, 1982].

5.3 Methods

5.3.1 Mapping of RTSs and landform classification

We manually digitized each RTS at a 1:2 000 scale using ArcMap (ESRI, version 10.3) from high-resolution satellite images acquired in July (13th and 18th), August (31st) and September (13th) 2011 (multispectral GeoEye-1 and WorldView-2 – 1.8 m resolution in multi-spectral and 0.5 m in panchromatic view). We exclusively mapped coastal RTSs, which we defined as features occurring within 500 m of the coast.

We classified RTSs according to their activity (Fig. 5.2). **Active** RTSs are characterized by steep headwalls exposing ice-rich permafrost, slump floors with thawed sediments and incised gullies. **Stable** RTSs comprise gently sloping and vegetated headwalls, vegetated slump floors and no visible active gully systems [Lantuit and Pollard, 2008; Wolfe *et al.*, 2001]. Stable polycyclic RTSs include the areas of active RTSs located within their boundaries. We additionally classified RTSs according to their initiation date, defining RTSs initiated after 1972 as occurring on surfaces that had never been affected by slumping processes before the 1970s. For this purpose, we used a series of 21 aerial photographs from 1972 and one photograph from 1976 (Supportive Information ds05), which jointly cover the entire study area [National Air Photo Library, Canada] and geo-coded all images to the 2011 satellite images using PCI Geomatic's Geomatica Orthoengine© software [2014]. Again, RTSs were digitized in ArcGIS 10.3 at a 1:2 000 scale. The aerial photographs have a resolution of 3 m (Supportive Information ds05). We distinguished between two kinds of RTSs. The first class comprised RTSs initiated after 1972, identified in 2011 on surfaces that were not affected by slumping on the historical aerial photographs. All the other RTSs (i.e., RTSs already detectable in 1972) were put into the second class. Even if we were not able to define the specific date of RTS initiation, the distinction between RTSs that initiated after 1972 and other RTSs allowed us to better understand RTS dynamics related to polycyclic activity. The use of different imagery for mapping RTSs might have affected the size of the RTSs that were detectable and introduced some limitations related to accuracy. However, differences in resolution between aerial photographs and satellite imagery were ca. 1.2 m and were deemed satisfactory for interpretation and mapping purposes.

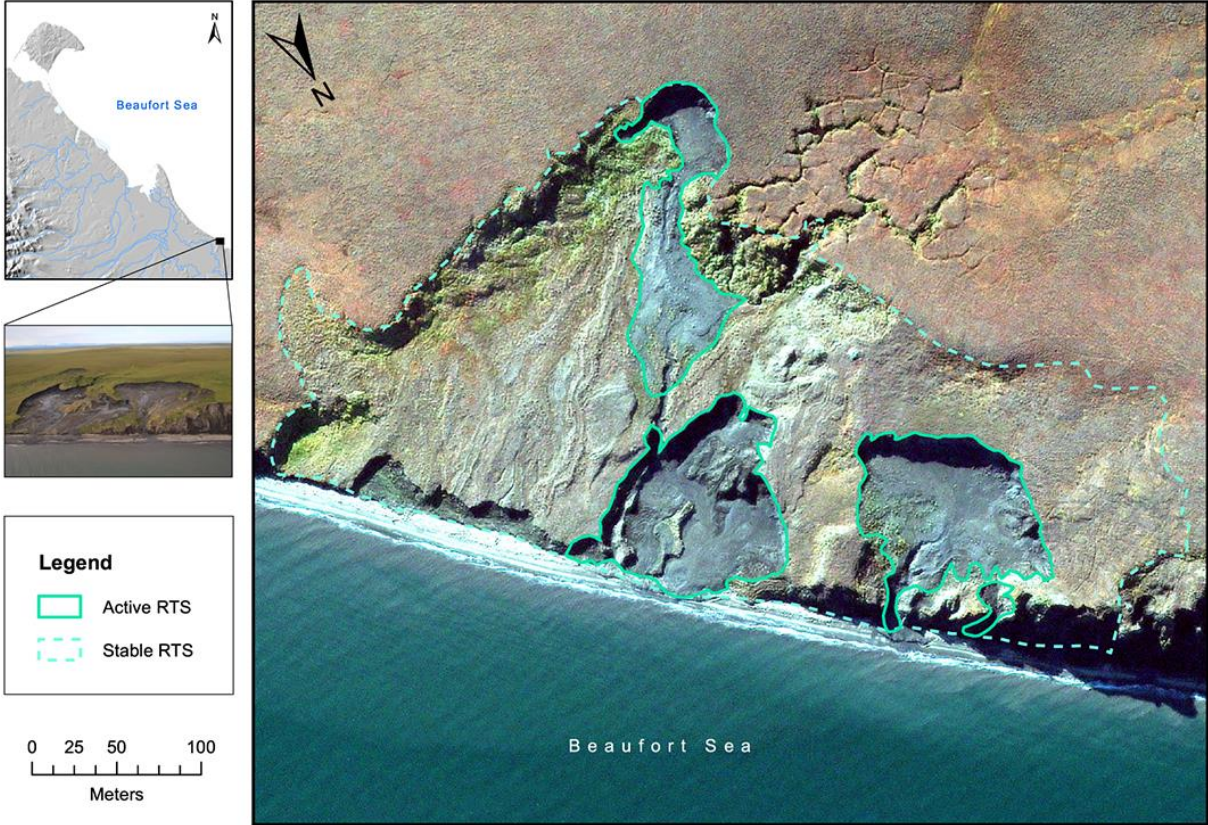


Figure 5.2: GeoEye image from 18 July 2011 illustrating the differences between active and stable RTSs. The depicted RTS is located in the eastern part of the study area, at King Point (segment 32). The oblique photograph was taken from a helicopter during fieldwork in July 2015.

Table 5.1: Summary of spatial information and terrain parameters extracted for each coastal segment. The data was calculated for this study based on satellite imagery from 2011, aerial photographs from 1972 and LiDAR dataset from 2013 or derived after [a] Rampton [1982] and [b] Couture [2010]. Environmental variables used as response variables in the model are indicated in bold. See Supportive Information ds02 and ds03.

Variable name	Description	Unit	Source
RTS characteristics			
Area_ha	Areal extent of a RTS	ha	Satellite imagery
Activity	Activity of the RTS in 2011: active or stable		Satellite imagery
Initiation	RTSs initiated after 1972 and their activity (active–stable)		Aerial photographs
Azimuth	Orientation of the RTS	°	Satellite imagery
Z_MEAN	Mean height within the slump floor of a RTS	m (a.s.l)	LiDAR
S_MEAN	Mean Slope within the slump floor of a RTS	°	LiDAR
Coastal_le	Width of the RTS lobe	m	Satellite imagery
NEAR_DIST	Distance from the RTS to the shore	m	Satellite imagery
Spatial information			
Segment_name	Name of the Coastal Segments		[b]
Glaciated	Glacial history - Yes: glaciated; No: non-glaciated		[b]
Geolunit	Surficial Geology		[a]
Area	Areal extent of the Coastal Segments	ha	Satellite imagery
CL	Coastal length	km	Satellite imagery
CH	Cliff height: median of elevation points (25 m inland)	m	LiDAR
S500	Slope 500m: average slope calculated over 500 m inland	°	LiDAR
Spit	Presence (1) or absence (0) of spit along the coast		Satellite imagery
E50-11	Erosion rate between 1952 and 2011	m yr ⁻¹	Satellite imagery
E70-11	Erosion rate between 1972 and 2011	m yr ⁻¹	Satellite imagery
Terrain characteristics			
PEI	Percentage of excess ice	%	[b]
PIV	Percentage of ice volume	%	[b]
AL	Active layer depth	cm	[b]
e	Soil porosity	g / cm ³	[b]
Dm	Depth to the top of massive ice	m (a.s.l)	[b]
Dbm	Depth to the bottom of massive ice	m (a.s.l)	[b]
DMI	Thickness of the massive ice (Dbm-Dm)	m (a.s.l)	[b]
Wt	Mean ice wedge width	m (a.s.l)	[b]
Ws	Mean ice wedge spacing	m (a.s.l)	[b]
PI	Pore ice	%	[b]
WI	Wedge ice	%	[b]
MI	Massive ice	%	[b]

5.3.2 Environmental variables

Environmental data that we used include local geomorphic parameters and coastal erosion rates. We did not take into account climatic factors. Geomorphic parameters and erosion rates are derived from various sources with different temporal and spatial resolution. For consistency, we refined the boundaries of the coastal segments defined by *Couture* [2010] based on the satellite imagery from 2011.

Table 5.2: List of the Response Variables Used in the Univariate Regression Tree Algorithms. The response variables are given for each coastal segment.

Response variables	Explanation
Density	Number of RTSs in segment / Total coastal length of segment
Coverage	(Sum of surface areas of RTSs in segment / Total surface area of segment) * 100
Activity	Percentage of active RTSs
Initiation	Percentage of RTSs that initiated after 1972

5.3.2.1 RTS characteristics

Using ArcMap 10.3, we derived RTS morphologies (Table 5.1, RTS characteristics) and extracted morphological and spatial information for each coastal segment (Table 5.1, spatial information) from an airborne LiDAR dataset acquired in July 2013 [*Kohnert et al.*, 2014]. The LiDAR dataset has a final georeferenced point cloud data vertical accuracy of 0.15 ± 0.1 m and covers most of the study area, with a scan width of 500 m. While visible on the satellite images, a total of 39 RTSs occurred in areas outside of the area covered by the LiDAR so we discarded those features from further analyses. RTS characteristics (Table 5.1) summarize the morphologic information for the area within each RTS shapefile. The mean elevation above sea level (Z_MEAN) provides information about the relative elevation of the slump floor of a RTS (Fig. 5.3). We used the mean slope of the slump floors (S_MEAN) as an indicator of the potential for removal of material from the slumps (Fig. 5.3).

Table 5.3: RTS Main Characteristics Derived From the Lidar Data set.

Type	N	Size (ha) (med, range)	Slope (°) (mean)	Aspect (°) (med)	Lobe width (m) (med, range)
Active	203	0.15, 20.8	15.3 ± 6.7	NE, 45.8	29.3, 1109
Stable	84	1.09, 19.9	13.3 ± 4.2	NE, 48.2	40.5, 963
All	287	0.24, 20.8	14.7 ± 6.1	NE, 46.7	31.1, 1109
Initiated after 1972	119	0.16, 16.7	11.3 ± 9.4	NE, 49.7	26.1, 1024

5.3.2.2 Spatial information

Information concerning the coastal segments on which the RTSs developed is summarized in the spatial information (Table 5.1). This information was calculated using the high-resolution satellite imagery, except for the mean cliff heights and coastal slopes, which we derived from the LiDAR dataset. The mean cliff height represents the mean values of elevation points 25 m inland from the shoreline, measured along transects placed every 100 m within a coastal segment. Elevation points that fell within a RTS were discarded. Coastal change rates from 1972 to 2011 were measured using the Esri ArcGIS extension Digital Shoreline Analysis System (DSAS) version 4.3 [Thieler *et al.*, 2009] applied on the satellite imagery from 2011 [Irrgang *et al.*, 2017].

5.3.2.3 Terrain characteristic

In addition to the spatial information, we used terrain characteristics from a study from Couture [2010] (see Data S1 in the Supportive Information). Terrain characteristics for each segment were either derived from direct measurements from bluff exposures and shallow cores or were estimated from published datasets. Couture and Pollard [2017] quantified ground ice at a landscape level and provided ice contents (volumes of each type of ice - pore ice, wedge ice and massive ice, volumetric ice content and volume of excess ice), for each coastal segment. The variable “Thickness of massive ice” (DMI) was estimated by subtracting the depth to the top of massive ice bodies (Dm) in a coastal segment from the depth to the bottom (Dbm) (Table 5.1). When the bottom of the massive ice was buried under reworked sediments, it was assumed to extend to the base of the bluff [Couture, 2010].

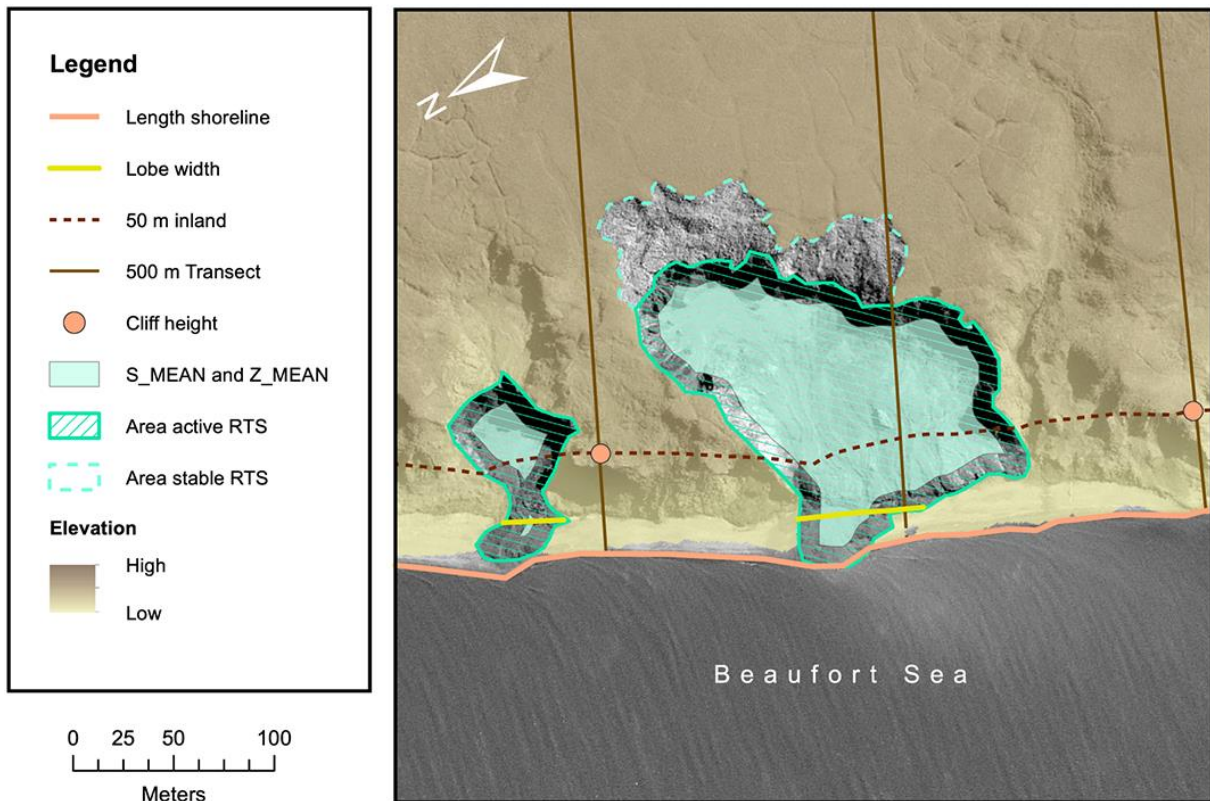


Figure 5.3: Scheme of RTSs showing RTS characteristics. All elevation data were derived from the lidar data set. The length of the shoreline was manually digitized for the entire study area. RTS elevation (Z_MEAN) and slope (S_MEAN) were calculated for the RTS floor, while the area of the RTS included the whole surface including the headwall. The cliff heights (CH) were defined for each segment as points located on transect every 100 m along the coast, 25 m inland. The segment slopes ($S500$) were an average of the slopes calculated for a whole segment, starting from 25 m inland to 500 m.

5.3.3 Univariate regression trees

Univariate regression tree models were fitted using R (The R Foundation, version 3.3.1) in order to characterize terrain controls on RTS distribution. We applied univariate regression trees (*rpart* package version 4.1-10, [Breiman *et al.*, 1984]) to highlight the environmental parameters (explanatory variables) that explained most variation in RTS abundance (univariate response variables) and the main thresholds in the datasets. Response variables used in the models (Table 5.2) are univariate and were tested against 16 environmental parameters (Table 5.1). Through recursive partitioning, the regression trees repeatedly split the dataset into binary groups (Supportive Information ds01). Each split is defined by a simple rule, which minimizes the sums of squares within the two groups formed by the split [Breiman *et al.*, 1984]. The optimal tree size was determined by the complexity parameter, which is used when pruning the tree to minimize the mean relative square error. This method is robust and can incorporate dependent variables as well as discrete data [De'ath and Fabricius, 2000]. The scripts are available in the Supportive Information.

5.4 Results

5.4.1 Characteristics of RTS along the coast

5.4.1.1 Distribution

Based on the 2011 satellite imagery, we detected 287 coastal RTSs along the Yukon Coast. All RTSs were located in the formerly glaciated part of the study area; more than half (53%) faced north-northeast, reflecting the general orientation of the coast. In total, 12% (28.1 km) of the entire coastline was incised by RTS lobes, which had a median width of 31 m. The size of RTSs varied both over the entire area and within the coastal segments (Fig. 5.4). The median size was 0.24 ha (mean = 1.52 ha) (Table 5.3). The largest RTS was observed on Herschel Island East (segment 13, 20.81 ha), the smallest at Stokes Point West (segment 20, 0.01 ha). On average, the largest RTSs were found on ice-thrust moraines (med = 0.27 ha, range = 20.80 ha) and lacustrine plains (med = 0.20 ha, range = 13.60 ha), while the smallest RTSs occurred on rolling moraines (med = 0.17 ha, range = 14.65 ha).

Among the 287 RTSs, 203 (71%) were active and had clear morphological differences compared to the stable RTSs (Table 5.3): active RTSs were 7 times smaller (med = 0.15 ha) than stable RTSs (med = 1.09 ha), their floors had slightly steeper slopes, and they had narrower slump lobes (Table 5.3).

In total, 119 of the 287 RTSs (41%) were initiated after 1972. Compared to the overall RTSs, RTSs initiated after 1972 were smaller (med = 0.18 ha), with gentler slopes and narrower slump lobes (Table 5.3). RTSs initiated after 1972 were found on 14 coastal segments. At Sabine Point West (segment 33) and Workboat Passage West (segment 8), the three observed RTSs initiated after 1972, and on Herschel Island North 77% of the RTSs initiated after 1972. In total, 51% of the RTSs occurring on ice-thrust moraines had developed since the 1970s, 35% of the RTSs initiated after 1972 on lacustrine plains and 24% of the RTSs initiated after 1972 on rolling moraines.

Of the RTSs that initiated after 1972, 72 were active and 47 were stable in 2011 (Supportive Information, Table S1, ds02). Active RTSs that initiated after 1972 had most likely remained active until 2011. On the other hand, stable RTSs that initiated after 1972 went through a period of activity and stabilized within this period. Forty percent of the RTSs that initiated after 1972 were stable, which is higher than the percentage of stable RTSs (22%). RTSs were more active, or reactivated, where slumping processes had previously affected the coast. Active RTSs that initiated after 1972 were smaller than stable RTSs that initiated after 1972 (0.10 ha vs. 0.68 ha), had steeper slopes (16.4° vs. 12.6°) and narrower slump lobes (20.7 m

vs. 46.0 m).

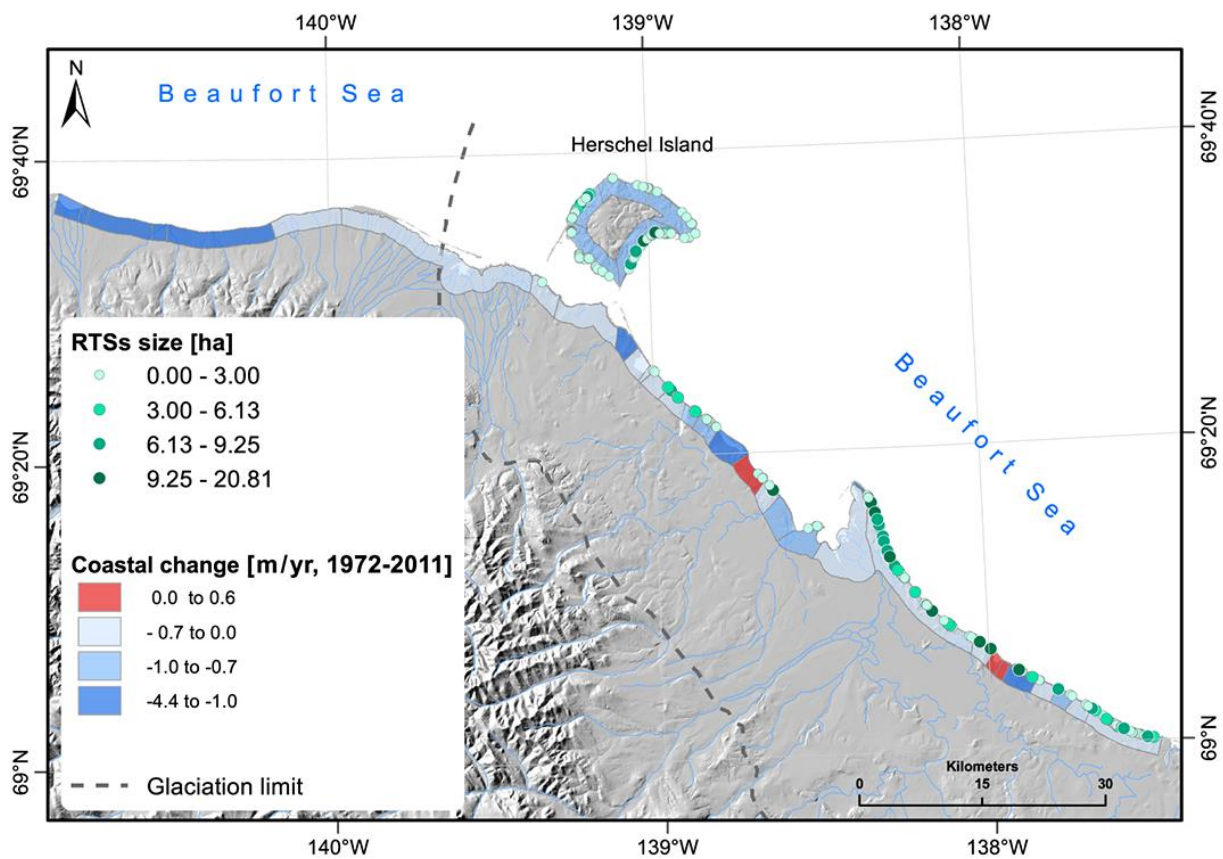


Figure 5.4: Distribution of RTSs according to their size and coastal erosion rates between the 1970s and 2011 along the study area. All RTSs were found in the eastern part of the study area, which was glaciated during the last glacial maximum. The largest RTSs were found on ice-thrust moraines. Rates of coastal change are described in Irrgang et al. [2017].

5.4.1.2 Terrain factors controlling the activity and initiation of the RTSs

Both the activity and the initiation of the RTSs were related to the geomorphology of the coastal segments (Fig. 5.5).

The slope (S500) and coastal height (CH) were the primary factors controlling the activity of RTSs (Fig. 5.5, a). The model did not show other factors because their contribution was not significant. Most of the active RTSs ($n = 200$, 98%) were found in coastal segments ($n = 21$) with a slope angle greater than 3.9° . Of these 200 active RTSs, 149 (74%) were found within coastal segments ($n = 9$) with cliff heights higher than 11.0 m. The median cliff height in the latter segments was 15.5 m.

RTSs initiated after 1972 (Fig. 5.5, b) occurred mainly on segments with a slope equal to or greater than 5.0° . We observed only two RTSs initiated after 1972 on a segment with a smaller slope angle (1.8°): Philips Bay (segment 25). However the mean slope did not represent the area on which RTSs occurred, because this coastal segment is characterized by the presence of different coastal types: the western and eastern parts of the segment are bay

areas, protected by spits. RTSs were observed along the central part of the segment, a north-facing coast open to the sea. The average slope angle on which RTSs occurred was 9.2° , while RTSs initiated after 1972 occurred on steeper slopes, with an average angle of 10.6° .

5.4.2 Density and areal coverage of RTSs along the Yukon Coast

5.4.2.1 Differences among coastal segments

Along the entire Yukon Coast, RTSs occurred with a density of 1.2 RTSs per km of coast. However there was great heterogeneity, with RTSs present in only 19 of 36 segments. They all occurred within the formerly glaciated area (Fig. 5.6), where the mean density was 2.3 RTSs per km of coast. RTSs were most abundant at Shingle Point West and Stokes Point West (segments 36 and 20, 4.2 RTSs per km of coast). At Shingle Point West, 87% of RTSs were active while at Stokes Point West, active RTSs represented 42% of the total RTSs. The study area as a whole was characterized by active slumping; active RTSs (71%) were more abundant than stable RTSs in most of the coastal segments. Differences in the occurrence of RTSs were observed between geological units (Table 5.4). In total, 60% of the RTSs occurred on ice-thrust moraines with a density of 2.4 RTSs per km of the coast. In contrast, 29% of the RTSs occurred on rolling moraines with a density of 2.0 RTSs per km of coast, and 11% on lacustrine plains with a density of 0.6 RTSs per km of coast.

RTSs covered a total area of 401.8 ha, which represents 3% of the 500 m-wide and 238-km long study area strip and 7% when considering only the coastal segments where RTSs occurred. In all segments except Herschel Island East (segment 13), West (segment 11), North (segment 12) and on Sabine Point East (segment 35) the area covered by stable RTSs was two thirds larger than the area covered by active RTSs. The coverage of RTSs was heterogeneous: the area covered by RTSs was less than 1% in 4 segments and more than 10% in 8 segments. King Point North West (segment 29) had the largest coverage of RTSs: 6 RTSs (4 active and 2 stable) covered 16% of the segment area. Herschel South (segment 10) had the smallest area covered by RTSs relative to the number of RTSs occurring on this segment (1% coverage, 31 RTSs). The total area occupied by RTSs that initiated after 1972 was proportionally smaller than the total area occupied by RTSs. Active RTSs represented 71% of the total number of RTSs and occupied 38% of the total area covered by RTSs while active RTSs that initiated after 1972 represented 25% of the total amount of RTSs and covered 4% of the total area covered by RTSs. Similarly, stable RTSs represented 29% of the total number of RTSs and occupied 62% of the total area covered by RTSs while stable RTSs that initiated after 1972 represented 16% of the total amount of RTSs and covered 20% of the total area covered by

RTSs. Those results emphasize the difference in size between RTSs that initiated after 1972 and the others.

Table 5.4: Number, density, and coverage of RTSs for each coastal segment. Abbreviations for the surficial geology are given in Table 5.1.

Seg ment #	Surficial Geology	Coastal Length (km)	Number of RTS	Density of RTS (RTS/km of coast)	Coverage of RTSs (%)
1	Ff	3.2	0	0.0	0.0
2	Ft	1.1	0	0.0	0.0
3	L	8.1	0	0.0	0.0
4	L	1.8	0	0.0	0.0
5	L	13.5	0	0.0	0.0
6	Ff	8.9	0	0.0	0.0
7	Ff	28.4	0	0.0	0.0
8	Mm	5.0	1	0.2	0.1
9	Gp	10.3	0	0.0	0.0
10	Mr	12.5	31	2.5	1.4
11	Mr	5.5	18	3.3	12.9
12	Mr	17.3	22	1.3	1.4
13	Mr	11.3	28	2.5	12.9
14	Gp	3.8	0	0.0	0.0
15	Mm	2.7	0	0.0	0.0
16	Mm	0.8	2	2.4	13.6
17	L	2.8	0	0.0	0.0
18	Mm	2.9	10	3.5	10.6
19	L	2.2	4	1.8	4.1
20	Mm	2.9	12	4.2	1.7
21	Mm	5.0	0	0.0	0.0
22	L	3.9	4	1.0	0.6
23	Mm	2.6	7	2.7	12.8
24	Mm	5.2	0	0.0	0.0
25	L	9.7	5	0.5	0.6
26	Fp	13.5	0	0.0	0.0
27	Gf	1.4	0	0.0	0.0
28	Mr	24.2	74	3.1	12.7
29	Mm	3.3	6	1.8	16.3
30	L	2.5	0	0.0	0.0

31	L	1.1	0	0.0	0.0
32	L	3.8	12	3.2	9.4
33	L	2.7	2	0.7	0.1
34	Mm	2.4	7	2.9	6.9
35	L	2.5	4	1.6	3.0
36	Mm	9.0	76	4.2	5.5

5.4.2.2 Terrain factors controlling the density and area coverage of RTSs

The main terrain factors controlling the density and coverage of RTSs are presented in Figure 5.7. The thickness of massive ice bodies within a coastal segment (DMI) was the main factor explaining the high density of RTSs (Fig. 5.7, a), whereas the percentage of massive ice by volume (MI) was the most influential factor for large coverage of RTSs (Fig. 5.7, b). The model showed that high densities of RTSs were found in coastal segments that contained massive ice with an average thickness of more than 1.5 m (DMI > 1.5). This was the case in 14 coastal segments and explained the occurrence of 240 RTSs (84%). In 22 coastal segments where massive ice was absent or less than 1.5 m thick – 47 RTSs (16%) – the slope angle was the main factor controlling the density of RTSs. Among those RTSs, 42 were located on segments which had a slope angle greater than 3.9°, with a median slope of 6.2. In one of the coastal segments (Philips Bay, segment 25, 5 RTSs), the occurrence of RTSs was not explained by either the thickness of the massive ice bodies or the degree of slope. However, as mentioned earlier, this coastal segment is characterized by the presence of different coastal types and average values might not reflect adequately the environment on which RTSs were occurring.

The main terrain control over the coverage of RTSs was the percentage of massive ice. RTSs affected a larger surface area of coastal segments that contained massive ice equal to or greater than 14%. For 13 coastal segments, mostly underlain by moraine deposits the massive ice was greater than 14%. Of those segments, 2 had no RTSs while 11% of the surface area of the remaining 11 segments was affected by RTSs.

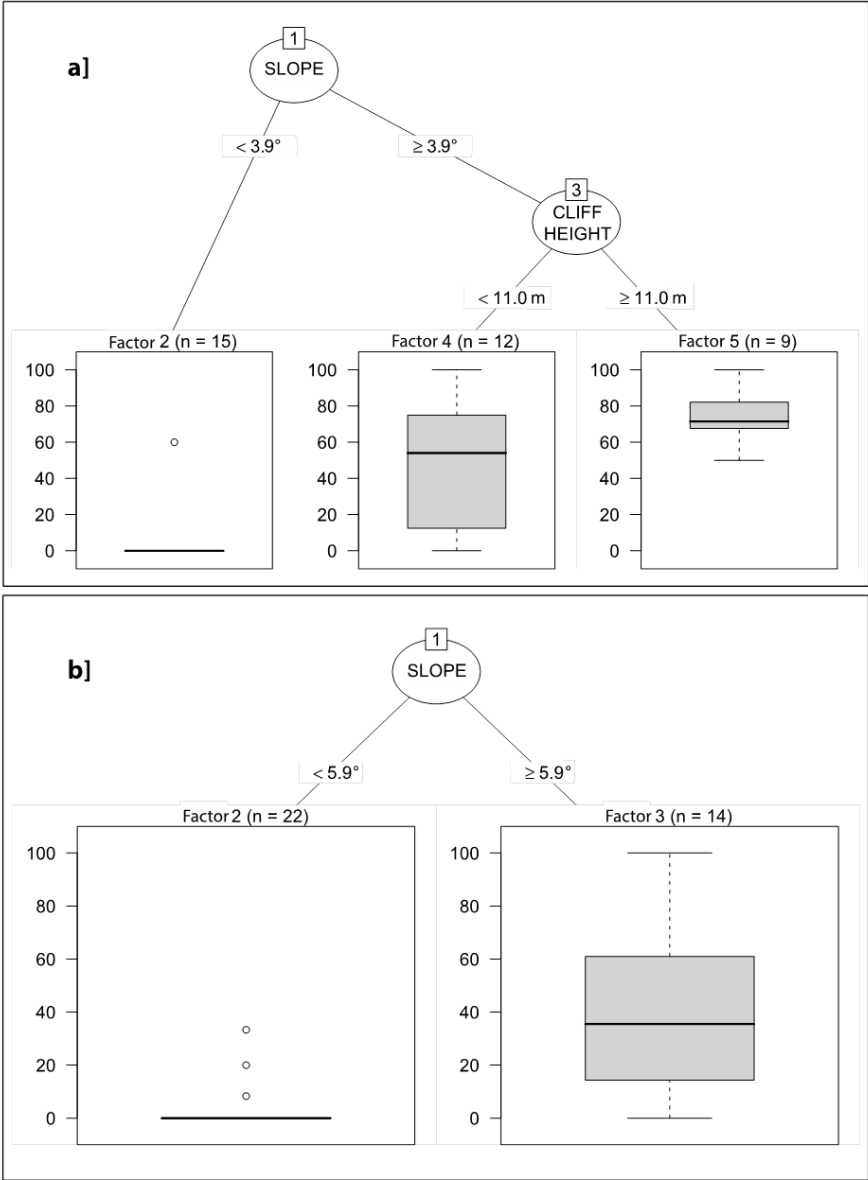


Figure 5.5: Univariate regression tree relating (a) the activity and (b) the initiation of RTSs to the 16 environmental variables used in the model; n indicates the number of segments included in each node. The slope and cliff height of the coastal segments were most influential in controlling both activity and initiation of RTSs. The box and whisker plots display variation in the activity and initiation of RTSs (%) for the segments (n) that fall in each node.

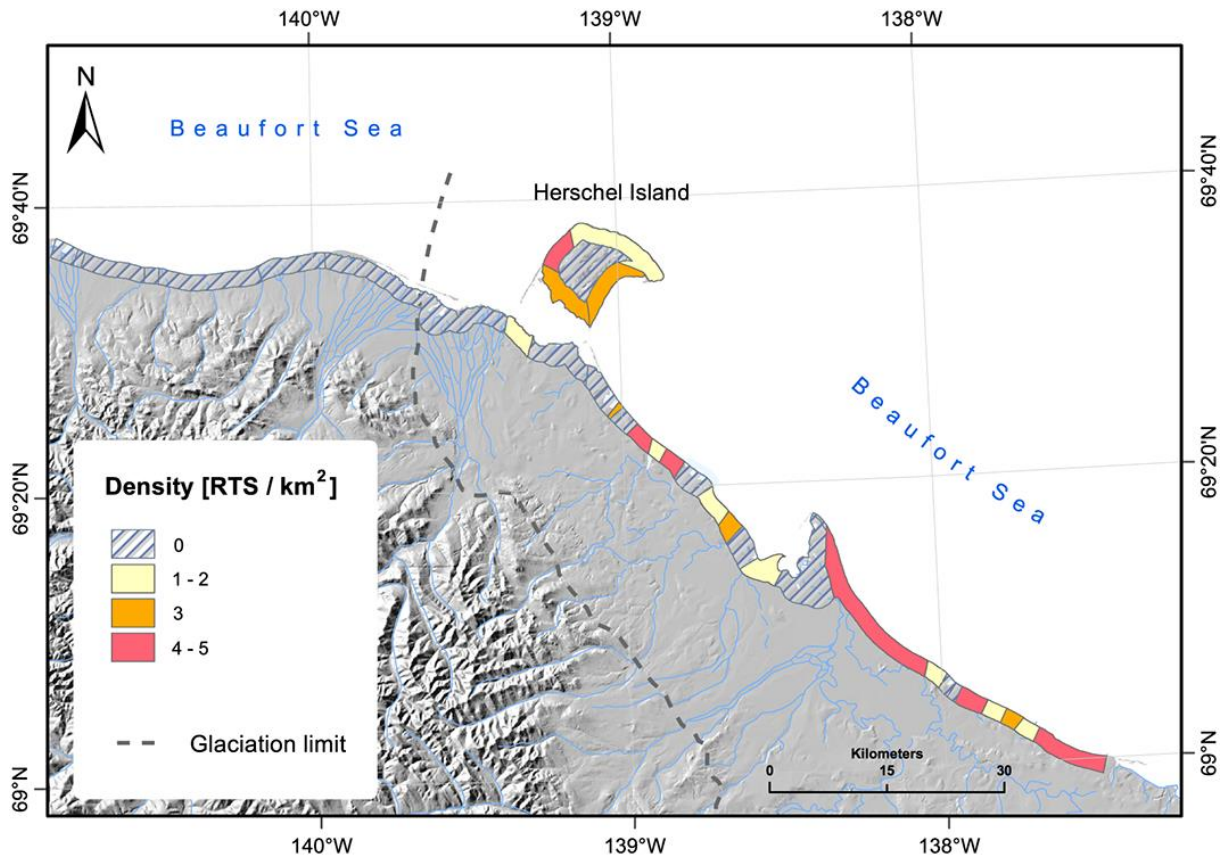


Figure 5.6: Density map of RTSs along the Yukon Coast. No RTSs were found in the formerly unglaciated area. The density varied greatly among the segments in the glaciated area.

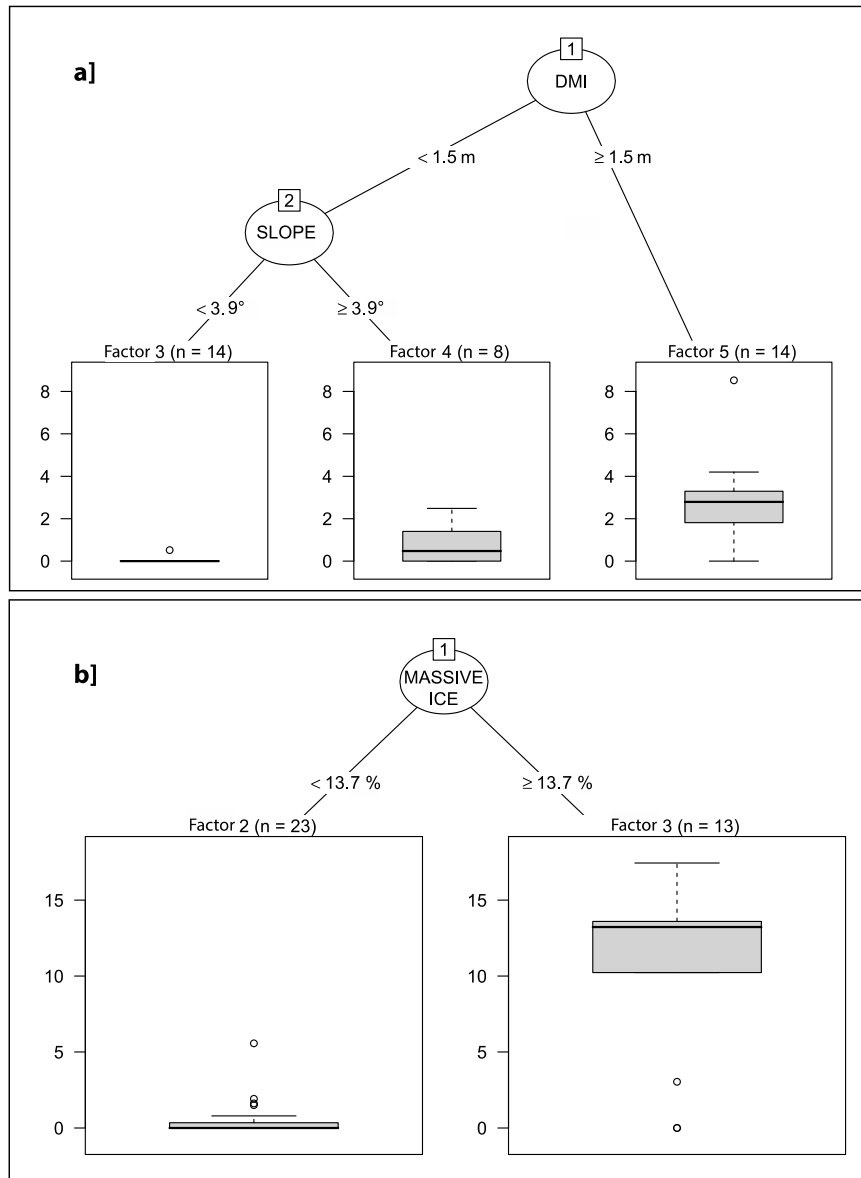


Figure 5.7: Univariate regression tree relating (a) the density and (b) the areal coverage of RTSs to the 16 environmental variables used in the model; n indicates the number of segments included in each node. Ground ice characteristics (DMI, the thickness of the massive ice bodies, and the percentage of massive ground ice) were the most influential factors for explaining the density and coverage of RTSs (Figure 7a). The box and whisker plots display variation in density (#RTS per km²) for the segments (n) that fall in each node. Slope angle explained the differences in coverage (ha) of RTSs (Figure 7b). The box and whisker plots display the variation in coverage for the segments (n) that fall in each node. Secondary factors were not named because they were not considered having a relative importance by the model.

5.5 Discussion

5.5.1 Characteristics and distribution of RTSs along the Yukon Coast

With a density of 1.2 RTSs per km of coast, the Yukon Coast is one of the Arctic areas most affected by retrogressive thaw slumping [Segal *et al.*, 2016; Kokelj *et al.*, 2015a; Lacelle *et al.*, 2010]. The Yukon Coast is undergoing a period of active slumping: 71% of all mapped RTSs were active in 2011 and 60% of the total number of RTSs initiated after 1972. Our results confirm the observations made by Lantuit *et al.* [2012a] and Wolfe *et al.* [2001] who show that RTSs increased greatly between 1970 and 2000 in some areas of the Yukon Coast: the number of RTSs increased by 22% on Herschel Island and by 25% along the eastern part of the Yukon Coast. With a median size of 0.16 ha, RTSs initiated after 1972 were smaller than RTSs, which initiated prior to 1972 (0.24 ha). Stable RTSs were 7 times larger than active RTSs, however they often conjoin several former active RTSs. For polycyclic RTSs, we could only identify stable RTSs whose extent exceeded the area of the active RTSs located within them and therefore only accounted for large stable RTSs. RTSs along the Yukon Coast had a median size of 0.24 ha, relatively small compared to the size of other RTSs occurring in the Arctic: Segal *et al.* [2016] found that in other previously glaciated areas of the Canadian Arctic, RTSs size varied on average between 0.98 ha and 5.35 ha, with the majority of the disturbances larger than 0.05 ha. Coastal RTSs were the smallest (0.98 ha on average in the Jesse Moraine area, Banks Island), but still larger than along the Yukon Coast. One reason for this peculiarity may be that compared to Segal *et al.* [2016] the high-resolution dataset from 2011 used in our study allowed identification of RTSs as small as 0.01 ha. However, when removing RTSs smaller than 0.05 ha, the median size of the RTSs still remained low with 0.28 ha. Overall, 30% of the active RTSs identified in 2011 developed on surfaces occupied by stable RTSs in the 1970s. The reactivation of formerly stabilized surfaces, combined with the small size of the RTSs in the region, reflects the polycyclic behavior of the RTSs along the coast. In coastal environments, stable RTSs can reactivate when erosion exposes buried massive ice bodies, often as a result of storm events [Lantuit *et al.*, 2012a; Kokelj *et al.*, 2009b; Lewkowicz, 1987b].

5.5.2 Terrain factors explaining RTS occurrence

Ground ice characteristics favored RTS occurrence and extent along the coast. As observed by Harper [1990], ground ice plays a crucial role in influencing coastal morphology and stability along the Yukon Coast and is of crucial importance for RTS development.

While focusing on coastal RTS dynamics, our results confirm the general patterns identified in previous studies on RTS occurrences in northern Canada. Kokelj et al. [2017] mapped RTSs in northern Canada and highlighted the strong correlation between RTS development and ice-rich moraine deposits found on the eastern margin of the late Wisconsinan glaciation. Our results support these observations; the density and coverage of RTSs along the Yukon Coast were higher on moraine deposits. Moraine deposits usually combine all factors favorable for RTS development: they form crested ridges made up of a mixture of sediments and ice - including massive ground ice - that had been deposited during the melt of the ice sheet, and remained as permafrost under cold conditions.

The thickness of the massive ice body was the most important factor explaining high densities of RTSs along the Yukon Coast. Lantuit et al. [2012a] showed that during polycyclic RTS activity, the first phase of RTS development depends on the pace of the headwall retreat and the angle of repose of the slump floor, while the second stage of RTS development depends on the depth of the remaining massive ice body and the coastal retreat rate. Our results – through the relationship between the density of RTSs and the thickness of the massive ice body – suggest that not only the depth but also the thickness of the massive ice bodies plays a role in the polycyclic nature of RTSs.

The volume (thickness and area) of massive ice was the main factor explaining the expansion of RTSs within a segment. In the case of reactivated RTSs, the size of the RTSs depends on the volume of the buried massive ice remaining underneath the stabilized RTS surface on which they reactivate. RTSs grow until ground ice is exhausted. This is supported by Burn [2000] following observations of RTSs along the Stewart River in Mayo, Canada. However, RTSs can stop growing if the remaining massive ice bodies become buried under thawed sediments. The condition for a RTS to grow therefore depends on the capacity of the slump headwall to remain exposed [Lantuit et al., 2012a], which is constrained by the geometry of the RTS [Lewkowicz, 1987a].

5.5.3 Coastal processes

Our statistical analyses highlight the direct relation between coastal geomorphology and RTS activity and initiation (Fig. 5.8). Active RTSs occurred in areas where the slope angle was greater than 3.9° and where cliff heights were higher than 11.0 m. RTSs that were initiated after 1972 were found on terrain with slope angles greater than 5.9° . Slope angle was one of the main factors sustaining RTSs in ice-rich permafrost terrain. In general, RTSs occurred only on terrain with slopes angles steeper than 3.9° and more specifically on terrain with mean slope angles of 6.2° . These results are in the same range as the observations from

Lantuit et al. [2012a] for coastal RTSs (Herschel Island; mean slope angles of 6.2° and 5.8° for stable and active RTSs, respectively) and Balsler et al. [2014] for inland RTSs (Noatak Basin; mean slope angles of 9.4°). The slope angle has an effect on the activity of RTSs because it influences the evacuation of thawed material, which is a precondition to expose massive ice and to perpetuate headwall retreat [Lantuit et al., 2012a; Lacelle et al., 2010]. The condition for a slope to remain at an angle that allows the headwall to be exposed depends on the intensity of coastal erosion processes on the coast.

Wave erosion at the base of the slope can lead to slope destabilization, thus triggering or reactivating RTSs through removal of the insulating soil layer fronting the massive ice [Lantuit et al., 2012a, 2008; Burn and Lewkowicz, 1990; Aré, 1988]. The intensity and direction of the waves lead to different dynamics along the coast [Harper, 1990] and are major factors controlling coastal erosion and potential RTS initiation. Contrary to our initial hypothesis, coastal erosion rates did not have a direct influence on the response variables in our model. The erosion rates used in the model did not emerge as significant predictors. This could be due to discrepancies related to the temporal scale of our dataset, or it could suggest an indirect influence of coastal erosion on the dynamics of coastal RTSs. We used mean erosion rates that were calculated for each segment over long time spans, 1972-2011 [Irrgang et al., 2017]. Those long-term erosion rates average out the effects of discrete storm events which crucially influence the magnitude of coastal erosion along the Yukon Coast [Lantuit et al., 2012a]. In turn, RTSs can also affect the rates of shoreline movement along the Yukon Coast [Obu et al., 2017a] by offsetting coastal retreat by sediments release to the shore and nearshore. For example, the shoreline may advance during a period of a RTS activity due to the accumulation of sediment on the shore, which forms the slump lobe. This fluctuating supply of material from the eroding RTS, combined with inter-seasonal variability in wave energy, can weaken the effect of waves in eroding the coast. The complexity of this interaction makes it challenging to estimate the impact of coastal erosion on RTS dynamics using long term averaged coastal erosion rates.

However, we suggest that coastal erosion processes – through their destabilization of the coast – contribute to maintaining RTSs activity and setting the pace of polycyclicality. Erosion impacts the dynamics of RTSs along the Yukon Coast through its indirect action on coastal geomorphology. Coastal erosion processes maintain preconditions for RTSs [Lantuit et al., 2012a]; they expose buried massive ice bodies and sustain the slope angle of the RTS floors, allowing further retreat of the headwall [Lewkowicz, 1987b].

5.6 Conclusions

From the 2011 imagery, we identified 287 RTSs along a 238 km coastal segment of the Yukon Coast. All RTSs occurred within the boundary of the last glacial maximum. The majority of the RTSs along the coast were polycyclic and active. Our study defined the main terrain factors controlling the development of RTSs along a 238 km coastal segment of the Yukon Coastal Plain. Geomorphology – slope angle and cliff height – explained the occurrence of both active coastal RTSs and coastal RTSs that initiated after 1972. Thickness of the massive ice bodies and slope angle explained high density of coastal RTSs. Likewise, areal coverage of coastal RTSs was related to the amount of massive ice within a segment. RTSs grow until all ice is thawed or is buried under thawed sediments [Burn, 2000].

Coastal erosion processes were not fully reflected by coastal erosion rates. However, by their action on coastal geomorphology, coastal erosion processes maintain the preconditions for reactivation of RTSs and thus have an indirect effect on the development of RTSs. This is the first study showing terrain controls on coastal RTSs using statistical analyses at a regional scale. It confirms earlier observations on terrain control over RTSs in the Arctic [Segal *et al.*, 2016; Kokelj *et al.*, 2015a; Lantuit *et al.*, 2012a; Lewkowicz, 1987b].

We emphasize the need for large-scale studies of RTSs to evaluate their impact on the ecosystem and to measure their contribution to the global carbon budget.

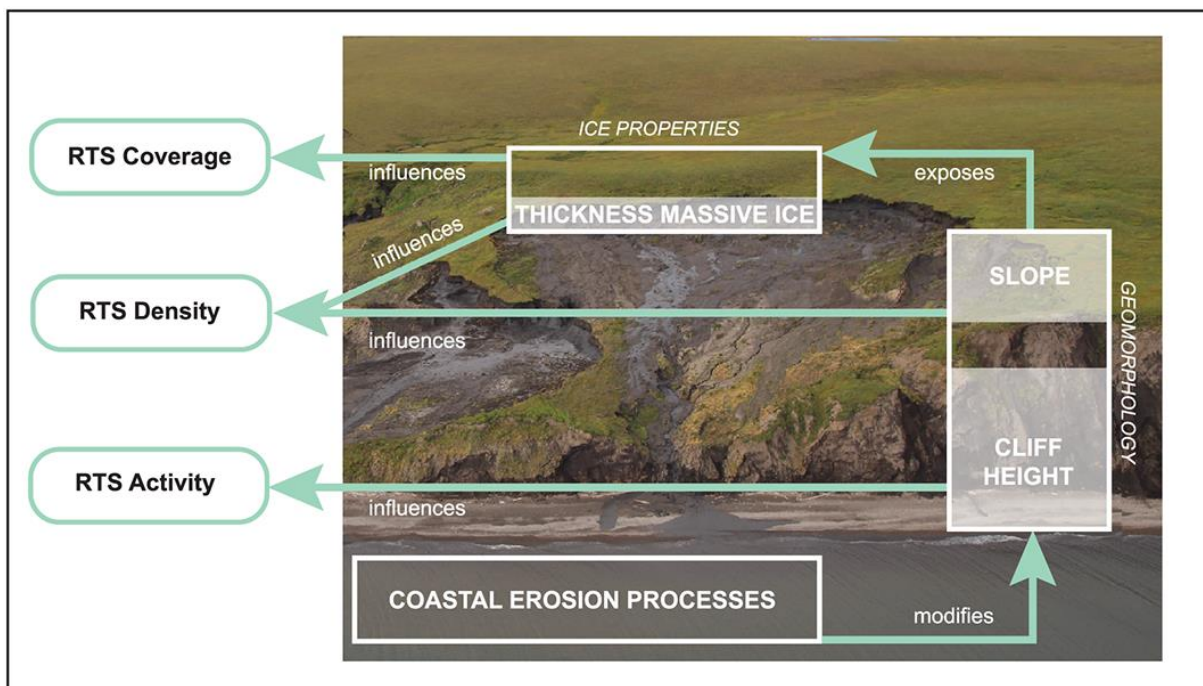


Figure 5.8: Scheme illustrating the processes contributing in the development of coastal RTSs, highlighted by the model. In the model, the response variables (RTS coverage, density, and activity) were explained by a complex interaction between the environmental variables (coastal erosion processes, geomorphology, and massive ice content). Thickness of the massive ice bodies and slope angle explained high density of coastal RTSs. Likewise, areal coverage of coastal RTSs was related to the amount of massive ice within a segment. Coastal erosion

processes indirectly create the preconditions for the development of coastal RTSs by destabilizing coastal geomorphology and maintaining massive ground ice exposed.

Acknowledgements

This study was supported by the Helmholtz Association through the COPER Young Investigators Group (VH-NG-801) and by the Alfred Wegener Institute in Potsdam. J. L. Ramage was financially supported by a PhD stipend by the University of Potsdam, by the Swedish National Board of Student Aid (Centrala studiestödsnämnden, CSN), and the ÅForsk Foundation. A.M. Irrgang was financially supported by a PhD stipend from the German Federal Environmental Foundation. It is a contribution [number 20170021] of the Natural Resources Canada, Canadian Crown Copyright reserved. The data used are listed in the references, tables, supplements and the PANGAEA repository at doi:10.1594/PANGAEA.869573. We acknowledge the detailed reviews and constructive comments of the reviewers.

Context

In the previous chapters rates of shoreline change, as well as the resulting carbon and sediment fluxes were quantified. The goal of the following chapter is to shed light on the impacts of coastal dynamics on the human component. Even though no permanently occupied settlements are existent along the Yukon coast, it is extensively and very diversely used by humans. While the Inuvialuit are for example using the coast for pursuing their traditional lifestyle (e.g., whaling), the sparse infrastructure in form of two landing strips is still used for the maintenance of the warning systems. The focus of the next chapter lays in showing how present and future coastal changes may influence living along the coast.

One of the main results of the PYRN Young Researchers workshop session called “Community-based research – Do’s and Don’ts in Arctic Research”, held prior to the ICOP 2016 conference was to earlier involve interested Arctic community members in Arctic research [Lenz *et al.*, 2017]. Taking this outcome into consideration, the following study was conducted with Richard Gordon, Inuvialuit Elder and Chief Ranger of Qikiqtaruk – Herschel Island Territorial Park, being part of the study from the stage of the study design on.

Impacts of past and future coastal changes on the Yukon coast – threats for cultural sites, infrastructure and travel routes

ABSTRACT

The Beaufort Sea coast of the Yukon Territory, Canada, is a highly dynamic landscape. Cultural sites, infrastructure, and travel routes used by the local population are particularly vulnerable to coastal erosion. To assess threats to cultural sites, infrastructure and travel routes, rates of coastal change for a 210 km length of the coast were analyzed and combined with socio-economic and cultural information. Rates of coastal change were derived from aerial imagery from the 1950s, 1970s, 1990s and 2011. Using these data, conservative (S1) and dynamic (S2) shoreline projection scenarios were constructed to predict shoreline positions for the year 2100. The locations of cultural features in the archives of a Parks Canada database, the Yukon Archeology Program, and derived from a review of existing literature were combined with projected coastal changes. Between 2011 and 2100, 846 ha (S1) and 2243 ha (S2) are expected to be eroded, which results in a loss of 46% (S1) to 50% (S2) of all cultural sites by 2100. The last actively used camp and two nearshore landing strips will likely be threatened by future coastal processes. Future coastal erosion and sedimentation processes will increasingly threaten cultural sites and influence travelling and living along the Yukon coast.

A manuscript with equal content is in review in the Journal: *Arctic Science*.

Irrgang, A.M., H. Lantuit, R. Gordon, A. Piskor and G.K. Manson (in review). Impacts of past and future coastal changes on the Yukon coast – threats for cultural sites, infrastructure and travel routes. *Arctic Science*.

6.1 Introduction

The Beaufort coast of the Yukon Territory is extensively used by the Inuvialuit and other Indigenous and non-Indigenous peoples. Settlements along the coast were present till the middle of the 20th century [Nagy, 1994; Thomson, 1998] reflecting the intimate relationship between the Inuvialuit and the coast [Nagy, 1994; Alunik *et al.*, 2003]. Thus, many cultural sites which give insight into the Inuvialuit way of life prior to contact with Europeans are situated along the Beaufort coast. Rare artifacts from their direct ancestors, the Thule Inuit, enrich the archaeological record of this region [Friesen and Arnold, 2008; Arnold, 2016; Friesen, 2016]. Also, numerous artifacts dating from the early 19th century, after the arrival of the first Europeans, can be found in the area; these cultural materials are evidence of the early explorers [Franklin, 1828, Amundsen, 1908], the whaling era [Bockstoe, 1986] and the presence of missionaries [Saxberg, 1993]. More recent history shows that the Yukon coast became both strategically and economically important in the last decades. During the cold war, three Distant Early Warning (DEW) line stations were built along the Yukon coast as part of a strategy to mitigate against attack by intercontinental ballistic missiles and these stations remain active as part of the North Warning System [Neufeld, 2002; Lackenbauer *et al.*, 2005]. Further, since the 1970s, the region has been episodically explored for the exploitation of potentially rich oil and gas resources [INAC, 2012, 2017b].

Roughly two-thirds of the Yukon coast is part of Ivvavik National Park. The archaeological legacies of Ivvavik National Park were inventoried systematically in the years of 1996 and 1997 [Thomson, 1998], and are supplemented by more detailed studies at the sites of Clarence Lagoon [Lyons, 2004], Nunaaluk Spit [Thomson, 2009], and Niaqulik Spit [Adams, 2004]. The archaeological studies were accompanied by coastal erosion studies, conducted at five main survey sites: Qainniurvik (Clarence Lagoon), Nunaaluk Spit, Qargialuk (Catton Point), Ikpiyuk west (Stokes Point west) and Niaqulik [Solomon, 1996; Forbes, 1997]. No other systematic analysis of archaeological sites has been conducted along the remaining Yukon mainland coast.

Un-lithified and ice-bonded coasts are particularly prone to coastal erosion, as is reflected in their high retreat rates [Brown *et al.*, 2003; Vasiliev *et al.*, 2005; Mars and Houseknecht, 2007; Jones *et al.*, 2009a; Lantuit *et al.*, 2012b; Günther *et al.*, 2013, 2015; Barnhart *et al.*, 2014a; Overduin *et al.*, 2014; Gibbs and Richmond, 2015; Obu *et al.*, 2017a]. Erosion rates can reach as high as -9 m a^{-1} along the Yukon coast [Irrgang *et al.*, 2017] and coastal erosion and flooding have the potential to put cultural heritage, existing infrastructure and travel routes at high risk [Jones *et al.*, 2008; Forbes, 2011; Radosavljevic *et al.*, 2015; Stern and

Gaden, 2015]. Many cultural sites along the Beaufort mainland coast, as well as along Qikiqtaruk (Herschel Island), have been or are about to be eroded [*Jones et al., 2008; Friesen, 2015; Radosavljevic et al., 2015; O'Rourke, 2017*]. Investigations of the DEW line site at Qamaqaaq (Komakuk Beach) show that the landing strip has been eroding on average by approximately -1 m a^{-1} since the 1950s [*Solomon, 1998; Konopczak et al., 2014*].

The objectives of this study are to assess the impacts of former and future coastline changes on cultural sites, infrastructure and travel routes in order to better understand how coastal dynamics are influencing living and traveling along the Yukon coast, and threatening evidence of past human activity and habitation.

6.2 Study Area

The study area spans approximately 210 km of the Yukon coast, from the international border with Alaska in the west to Tapqaaq (Shingle Point) in the east (Figure 6.1) and comprises the 10 km to 40 km wide Yukon Coastal Plain. Qikiqtaruk (Herschel Island) is not included in the study area. During the Wisconsinan Glaciation, the Laurentide Ice sheet extended to the west as far as Firth River and roughly two-thirds of the study area was covered by ice [*Rampton, 1982; Fritz et al., 2012*]. Fine-grained lacustrine and alluvial sediments occur west of the Firth River. East of the Firth River, fine-grained lacustrine and outwash plains as well as rolling moraines are prevalent in the surficial geology [*Rampton, 1982*]. Qikiqtaruk (Herschel Island) became separated from the mainland most probably between 650 and 1600 years ago by a narrow and shallow ($< 3 \text{ m}$) channel, known as Workboat Passage (Canadian Hydrographic Service, 1986; Burn, 2009; Burn, 2016). Backshore elevations vary from around 6 m near the Canadian – U.S. American border to 2 m within Workboat Passage, and up to 60 m east of Tikiraq (Kay Point). Ground-ice contents are high along the entire coast and reach as high as 74% in the formerly glaciated area where massive ground ice beds are found [*Harry et al., 1988; Couture and Pollard, 2017*]. The whole study area is underlain by continuous permafrost [*Rampton, 1982*]. Permafrost temperatures rose by $2.6 \text{ }^{\circ}\text{C}$ since 1905 [*Burn and Zhang, 2009*], which reflects the above-average rise of air temperatures in the Arctic in comparison to more temperate regions [*Kaufman et al., 2009; Richter-Menge and Mathis, 2016*].

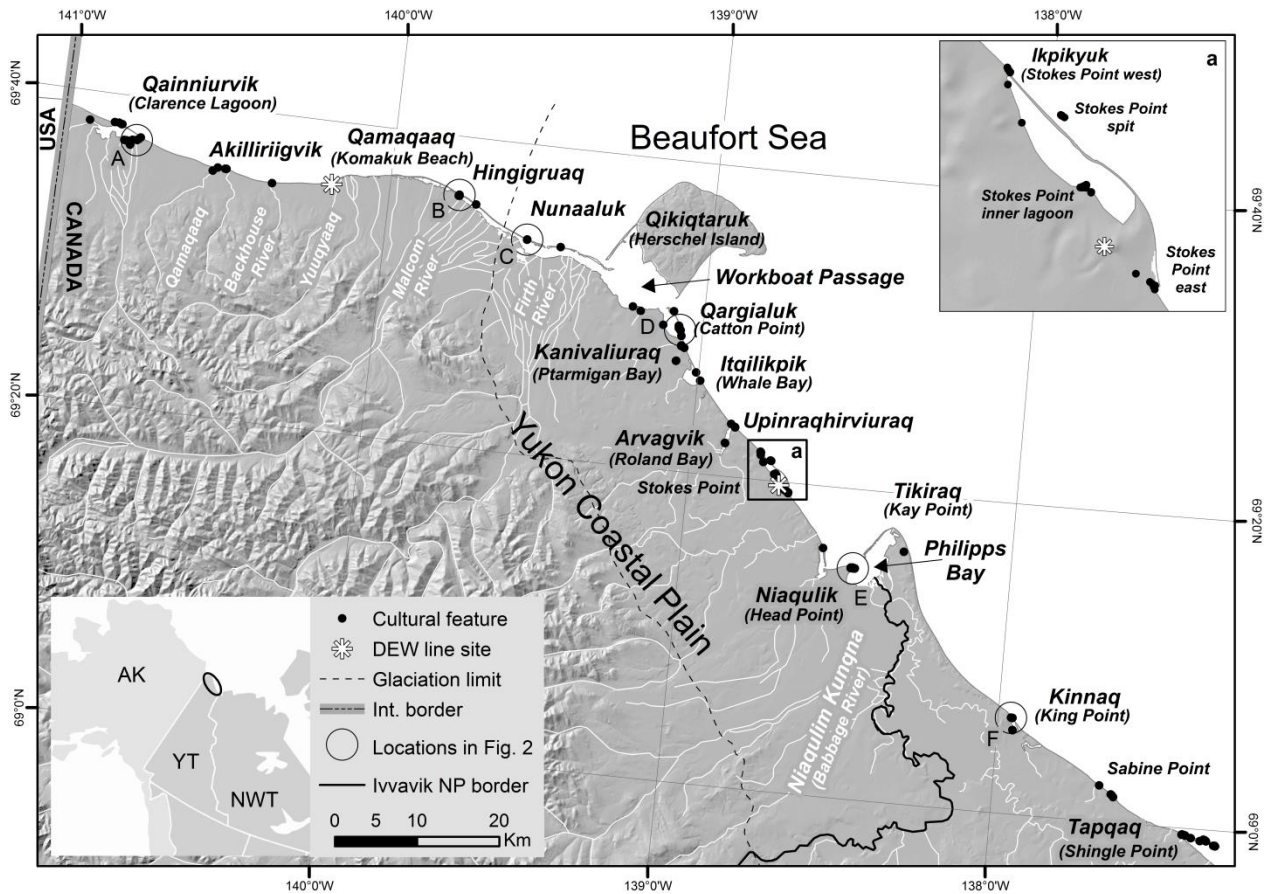


Figure 6.1: Study area of the Yukon coast showing the locations of cultural features and infrastructure. Basemap: 30 m Yukon DEM, interpolated from the digital 1:50 000 Canadian Topographic Database [Yukon Department of Environment, 2016].

The Yukon coast has diverse coastal dynamics. Mean shoreline change rates are highest in the regions west of Firth River with rates of -0.9 to -1.4 m a^{-1} and lowest in the region of Tapqaq (Shingle Point) with -0.1 m a^{-1} [Irrgang *et al.*, in review]. However, locally along gravel features, for example along the barrier islands of Nunaaluk Spit and the spit of Tapqaq (Shingle Point), high accumulation rates of up to 5 m a^{-1} occur [Irrgang *et al.*, in review]. Coastal dynamics are limited to the ice-free period which occurs from the end of June to early October [Galley *et al.*, 2016]. Storms, which are very effective in forcing coastal erosion and accumulation, peak in October during ice freeze up [Hudak and Young, 2002; Atkinson, 2005]. The mean maximum wind speed in October is 12.8 m s^{-1} for the Beaufort Sea [Atkinson, 2005]. Most common wind directions are from the south-east and north-west, however the storms most effective in causing coastal change originate from the north-west [Hill *et al.*, 1991b; Hudak and Young, 2002; Manson *et al.*, 2005; Manson and Solomon, 2007]. Astronomical tides are semidiurnal and with amplitudes of 0.3 to 0.5 m in the micro-tidal range [Harper, 1990]. Sea level rise in this region amounts to approximately 3.5 ± 1.1 mm a^{-1} [Manson and Solomon, 2007].

Infrastructure within the study area is sparse. The two DEW line stations at Qamaqaaq (Komakuk Beach) and Ikipikyuk (Stokes Point) with their respective landing strips are the only permanent structures [Lackenbauer *et al.*, 2005]. The landing strip at Qamaqaaq (Komakuk Beach) is built on approximately 6 m high, flat polygonal tundra, while the landing strip at Ikipikyuk (Stokes Point) is built on a set of approximately 1 m high beach ridges. Transportation along the Yukon coast during the ice-free season is mainly done by boat. Workboat Passage is an important travel route which is taken by local travellers in order to avoid navigating the potentially rough water north of Qikiqtaruk (Herschel Island) and is also used as shelter by barges. Pauline Cove, a former Inuvialuit and whalers settlement at Qikiqtaruk (Herschel Island) [Bockstoece, 1986] is part of the Qikiqtaruk- Herschel Island Territorial Park and is well-frequented by local travellers. Along the mainland coast, other than a few widely spread single cabins, the only regularly used remaining camp is at Tapqaaq (Shingle Point). Since the abandonment of the last settlements in the 1950s, no settlements are present along the Yukon coast [Nagy, 1994].

6.3 Methods

6.3.1 Data for shoreline projections

The calculation of shoreline projections is based on shoreline change data from Irrgang *et al.* [in review]. The shoreline position was digitized using orthorectified aerial images from the 1950s, 1970s, 1990s and for 2011 on GeoEye-1 and WorldView-2 satellite images [Digital Globe, 2014, 2016]. The Esri ArcGIS extension Digital Shoreline Analysis System (DSAS) version 4.3 [Thieler *et al.*, 2009] was used to calculate shoreline change rates in the study area for three time periods, being 1950s-2011, 1970s-1990s and 1990s-2011. A total of 1967 transects at 100 m alongshore intervals were analysed to obtain annual mean rates of change using the method of end point rates (EPRs) [Thieler *et al.*, 2009]. The coastal landform classification from Irrgang *et al.* (in review) was used to associate the change (i.e., acceleration or deceleration) of the EPRs to different coastal landforms. This information was used for a differentiated shoreline projection (section 3.1.2). The landforms were distinguished in the 2011 images and were grouped into five classes: 1. beach, barrier island, spit, 2. inundated tundra, 3. tundra flats, 4. tundra slopes and 5. active tundra cliff. (Table 6.1, after Irrgang *et al.*, in review).

Table 6.1: Coastal landform classification.

Class number	Coastal landform class	Definition
1	Beach, barrier island, spit	Subaerial sand and gravel beaches which are surrounded by water from both sites, such as spit extensions from the mainland, barrier islands fronting the mainland, lagoons and river inlets
2	Inundated tundra	Tundra inundated due to thaw subsidence and/or coastal flooding as an effect of sea level rise. This class includes wetlands and tidal flats.
3	Tundra flats	low lying tundra with no evident active cliff or inactive cliff
4	Tundra slopes	Inactive cliffs and inactive retrogressive thaw slumps which are flattened and vegetated due to the absence of coastal erosion
5	Active tundra cliff	Cliffs and bluffs which are actively eroding

6.3.2 Shoreline projection for the conservative scenario (S1)

In the conservative scenario (S1), a purely linear shoreline projection was used. S1 is based on the EPRs from the 1950s to 2011. The EPR at each transect was multiplied by the number of years between 2011 and 2100 (89 years) to derive a transect-wise projected shoreline using ArcMap 10.3. Since this approach uses rates of coastal change which were averaged over 60 years, the effects of severe storm events are smoothed. Thus, we consider the S1 scenario the “better case” scenario for future shoreline evolution.

6.3.3 Shoreline Projection for the dynamic scenario (S2)

In the dynamic scenario (S2), a different strategy to project shoreline position was used. We used the changes in EPRs from the 1970s to 1990s period to the 1990s to 2011 period to project the shoreline position.

The transect-wise change in EPR was calculated by comparing the EPR from the 1970s to 1990s to the EPR from the 1990s to 2011. To do this, a change index was calculated for each transect as follows:

$$Ci = (EPR_{1990s-2011}) / (EPR_{1970s-1990s}) , \quad (6.1)$$

where Ci is the change index, $EPR_{1990s-2011}$ is the rate of change from the 1990s to 2011 and $EPR_{1970s-1990s}$ is the rate of change from the 1970s to 1990s. A median change index was then calculated for each coastal landform class. For the coastal landform classes 1, 2 and 3 (Table 6.1), the calculations resulted in a net acceleration of shoreline changes, with positive change indexes of 1.86, 1.24 and 1.41, respectively. For the coastal landform classes 4 and 5 (Table 6.1) a net deceleration of shoreline changes was calculated, with negative change indices of -1.46 and -1.25, respectively.

The EPRs from the 1950s-2011 period were then multiplied by the respective change index to estimate the EPRs for the 2011-2030 period. The same method was then used to project rates of change to 2100 and subsequently project the shoreline position in 2100. This approach results in much greater EPRs for all classes with a positive change index, which cover the majority of the study area. Thus we consider the S2 scenario the “worse case” scenario for future shoreline evolution.

6.3.4 Positioning and characterizing of cultural sites

The positions and character of cultural features were provided for Ivvavik National Park between the Canada- U.S. American border and the Babbage River Delta by Parks Canada [Parks Canada Agency, 2007] (Figure 6.1). The Parks Canada database was expanded by combining it with a database of cultural features from the Yukon Archaeological Program [Yukon Government, 2016] which includes features outside Ivvavik National Park. The accuracy of points within the combined database is considered to be approximately 500 m which is lower than the projected average net shoreline movement by 2100. Since this would influence the calculations of the loss of cultural features, the point positions were improved, where possible. Therefore, GeoEye-1 and WorldView-2 satellite images from 2011 [Digital Globe 2014, 2016], geo-coded aerial images from the 1950s and 1970s [Irrgang *et al.*, in review], aerial video collected by the Geological Survey of Canada in 1984 and 1999 [Forbes and Frobel, 1986, Solomon and Frobel, 1999], the location descriptions from Thomson [Thomson, 1998], site visits and imagery interpretation were used to review the position of each site. We were able to expand the original database by adding more detailed information about the nature and quantity of the features. In total, 137 points were added to the database, even though not all cultural features described in Thomson [1998] could be positioned on the imagery. The sites were separated into three groups: 1) housing, 2) burial sites and 3) miscellaneous features (Table 6.2).

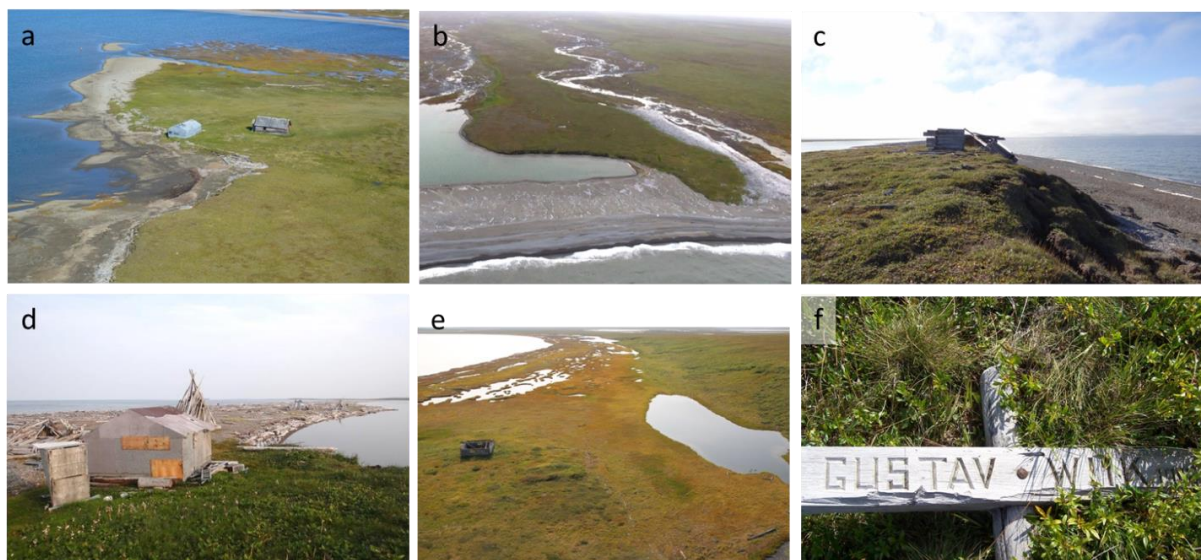


Figure 6.2: Photos showing cultural features along the Yukon coast. From west to east: A) Qainniurvik (Clarence Lagoon): One wooden store house and one sheet metal structure at a Hudson's Bay Company post, B) Nunaaluk Spit: Site of the former Inuvialuit settlement Hingigruaq, C) Nunaaluk Spit: Relicts of a cabin built by Alexander Steffanson in 1934, D) Qargialuk (Catton Point): Modern cabin together with several traditional Inuvialuit graves (possible pre-contact), E) Niaqulik Spit: Relicts of a cabin and the outline of the foundation of a second building – both were part of an Inuvialuit settlement, F) Kinnaq (King Point): grave of Gustav Juel Wiik, who died in 1906 at the Gjøa expedition led by Roald Amundsen. Grave was moved inland several times [Hill, 1990]. The site locations are indicated in Figure 6.1.

Table 6.2: Cultural feature classes

Cultural feature class	Features included
Housing	Tent structures, sod houses and cabins
Burial sites	Inuvialuit and European burial sites
Miscellaneous features	Ice houses, lean-tos, windbreaks, drying racks, stages, refuse areas and unidentified or not further defined features and wooden structures

6.3.5 Calculation of losses under the S1 and S2 scenarios

Using Esri ArcMap 10.3, two polygon feature classes were created out of the S1 shoreline and the 2011 shoreline and the S2 shoreline, and the 2011 shoreline. The respective polygons were used to identify the cultural features that might be affected by shoreline changes under the S1 and S2 scenarios and to quantify future Yukon land loss along the coast. To provide more detailed information at permanent infrastructure, the landing strips of the DEW line stations at Qamaqaaq (Komakuk Beach) and Stokes Point were digitized and the airstrip polygons were used to quantify the length of landing strips which could be eroded under both scenarios.

6.3.6 Estimation of future dynamics in very dynamic areas

Workboat Passage and Tapqaq (Shingle Point) are both areas of high importance for local transportation and recreation. Workboat Passage is enclosed by gravel spits, barrier islands and sand bars. Tapqaq (Shingle Point) is also a gravel spit. The S1 and S2 scenarios were not capable of drawing reasonable pathways of future coastal dynamics, because the past sediment movements were too dynamic. Instead, a detailed investigation of the shape of these gravel features was done for the 1950s, the 1970s and 2011 in order to understand their past development. This information is used to draw scenarios for the future development of Workboat Passage and Tapqaq (Shingle Point).

6.4 Results and discussion

6.4.1 Past and future shoreline change rates

The mean rate of change from the 1950s to 2011 period amounts to -0.7 m a^{-1} and varies considerably within the study area [Irrgang *et al.*, in review]. A general eastward decrease in shoreline change rates was identified. The highest mean shoreline change rates were measured from Qikiqtaruk (Herschel Island) towards the west, whereas the lowest shoreline change rates were measured in the east between Kinnaq (King Point) and Tapqaq (Shingle Point) (Figure 6.1). We attribute this pattern to the exposure of the western part of the coast to the most effective storms which originate from the northwest [Solomon, 2005; Manson and Solomon, 2007] and the comparatively low cliffs. In the eastern part of the study area, the coast is considerably higher and sheltered from northwesterly storms by its orientation towards the east and by Qikiqtaruk (Herschel Island) (Figure 6.1).

Further, a link between EPRs and coastal landforms was detected. While sections of in the coastal landform class 2 and 5 were eroding particularly fast, landforms classified 4, for instance, were more stable. Coastal segments classified as 1 were, by far, the most dynamic. Both highest rates of accumulation and highest rates of erosion were measured in this class [Irrgang *et al.*, in review].

The EPRs for the 1950s to 2011 time period build the foundation for both scenarios of future shoreline evolution. The S1 projection is solely based on the EPRs from the last 60 years. The S2 projection additionally incorporates changes of EPRs, which were calculated for each landform class (Chpt. 3.3.4).

For the S1 scenario, the mean EPR for the study area amounted to -0.7 m a^{-1} over the 2011-2100 period. The resulting mean land loss amounted to approximately -9.5 ha a^{-1} . This could lead to a total loss of land of approximately 846 ha by 2100.

For the S2 projection, the mean EPR for the study area amounted to -2.2 m a^{-1} over the 2011-2100 period. The resulting mean land loss amounted to approximately -25 ha a^{-1} . This could lead to a total loss of land of approximately 2 243 ha by 2100. Since the change indices were found to be largest for the coastal landform classes 2 and 5, coastal retreat in these areas is expected to be fastest by 2100. Thus, cultural features lying in these areas are particularly prone to erosion. The landform classes 1 and 4 had negative change indices. While cultural features lying in the landform class 4 are considered to be less threatened by coastal erosion, cultural features lying in the landform class 1 are considered to be particularly threatened, because of the high natural dynamics of these landforms.

The results of the S1 and S2 scenarios show reasonable lower and upper limits of projections for future shoreline positions, but also contain some simplifications. The change indices reflect past coastal dynamics that occurred during the 1990s to 2011 time period, including duration of the open water season, frequency and severity of storms and sea level rise. Any future increases in forcing which will exceed the order of magnitude of the past forcing are not considered by either projection. Prominent amplifying forcing factors are, for example, a further acceleration of sea level rise, or a complete loss of summer sea-ice. The rapid reduction of summer sea-ice already has had major effects on the sea state of the Beaufort Sea [Stroeve *et al.*, 2011, 2014; Stammerjohn *et al.*, 2012; Jeffries *et al.*, 2013; Thomson *et al.*, 2016]. Together with the observed trend towards stronger autumn storms [Zhang *et al.*, 2004], the height of the sea state is expected to rise [Vermaire *et al.*, 2013; Thomson and Rogers, 2014]. We expect these interactions to lead to an intensification of coastal erosion. Consequently, shoreline changes might get even more severe than in the S2 projection, which we considered our worst case scenario.

6.4.2 Cultural sites

In total, 168 cultural features along the Yukon coast are found at 19 separate areas, termed cultural sites (Table 6.3). At least 11 of the cultural sites are known to be former small settlements: Qainniurvik (Clarence Lagoon), Akilliriigvik, Hingigruaq, Nuunaluk, Qargialuk (Catton Point), Itpiliqipik (Whale Bay), Ikpikyuk west (Stokes Point west), Niaqulik (Head Point), Tikiraq (Kay Point), Kinnaq (King Point) and Tapqaq (Shingle Point) [Nagy, 1994, Thomson, 1998] (Figure 6.2). Out of the 168 cultural features, 48 features were categorized as housing, 28 features were burial sites and 82 features were added to the miscellaneous features group (Table 6.2, 6.3). Ten out of 42 known features at Hingigruaq [Thomson, 1998] could be located on satellite images and aerial photographs, but the data did not allow a further characterization of these features. No cultural features from the settlements at Tikiraq

(Kay Point) and Kinnaq (King Point) could be accurately positioned. No specific information about the quantity and position of cultural features could be obtained for Tapqaq (Shingle Point), aside from the identification of roof tops on imagery. A total of 52 roof tops could be detected on the satellite imagery from 2011. Since the broad majority of identified roof tops is presumably of modern origin and no confirming material specifying the nature of these roof tops was available, we did not include these features in the statistics about cultural features losses. In the past, coastal erosion has led to the loss of 44 cultural features, 26% of the total (Table 6.3). Under the S1 and S2 scenarios, 34 and 43 additional cultural features are going to be eroded, respectively. This amounts to 20% and 26% of the total inventoried cultural features. Consequently, 46% to 52% of all recorded cultural features could be eroded by 2100. Since not all sites could be digitized, this is considered a conservative estimate. Thus, coastal erosion is causing a reduction in the diversity of cultural features, some of which have already been eroded. However, the vulnerability varies between sites. While, for example, a cemetery at Igpikyuk west (Stokes Point, west) and several features at Ikpikyuk spit (Stokes Point spit) have been lost to erosion, so far no losses have been recorded at Qargialuk (Catton Point), Itpiliqpik (Whale Bay) and Arvagvik (Roland Bay). The former settlement of Niaqulik is particularly threatened under both scenarios (Figure 6.3). In the S1 scenario, 9 cultural features are expected to be eroded, whereas under the S2 scenario all cultural features are expected to be eroded by 2100. Figure 6.3 also demonstrates the relative performance of both shoreline projections. The projection algorithms linearly extrapolate the 2011 position of the shoreline based on measured shoreline change rates, but do not account for the topography of the inland area. On the eastern shore of Niaqulik, the 1950s-2011 EPR is related to the erosion of a low-lying inundating area and is thus comparatively high (Figure 6.3). Yet, this section of coast is backed by a much higher hinterland, which will most likely not erode at similar rates. The S2 scenario probably grossly overestimates the erosion of the shoreline. Erosion will most likely decelerate when the shoreline reaches higher topography.

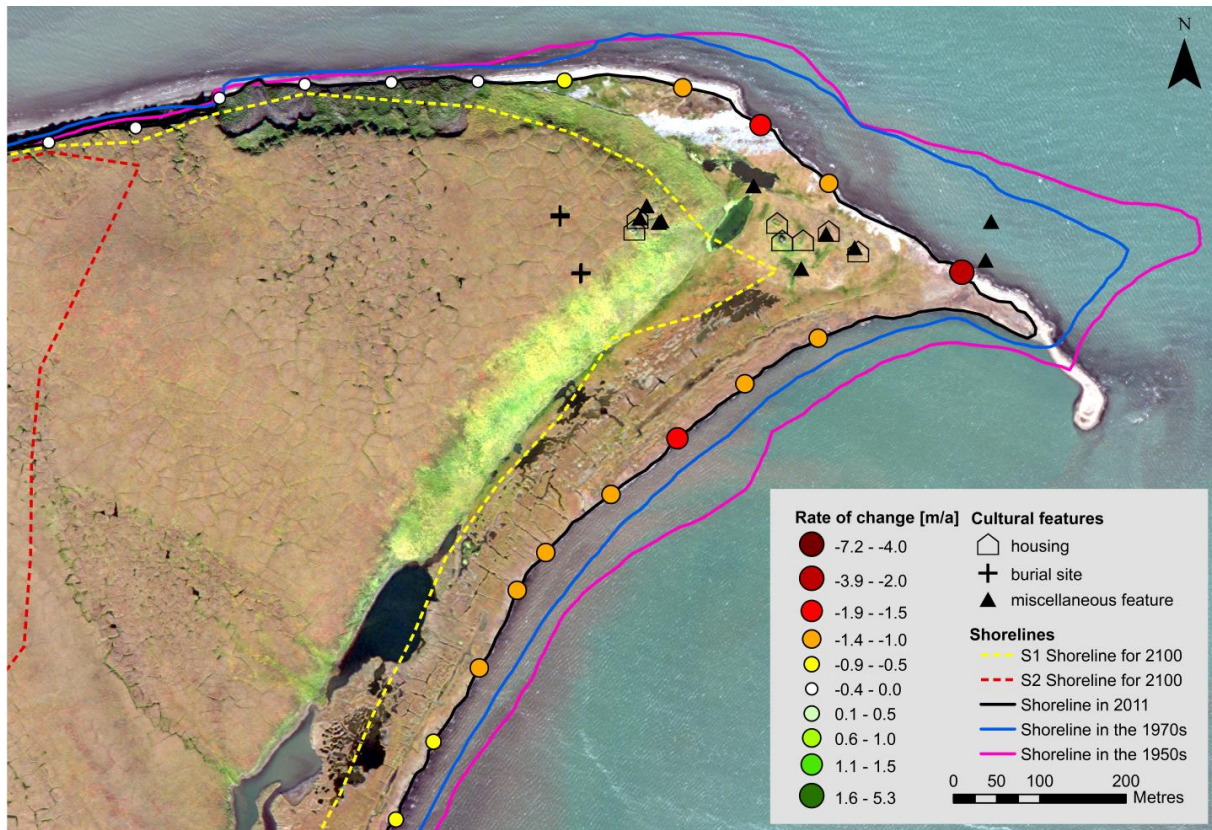


Figure 6.3: Former settlement of Niaqulik. Base image: WorldView-2 scene from August 2011.

The cultural features of the former settlement of Hingigruaq which could be digitized on the 2011 images are not considered to be threatened in either scenario (Figure 6.4). By 2100, the shoreline in the S1 and S2 scenarios is expected to be 17 m to 20 m from the site (Figure 6.4). Even though the shoreline was 70 m apart from the site in 2011, driftwood lines present at 1.8 m elevation relative to sea level and visible on the 2011 satellite images suggest that the surrounding lower-lying area is subject to large-scale flooding. Observations from Tuktoyaktuk, east of the Mackenzie River, and the Alaskan Beaufort coast to the west show that large scale flooding can inundate areas up to 2.4 m (relative to sea level) and 3.4 m (relative to sea level), respectively [Harper *et al.*, 1988, Reimnitz and Maurer, 1979]. With an elevation of 2.8 m relative to sea level, Hingigruaq is low enough to be at risk for storm surge flooding. Continued erosion together with projected rise in relative sea level up to 1 m by 2100 [NT Government, 2015; Horton, 2014] and the trend towards stronger autumn storms [Zhang *et al.*, 2004] will make Hingigruaq more vulnerable towards flooding. Hingigruaq shows that the distance of the cultural site from the coast is no systematic protection against coastal processes, specifically against episodic flooding during storms.

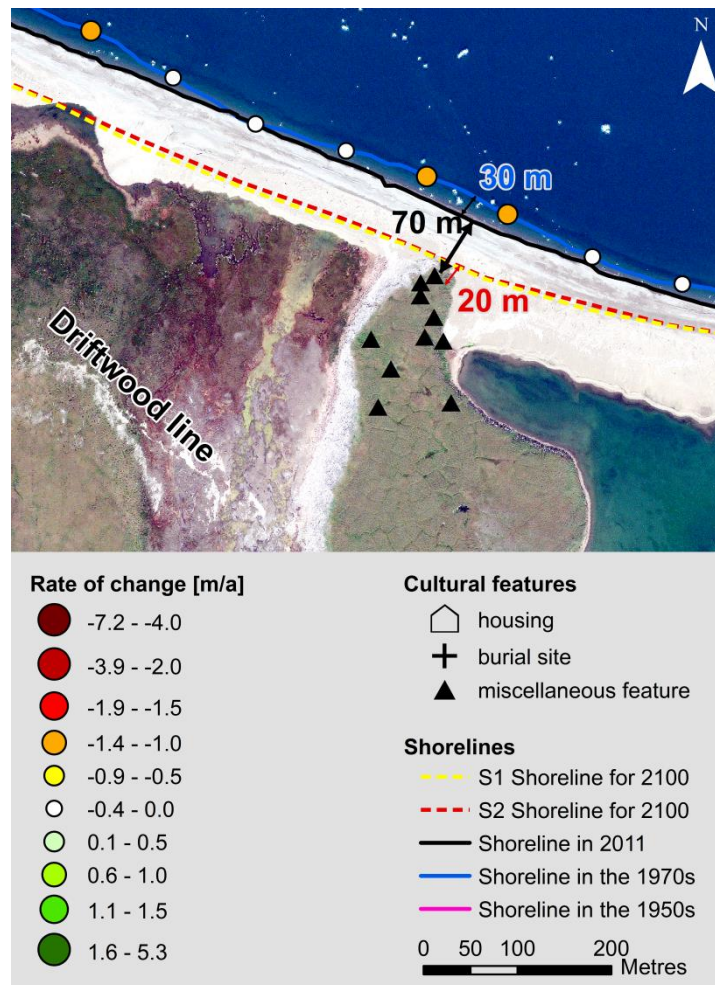


Figure 6.4: Former settlement area of Hingigruaq. Ten out of 42 known cultural features could be located on the satellite image. Some of the features which could not be located on the images are considered to have been eroded by 2011 [Thomson, 1998].

Tapqaq (Shingle Point) is the last remaining periodically occupied camp along the Yukon mainland coast (Figure 6.5). There are three areas of occupation on the spit: Down the Hill Camp, Middle Camp and Point Camp. As already stated in Chapter 6.3.4, most gravel features are too dynamic to develop reasonable shoreline projections. Thus, the past development of the spit was taken as a foundation for the estimation of future dynamics. A comparison of the area in the 1950s, the 1970s and 2011 reveals that the spit is largest in 2011. The length of the spit was approximately 6 000 m in the 1950s, and lengthened approximately 500 m to 6 500 m by 2011 (Figure 6.5). The spit widened considerably between the 1950s and 2011 in the area of Down the Hill Camp, where in 2011 it was 110 m wide (Figure 6.5, inset a). In the area between Down the Hill Camp and Middle Camp, the spit migrated 100 m to the south and narrowed from approximately 100 m to 60 m between the 1950s and 2011. In the area of Middle Camp, the spit widened from approximately 50 m in the 1950s to 100 m in 2011 (Figure 6.5, inset b). The greatest changes are in the area of Point Camp where the spit extended by approximately 500 m to the east between the 1950s and 2011 (Figure 6.5, inset

d). Some of the structures are therefore built on sediments that were deposited after the 1950s. Where the distal end of the spit was located in the 1950s with a width of 40 m, it is now as wide as 100 m (Figure 6.5, inset c). In summary, all camps lie in areas where the spit widened since the 1950s.

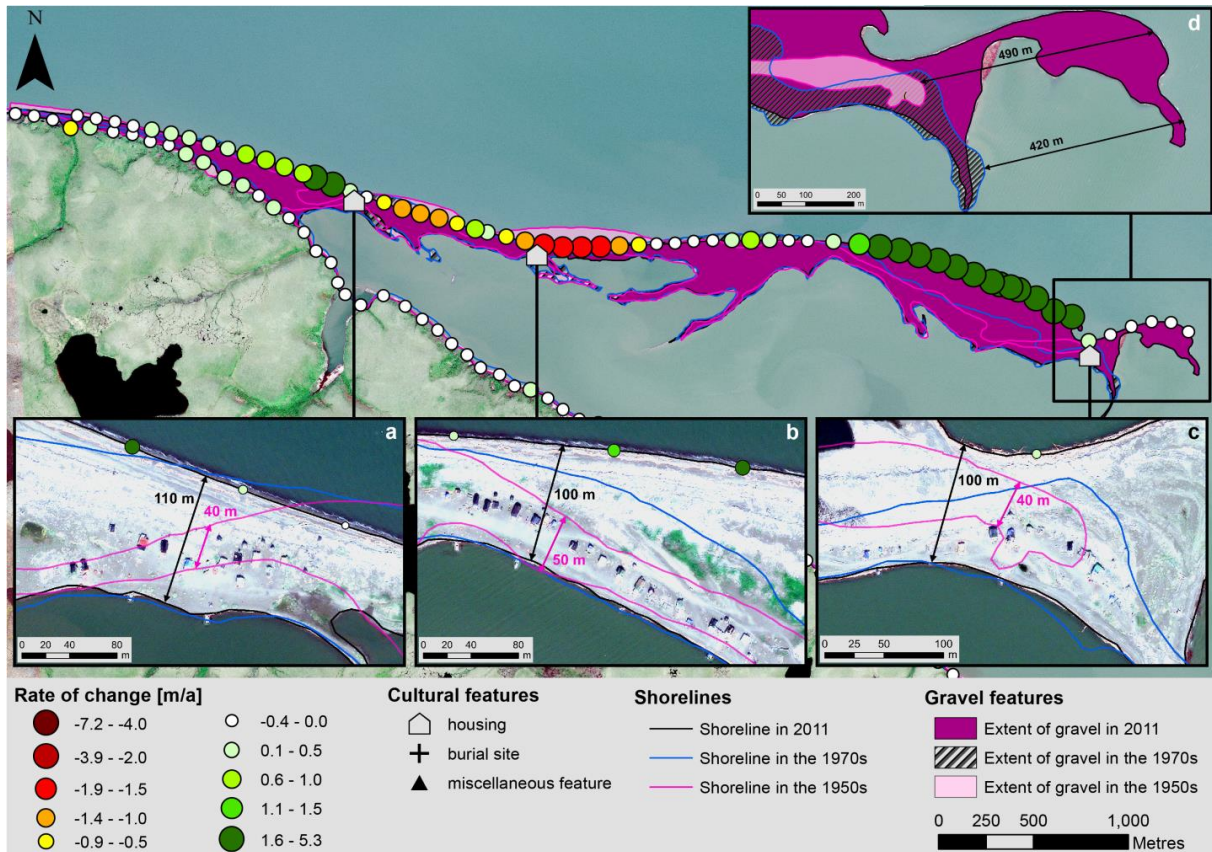


Figure 6.5: Tapqaq (Shingle Point) with its three camps. From west to east: a) Down the Hill Camp, b) Middle Camp and c) Point Camp. The upper right inset d) is a zoom on the distal end of the spit. Base image: GeoEye-1 scene from July 2011.

The shoreline north of Down the Hill Camp has been retreating since the 1950s and erosion has accelerated since the 1970s. If this process continues in the future, Down the Hill Camp could be threatened by coastal erosion. Towards the north of Middle Camp is an area which has been accumulating sediment since the 1950s and thus Middle Camp is not considered immediately threatened by coastal erosion. Point Camp is also not considered immediately threatened.

With projected relative sea level rise of up to 1 m by 2100 [NT Government, 2015; Horton *et al.*, 2014], all three camps will become more prone to the risk of periodical flooding during storms, and eventually to permanent flooding due to sea level rise. Since storms have been observed to increase in frequency and intensity with ongoing climate change [McCabe *et al.*, 2001; Zhang *et al.*, 2004; Vermaire *et al.*, 2013], the risk of spit breaching is likely to increase

[*Héquette and Ruz, 1991; Morton and Sallenger Jr., 2003*]. The most vulnerable area was found to be between Down the Hill Camp and Middle Camp because it has been decreasing in width since the 1950s. With the predicted rise in sea level [*Horton et al., 2014*], extension of the open water season [*Overland and Wang, 2007; Wang and Overland, 2009; Stroeve et al., 2011, 2014; Barnhart et al., 2015*] and increase in storminess [*Vermaire et al., 2013*], coastal erosion to the west of Tapqaq (Shingle Point) is expected to increase [*Barnhart et al., 2014b*] potentially providing more sediment to Tapqaq (Shingle Point) through alongshore drift processes.

Whether sediment supply to Tapqaq (Shingle Point) from alongshore drift will be sufficient to effectively counteract inundation caused by sea level rise remains an important question of interest, both scientifically, and for the longevity of Tapqaq (Shingle Point). A subsequent study incorporating topography (e.g., LiDAR) data and bathymetry data, combined with hydrodynamic modelling would be necessary to more accurately estimate the flood risk and breaching risk for Tapqaq (Shingle Point).

Table 6.3: Results of the cultural sites investigations. Cultural class definitions are given in Table 6.2.

Cultural site	All cultural features			Housing			Burial sites			Remaining features		
	Total number	Eroded	Eroded by 2100 (S1)	Eroded by 2100 (S2)	Total number	Eroded	Eroded by 2100 (S1)	Eroded by 2100 (S2)	Total number	Eroded	Eroded by 2100 (S1)	Eroded by 2100 (S2)
Qainniurvik	14	5	6	6	5	1	4	4	0	0	0	0
Akilliriigvik	8	3	1	1	3	1	2	1	0	0	0	0
Backhouse River	2	0	5	1	1	0	1	1	0	0	0	0
Hingignuaq	10	0	0	0	n/a	n/a	n/a	n/a	n/a	n/a	n/a	n/a
Nunaaluk	5	3	2	2	2	1	1	1	0	0	0	0
Workboat Passage	3	1	0	0	1	0	0	0	1	1	0	0
Kanivaliuraq	7	0	1	6	4	0	1	3	0	0	0	3
Qargialuk	30	0	0	0	5	0	0	0	8	0	0	0
Iptiliqpiq	3	0	0	0	3	0	0	0	0	0	0	0
Arvagvik	2	0	0	0	1	0	0	0	0	0	0	0
Upinraqhirviuraq	11	10	1	1	2	2	0	0	0	0	1	1
Ikpikyuk west	9	9	0	0	0	0	0	0	7	7	0	0
Ikpikyuk spit	6	6	0	0	2	2	0	0	0	0	0	0
Ikpikyuk lagoon	17	2	3	1	0	0	0	0	6	0	6	1
Ikpikyuk east	6	0	0	0	6	0	0	0	0	0	0	0
Niaquilik	21	2	9	15	7	0	5	7	4	0	0	4
Kinnaq	5	0	2	2	3	0	1	1	1	0	0	0
Sabine Point	4	2	2	2	2	1	1	1	0	0	0	0
Remaining sites (isolated finds)	5	1	2	2	1	0	0	0	1	0	1	1
Total	168	44	34	43	48	8	16	19	28	8	6	10
									82	28	17	19

6.4.3 Infrastructure and travel routes

The DEW line stations of Qamaqaaq (Komakuk Beach) and Stokes Point each have one landing strip (Figure 6.6 a and b). At Qamaqaaq (Komakuk Beach), 46 m of the landing strip was eroded since the 1970s. In the S1 scenario, a further 140 m may be eroded, shortening the landing strip to 980 m. In the S2 scenario 395 m are expected to be eroded, which will shorten the landing strip to 725 m. Additionally, changes in the state of permafrost, such as thawing and frost heaving, have the potential to cause damages to the landing strip [Hunter, 2013; Stern and Gaden, 2015]. At Stokes Point, the length of the landing strip was approximately 1 100 m in the 1970s. Between the 1970s and 2011, 180 m was eroded. Both scenarios project a shortening of the landing strip to approximately 500 m. Further, the landing strip is situated on an average height of 1.2 m. With the regression of the shoreline and a further rise of sea level, the risk of flooding and permanent inundation might threaten the landing strips. Consequently, the shoreline projections and interpretation suggest that by 2100 the landing strips along the Yukon coast will be increasingly affected by erosion and flooding to the extent that they may become unsafe for loaded fixed-wing aircraft.

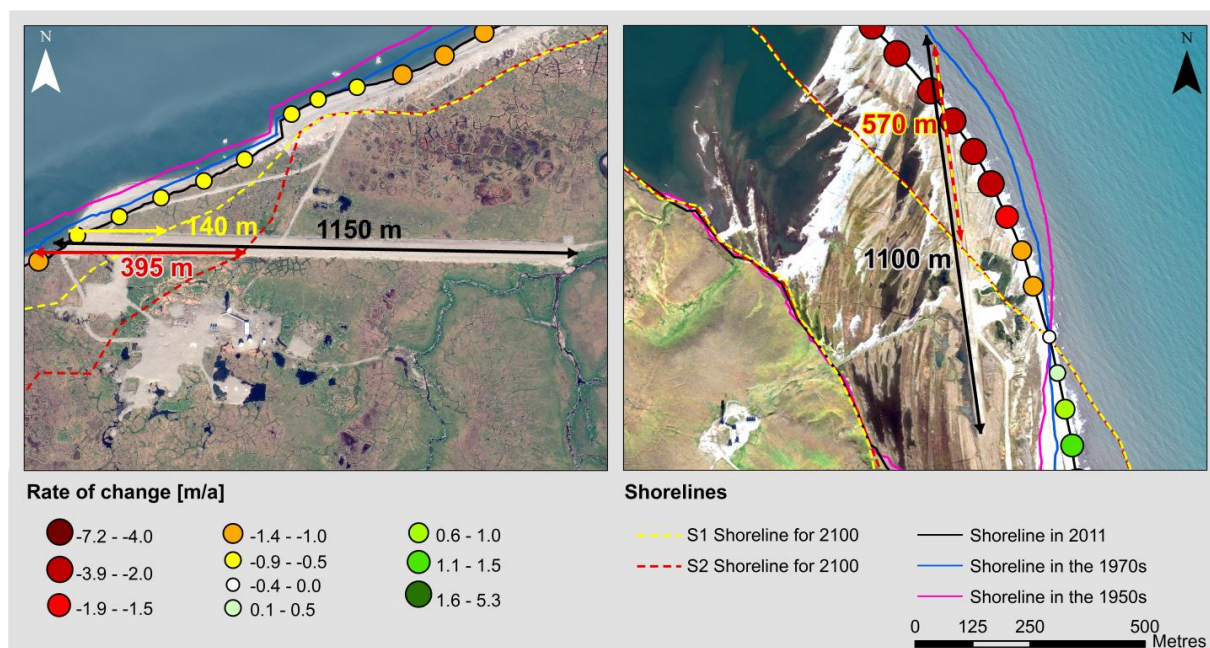


Figure 6.6: a) Qamaqaaq (Komakuk Beach) DEW line station. The landing strip is built on approximately 6 m high, polygonal tundra. Base image: GeoEye-1 scene from July 2011, b) Stokes Point DEW line station. The landing strip is built on a set of approximately 1.2 m high beach ridges. Base image: WordView-2 scene from August 2011.

Workboat Passage is an important travel route used by the local population in order to avoid exposed waters north of Qikiqtaruk (Herschel Island). Both entrances to Workboat Passage are defined by gravel spits and are highly dynamic (Figure 6.7). In the 1950s, the western

entrance was approximately 690 m wide, and widened by 20 m to 710 m by 2011. During the same time period, the Nunaaluk barrier island system migrated to the east and north, which increases the risk of boats and barges running aground while entering the passage. The eastern entrance narrowed from 1800 m in the 1970s to 690 m by 2011. The average depth within the passage is around 2 m with wide areas of shallow banks of -0.5 m in the southern part of the passage [Canadian Hydrographic Service, 1986]. Since coastal erosion and hence the amount of sediment in nearshore waters is expected to increase in the future (see above) we expect the sediment supply for all spits to remain stable or increase, even though further sea level rise may also lead to increased erosion of the spits. Since the tidal and wind-driven currents on both sites are strong and the entrances to the passage on both sites are up to 10 m deep [Canadian Hydrographic Service, 1986], the closure of either entrance is unlikely. Occasional strong storms from the west and from the east will help to maintain the entrances. Independent from the prevailing wind direction, the water is in constant movement through the passage and does not stagnate. Due to additional sediment transported into Workboat Passage, we expect that sediment deposition will increase and the passage will become shallower. We predict that, while Workboat Passage is very unlikely to fully close, overall shallowing and shifting shoals at the entrances will make travel in even small boats increasingly difficult.

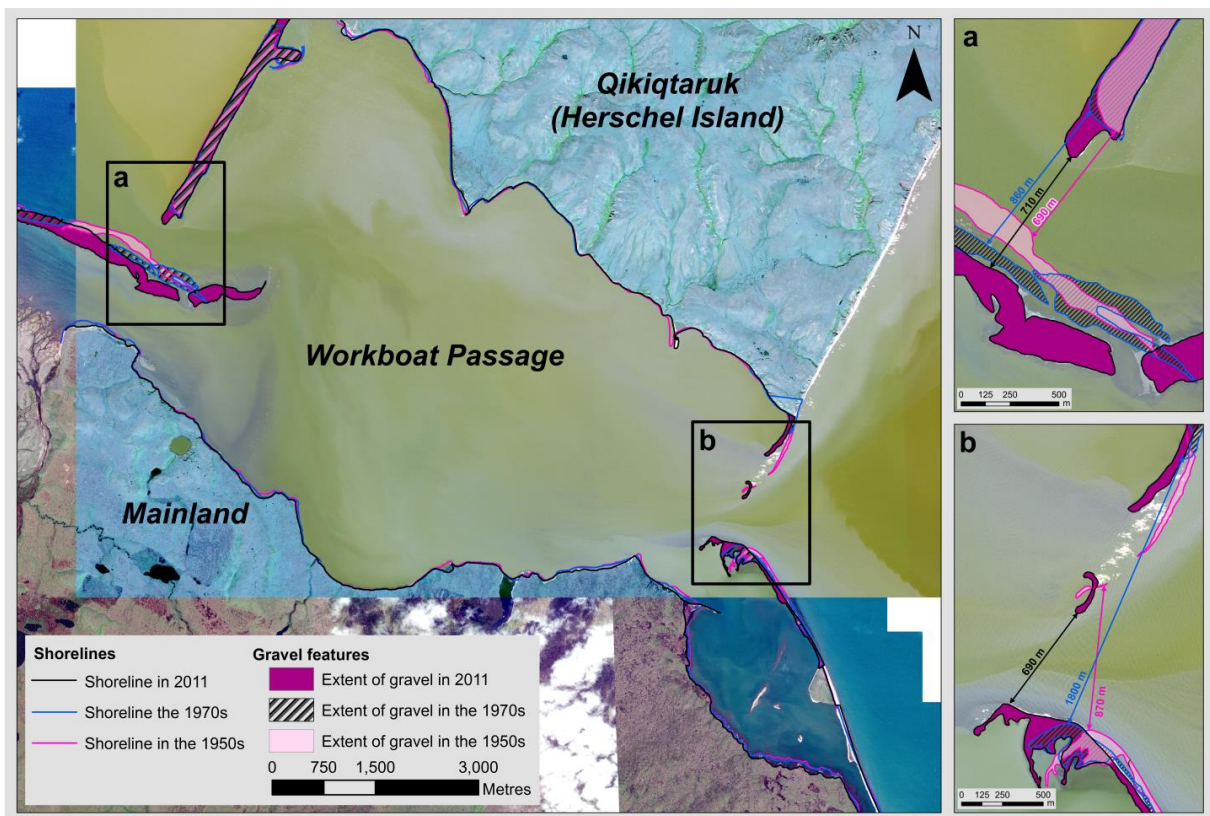


Figure 6.7: Workboat Passage. Inset a) zoom to its western entrance. Inset b) zoom to its eastern entrance. Lower base image: GeoEye-1 scene from July 2011. Upper base image: GeoEye-1 scene from August 2011.

6.5 Conclusions

Shoreline change rates derived from air- and satellite-borne imagery from the 1950s, 1970s, 1990s, and 2011 were used to assess the impact of shoreline changes on cultural features, infrastructure, and travel routes along a 210 km length of the Yukon coast. These data were used to create conservative (S1) and dynamic (S2) scenarios to project two shoreline positions for the year 2100 in order to estimate how future shoreline changes may affect cultural sites, infrastructure, and travel routes. The main results are as follows:

- Under the S1 scenario, a mean rate of change of -0.7 m a^{-1} was calculated. This results in a mean future land loss of 9.5 ha a^{-1} along the entire study area and a total loss of land of approximately 846 ha between 2011 and 2100. Under the S2 scenario, a mean rate of change of -2.2 m a^{-1} was calculated, resulting in a mean future land loss of 25 ha a^{-1} along the entire study area and a total loss of land of approximately 2 243 ha between 2011 and 2100.
- Past shoreline changes led to the erosion of 26% of all inventoried cultural features. Additional 20% to 26% are expected to be eroded under the S1 and S2 scenarios, leading to a loss of 46% (S1) to 52% (S2) of the inventoried cultural features along the Yukon coast by 2100. Since not all existent cultural features could be mapped, this is still a conservative estimate. Further, both shoreline projections do not incorporate ground elevation data. Some cultural features which are not considered threatened due to erosion under both scenarios may nevertheless be threatened due to coastal flooding. In the future, coastal processes are expected to further reduce the diversity of cultural features along the Yukon coast.
- All three camps at Tapqaq (Shingle Point) are built in areas in which the spit has been widening since the 1950s and are not directly threatened by erosion. However, future sea level rise and more intense storms have the potential to seriously threaten all three camps. Highly resolved topography and bathymetry data would allow for more accurate analyses and better prediction of the future risk of coastal erosion, spit breaching and floodings at Tapqaq (Shingle Point).
- The landing strips of the two DEW line stations of Ikpikyuk (Stokes Point) and Qamaqaaq (Komakuk Beach) are expected to be substantially shortened by 2100 to 530 m and 755 m, respectively. Additionally, due to its low elevation, the landing strip at Ikpikyuk (Stokes Point) is in danger of becoming periodically or permanently flooded. The projections suggest that all landing strips near the Yukon mainland coast will be directly impacted by erosion and/or flooding by 2100.

- The travel route through Workboat Passage between the mainland and Qikiqtaruk (Herschel Island) is likely to remain open at both entrances. Nevertheless, increasing sedimentation as a result of increased erosion of cliffs on Qikiqtaruk (Herschel Island) might cause the passage to gradually shallow. Thus, we expect that Workboat Passage will be increasingly challenging to navigate in the future.

Acknowledgements

A. M. Irrgang was financed by the German Federal Environmental Foundation and was part of the Helmholtz Young Investigator Group “COPER” (grant VH-NG-801 to H. Lantuit). G. K. Manson was funded by the Climate Change Geoscience Program of the Earth Science Section of Natural Resources Canada. We thank Peter Demontigny and Hayleigh Conway (Parks Canada, Western Arctic Field Unit) and Ruth Gotthardt (Yukon Government – Dept. of Tourism and Culture) for data sharing and collaboration. We thank Patrick Potter for a thoughtful internal review. This comprises GSC contribution #XXXX. The DSAS data and coastal landform classification data presented here are available through the PANGAEA data repository [Irrgang *et al.*, 2017].

Discussion

7.1 The importance of understanding climatic drivers of coastal changes

The results from the first study (Chpt. 3) indicated that no coastal-wide acceleration in shoreline retreat was measurable between the 1950s and 2011. However, along six shorter sections of the coast, the key sites, for which additional imagery from the 1990s was available, the rates of change decreased from the 1970s to the 1990s and increased again over the 1990s to 2011 time period. Geodetic survey data from three field sites confirm these observations. These results correspond well with the continuous decrease in sea ice extent and longer open water seasons [Markus *et al.*, 2009; Stroeve *et al.*, 2014], as well as with the increasing intensity of storms and general warming of air, soil and water temperatures [AMAP, 2011; Overland *et al.*, 2016; Timmermans, 2016]. However, the exact linkages between Arctic coastal dynamics and changing environmental forcing factors are still not fully understood. This is detrimental to the elaboration of models able to project future coastal evolution. To examine the combined and individual contribution of various forcing factors to the coastal dynamics, multivariate statistical models need to be developed. This would form a first step in increasing the capacity of projecting coastal response to future climatic changes and the impacts which come along therewith. Further, the development of statistical models is the first step towards the inclusion of Arctic coastal erosion processes in Earth system models. This is particularly important because, despite their large quantity, carbon fluxes from coastal erosion are not accounted for in these Earth system models.

Previous studies are inconsistent when it comes to the statistical relationship between shoreline retreat and environmental variables. Some studies came to the conclusion that oceanic forcing (sea level rise, waves and storms) is of particular significance for shoreline retreat [Reimnitz and Maurer, 1979; Héquette and Barnes, 1990; Solomon *et al.*, 1994; Héquette *et al.*, 1995; Manson and Solomon, 2007]. Other studies emphasized that the

sedimentological and geocryological characteristics of the coast, consisting of fine grained sediments which are bond by ice, or the presence of ice in the water column renders Arctic coasts particularly vulnerable towards shoreline retreat [Reimnitz *et al.*, 1985, 1988; Dallimore *et al.*, 1996; Aré *et al.*, 2008; Barnhart *et al.*, 2014a]. One reason for these inconsistent conclusions is likely the dependence of these results on the scale at which the studies were conducted, and on regional variability. Some variables will explain the variance in shoreline retreat much better at the local scale than regionally or Arctic-wide. Another reason for the inconsistencies is the very limited availability of high spatial and temporal shoreline change and environmental forcing data. This greatly limits the capacity to derive robust statistical relationships between shoreline retreat and environmental forcing. Some studies have attempted to do so at the local scale [Lantuit *et al.*, 2011; Jones *et al.*, 2013; Barnhart *et al.*, 2014a; Günther *et al.*, 2015], yet regional analyses are still missing.

7.2 The influence of shoreline change rates on retrogressive thaw slump activity

In the fourth chapter, the spatial distribution and temporal activity of retrogressive thaw slumps along the Yukon coast was investigated. The chapter also determined the factors underpinning retrogressive thaw slump initiation and activity. With the help of univariate regression tree models, the main terrain controls for slump initiation and upkeep were found to be terrain slope and cliff height. The density and areal coverage were best explained by volume and thickness of massive ice bodies. Coastal erosion did not appear to be one of the driving factors for retrogressive thaw slump initiation. If the coast is not steep and high enough and not characterized by high ground ice contents, coastal erosion can be very intense but will not lead to the initiation of a retrogressive thaw slump. Instead, the cliff will either retreat more uniformly, like for example at the US-Canadian border (Figure 2.5 inset a), or at Stokes Point west (Figure 2.5, inset d), or shoreline retreat will occur in the form of block failures, like at Kay Point (Figure 2.5, inset e). Coastal erosion, however, plays an important role in facilitating retrogressive thaw slump initiation by removing the insulation layer which is protecting the massive ice body from thawing. Coastal processes also play an important role in sustaining retrogressive thaw slump activity by eroding the outflow material. In order to quantify the exact role of coastal erosion for retrogressive thaw slump initiation, a separate statistical analysis would be needed. In this analysis, the respective contribution of each process leading to the disturbance of the insulation layer would need to be investigated. Along the coast, these processes are mainly coastal erosion, active layer detachments and thermo-erosional gully expansion. Since no data is available on the latter two processes, the relative

contribution of different triggering mechanisms to retrogressive thaw slump initiation cannot be determined. It is also very difficult to link distinct triggering mechanisms to the initiation of retrogressive thaw slumps, since retrogressive thaw slumps take years to develop, after being initiated [Kokelj and Jorgenson, 2013]. However, coastal erosion, as well as active layer detachments and thermo-erosional gully expansion, are processes which are likely to intensify in response to warming temperatures [Lantuit and Pollard, 2008; Lantz and Kokelj, 2008; Gooseff *et al.*, 2009]. Thus, the increased occurrence and activity of retrogressive thaw slumps [Wolfe *et al.*, 2001; Lantuit and Pollard, 2005; Lantuit *et al.*, 2012a; Kizyakov *et al.*, 2013; Segal *et al.*, 2016] is very likely the direct effect of the intensification of multiple triggering mechanisms.

The lack of a statistical relationship between retrogressive thaw slump triggering and coastal erosion rates mentioned above is also likely due to the method used to compute rates of shoreline change. The shoreline indicator used for shoreline digitalisation might have influenced the shoreline change rates and thus the multiple regression analyses results. Along sections of the coast where retrogressive thaw slumps were present, the digitalization of shoreline was done along the cliff toe and the rates of change were computed by comparing two successive shorelines in 2 dimensions (planimetric shoreline mapping). However, since mud lobes at the retrogressive thaw slump outflows in some cases temporarily displaced the shoreline seaward, accurate shoreline detection was hampered and DSAS analyses less accurate. Obu *et al.* [2016a] showed that the detection of volumetric erosion measurements reflects changes in environmental forcing more adequately than planimetric erosion measurements. Feeding the results of volumetric erosion measurements into the statistical model likely would reflect the importance of coastal erosion processes for retrogressive thaw slump initiation better. However, due to the lack of a digital elevation model for the Yukon coast for 1972, this method could not be applied in the present study.

The non-significant link between shoreline change rates and retrogressive thaw slump initiation might also be associated with the long-time spans used to compute shoreline change rates. By using long term (39 years) rates of change, the impact of extreme events was averaged out. As described above, the initiation of a retrogressive thaw slump is caused by the destruction of the insulating soil and vegetation layer, which can be initiated by one severe storm. However, shoreline rates of change averaged over 39 years (1972-2011) do not reflect these single events. Instead, sub-decadal shoreline change rates would be more suitable, which would allow the detection of the effect of single storm events on shoreline recession. As the results from the geodetic surveys (Figure 3.5) show, the variation of year-to-year

erosion rates can be up to 10 times the long-term average rate. In order to alleviate this issue, repeat satellite imagery coverage on a yearly, if not on an intra-annual basis, would need to be acquired to capture geomorphological change at the coast in relation to storms. Geodetic surveys alone could not provide this kind of validation, because of the lack of information on the distribution of slumps along the entire coast.

7.3 On the calculation of carbon fluxes from coastal erosion along the Yukon coast

Chapter four aimed at calculating current fluxes of sediment and soil organic carbon from the coast. In the fourth chapter, the amounts of sediment and carbon fluxes mobilized by shoreline retreat were estimated at 1.801×10^{12} g and 0.035×10^{12} g, respectively. In the fifth chapter, it was shown that retrogressive thaw slumps occur along 28.1 km of the Yukon coast and that they are undergoing a phase of increased activity. Yet, the fluxes of sediment and soil organic carbon from retrogressive thaw slumps were not included.

In soils of the Yukon coast, 44% of the total soil organic carbon in the soil column is stored within the top soil meter (Chpt. 4). In retrogressive thaw slumps, this top meter of soil is always eroded. Thus, retrogressive thaw slumps, even though they occur along a relatively short section of the shoreline likely contribute large amounts of carbon and sediments from the hinterland. Consequently, the soil organic carbon and sediment fluxes from shoreline retreat presented in chapter four are a lower-end estimation of past and current fluxes. The inclusion of carbon fluxes from retrogressive thaw slumps would provide a much greater flux of carbon to the Beaufort Sea.

To get a rough estimate of these fluxes, the combination of the area affected by retrogressive thaw slumps with the carbon content of the top meter of soil would already give a first approximation. However, the carbon which is mobilized by thermokarst features, such as retrogressive thaw slumps, is subject to degradation prior to entering the ocean [*Knoblauch et al.*, 2013; *Tanski et al.*, 2017] and thus cannot be equated to the volumes computed with the simple estimation method outlined above. This outlines the need for identifying and quantifying the carbon degradation processes associated with permafrost degradation in the coastal zone. These processes have the potential to greatly alter the bioavailability of organic carbon and to change the magnitude of the flux estimates. This important field of study is necessary to the understanding of the whole spectrum of processes acting upon the material transferred to the nearshore zone, but is beyond the scope of this thesis.

7.4 Impacts of present and future coastal erosion on the natural and human environment

The prediction of two different shoreline positions for the year 2100 in chapter six, allowed an estimation of the destroying effect of future shoreline changes on heritage sites. Under the more extreme scenario of shoreline change, 52% of the listed heritage sites would be lost to the ocean by 2100 (Chpt. 6). Thus, the diversity of historical sites as it is known at present times is successively destroyed by coastal processes. These estimates have a direct impact on coastal zone management. They can be used to prioritize which cultural sites to investigate first, in order to foster the preservation of archaeological goods and knowledge. Also the usage of the sparse infrastructure, in the form of two landing strips, will be severely restricted by 2100. Travelling on traditional boat routes is already affected due to increased sedimentation processes.

The results of the studies in chapter three, four and five suggest that further climate warming might enhance sediment, nutrient, and carbon release to the Arctic Ocean. Increasing sediment fluxes into the Arctic Ocean will enhance the turbidity of the water and alter light availability, which is important for the nearshore fauna and flora [Eicken *et al.*, 2005; Walsh, 2005; Gradinger *et al.*, 2009]. The entrainment of nutrients into the nutrient-deficient nearshore zone will also likely stimulate primary production, which can lead to enhanced algae blooms [Walsh, 2005]. On the other hand, higher light availability due to a shorter sea ice coverage will favour the development of new vegetated habitats at coastal seafloors, which will be able to store more carbon than is stored at the seafloor in present times [Walsh, 2005; Krause-Jensen and Duarte, 2014]. A further consequence of increasing carbon dioxide values in the Arctic atmosphere and a reduced seasonal sea ice cover is the increase in carbon dioxide uptake in the Arctic Ocean and the resulting ocean acidification [Bates and Mathis, 2009]. All these changes will impact the species composition of higher trophic levels like for example fishes, or whales. This in turn will influence the peoples' traditional lifestyle and on the economy (e.g., fishing industry) in the North [Walsh, 2005; Forbes, 2011]. A further implication of a warming Arctic is, that the Arctic Ocean will get more accessible for industrial and commercial shipping [Smith and Stephenson, 2013; Stephenson and Smith, 2015]. The successive opening of the North-West Passage to industrial shipping is leading to significant savings in time and expenses. However, the increasing ship traffic has negative effects on the surrounding environment. Two of main impacts are the introduction of pollutants to the atmosphere and to the water and the destabilizing effect which ships have on sea ice [Forbes, 2011]. On the other hand, the increasing accessibility of the Arctic to tourists

creates the opportunity to raise public awareness on the impacts of climate change and the great value of the Arctic as a unique ecosystem and living environment, as well as its importance for the global climate.

7.5 Synthesis

The increasing availability of remote sensing and ground-based information for the Yukon coast will help provide answers to the open research questions outlined in the previous sections. There is now high resolution altimetry data [*Obu et al.*, 2016b; *Kohnert et al.*, 2014], a shoreline change database (Chpt. 3), a sediment content, and ice content database (Chpt. 4), as well as a georeferenced set of images which allows the mapping of landforms such as retrogressive thaw slumps (Chpt. 5). Further, the cultural heritage site database (Chpt. 6) enriches the data by adding the human component to the biophysical system.

This unique set of data, together with the results from this thesis, bears high potential for future studies. Cliff height and slope are the driving factors for slump initiation and ground ice content determines the areas where retrogressive thaw slumps occur (Chpt. 5). Part of these factors can already be retrieved using some of these new datasets. Some, like ground ice occurrence are more challenging to extract, but should form the focus of future research. The invention of a methodology to remotely sense the occurrence of ground ice combined with LiDAR data could help to detect areas which are prone to retrogressive thaw slump initiation. This would enable the establishment of a predictive system for retrogressive thaw slump occurrence. This would complement existing hazard potential maps, such as the ones devised for active layer detachments [*Rudy et al.*, 2017]. An estimation of future retrogressive thaw slump initiation would also provide a more accurate estimation of future carbon fluxes from the Yukon coast into the Arctic Ocean.

Since many factors driving coastal dynamics are expected to intensify, the need for an enhanced monitoring of Arctic shoreline change dynamics is becoming more acute. The usage of advanced technology, like for example UAVs (unmanned aerial vehicles), bears high potential for improving the spatial resolution of volumetric shoreline change data. The set-up of a tide gauge at the Yukon coast would allow to accurately relate coastal erosion to local sea level changes on sub-decadal periods. In combination, these additional observation techniques would provide valuable data for an in-depth understanding of coastal responses to an increasingly changing environment. The collection and standardization of coastal change data across all Arctic coasts in programs like “Arctic Coastal Dynamics” [*Rachold et al.*, 2005;

Lantuit et al., 2012b] is crucial for a better understanding of coastal processes on an Arctic-wide scale.

In the Arctic coastal zone, terrestrial, atmospheric and oceanic processes, which are all influenced by the presence of ice, interact to shape the physical environment. This makes Arctic coasts very complex areas to study. Consequently, it is essential to account for processes from all spheres and their interrelationships in order to understand which role climatic change has on the Arctic coast and how changing coastal dynamics are influencing the living conditions in the Arctic.

Summary and Conclusions

The overarching goal of this thesis was 1. to contribute to an improved understanding of the role coastal dynamics are playing for material fluxes and landscape evolution along the Yukon coast, as well as 2. to determine which impacts they have on infrastructure, travel routes and cultural sites. These objectives have been pursued in four separate studies which build the main body of this thesis.

The investigation of spatial and temporal variability of shoreline changes along the ice-rich Yukon coast were done by using geo-coded aerial photographs from the 1950s, 1970s and 1990s and satellite images from 2011. Shorelines were digitized from these images and DSAS analyses were performed. These analyses were complemented by geodetic field surveys performed along seven field sites in 2014 and 2015. The results showed no acceleration in the mean rate of shoreline change (-0.7 m a^{-1}) along the whole Yukon coast, but the percentage of transects recording erosion increased through time. In 2011, 85% of all transects, covering 210 km of the Yukon coast with a spacing of 100 m, recorded erosion. Further, analyses of shoreline dynamics along selected key sites revealed a significant acceleration in shoreline retreat over the last 20 years from -0.54 m a^{-1} between the 1970s-1990s, to -1.30 m a^{-1} between the 1990s-2011. This development is also reflected in the results of the geodetic field site measurements. Along three sites, an increase of erosion rates was measured since 2006. Thus, the Yukon coast is experiencing the highest measured erosive activity since 64 years, which corresponds well with observations of further parts of the Beaufort coast, as well as with observations from the Siberian coasts. Since 16% of the coast was classified as inundated tundra, or low-lying tundra, the expected increase in severe storms and sea level rise might render these stretches of coast particularly vulnerable towards future coastal erosion.

The mean annual sediment and soil organic carbon fluxes which were mobilized by coastal erosion within the time period from 1953 to 2011 amounted to $5.3 \times 10^3 \text{ kg m}^{-1} \text{ a}^{-1}$ and

131 kg C m⁻¹ a⁻¹, respectively. An extrapolation of these rates to the area east of the Mackenzie Delta results in carbon fluxes which are almost three times as high as the values used to date for budget calculations. This was the first study performed along the Yukon coast which accounted for ground ice within the cliff, as well as for the sediment and carbon stored in the entire soil column. Since on average only 44% of the total soil organic carbon was stored in the first metre of soil, accounting for the whole soil column significantly increased the amount of carbon being mobilized by coastal erosion. However, accounting for ground ice in the soil column reduced the amount of soil organic carbon on average by 19%, and the amount of sediments by 16%. The usage of high resolved altimetry data for the estimation of mean cliff heights and erosion areas instead of shoreline lengths and mean erosion rates for the estimation of area losses further increased the accuracy of the results in comparison to previous estimates.

The analysis of the role of coastal erosion for the initiation of retrogressive thaw slumps revealed that coastal erosion does not play a significant role statistically. Field observations and previous publications suggest, however, that shoreline retreat plays a crucial role for setting the preconditions for retrogressive thaw slump development and for sustained activity. Ground ice volume and thickness appeared to be the driving factors for retrogressive thaw slump initiation and the high ground ice volumes of the Yukon coast seem to be favorable for retrogressive thaw slump occurrence since the analyses revealed that the Yukon coast is one of the regions most affected by retrogressive thaw slumps along all Arctic coasts. Further, the study showed that a total area of 402 ha was occupied by retrogressive thaw slumps in 2011. Although this area is relatively small, retrogressive thaw slumps deliver high amounts of sediments, carbon and nutrients from the hinterland. Thus, when calculating the amount of sediment and carbon fluxes mobilized by coastal erosion, it is important to account for fluxes derived from retrogressive thaw slump activity.

In order to expand the scope of this thesis to the human environment, the present and potential future impacts of coastal dynamics on the people who are interacting with the coast were studied. The focus was on threats to cultural sites, since their relatively high abundance and diversity provides them a particular relevance of the preservation the cultural heritage of the Yukon coast. According to projected shoreline positions, 46% to 52% of all cultural features will be eroded by 2100, which will result in a great loss of cultural heritage along the Yukon coast. Since the projections are built on past rates of shoreline change, these are still conservative estimations. A quantitative analysis of shoreline dynamics along three main Inuvialuit summer camps at Tapqaq (Shingle Point) revealed that the three camps are not in

immediate danger at the present. However, further analyses, incorporating onshore and nearshore topography data are needed in order to give a more accurate estimation of the vulnerability of Shingle Point to future storms and floods. Therefore, and for further research, the installation of a tide gauge for a better monitoring of sea level along the Yukon coast is urgently needed.

An investigation of the present and future conditions of transportation routes and infrastructure revealed that traveling along the Yukon coast will require a higher flexibility of the people in the future. The usage of the two landings strips at the Komakuk and Shingle Point DEW line stations will be increasingly restricted. Travelling by boat along the coast will get more challenging, since increasing sediment entrainment from coastal erosion results in the built up of new dynamic sand bars and shoals. Together with the fast changing extent and thickness of sea and river ice, which is traditionally used for transportation routes during the winter, people in the North will need to adapt to an increasingly dynamic coastal environment.

The variability of shoreline dynamics along the Yukon coast (Chpt. 3) constituted an important part for the analyses conducted in the three consequent studies (Chpt. 4, 5, 6). These subsequent studies focused on impacts of coastal changes on the natural environment (Chpt. 4, 5), as well as on the human environment (Chpt. 6). Together, these four studies contribute to the current understanding of the interplay of natural processes in the coastal zone and their impacts on the human realm. With continuously warming climate, coastal erosion is expected to further increase. The estimation of a future shoreline position, which is based on a dynamic scenario in chapter six, exemplifies how the future coast along the Yukon might look like. A three-fold increase in mean rates of change, as is suggested in the S2 scenario, would result in an amplified mobilization of sediments and carbon from the coast by direct erosion, and through an intensification of thermokarst processes such as retrogressive thaw slumps. The release of greater amounts of carbon to the atmosphere will contribute to further warming. The enhanced entrainment of carbon, sediments and nutrients into the nearshore zone will affect the ecosystem, which, in turn, is supporting people and economy in the North. These intertwined components in the coastal zone call on novel interdisciplinary research approaches to provide a thorough understanding of the role coastal dynamics are playing in the change of the complex Arctic living environment.

Bibliography

- Abbott, B. W., J. B. Jones, E. A. G. Schuur, F. Stuart Chaplin III, W. B. Bowden, et al. (2016), Biomass offsets little or none of permafrost carbon release from soils, streams, and wildfire: An expert assessment, *Environ. Res. Lett.*, 11(3), 034014.
- ACD (Arctic Coastal Dynamics) (2016), The Arctic Coastal Research Forum. <https://arcticcoast.info> (accessed: 04.09.2017)
- Adams, G. (2004), Niaqulik - A Chapter in Inuvialuit Lifestyles. Cultural Resource Services. Parks Canada. Internal document.
- Alunik, I., E. D. Kolausok, and D. Morrison (2003), *Across Time and Tundra: The Inuvialuit of the Western Arctic*. 1st edition. Canadian Museum of Civilisation. Gatineau. Canada.
- Arctic Monitoring and Assessment Programme (AMAP) (2011), *Snow, water, ice and permafrost in the Arctic (SWIPA): Climate change and the cryosphere*, 538 pp, Oslo, Norway.
- Amundsen, R. (1908), *The North West Passage. Being the Record of a Voyage of Exploration of the Ship "Gjøa", 1903-1907*. 2nd vol. 430 pp. London, UK.
- Arctic Monitoring and Assessment Programme (AMAP) (2011), *Snow, water, ice and permafrost in the Arctic (SWIPA): Climate change and the cryosphere*, 538 pp, Oslo, Norway.
- Aré, F. E. (1988), Thermal abrasion of sea coasts (part I), *Polar Geogr. Geol.*, 12(1), 1–86, doi:10.1080/10889378809377343.
- Aré, F. E., E. Reimnitz, M. Grigoriev, H.-W. Hubberten, and V. Rachold (2008), The Influence of Cryogenic Processes on the Erosional Arctic Shoreface, *J. Coast. Res.*, 241, 110–121, doi:10.2112/05-0573.1.
- Arnold, C. (2016), Development of the Mackenzie Inuit culture, in *The Oxford Handbook of the prehistoric Arctic*, in M. T. Friesen and O. K. Mason (Eds.), pp. 585–606, New York, USA.
- Arp, C. D., B. M. Jones, J. A. Schmutz, F. E. Urban, and M. T. Jorgenson (2010), Two mechanisms of aquatic and terrestrial habitat change along an Alaskan Arctic coastline, *Polar Biol.*, 33(12), 1629–1640, doi:10.1007/s00300-010-0800-5.
- Atkinson, D. (2005), Observed storminess patterns and trends in the circum-Arctic coastal regime, *Geo-Marine Lett.*, 25(2–3), 98–109, doi:10.1007/s00367-004-0191-0.
- Balser, A. W., J. B. Jones, and R. Gens (2014), Timing of retrogressive thaw slump initiation in the Noatak Basin, northwest Alaska, USA, *J. Geophys. Res. Earth*, 119, 1106–1120, doi:10.1002/2013JF002889.
- Barnhart, K. R., R. S. Anderson, I. Overeem, C. Wobus, G. D. Clow, and F. E. Urban (2014a), Modeling erosion of ice-rich permafrost bluffs along the Alaskan Beaufort Sea coast, *J. Geophys. Res.*, 1155–1179, doi:10.1002/2013JF002845.
- Barnhart, K. R., I. Overeem, and R. S. Anderson (2014b), The effect of changing sea ice on the physical vulnerability of Arctic coasts, *Cryosph.*, 8(5), 1777–1799, doi:10.5194/tc-8-1777-2014.
- Barnhart, K. R., C. R. Miller, I. Overeem, and J. E. Kay (2015), Mapping the future expansion of Arctic open water, *Nat. Clim. Chang.*, 6, 280-285, doi:10.1038/nclimate2848.

- Bates, N. R., and J. T. Mathis (2009), The Arctic Ocean marine carbon cycle: evaluation of air-sea CO₂ exchanges, ocean acidification impacts and potential feedbacks, *Biogeosciences*, 6(4), 2433–2459, doi:10.5194/bgd-6-6695-2009.
- Battin, T. J., L. A. Kaplan, S. Findlay, C. S. Hopkins, E. Marti, A. I. Packman, J. D. Newbold, and F. Sabater (2009), Biophysical controls on organic carbon fluxes in fluvial networks, *Nat. Geosci.*, 2(8), 595–595, doi:10.1038/ngeo602.
- Belicka, L. L., and H. R. Harvey (2009), The sequestration of terrestrial organic carbon in Arctic Ocean sediments: a comparison of methods and implications for regional carbon budgets, *Geochimica et Cosmochimica Acta*, 73, 6231–6248, doi:/10.1016/j.gca.2009.07.020.
- Belicka, L. L., R. W. MacDonald, and H. R. Harvey (2002), Sources and transport of organic carbon to shelf, slope, and basin surface sediments of the Arctic Ocean, *Deep-Sea Research*, I49, 1463–1483. doi:10.1016/S0967-0637(02)00031-6.
- Belicka, L. L., R. W. MacDonald, and H. R. Harvey (2009), Trace element and molecular markers of organic carbon dynamics along a shelf–basin continuum in sediments of the western Arctic Ocean, *Marine Chemistry*, 115, 72–85, doi:10.1016/j.marchem.2009.06.007.
- Bird, E. (2009), *Coastal Geomorphology – an introduction*, 434 pp, 2nd edition, Chichester, UK.
- Bockheim, J. G., and K. M. Hinkel (2007), The importance of “deep” organic carbon in permafrost-affected soils of Arctic Alaska, *Soil Science Society of America Journal*, 71, 1889–1892, doi:10.2136/sssaj2007.0070N.
- Bockheim, J. G., and C. Tarnocai (1998), Recognition of cryoturbation for classifying permafrost-affected soils. *Geoderma*, 81, 281–293, doi:10.1016/S0016-7061(97)00115-8.
- Bockheim, J. G., D. A. Walker, and L. R. Everett (1998), Soil carbon distribution in nonacidic and acidic tundra of arctic Alaska, in R. Lal, J.M. Kimble, R.F. Follett, B.A. Stewart (Eds.), *Soil processes and the carbon cycle*, pp. 143–155, Boca Raton, FL: CRC Press.
- Bockheim, J. G., L. R. Everett, K. M. Hinkel, F. E. Nelson, and J. Brown (1999), Soil organic carbon storage and distribution in arctic tundra, Barrow, Alaska, *Soil Science Society of America Journal*, 63, 934–940, doi:10.2136/sssaj1999.634934x.
- Bockheim, J. G., K. M. Hinkel, and F. E. Nelson (2003), Predicting carbon storage in tundra soils of arctic Alaska, *Soil Science Society of America Journal*, 67, 648–650, doi:10.2136/sssaj2003.9480.
- Bockheim, J.G., K.M. Hinkel, W.R. Eisner, and X.Y. Dai (2004), Carbon pools and accumulation rates in an age-series of soils in drained thaw-lake basins, Arctic Alaska, *Soil Science Society of America Journal*, 68, 697–704, doi:10.2136/sssaj2004.6970.
- Bockstoe J. R. (1986), *Whales, ice, and men: the history of whaling in the western Arctic*. University of Washington Press, Seattle, USA.
- Bowden, W. B., M. N. Gooseff, A. Balsler, A. Green, B. J. Peterson, and J. Bradford (2008), Sediment and nutrient delivery from thermokarst features in the foothills of the North Slope, Alaska: Potential impacts on headwater stream ecosystems, *J. Geophys. Res.*, 113, G02026, doi:10.1029/2007JG000470.
- Breiman, L., J. Friedman, C. J. Stone, and R. A. Olshen (1984), *Classification and Regression Trees*, CRC Press, Wadsworth, Belmont, USA.
- Bouchard, M. (1974), *Surficial geology of Herschel Island, Yukon Territory*, M.Sc. Thesis, University of Montréal, Montréal, Canada.
- Brown, J., M. Jorgenson, O. Smith, and W. Lee (2003), Long-term rates of coastal erosion and carbon input, Elson Lagoon, Barrow, Alaska, *Eighth International Conference on Permafrost*, 21–25, Zürich, Switzerland.

-
- Brown, E., A. Colling, D. Park, J. Phillips, D. Rothery, and J. Wright (1999), *Waves, Tides and Shallow-Water Processes*, 227 pp., The Open University, Milton Keynes, UK.
- Brown, J., M. Jorgenson, O. Smith, and W. Lee (2003), Long-term rates of coastal erosion and carbon input, Elson Lagoon, Barrow, Alaska, Eighth International Conference on Permafrost, 21–25, Zürich, Switzerland.
- Brown, R. J. E., and W. O. Kupsch (1974), Permafrost terminology, National Research Council of Canada.
- Bruun, P. (1988), The Bruun rule of erosion by sea-level rise: a discussion on large-scale two- and three-dimensional usages, *J. Coast. Res.*, 4(4), 627–648, doi:10.2307/4297466.
- Burn, C. R., and A. G. Lewkowitz (1990), Canadian Landform Examples - 17 Retrogressive thaw Slumps, *Can. Geogr.*, 34(3), 273–276.
- Burn, C. R. (1997). Cryostratigraphy, paleogeography, and climate change during the early Holocene warm interval, western Arctic coast, Canada, *Canadian Journal of Earth Sciences*, 34, 912-925. doi:10.1139/e17-076.
- Burn, C. R. (2000), The thermal regime of a retrogressive thaw slump near Mayo, Yukon Territory, *Can. J. Earth Sci.*, 37, 967–981.
- Burn, C. R. (2009), After Whom is Herschel Island Named?, *Arctic*, 62(3), 317–323.
- Burn, C. R., and Y. Zhang (2009), Permafrost and climate change at Herschel Island (Qikiqtaruq), Yukon Territory, Canada, *J. Geophys. Res. Earth Surf.*, 114(2), F02001, doi:10.1029/2008JF001087.
- Burn, C. R. (2016), Herschel Island (Qikiqtaryuk), Yukon's Arctic Island, in *Landscapes and Landforms of Western Canada Beaufort Sea*, in O. Slaymaker (Ed.), pp. 335–348, Switzerland.
- Cannone, N., A. G. Lewkowitz, and M. Guglielmin (2010), Vegetation colonization of permafrost-related landslides, Ellesmere Island, Canadian High Arctic, *J. Geophys. Res.*, 115, G04020, doi:10.1029/2010JG001384.
- Callaghan, T. V., M. Johansson, T. D. Prowse, M. S. Olsen, and L.-O. Reiersen (2011), Arctic Cryosphere: Changes and Impacts, *Ambio*, 40(S1), 3–5, doi:10.1007/s13280-011-0210-0.
- Canadian Hydrographic Service, (1986), Nautical Chart 7661: Demarcation Bay to Phillips Bay. Scale 1:150000. Minister of Fisheries and Oceans Canada.
- Chin, K. S., J. Lento, J. M. Culp, D. Lacelle, and S. V. Kokelj (2016), Permafrost thaw and intense thermokarst activity decreases abundance of stream benthic macroinvertebrates, *Global Change Biol.*, 22, 2715–2728.
- Cohen, J., J. A. Screen, J. C. Furtado, M. Barlow, D. Whittleston, et al. (2014), Recent Arctic amplification and extreme mid-latitude weather, *Nat. Geosci.*, 7(9), 627–637, doi:10.1038/ngeo2234.
- Couture, N. (2010), Fluxes of Soil Organic Carbon from Eroding Permafrost Coasts, Canadian Beaufort Sea, Phd Thesis, 155 pp, McGill University, Montréal, Canada.
- Couture, N., D. L. Forbes, P. R. Fraser, D. Frobel, K. A. Jenner, G. K. Manson, S. M. Solomon, B. Szlavko, and B. Taylor (2015a), A coastal information system for the southeastern Beaufort Sea, Yukon and Northwest Territories. Geological Survey of Canada Open File Report 7778. 17pp. [Available at: <http://geoscan.nrcan.gc.ca/starweb/geoscan/servlet.starweb>]
- Couture, N. and W. H. Pollard (2017), A Model Quantifying Ground-Ice Volume, Yukon Coast, Western Arctic Canada, *Permafr. Periglac. Process.*, pp. 1–9, doi: 10.1002/ppp.1952.
- Cray, H. A., and W. H. Pollard (2015), Vegetation recovery patterns following permafrost disturbance in a low Arctic setting: Case study of Herschel Island, Yukon, Canada, *Arct. Antarct. Alp. Res.*, 47(1), 99–113.

- Dallimore, S. R., S. Wolfe, and S. M. Solomon (1996), Influence of ground ice and permafrost on coastal evolution, Richards Island, Beaufort Sea coast, N.W.T., Can. J. Earth Sci., 33(5), 664–675, doi:10.1139/e96-050.
- De'ath, G., and K. E. Fabricius (2000), Classification and regression trees: A powerful yet simple technique for ecological data analysis, *Ecology*, 81(11), 3178–3192.
- de Haas, H., T. C. E. van Weering, and H. de Stigter (2002), Organic carbon in shelf seas: sinks or sources, processes and products. *Continental Shelf Research*, 22, 691–717, doi:10.1016/S0278-4343(01)00093-0.
- Digital Globe, (2016), WorldView-2 data sheet. [Available at <https://dg-cms-uploads-production.s3.amazonaws.com/uploads/document/file/98/WorldView2-DS-WV2-rev2.pdf>]
- Digital Globe, (2014), GeoEye-1 data sheet. [Available at: https://dg-cms-uploads-production.s3.amazonaws.com/uploads/document/file/97/DG_GeoEye1.pdf]
- Dittmar, T., and G. Kattner (2003), The biogeochemistry of the river and shelf ecosystem of the Arctic Ocean: a review, *Mar. Chem.*, 83(3–4), 103–120, doi:10.1016/S0304-4203(03)00105-1.
- Dolan, R., M. S. Fenster, and S. J. Holme (1991), Temporal Analysis of Shoreline Recession and Accretion, *J. Coast. Res.*, 7(3), 723–744.
- Dunton, K. H., T. Weingartner, and E. C. Carmack (2006), The nearshore western Beaufort Sea ecosystem: Circulation and importance of terrestrial carbon in arctic coastal food webs, *Prog. Oceanogr.*, 71(2–4), 362–378, doi:10.1016/j.pocean.2006.09.011.
- Dupeyrat, L., F. Costard, R. Randriamazaoro, E. Gailhardis, E. Gautier, and A. Fedorov (2011), Effects of Ice Content on the Thermal Erosion of Permafrost: Implications for Coastal and Fluvial Erosion, *Permafr. Periglac. Process.*, 22(2), 179–187, doi:10.1002/ppp.722.
- Dyke, A., and V. Prest (1987), Late Wisconsinan and Holocene history of the Laurentide ice sheet, *Geog. Phys. Quater.*, 41(2), 237–263.
- Eckert, C. D., D. Cooley, and R. R. Gordon (2005), Monitoring Black Guillemot population and nesting success at Herschel Island, Yukon Territory – 2005, Yukon Environment, Whitehorse, Canada.
- Eicken, H., R. Gradinger, A. Gaylord, A. Mahoney, I. Rigor, and H. Melling (2005), Sediment transport by sea ice in the Chukchi and Beaufort Seas: Increasing importance due to changing ice conditions?, *Deep Sea Res. Part II Top. Stud. Oceanogr.*, 52(24–26), 3281–3302, doi:10.1016/j.dsr2.2005.10.006.
- Elberling, B., A. Michelsen, C. Schädel, E. A. G. Schuur, H. H. Christiansen, L. Berg, M. P. Tamstorf, and C. Sigsgaard (2013), Long-term CO₂ production following permafrost thaw, *Nat. Clim. Chang.*, 3(10), 890–894, doi:10.1038/nclimate1955.
- Environment Yukon (2016), 30 m Yukon digital elevation model. [Available at: http://www.env.gov.yk.ca/publications-maps/geomatics/data/30m_dem.php]
- Environment Canada (2015), Beaufort Coastal Sensitivity Atlas. Environment Canada, Gatineau, Canada. [Available at: <http://publications.gc.ca/site/eng/9.629783/publication.html>]
- Environment Canada (2016), Historical Climate data. [Available at: <http://climate.weather.gc.ca/>]
- Environment Canada (2017), Canadian climate normals 1971–2000 station data. [Available at: http://climate.weather.gc.ca/climate_normals/]
- Forbes, D. L. and D. Frobel (1986), Coastal video survey: Canadian Beaufort Sea coast, Yukon and Northwest Territories; Geological Survey of Canada, Open File 1256, doi:10.4095/120474.
- Forbes, D. L., S. M. Solomon, and D. Frobel (1995), Report of the 1992 coastal surveys in the Beaufort Sea.

- Forbes, D. L. (1997), Coastal erosion and nearshore variability in the southern Beaufort Sea, Ivvavik National Park, Yukon Territory, Geological Survey of Canada Open File report 3531.
- Forbes, D. L. (ed.) (2011), State of the Arctic Coast 2010 – Scientific Review and Outlook. International Arctic Science Committee, Arctic Monitoring and Assessment Programme, International Polar Association, Helmholtz-Zentrum, 168 pp, Geesthacht, Germany. [Available at: <http://www.futureearthcoasts.org/state-of-the-arctic-coast-2010-scientific-review-and-outlook/>]
- Forbes, D. L., D. J. R. Whalen, B. Jacobson, P. Fraser, G. K. Manson, N. J. Couture, R. Simpson (2013), Co-design of coastal risk assessment for subsistence infrastructure in the Inuvialuit Settlement Region, western Arctic Canada in, ArcticNet (ASM2013), Programme. 2013, 141-142.
- Forrest, M. (2017), Going, going, gone: Canadian Arctic faces threat of coastal erosion. <https://www.newsdeeply.com/arctic/articles/2017/01/25/going-going-gone-canadian-arctic-faces-threat-of-coastal-erosion> (accessed: 06.09.2017)
- Foster, E. R., and R. J. Savage (1989), Methods of Historical Shoreline Analysis, Coastal Zone'89, 4434–4448.
- Francis, J. A., and S. J. Vavrus (2012), Francis_2012_Evidence linking Arctic Amplification to Extreme Weather.pdf, Geophys. Res. Lett., 39, 1–6, doi:10.1029/2012GL051000.
- Franklin, J. (1828), The Polar Sea, in the years 1825, 1826 and 1827, London.
- Friesen, M. T. (2015), The Arctic CHAR Project: Climate Change Impacts on the Inuvialuit Archaeological Record, Les Nouv. l'Archeologie, 141, 31–37.
- Friesen, M. T. (2016), Pan-Arctic population movements, in The Oxford handbook of the prehistoric Arctic, in M. T. Friesen and O. K. Mason (Eds.), pp. 673–692, New York.
- Friesen, T. M., and C. D. Arnold (2008), The Timing of the Thule Migration: New Dates from the Western Canadian Arctic, Am. Antiq., 73(3), 527–538.
- Fritz, M., S. Wetterich, L. Schirrmeister, H. Meyer, H. Lantuit, F. Preusser, and W. H. Pollard (2012), Eastern Beringia and beyond: Late Wisconsinan and Holocene landscape dynamics along the Yukon Coastal Plain, Canada, Palaeogeogr. Palaeoclimatol. Palaeoecol., 319–320, 28–45, doi:10.1016/j.palaeo.2011.12.015.
- Fritz, M., H. Lantuit and J. Vonk (2017), Collapsing Arctic coastlines, Nature Clim. Change, 7(1), 6-7, doi: 10.1038/nclimate3188.
- Galley, R. J., D. Babb, M. Ogi, B. G. T. Else, N. X. Geilfus, O. Crabeck, D. G. Barber, and S. Rysgaard (2016), Replacement of multiyear sea ice and changes in the open water season duration in the Beaufort Sea since 2004, J. Geophys. Res. Ocean., 121(3), 1806–1823, doi:10.1002/2015JC011583.
- Gibbs, A. E., and B. M. Richmond (2015), National Assessment of Shoreline Change — Historical Shoreline Change Along the North Coast of Alaska, U.S.-Canadian Border to Icy Cape, U.S. Geological Survey Open File Report 2015 – 1048, 96 pp. [Available at <https://pubs.usgs.gov/of/2015/1030/>]
- Goñi, M.A., M.B. Yunker, R.W. Marcdonald, and T.I. Eglinton (2000), Distribution and sources of organic biomarkers in arctic sediments from the Mackenzie River and Beaufort Shelf. Marine Chemistry, 71, 23-51, doi:10.1016/S0304-4203(00)00037-2.
- Gooseff, M. N., A. Balsler, W. B. Bowden, and J. B. Jones (2009), Effects of hillslope thermokarst in Northern Alaska, Eos (Washington. DC), 90(4), 29–30, doi:10.1029/2009EO040001.
- Gradinger, R. R., M. R. Kaufman, and B. A. Bluhm (2009), Pivotal role of sea ice sediments in the seasonal development of near-shore Arctic fast ice biota, Mar. Ecol. Prog. Ser., 394, 49–63, doi:10.3354/meps08320.

- Grosse, G., S. Goetz, A. D. McGuire, V. E. Romanovsky, and E. A. G. Schuur (2016), Changing permafrost in a warming world and feedbacks to the Earth system, *Environ. Res. Lett.*, 11(4), 40201, doi:10.1088/1748-9326/11/4/040201.
- Günther, F., P. P. Overduin, A. V. Sandakov, G. Grosse, and M. N. Grigoriev (2013), Short- and long-term thermo-erosion of ice-rich permafrost coasts in the Laptev Sea region, *Biogeosciences*, 10(6), 4297–4318, doi: 10.5194/bg-10-4297-2013.
- Günther, F., P. P. Overduin, I. A. Yakshina, T. Opel, A. V. Baranskaya, and M. N. Grigoriev (2015), Observing Muostakh disappear: Permafrost thaw subsidence and erosion of a ground-ice-rich Island in response to arctic summer warming and sea ice reduction, *Cryosphere*, 9(1), 151–178, doi:10.5194/tc-9-151-2015.
- Gustafsson, E., C. Humborg, G. Björk, C. Stranne, L. G. Anderson, et al. (2017), Carbon cycling on the East Siberian Arctic Shelf – a change in air-sea CO₂ flux induced by mineralization of terrestrial organic carbon, *Biogeosciences Discuss.*, (April), 1–31, doi:10.5194/bg-2017-115.
- Hacquebord, L (2011). Cultural heritage sites on a changing Arctic coast; in Forbes (Ed.), *State of the Arctic Coast*. Geesthacht, Germany.
- Hansom, J. D., N. D. P. Barltrop, and A. M. Hall (2008), Modelling the processes of cliff-top erosion and deposition under extreme storm waves, *Mar. Geol.*, 253(1–2), 36–50, doi:10.1016/j.margeo.2008.02.015.
- Hapke, C. J., and D. Reid (2007), National Assessment of Shoreline Change, Part 4: Historical Coastal Cliff Retreat along the California Coast. U.S. Geological Survey Open File Report 1133, 51 pp. [Available at <https://pubs.usgs.gov/of/2007/1133/>]
- Harper, J. R. (1990), Morphology of the Canadian Beaufort Sea coast, *Mar. Geol.*, 91(1), 75–91, doi:10.1016/0025-3227(90)90134-6.
- Harper, J. R., and P. S. Penland (1982), Beaufort Sea sediment dynamics, technical report of Woodward- Clyde Consult for Geological Survey of Canada, 125 pp., Victoria, Canada.
- Harper, J. R., P. D. Reimer, and A. D. Collins (1985), Canadian Beaufort Sea physical shore-zone analysis, Report for Northern Oil and Gas Action Plan, Indian and Northern Affairs Canada Ottawa, Canada, 105 pp. [Available at <http://engineerradcc.library.link/portal/Canadian-Beaufort-Sea-physical-shore-zone/Gu3YaBSD3Pk/>]
- Harper, J. R., R. F. Henry, and G. G. Stewart (1988), Maximum Storm Surge Elevations in the Tuktoyaktuk Region of the Canadian Beaufort Sea, *Arctic*, 1(1), 48–52, doi:10.14430/arctic1691.
- Harry, D. G., H. M. French, and W. H. Pollard (1988), Massive ground ice and ice-cored terrain near Sabine Point, Yukon Coastal Plain, *Can. J. Earth Sci.*, 25(11), 1846–1856, doi:10.1139/e88-174.
- Hedges, J. I., R. J. Keil, and R. Benner (1997), What happens to terrestrial organic matter in the ocean? *Organic Geochemistry*, 27, 195-212, doi:10.1016/S0146-6380(97)00066-1.
- Henry, R. F. (1975), Storm Surges, Beaufort Sea Project, Beaufort Sea Technical Report No. 19, 41 pp.
- Héquette, A., and P. W. Barnes (1990), Coastal retreat and shoreface profile variations in the Canadian Beaufort Sea, *Mar. Geol.*, 91(1–2), 113–132, doi:10.1016/0025-3227(90)90136-8.
- Héquette, A., and M. H. Ruz (1991), Spit and Barrier-Island Migration in the Southeastern Canadian Beaufort Sea, *J. Coast. Res.*, 7(3), 677–698.
- Héquette, A., M.-H. Ruz, and P. R. Hill (1995), The effects of the Holocene sea-level rise on the evolution of the southeastern coast of the Canadian Beaufort Sea, *J. Coast. Res.*, 11(2), 494–507.

- Hill, P. R. (1990), Coastal geology of the King Point area, Yukon Territory, Canada, *Mar. Geol.*, 91, 93–111.
- Hill, P. R., A. Héquette, M.-H. Ruz, and A. J. Kimberley (1991a), Geological investigations of the Canadian Beaufort Sea coast. Geological Survey of Canada Open File Report 2378. 348 pp.
- Hill, P. R., S. M. Blasco, J. R. Harper, and D. B. Fissel (1991b), Sedimentation on the Canadian Beaufort Shelf, *Cont. Shelf Res.*, 11(8–10), 821–842, doi:10.1016/0278-4343(91)90081-G.
- Hilton, R. G., V. Galy, J. Gaillardet, M. Dellinger, C. Bryant, et al. (2015), Erosion of organic carbon in the Arctic as a geological carbon dioxide sink, *Nature*, 524, 84–87. doi:10.1038/nature14653
- Hinzman, L. D., N. D. Bettez, W. R. Bolton, F. S. Chaplin, M. B. Dyurgerov, et al. (2005), Evidence and Implications of Recent Climate Change in Northern Alaska and Other Arctic Regions, *Clim. Change*, 72(3), 251–298, doi:10.1007/s10584-005-5352-2.
- Hjulström, F. (1932), Das Transportvermögen der Flüsse und die Bestimmung der Erosionsbetrages, *Geogr. Ann.*, 14, 244–258.
- Holmes, R. M., J. McClelland, B. J. Peterson, S. E. Tank, E. Bulygina, et al. (2012), Seasonal and Annual Fluxes of Nutrients and Organic Matter from Large Rivers to the Arctic Ocean and Surrounding Seas, *Estuaries and Coasts*, pp. 369–382. doi:10.1007/s12237-011-9386-6.
- Horton, B. P., S. Rahmstorf, S.E. Engelhart, and A.C. Kemp (2014), Expert assessment of sea-level rise by AD 2100 and AD 2300, *Quaternary Science Reviews* (84), 1–6.
- Hoque, M. A., and W. H. Pollard (2009), Arctic coastal retreat through block failure, *Can. Geotech. J.*, 46(10), 1103–1115, doi:10.1139/T09-058.
- Hoque, Md. A., and W.H. Pollard (2015), Stability of permafrost dominated coastal cliffs in the Arctic, *Polar Science*, 10(1), 79–88, doi:10.1016/j.polar.2015.10.004.
- Houghton, R.A. (2007), Balancing the Global Carbon Budget, *Annual Review of Earth and Planetary Sciences*, 35, 313–47, doi:10.1146/annurev.earth.35.031306.140057.
- Huber, M., A. Gruber, A. Wendleder, B. Wessel, A. Roth, and A. Schmitt (2012), The Global TanDEM-X DEM: Production Status and First Validation Results, *Int. Arch. Photogramm. Remote Sens. Spat. Inf. Sci.*, XXXIX-B7, 45–50, doi:10.5194/isprsarchives-XXXIX-B7-45-2012.
- Hudak, D. R., and J. M. C. Young (2002), Storm climatology of the Southern Beaufort Sea, *Atmosphere-Ocean*, 40(2), 145–158, doi:10.3137/ao.400205.
- Hunter, C. (2013), Sustaining Infrastructure in Canada's North, <http://www.nrcan.gc.ca/science/story/11700> (accessed: 10.07.2017).
- Hugelius, G., C. Tarnocai, G. Broll, J. G. Canadell, P. Kuhry, and D. K. Swanson (2013), The Northern Circumpolar Soil Carbon Database: spatially distributed datasets of soil coverage and soil carbon storage in the northern permafrost regions, *Earth Syst. Sci. Data*, 5(1), 3–13, doi:10.5194/essd-5-3-2013.
- Hugelius, G., J. Strauss, S. Zubrzycki, J. W. Harden, E. A. G. Schuur, et al. (2014), Estimated stocks of circumpolar permafrost carbon with quantified uncertainty ranges and identified data gaps, *Biogeosciences*, 11(23), 6573–6593, doi:10.5194/bg-11-6573-2014.
- Hughes, O. L. (1972), Surficial geology of northern Yukon Territory and northwestern district of Mackenzie, Northwest Territories, Geological Survey of Canada Report 69-36.
- Hume, J. D., and M. Schalk (1964), The effects of ice push on Arctic beaches, *Am. J. Sci.*, 262(2), 267–273, doi:10.2475/ajs.262.2.267.
- IBA (Important Bird Areas) (2017a), Babbage River delta, <https://www.ibacanada.ca/site.jsp?siteID=YK007> (accessed: 12.09.2017)

- IBA (Important Bird Areas) (2017b), Nunaluk Spit to Herschel Island, <http://www.ibacanada.com/site.jsp?siteID=YK005> (accessed: 12.09.2017)
- INAC (Indigenous and Northern Affairs Canada) (2012), Oil and Gas in Canada's North – Active Exploration and New Development, <https://www.aadnc-aandc.gc.ca/eng/1100100037301/1100100037302> (accessed: 25.06.2017).
- INAC (Indigenous and Northern Affairs Canada) (2017a): Historical Northern Oil and Gas Research Initiatives, <https://www.aadnc-aandc.gc.ca/eng/1310570943643/1310572541138> (accessed: 06.09.2017)
- INAC (Indigenous and Northern Affairs Canada) (2017b), Northern Oil and Gas Annual Report 2016. Available at: <https://www.aadnc-aandc.gc.ca/eng/1490033456946/1490033563379>.
- IPCC (Intergovernmental Panel on Climate Change), (2014). Coastal Systems and Low-Lying Areas. In: *Climate Change 2014 – Impacts, Adaptation and Vulnerability: Part A: Global and Sectoral Aspects, Contribution of Working Group II to the Fifth Assessment Report of the IPCC*, 361-410, Cambridge, UK, doi:10.1017/CBO9781107415379.010
- IPCC (Intergovernmental Panel on Climate Change), (2013), *Climate Change 2013: The Physical Science Basis, Contribution of Working Group I to the Fifth Assessment Report of the IPCC*, in T. F. Stocker et al. (Eds.), 1535 pp., Cambridge, UK.
- Irrgang, A.M., H. Lantuit, G. Manson, F. Günther, G. Grosse, and P.P. Overduin (2017), Quantification of shoreline movements along the Yukon Territory mainland coast between 1951 and 2011, Dataset #874343, doi:10.1594/PANGAEA.874343.
- Irrgang, A.M., H. Lantuit, G. Manson, F. Günther, G. Grosse, and P.P. Overduin (in review): Variability in rates of coastal change along the Yukon coast, 1951 to 2015. Submitted to *J. Geophys. Res.: Earth Surface*.
- Jahn, A., J. E. Kay, M. M. Holland, and D. M. Hall (2016), How predictable is the timing of a summer ice-free Arctic?, *Geophys. Res. Lett.*, 43(17), 9113–9120, doi:10.1002/2016GL070067.
- Jeffries, M. O., J. E. Overland, D. K. Perovich (2013), The Arctic shifts to a new normal, *Phys. Today*, 66(10), doi:10.1063/PT.3.2147.
- Jensen, A. M. (2016), Archaeology of the late western Inuit/ Inupiat in north Alaska (A.D. 1300-1750), in *The Oxford handbook of the prehistoric Arctic*, M. T. Friesen and O. K. Mason (Eds.), pp. 513–536, New York, USA.
- Johnson, K., S. Solomon, D. Berry, and P. Graham (2003), Erosion Progression and Adaptation Strategy in a Northern Coastal Community, 8th International Conference on Permafrost, pp. 21-25.
- Jones, B. M., K. M. Hinkel, C. D. Arp, and W. R. Eisner (2008), Modern erosion rates and loss of coastal features and sites, Beaufort Sea coastline, Alaska, *Arctic*, 61(4), 361–372, doi:<http://dx.doi.org/10.14430/arctic44>.
- Jones, B. M., C. D. Arp, M. T. Jorgenson, K. M. Hinkel, J. A. Schmutz, and P. L. Flint (2009a), Increase in the rate and uniformity of coastline erosion in Arctic Alaska, *Geophys. Res. Lett.*, 36(3), 1–5, doi:10.1029/2008GL036205.
- Jones, B. M., C. D. Arp, R. A. Beck, G. Grosse, J. M. Webster, and F. E. Urban (2009b), Erosional history of Cape Halkett and contemporary monitoring of bluff retreat, Beaufort Sea coast, Alaska, *Polar Geogr.*, 32(3–4), 129–142, doi:10.1080/10889370903486449.
- Jones, B. M., J. M. Stoker, A. E. Gibbs, G. Grosse, V. E. Romanovsky, T. A. Douglas, N. E. M. Kinsman, and B. M. Richmond (2013), Quantifying landscape change in an arctic coastal lowland using repeat airborne LiDAR, *Environ. Res. Lett.*, 8(4), 45025 – 10 pp, doi:10.1088/1748-9326/8/4/045025.

- Jorgenson, M. T., and J. Brown (2005), Classification of the Alaskan Beaufort Sea Coast and estimation of carbon and sediment inputs from coastal erosion, *Geo-Marine Lett.*, 25(2–3), 69–80, doi:10.1007/s00367-004-0188-8.
- Kaufman, D. S., D. P. Schneider, N. P. McKay, C. M. Ammann, R. S. Bradley, K. R. Briffa, G. H. Miller, B. L. Otto-Bliesner, J. T. Overpeck, B. M. Vinther, and Arctic Lakes 2k Project Members (2009), Recent Warming Reverses Long-Term Arctic Cooling, *Science* 325(5945), 1236–1239, doi:10.1126/science.1173983.
- Kizyakov, A. I., M. V. Zimin, M. O. Leibman, and N. V. Pravikova (2013), Monitoring of the rate of thermal denudation and thermal abrasion on the western coast of Kolguev Island, using high resolution satellite images, *Earth Cryosphere*, 17(4), 36–47.
- Knoblauch, C., C. Beer, A. Sosnin, D. Wagner, and E. M. Pfeiffer (2013), Predicting long-term carbon mineralization and trace gas production from thawing permafrost of Northeast Siberia, *Glob. Chang. Biol.*, 19(4), 1160–1172, doi:10.1111/gcb.12116.
- Kobayashi, N., J. C. Vidrine, R. B. Nairn, and S. M. Soloman (1999), Erosion of Frozen Cliffs Due to Storm Surge on Beaufort Sea Coast, *J. Coast. Res.*, 15(2), 332–344.
- Kohnert K., A. Serafimovich, J. Hartmann, and T. Sachs (2014), Airborne measurements of methane fluxes in Alaskan and Canadian tundra with the research aircraft Polar 5, *Reports on Polar and Marine Research* (673), 76 pp, Bremerhaven: Alfred Wegener Institute, hdl:10013/epic.43357.d001.
- Kokelj, S.V., C.A.S. Smith, and C.R. Burn (2002), Physical and chemical characteristics of the active layer and permafrost, Herschel Island, western Arctic coast, Canada, *Permafrost and Periglacial Processes*, 13, 171–185, doi:10.1002/ppp.417.
- Kokelj, S. V., T. C. Lantz, J. Kanigan, S. L. Smith, and R. Coutts (2009a), Origin and polycyclic behaviour of tundra thaw slumps, Mackenzie Delta region, Northwest Territories, Canada, *Permafrost Periglac*, 20(2), 173–184.
- Kokelj, S. V., B. Zajdlik, and M. S. Thompson (2009b), The impacts of thawing permafrost on the chemistry of lakes across the subarctic borealtundra transition, Mackenzie Delta region, Canada, *Permafrost Periglac*, 20(2), 185–199.
- Kokelj, S. V., and M. T. Jorgenson (2013), Advances in thermokarst research, *Permafr. Periglac. Process.*, 24(2), 108–119, doi:10.1002/ppp.1779.
- Kokelj, S. V., D. Lacelle, T. C. Lantz, J. Tunnicliffe, L. Malone, I. D. Clark, and K. S. Chin (2013), Thawing of massive ground ice in mega slumps drives increases in stream sediment and solute flux across a range of watershed scales, *J. Geophys. Res. Earth*, 118, 681–692, doi:10.1002/jgrf.20063.
- Kokelj, S. V., J. Tunnicliffe, D. Lacelle, T. C. Lantz, K. D. Chin, and R. Fraser (2015a), Increased precipitation drives mega slump development and destabilization of ice-rich permafrost terrain, northwestern Canada, *Global Planet. Change*, 129, 56–68.
- Kokelj, S. V., J. Tunnicliffe, D. Lacelle, T. C. Lantz, and R. H. Fraser (2015b), Retrogressive thaw slumps: From slope process to the landscape sensitivity of northwestern Canada, in *GEOQuébec 2015, Proceedings of 7th Canadian Permafrost Conference*, Sept. 20–23, Quebec City, Canada.
- Kokelj, S. V., T. C. Lantz, J. Tunnicliffe, R. Segal, and D. Lacelle (2017), Climate-driven thaw of permafrost preserved glacial landscapes, northwestern Canada, *Geology*, 45(4), 371–374.
- Konopczak, A. M., G. K. Manson, and N. J. Couture (2014), Variability of coastal change along the western Yukon coast, Geological Survey of Canada Open File Report 7516, 61 pp. [Available at <http://geoscan.nrcan.gc.ca/starweb/geoscan/servlet.starweb?path=geoscan/shorte.web&search1=R=293788>]
- Kovacs, A. (1983), Shore ice ride-up and pile-up features Part II: Alaska's Beaufort Sea coast, U.S. Army Corps of Engineers, 51 pp, Hanover, USA.

- Koven, C. D., B. Ringeval, P. Friedlingstein, P. Ciais, P. Cadule, D. Khvorostyanov, G. Krinner, and C. Tarnocai (2011), Permafrost carbon-climate feedbacks accelerate global warming., *Proc. Natl. Acad. Sci. U. S. A.*, 108(36), 14769–74, doi:10.1073/pnas.1103910108.
- Krause-Jensen, D., and C. M. Duarte (2014), Expansion of vegetated coastal ecosystems in the future Arctic, *Front. Mar. Sci.*, 1, 1–10, doi:10.3389/fmars.2014.00077.
- Kroon, A., B. H. Jakobsen, and J. B. T. Pedersen (2010), Coastal environments around Thule settlements in Northeast Greenland, *J. Geog.*, 110(2), 143–154, doi:10.1080/00167223.2010.10669504.
- Kroon, A., (2014), 14. High-Latitude Coasts in Masselink G. and R. Gehrels (Eds.): *Coastal Environments and Global Change*, pp. 338-355. 1st edition, 448 p, Chichester, UK.
- Kwok, R., and D. a. Rothrock (2009), Decline in Arctic sea ice thickness from submarine and ICESat records: 1958-2008, *Geophys. Res. Lett.*, 36(15), L15501, doi:10.1029/2009GL039035.
- Lacelle, D., J. Bjornson, and B. Lauriol (2010), Climatic and geomorphic factors affecting contemporary (1950-2004) activity of retrogressive thaw slumps on the Aklavik Plateau, Richardson Mountains, NWT, Canada, *Permafrost Periglac.*, 21(1), 1–15.
- Lacelle, D., A. Brooker, R. H. Fraser, and S. V. Kokelj (2015), Distribution and growth of thaw slumps in the Richardson Mountains–Peel Plateau region, northwestern Canada, *Geomorphology*, 235, 40–51.
- Lackenbauer, W. P., M. J. Farish, and J. Arthur-Lackenbauer (2005), *The Distant Early Warning (DEW) Line: A Bibliography and Documentary Resource List*, Arctic Institute of North America.
- Lantuit, H., and W. H. Pollard (2005), Temporal stereophotogrammetric analysis of retrogressive thaw slumps on Herschel Island, Yukon Territory, *Nat. Hazards Earth Syst. Sci.*, 5(3), 413–423, doi:10.5194/nhess-5-413-2005.
- Lantuit, H., and W. H. Pollard (2008), Fifty years of coastal erosion and retrogressive thaw slump activity on Herschel Island, southern Beaufort Sea, Yukon Territory, Canada, *Geomorphology*, 95(1–2), 84–102, doi:10.1016/j.geomorph.2006.07.040.
- Lantuit, H., P. P. Overduin, and N. Couture (2008), Sensitivity of Coastal Erosion to Ground Ice Contents: An Arctic-Wide Study Based on the ACD Classification of Arctic Coasts, 4 pp, Ninth International Conference on Permafrost. Fairbanks, USA.
- Lantuit, H., D. Atkinson, P. P. Overduin, M. Grigoriev, V. Rachold, G. Grosse, and H.-W. Hubberten (2011), Coastal erosion dynamics on the permafrost-dominated Bykovsky Peninsula, north Siberia, 1951–2006, *Polar Res.*, 30(7341), doi:10.3402/polar.v30i0.7341.
- Lantuit, H., W. H. Pollard, N. Couture, M. Fritz, L. Schirrmeister, H. Meyer, and H.-W. Hubberten (2012a), Modern and Late Holocene Retrogressive Thaw Slump Activity on the Yukon Coastal Plain and Herschel Island, Yukon Territory, Canada, *Permafrost Periglac. Process.*, 23(1), 39–51, doi:10.1002/ppp.1731.
- Lantuit, H., P. P. Overduin, N. J. Couture, S. Wetterich, F. Aré, et al. (2012b), The Arctic Coastal Dynamics Database: A New Classification Scheme and Statistics on Arctic Permafrost Coastlines, *Estuaries and Coasts*, 383-400, doi:10.1007/s12237-010-9362-6.
- Lantz, T. C., and S. V. Kokelj (2008), Increasing rates of retrogressive thaw slump activity in the Mackenzie Delta region, N.W.T., Canada, *Geophys. Res. Lett.*, 35(6), 1–5, doi:10.1029/2007GL032433.
- Lantz, T. C., S. V. Kokelj, S. E. Gergel, and G. H. R. Henry (2009), Relative impacts of disturbance and temperature: Persistent changes in microenvironment and vegetation in retrogressive thaw slumps, *Global Change Biol.*, 15(7), 1664–1675.

- Lawrence, M., B.R. Pelletier, and G. Lacho (1984), Sediment sampling of beaches along the Mackenzie Delta and Tuktoyaktuk Peninsula, Beaufort Sea, Geological Survey of Canada Paper (84-1 A, 633-640), Ottawa, ON: Geological Survey of Canada.
- Lenz, J., Kutnezowa, E. , Choy, E. , Brown, K. , Roy, L. P. and Way, R. (2017): Do's and Don'ts in Arctic Research? An interactive Workshop on Community-based Research with Early Career Scientists, Arctic Science Summit Week, Prague, Czech Republic, 31 March 2017 - 7 April 2017.
- Lewis, C. P., and D. L. Forbes (1974), Sediments and sedimentary processes, Yukon Beaufort Sea coast. Canada, Environmental-Social Committee, Northern Pipelines, Task Force on Northern Oil Development, Report 74-29, 40 p.
- Lewkowicz, A. G. (1987a), Headwall retreat of ground-ice slumps, Banks Island, Northwest Territories, *Can. J. Earth Sci.*, 24(1), 1077–1085, doi:10.1139/e87-105.
- Lewkowicz, A. G. (1987b), Nature and importance of thermokarst processes, Sand Hills Moraine, Banks Island, Canada, *Geogr. Ann. A*, 69(2), 321–327.
- Lewkowicz, A. G. (1988), Ablation of massive ground ice, Mackenzie Delta, in *Proceedings, 5th International Conference on Permafrost*, vol. 1, pp. 605–610.
- Lyons, N. (2004), Early 20th Century Lifeways in Qainiuvik (Clarence Lagoon): Report on the 2003 Archaeological Investigations at Site 76Y. Parks Canada. Internal document.
- Macdonald, R. W., S. M. Solomon, R. E. Cranston, H. E. Welch, M. B. Yunker, and C. Gobeil (1998), A sediment and organic carbon budget for the Canadian beaufort shelf, *Mar. Geol.*, 144(4), 255–273, doi:10.1016/S0025-3227(97)00106-0.
- Macdonald, R. W., A. S. Naidu, M. B. Yunker, and C. Gobeil (2004), The Beaufort Sea: Distribution, sources, fluxes and burial of organic carbon, in R. Stein, R.W. Macdonald (Eds.), *The organic carbon cycle in the Arctic Ocean* (pp. 177-193), Berlin: Springer.
- Macdonald, R. W., Z. Z. A. Kuzyk, and S. C. Johannessen (2015), The vulnerability of Arctic shelf sediments to climate change, *Environ. Rev.*, 479(September), 1–19, doi:10.1139/er-2015-0040.
- Mackay, J. R. (1959), Glacier ice thrust features of the Yukon coast, *Geographical Bull.* 5–21.
- Mackay, J. R. (1963), Notes on the shoreline recession along the coast of the Yukon Territory, *Short Pap. Notes*, 195–197.
- Malone, L., D. Lacelle, S. Kokelj, and I. D. Clark (2013), Impacts of hillslope thaw slumps on the geochemistry of permafrost catchments (Stony Creek watershed, NWT, Canada), *Chem. Geol.*, 356, 38–49.
- Manson, G. K., S. M. Solomon, D. L. Forbes, D. E. Atkinson, and M. Craymer (2005), Spatial variability of factors influencing coastal change in the Western Canadian Arctic, *Geo-Marine Lett.*, 25(2–3), 138–145, doi:10.1007/s00367-004-0195-9.
- Manson, G. K., and S. M. Solomon (2007), Past and future forcing of Beaufort Sea coastal change, *Atmosphere-Ocean*, 45(2), 107–122, doi:10.3137/ao.450204.
- Markus, T., J. C. Stroeve, and J. Miller (2009), Recent changes in Arctic sea ice melt onset, freezeup, and melt season length, *J. Geophys. Res. Ocean.*, 114(12), C12024, doi:10.1029/2009JC005436.
- McCabe, G., M. Clark, and M. Serreze (2001), Trends in Northern Hemisphere surface cyclone frequency and intensity, *J. Clim.*, (1993), 2763–2768.
- McDonald, B. C. and C. P. Lewis (1973), Geomorphic and sedimentologic processes of rivers and coasts, Yukon Coastal Plain. *Environ.-Soc. Comm. Northern Pipelines Task Force on Northern Oil Dev.*, Rep. 73-79, 245 pp.
- McGuire, A. D., J. M. Melillo, D. W. Kicklighter, and L. A. Joyce (1995), Equilibrium Responses of Soil Carbon to Climate Change: Empirical and Process-Based Estimates, *J. Biogeogr.*, 22(4/5), 785–796, doi:10.2307/2845980.

- McGuire, A.D., L.G. Anderson, T.R. Christensen, S. Dallimore, L. Guo, D.J. Hayes, M. Heimann, T.D. Lorenson, R.W. Macdonald, and N. Roulet (2009), Sensitivity of the carbon cycle in the Arctic to climate change, *Ecological Monographs*, 79, 523-555, doi:10.1890/08-2025.1.
- Mars, J. C., and D. W. Houseknecht (2007), Quantitative remote sensing study indicates doubling of coastal erosion rate in past 50 yr along a segment of the Arctic coast of Alaska, *Geology*, 35(7), 583–586, doi:10.1130/G23672A.1.
- Maslakov, A., and G. Kraev (2016), Erodibility of permafrost exposures in the coasts of Eastern Chukotka, *Polar Sci.*, 10(3), 374–381, doi:10.1016/j.polar.2016.04.009.
- Michaelson, G. J., C. L. Ping, and J. M. Kimble (1996), Carbon storage and distribution in tundra soils of arctic Alaska, U.S.A. *Arctic and Alpine Research*, 28, 414-424.
- Nagy, M. I. (1994), Yukon North Slope Inuvialuit Oral History, *Occas. Pap. Yukon Hist.*, 1, 119.
- Naidu, A. S., S. W. Cooper, B. P. Finney, R. W. Macdonald, C. Alexander, and I. P. Semiletov (2000). Organic carbon isotope ratios ($\delta^{13}\text{C}$) of Amerasian continental shelf sediments. *International Journal of Earth Sciences*, 89, 522-532, doi:10.1007/s005310000121.
- Neff, J. C., and G. P. Asner (2001), Dissolved organic carbon in terrestrial ecosystems: Synthesis and a model, *Ecosystems*, 4(1), 29–48, doi:10.1007/s100210000058.
- Neufeld, D. (2002), The Distant Early Warning (DEW) Line - A Preliminary Assessment of its Role and Effects upon Northern Canada. Arctic Institute of North America.
- NRCan (Natural Resources Canada), (2016a), National air photo library, <http://www.nrcan.gc.ca/earth-sciences/geomatics/satellite-imagery-air-photos/9265>. (last access: 18.09.2016)
- NRCan (Natural Resources Canada), (2016b), Canadian Spatial Reference System – Precise Point Positioning (CSRS-PPP), <http://www.nrcan.gc.ca/earth-sciences/geomatics/geodetic-reference-systems/tools-applications/10925#ppp>. [accessed: 11.03.2017]
- NRCan (Natural Resources Canada), (2013), Guidelines for RTK/RTN GNSS surveying in Canada. [Available at: <http://publications.gc.ca/site/eng/9.822881/publication.html>]
- NT Government (Northwest Territories Government) (2015), Projected trends in Beaufort Sea levels, in: NWT State of the Environment Report. Environment and Natural Resources. [Available at: <http://www.enr.gov.nt.ca/en/state-environment/17-projected-trends-beaufort-sea-levels>.]
- O'Brien, M. C., R. W. Macdonald, H. Melling, and K. Iseki (2006), Particle fluxes and geochemistry on the Canadian Beaufort Shelf: Implications for sediment transport and deposition. *Continental Shelf Research*, 26, 41-81, doi:10.1016/j.csr.2005.09.007.
- Obu, J., H. Lantuit, M. Fritz, W. H. Pollard, T. Sachs, and F. Günther (2016a), Relation between planimetric and volumetric measurements of permafrost coast erosion: A case study from Herschel Island, western Canadian Arctic, *Polar Res.*, 35(2016), 1–13, doi:10.3402/polar.v35.30313.
- Obu, J., H. Lantuit, M. Fritz, G. Grosse, F. Günther, et al. (2016b), LiDAR elevation data of Yukon Coast and Herschel Island in 2012 and 2013. doi:10.1594/PANGAEA.859046, Supplement to: Obu, J. et al. (2016), Dynamics of permafrost coasts along the Canadian Beaufort Sea based on annual airborne LiDAR elevation data. *Geomorphology*. [Available at: <https://doi.pangaea.de/10.1594/PANGAEA.859046>]
- Obu, J., H. Lantuit, G. Grosse, F. Günther, T. Sachs, V. Helm, and M. Fritz (2017a), Coastal erosion and mass wasting along the Canadian Beaufort Sea based on annual airborne LiDAR elevation data, *Geomorphology*, doi:10.1016/j.geomorph.2016.02.014.
- Obu, J., H. Lantuit, I. Myers-Smith, B. Heim, J. Wolter, and M. Fritz (2017b), Effect of terrain characteristics on soil organic carbon and total nitrogen stocks in soils of

- Herschel Island, western Canadian Arctic. *Permafrost and Periglacial Processes*, 28, 92-107, doi: 10.1002/ppp.1881.
- Ogorodov, S. A., A. V. Baranskaya, N. G. Belova, A. M. Kamalov, D. E. Kuznetsov, P. P. Overduin, N. N. Shabanova, and A. P. Vergun (2016), Coastal dynamics of the Pechora and Kara Seas under changing climatic conditions and human disturbances, *Geogr. Environ. Sustain.*, 9(3), 53–73, doi:10.15356/2071-9388.
- Olsen, M. S., T. V. Callaghan, J. D. Reist, L. O. Reiersen, D. Dahl-Jensen, et al. (2011), The Changing Arctic Cryosphere and Likely Consequences: An Overview, *Ambio*, 40(S1), 111–118, doi:10.1007/s13280-011-0220-y.
- O'Rourke, M. J. E. (2017), Archaeological Site Vulnerability Modelling: The Influence of High Impact Storm Events on Models of Shoreline Erosion in the Western Canadian Arctic, *Open Archaeol.*, 3(1), 1–16, doi:10.1515/opar-2017-0001.
- Overduin, P. P., M. C. Strzelecki, M. N. Grigoriev, N. Couture, H. Lantuit, D. St-Hilaire-Gravel, F. Gunther, and S. Wetterich (2014), Coastal changes in the Arctic, in *Sedimentary Coastal Zones from High to Low Latitudes: Similarities and Differences.*, in I. P. Martini, I. P. and H. R. Wanless (Eds.), 103–129, Geological Society, London, Special Publications, 388 pp, London. UK.
- Overeem, I., R. S. Anderson, C. W. Wobus, G. D. Clow, F. E. Urban, and N. Matell (2011), Sea ice loss enhances wave action at the Arctic coast, *Geophys. Res. Lett.*, 38(17), L17503, doi:10.1029/2011GL048681.
- Overland, J., J. A. Francis, R. Hall, E. Hanna, S. J. Kim, and T. Vihma (2015), The melting arctic and midlatitude weather patterns: Are they connected?, *J. Clim.*, 28(20), 7917–7932, doi:10.1175/JCLI-D-14-00822.1.
- Overland, J. E., M. Wang, J. E. Walsh, and J. C. Stroeve (2013), Future Arctic climate changes: Adaptation and mitigation time scales, *Earth's Futur.*, 2, 68–74, doi:10.1002/2013EF000162.
- Overland, J. E., K. Dethloff, J. A. Francis, R. J. Hall, E. Hanna, S.-J. Kim, J. A. Screen, T. G. Shepherd, and T. Vihma (2016a), Nonlinear response of mid-latitude weather to the changing Arctic, *Nat. Clim. Chang.*, 6(11), 992–999, doi:10.1038/nclimate3121.
- Overland, J., E. Hanna, I. Hanssen-Bauer, S.-J. Kim, E. J. Walsh, M. Wang, U. S. Bhatt, and R. L. Thoman (2016b), Arctic Report Card, 2016, Surface Air Temperature <http://www.arctic.noaa.gov/Report-Card/Report-Card-2016/ArtMID/5022/ArticleID/271/Surface-Air-Temperature> (accessed: 18.09.2017)
- Overland, J. E., and M. Wang, (2007), Future regional Arctic sea ice decline. *Geophys. Res. Lett.*, 34, L17705, doi:10.1029/2007GL030808.
- Owens, E. H., and J. R. Harper (1977), Frost-Table and Thaw Depths in the Littoral Zone near Peard Bay, Alaska, Arctic, 30(3), 155–168.
- Parks Canada Agency (2007), Ivvavik Archaeological Sites Database. Winnipeg: Government of Canada. Not published.
- Parkinson, C. L., and J. C. Comiso (2013), On the 2012 record low Arctic sea ice cover: combined impact of preconditioning and an August storm, *Geophys. Res. Lett.*, 40(7), 1356–1361, doi:10.1002/grl.50349.
- Pelletier, B. R. and B. E. Medioli (2014), Environmental Atlas of the Beaufort Coastlands, Geological Survey of Canada Open File Report 7619. [Available at: <http://geoscan.nrcan.gc.ca/starweb/geoscan/servlet.starweb?path=geoscan/fulle.web&search1=R=294601>]
- Pinchin, B. M., R. B. Nairn, and K. L. Philpott (1985), Beaufort Sea Coastal Sediment Study Numerical Estimation of Sediment Transport and Nearshore Profile Adjustment. Geological Survey of Canada Open File Report 1259.

- Ping, C.-L., G. J. Michaelson, M. T. Jorgenson, J. M. Kimble, H. Epstein, V. E. Romanovsky, and D. A. Walker (2008), High stocks of soil organic carbon in the North American Arctic region, *Nature Geoscience*, 1, 615 – 619, doi:10.1038/ngeo284.
- Ping, C.-L., G. J. Michaelson, L. Guo, M. T. Jorgenson, M. Kanevskiy, Y. Shur, F. Dou, and J. Liang (2011), Soil carbon and material fluxes across the eroding Alaska Beaufort Sea coastline, *J. Geophys. Res.*, 116(G02), G02004, doi:10.1029/2010JG001588.
- Malone, L., D. Lacelle, S. Kokelj, and I. D. Clark (2013), Impacts of hillslope thaw slumps on the geochemistry of permafrost catchments (Stony Creek watershed, NWT, Canada), *Chem. Geol.*, 356, 38–49.
- Proshutinsky, A., D. Dukhovskoy, M. Timmermans, R. Krishfield, and J. L. Bamber (2015), Arctic circulation regimes, *Philosophical Trans. A*, 373(20140160), 1-18.
- Rachold, V., M. N. Grigoriev, F. E. Aré, S. Solomon, E. Reimnitz, H. Kassens, and M. Antonow (2000), Coastal erosion vs riverine sediment discharge in the Arctic Shelf seas, *Int. J. Earth Sci.*, 89(3), 450–460, doi:10.1007/s005310000113.
- Rachold, V., F. E. Aré, D. E. Atkinson, G. Cherkashov, and S. M. Solomon (2004a), Arctic Coastal Dynamics (ACD): an introduction, *Geo-Marine Lett.*, 25(2–3), 63–68, doi:10.1007/s00367-004-0187-9.
- Rachold, V., H. Eicken, V. V. Gordeev, M. N. Grigoriev, H.-W. Hubberten, A. P. Lisitzin, V. P. Shevchenko, and L. Schirrmeister (2004b), Modern terrigenous organic input to the Arctic Ocean, in *The Organic Carbon Cycle in the Arctic Ocean*, R. Stein and R. W. Macdonald (Eds.), pp. 33–55, Springer, Berlin / Heidelberg, Germany.
- Rachold, V., H. Lantuit, N. Couture, and W. H. Pollard (eds.) (2005), *Arctic Coastal Dynamics: Report of the 5th International Workshop*. *Berichte zur Polar- und Meeresforschung*, 506, 1–143.
- Radosavljevic, B., H. Lantuit, W. Pollard, P. Overduin, N. Couture, T. Sachs, V. Helm, and M. Fritz (2015), Erosion and Flooding - Threats to Coastal Infrastructure in the Arctic: A Case Study from Herschel Island, Yukon Territory, Canada, *Estuaries and Coasts*, doi:10.1007/s12237-015-0046-0.
- Ramage J. L., A. M. Irrgang, U. Herzsuh, A. Morgenstern, N. Couture, and H. Lantuit (2017), Terrain Controls on the Occurrence of Coastal Retrogressive Thaw Slumps along the Yukon Coast, Canada, *J. Geophys. Res.: Earth Surface*, 122, doi:10.1002/2017JF004231.
- Rampton, V. N. (1982), Quaternary Geology of the Yukon Coastal Plain, Geological Survey of Canada, Bulletin 317, 49 pp. [Available at: <http://geoscan.nrcan.gc.ca/starweb/geoscan/servlet.starweb?path=geoscan/shorte.web&search1=R=111347>]
- Reimnitz, E., and D. K. Maurer (1979), Effects of Storm Surges on the Beaufort Sea Coast, Northern Alaska, *Arctic*, 32(4), 329–344, doi: <http://dx.doi.org/10.14430/arctic2631>.
- Reimnitz, E., S. M. Graves, and P. W. Barnes (1985), Beaufort Sea coastal erosion, shoreline evolution and sediment flux, U.S. Geological Survey Open File Report 85-380.
- Reimnitz, E., S. M. Graves, and P. W. Barnes (1988), Beaufort Sea coastal erosion, sediment flux, shoreline evolution, and the erosional shelf profile, U.S. Geological Survey Open File Report 85-380.
- Reimnitz, E., P. W. Barnes, and J. R. Harper (1990), A Review of Beach Nourishment from Ice Transport of Shoreface Materials, Beaufort Sea, Alaska, *J. Coast. Res.*, 6(2), 439–469.
- Richter-Menge, J., and J. Mathis (2016), The Arctic, in *State of the climate in 2015*, in J. Blunden and D. S. Arndt (Eds.), *Bulletin of the American Meteorological Society*, 97 (8), S131–S152.

- Richter-Menge, J., J. E. Overland and J. Mathis (2016), Arctic Report Card, Update for 2016, Executive Summary. <http://www.arctic.noaa.gov/Report-Card/Report-Card-2016/ArtMID/5022/ArticleID/270/Executive-Summary> (accessed: 18.09.2017)
- Rudy, A. C. A., S. F. Lamoureux, P. Treitz, K. Van Ewijk, P. P. Bonnaventure, and P. Budkewitsch (2017), Terrain Controls and Landscape-Scale Susceptibility Modelling of Active-Layer Detachments, Sabine Peninsula, Melville Island, Nunavut, Permafrost. *Periglac. Process.*, 28(1), 79–91, doi:10.1002/ppp.1900.
- Saxberg, N. (1993), The archaeology and history of an arctic mission, Herschel Island, Yukon, *Occas. Pap. Archaeol.*, 4, 103.
- Schaefer, K., H. Lantuit, V. E. Romanovsky, E. A. G. Schuur, and R. Witt (2014), The impact of the permafrost carbon feedback on global climate, *Environ. Res. Lett.*, 9(8), 85003, doi:10.1088/1748-9326/9/8/085003.
- Schuur, E. A. G., J. Brockenheim, J. G. Canadell, E. Euskirchen, C. B. Field, et al. (2008), Vulnerability of Permafrost Carbon to Climate Change: Implications for the Global Carbon Cycle, *Bioscience*, 58(8), 701, doi:10.1641/B580807.
- Schuur, E. A. G., A. D. McGuire, G. Grosse, J. W. Harden, D. J. Hayes, G. Hugelius, C. D. Koven, and P. Kuhry (2015), Climate change and the permafrost carbon feedback, *Nature*, 520, 171–179, doi:10.1038/nature14338.
- Segal, R. A., T. C. Lantz, and S. V Kokelj (2016), Acceleration of thaw slump activity in glaciated landscapes of the Western Canadian Arctic, *Environ. Res. Lett.*, 11(3), 34025, doi:10.1088/1748-9326/11/3/034025.
- Serreze, M. C., J. E. Walsh, T. Osterkamp, M. Dyurgerov, V. Romanovsky, W. C. Oechel, J. Morison, T. Zhang, and R. G. Barry (2000), Observational evidence of recent change in the northern high-latitude environment, *Clim. Chang.*, 46, 159–207.
- Serreze, M. C., A. P. Barrett, J. C. Stroeve, D. N. Kindig, and M. M. Holland (2009), The emergence of surface-based Arctic amplification, *Cryosph.*, 3, 11–19, doi:10.5194/tc-3-11-2009.
- Serreze, M. C., and R. G. Barry (2011), Processes and impacts of Arctic amplification: A research synthesis, *Glob. Planet. Change*, 77(1–2), 85–96, doi:10.1016/j.gloplacha.2011.03.004.
- Smith, C. A. S., C. E. Kennedy, A. E. Hargrave, and K.M. McKenna (1989), Soil and vegetation of Herschel Island, Yukon Territory, Yukon Soil Survey Report (No. 1, 101 pp.), Ottawa, ON: Land Resource Research Centre, Agriculture Canada.
- Smith, L. C., and S. R. Stephenson (2013), New Trans-Arctic shipping routes navigable by midcentury, *Proc. Natl. Acad. Sci.*, 110(13), E1191–E1195, doi:10.1073/pnas.1214212110.
- Smith, S. L., V. E. Romanovsky, A. G. Lewkowicz, C. R. Burn, M. Allard, G. D. Clow, K. Yoshikawa, and J. Throop (2010), Thermal state of permafrost in North America: a contribution to the International Polar Year, *Permafrost. Periglac. Process.*, 21(2), 117–135, doi:10.1002/ppp.690.
- Solomon, S. M., D. L. Forbes, and B. Kierstead (1994), Coastal impacts of climate change: Beaufort sea erosion study, Geological Survey of Canada Open File 2890, 35 pp. [Available at: <http://geoscan.nrcan.gc.ca/starweb/geoscan/servlet.starweb?path=geoscan/shorte.web&search1=R=194148>]
- Solomon, S. M. (1996), Ivvavik National Park coastal erosion study. Open File Report 3323.
- Solomon, S. M. (1998), Draft Report to Department of National Defense and Ivvavik National Park on Coastal Erosion at the Komakuk DEW Line Site. Unpublished.
- Solomon, S. M. and D. Frobel (1999), Coastal video survey: aerial video surveys – Beaufort Sea coast; Geological Survey of Canada.

- Solomon, S. M. (2005), Spatial and temporal variability of shoreline change in the Beaufort-Mackenzie region, northwest territories, Canada, *Geo-Marine Lett.*, 25(2–3), 127–137, doi:10.1007/s00367-004-0194-x.
- Stammerjohn, S., R. Massom, D. Rind, and D. Martinson (2012), Regions of rapid sea ice change: An inter-hemispheric seasonal comparison, *Geophys. Res. Lett.*, 39, 1–8, doi:10.1029/2012GL050874.
- Stein, R., and R.W. Macdonald (Eds.). (2004). *The organic carbon cycle in the Arctic Ocean*. Berlin, Germany.
- Stephenson, S. R., and L. C. Smith (2015), Influence of climate model variability on projected Arctic shipping futures, *Earth's Future*, 3(11), 331–343, doi:10.1002/2015EF000317.
- Stern, G.A. and A. Gaden (2015), *From Science to Policy in the Western and Central Canadian Arctic: An Integrated Regional Impact Study (IRIS) of Climate Change and Modernization*. ArcticNet, Québec City, 432 pp.
- Strauss, J., L. Schirmermeister, G. Grosse, S. Wetterich, M. Ulrich, U. Herzschuh, and H.-W. Hubberten (2013), The deep permafrost carbon pool of the Yedoma region in Siberia and Alaska, *Geophys. Res. Lett.*, 40, 2013GL058088, doi:10.1002/2013GL058088.
- Streicker, J. (2016), *Yukon Climate Change Indicators and Key Findings 2015*. Northern Climate Exchange, 84 pp., Yukon Research Centre, Yukon College, Whitehorse, Canada.
- Streletskaia, I. D., A. A. Vasiliev, and B. G. Vanstein (2009), Erosion of sediment and organic carbon from the Kara Sea coast, Arctic, Antarctic, and Alpine Research, 41, 79–87, doi:10.1657/1938-4246(08-017).
- Stroeve, J., M. M. Holland, W. Meier, T. Scambos, and M. Serreze (2007), Arctic sea ice decline: Faster than forecast, *Geophys. Res. Lett.*, 34(9), L09501, doi:10.1029/2007GL029703.
- Stroeve, J. C., M. C. Serreze, M. M. Holland, J. E. Kay, J. Malanik, and A. P. Barrett (2011), The Arctic's rapidly shrinking sea ice cover: a research synthesis, *Clim. Change*, 110(3–4), 1005–1027, doi:10.1007/s10584-011-0101-1.
- Stroeve, J. C., T. Markus, L. Boisvert, J. Miller, and A. Barrett (2014), Changes in Arctic melt season and implications for sea ice loss, *Geophys. Res. Lett.*, 41, 1216–1225, doi:10.1002/2013GL058951.
- Tanski, G., N. Couture, H. Lantuit, A. Eulenburg, and M. Fritz (2016), Eroding permafrost coasts release low amounts of dissolved organic carbon (DOC) from ground ice into the nearshore zone of the Arctic Ocean, *Global Biogeochem. Cycles*, 30, 1054–1068, doi:10.1002/2015GB005337.
- Tanski, G., H. Lantuit, S. Ruttore, C. Knoblauch, B. Radosavljevic, J. Strauss, J. Wolter, A. M. Irrgang, J. Ramage, and M. Fritz (2017), Transformation of terrestrial organic matter along thermokarst-affected permafrost coasts in the Arctic, *Sci. Total Environ.*, 581–582, 434–447, doi:10.1016/j.scitotenv.2016.12.152.
- Tarnocai, C. (1998), The amount of organic carbon in various soil orders and ecological provinces in Canada, in R. Lal, J.M. Kimble, R.F. Follett, B.A. Stewart (Eds.), *Soil processes and the carbon cycle*, pp. 81–92, Boca Raton, FL: CRC Press.
- Tarnocai, C., and B. Lacelle (1996), *The soil organic carbon digital database of Canada*. Ottawa, ON: Research Branch, Agriculture Canada.
- Tarnocai, C., J. Kimble and G. Broll (2003), Determining carbon stocks in cryosols using the northern and mid latitudes soil database, *Proceedings 8th International Conference on Permafrost* (pp. 10129–1134), Zürich, Switzerland.
- Tarnocai, C., C.-L. Ping, and J. Kimble (2007), Carbon Cycles in the Permafrost Region of North America, in A. W. King, L. Dilling, G.P. Zimmerman, D.M. Fairman, R.A. Houghton, G. Marland, A. Z. Rose, T. J. Wilbanks (Eds.), *The first state of the carbon*

- cycle report (SOCCR): The North American carbon budget and implications for the global carbon cycle, pp. 127-138, Asheville, USA.
- Tarnocai, C., J. G. Canadell, E. A. G. Schuur, P. Kuhry, G. Mazhitova, and S. Zimov (2009), Soil organic carbon pools in the northern circumpolar permafrost region, *Global Biogeochem. Cycles*, 23(2), 1–11, doi:10.1029/2008GB003327.
- Thieler, E. R., E. A. Himmelstoss, J. L. Zichichi, and E. Ayhan (2009), Digital Shoreline Analysis System (DSAS) version 4.0 - An ArcGIS extension for calculating shoreline change, U.S. Geological Survey Open-File Rep. 2008 - 1278, 79 pp. [Available at <https://woodshole.er.usgs.gov/project-pages/DSAS/version4/>]
- Thompson, F. (1994), An interpretive manual for reports on granular deposits in the Inuvialuit settlement region, Indian and Northern Affairs Canada, Part of the Inuvialuit Final Agreement Implementation Program Task 7 - Sand and Gravel, 70 pp.
- Thomson, J., and W. E. Rogers (2014), Swell and sea in the emerging Arctic Ocean, *Geophys. Res. Lett.*, 1–5, doi:10.1002/2014GL059983.
- Thomson, J., Y. Fan, S. Stammerjohn, J. Stopa, W. E. Rogers, et al. (2016), Emerging trends in the sea state of the Beaufort and Chukchi seas, *Ocean Model.*, 105, 1–12, doi:10.1016/j.ocemod.2016.02.009.
- Thomson, S. (1998), 1996-97 coastal archaeological survey, Ivvavik National Park. Parks Canada. Western Canada Service Center, Winnipeg, Canada.
- Thomson, S. (2009), 2008 Cultural Resource Investigations, Ivvavik National Park of Canada. Western and Northern Service Centre. Parks Canada Agency. Winnipeg, Canada.
- Timmermans, M.-L., (2016), Arctic Report Card 2016, Sea Surface Temperatures. <http://www.arctic.noaa.gov/Report-Card/Report-Card-2016/ArtMID/5022/ArticleID/285/Sea-Surface-Temperature> (accessed: 18.09.2017)
- Timmermans, M.-L., and A. Proshutinsky (2016), (The Arctic) Sea Surface Temperature, in J. Blunden, D.S. Arndt (Eds.), *State of the Climate in 2015*. Bulletin of the American Meteorological Society, 97(8), S137-S138.
- Tweedie, C.E., Aguirre, A., Cody, R., Vargas, S. and J. Brown (2012), Spatial and Temporal Dynamics of Erosion Along the Elson Lagoon Coastline near Barrow, Alaska (2002-2011), *Proceedings of the Tenth International Conference on Permafrost, Volume 1: International Contribution*, 405-430.
- Ulrich, M., G. Grosse, J. Strauss, and L. Schirmermeister (2014), Quantifying wedge-ice volumes in yedoma and thermokarst basin deposits, *Permafrost and Periglacial Processes*, 25, 151-161. doi:10.1002/ppp.1810.
- UNESCO (United Nations Educational, Scientific and Cultural Organization) (2004), Ivvavik/Vuntut/ Herschel Island (Qikiqtaruk). <http://whc.unesco.org/en/tentativelists/1939/>. (accessed: 07.09.2017)
- Vasiliev, A., M. Kanevskiy, G. Cherkashov, and B. Vanshtein (2005), Coastal dynamics at the Barents and Kara Sea key sites, *Geo-Marine Lett.*, 25(2–3), 110–120, doi:10.1007/s00367-004-0192-z.
- Vermaire, J. C., M. F. J. Pisaric, J. R. Thienpont, C. J. Courtney Mustaphi, S. V. Kokelj, and J. P. Smol (2013), Arctic climate warming and sea ice declines lead to increased storm surge activity, *Geophys. Res. Lett.*, 40(7), 1386–1390, doi:10.1002/grl.50191.
- Vetrov, A.A., and E.A. Romankevich (Eds.) (2004), *Carbon cycle in the Russian Arctic seas*. Berlin, Germany.
- Vonk, J. E. (2014), Preferential burial of permafrost-derived organic carbon in Siberian-Arctic shelf waters, *J. Geophys. Res. Ocean.*, 8410–8421, doi:10.1002/2014JC010261.
- Vonk, J. E., L. Sanches-Garcia, B.E. van Dongen, V. Alling, D. Kosmach, et al. (2012), Activation of old carbon by erosion of coastal and subsea permafrost in Arctic Siberia, *Nature*, 489(7414), 137–40, doi:10.1038/nature11392.

- Walker, D. A., M. K. Raynolds, F. J. A. Daniëls, E. Einarsson, A. Elvebakk, W. A. Gould, and A. E. Katenin (2005), The Circumpolar Arctic vegetation map, *J. Veg. Sci.*, 16, 267–282, doi:10.1111/j.1654-1103.2005.tb02365.x.
- Walsh, J. E. (2005), Cryosphere and Hydrology, in ACIA Scientific Report, pp. 183–242, Cambridge, UK.
- Wang, M., and J. E. Overland (2009), A sea ice free summer Arctic within 30 years?, *Geophys. Res. Lett.*, 36(7), 2–6, doi:10.1029/2009GL037820.
- Wegner, C., K. E. Bennett, A. de Vernal, M. Forwick, M. Fritz, et al. (2015), Variability in transport of terrigenous material on the shelves and the deep Arctic Ocean during the Holocene, *Polar Res.*, 34, 1–19, doi:10.3402/polar.v34.24964.
- Winton, M. (2006), Amplified Arctic climate change: What does surface albedo feedback have to do with it?, *Geophys. Res. Lett.*, 33(3), 1–4, doi:10.1029/2005GL025244.
- Wobus, C., R. Anderson, I. Overeem, N. Matell, G. Clow, and F. Urban (2011), Thermal Erosion of a Permafrost Coastline: Improving Process-Based Models Using Time-Lapse Photography, *Arctic, Antarct. Alp. Res.*, 43(3), 474–484, doi:10.1657/1938-4246-43.3.474.
- Wolfe, S. A., S. R. Dallimore, and S. M. Solomon (1998), Coastal permafrost investigations along a rapidly eroding shoreline, Tuktoyaktuk, N.W.T, in PERMAFROST - 7th International Conference, pp. 1125–1131, Yellowknife, Canada.
- Wolfe, S. A., E. Kotler, and S. R. Dallimore (2001), Surficial characteristics and the distribution of thaw landforms (1970 to 1999), Shingle Point to Kay Point, Yukon Territory, Geological Survey of Canada Open File 4115, 18 pp. [Available at <http://geoscan.nrcan.gc.ca/starweb/geoscan/servlet.starweb?path=geoscan/shorte.web&search1=R=212842>]
- Woodroffe, C. D., and C. V. Murray-Wallace (2012), Sea-level rise and coastal change: The past as a guide to the future, *Quat. Sci. Rev.*, 54, 4–11, doi:10.1016/j.quascirev.2012.05.009.
- Yukon Department of Environment (2016), 30 Meter Yukon Digital Elevation Model. [Available at: http://www.env.gov.yk.ca/publications-maps/geomatics/data/30m_dem.php/]
- Yukon Government (2016), Yukon Archaeology Sites Database. Whitehorse, Canada.
- Yunker, M. B., F. A. McLaughlin, B. R. Fowler, T. A. Smyth, W. J. Cretney, R. W. Macdonald, and D. McCullough (1990), Hydrocarbon Determinations; Mackenzie River and Beaufort, Sea Shoreline Peat Samples. Canadian Data Report of Hydrography and Ocean Sciences (NOGAP), 7(60), 81 pp., Ottawa, ON: Department of Fisheries and Oceans.
- Yunker, M. B., R. W. Macdonald, B. R. Fowler, W. J. Cretney, S. R. Dallimore, and F. A. McLaughlin (1991), Geochemistry and fluxes of hydrocarbons to the Beaufort Sea shelf: A multivariate comparison of fluvial inputs and coastal erosion of peat using principal components analysis. *Geochimica et Cosmochimica Acta*, 55, 255–213, doi:10.1016/0016-7037(91)90416-3.
- Yunker, M. B., R. W. Macdonald, W. J. Cretney, B. R. Fowler, and F. A. McLaughlin (1993), Alkane, terpene, and polycyclic aromatic hydrocarbon geochemistry of the Mackenzie River and Mackenzie shelf: Riverine contributions to Beaufort Sea coastal sediment. *Geochimica et Cosmochimica Acta*, 57, 3041–3061, doi:10.1016/0016-7037(93)90292-5.
- Zhang, K., B. C. Douglas, and S. P. Leatherman (2004), Global Warming and Coastal Erosion. *Climatic Change*, 64, 41–58. doi:10.1023/b:clim.0000024690.32682.48.
- Zhang, Y., and W. Chen (2005), Soil temperature in Canada during the twentieth century: Complex responses to atmospheric climate change, *J. Geophys. Res.*, 110(D3), D03112, doi:10.1029/2004JD004910.

-
- Zimov, S. A., E. A. G. Schuur, and F. S. Chapin III (2006), Permafrost and the global carbon budget, *Science*, 312, 1612 – 1613, doi:10.1126/ science.1128908.
- Zöckler, C., T. Douglas (Eds.) (2011), 2.2 Ecological State of the Circum-Arctic Coast, in Forbes (Ed.) (2011): *State of the Arctic Coast*, 2010, Geesthacht, Germany.

Supporting Material

All supporting material is available at:

<http://onlinelibrary.wiley.com/doi/10.1002/2017JF004231/full>

Data Set ds01: Shapefile containing 287 polygons, which represent retrogressive thaw slumps and associated geographic information. The shapefile is available online: doi:10.1594/PANGAEA.869573.

Table S1: RTSs characteristics. The table includes morphological information for the 287 retrogressive thaw slumps that occurred in 2011 along the Yukon Coast.

Name	Segment	Segment_name	Glaciated	GEOLUNIT	Area	Coastal length	Number of R	Number of A	Active RTS	Number of N	New RTS	Density of R
Information	Segment	Segment_name	Glaciated	Geolunit	Area	CL	Number_RTS	Number_AR	ARTS_p	Number_NR	NRTS_p	Density_RT
Unit					(ha)	(km)			(%)		(%)	(RTS per km
Source	Rampton, 19	Rampton, 1982	This study	Rampton, 19	This study	This study	This study	This study	This study	This study	This study	This study
BRD	Babbage River Delta		Yes	Fp	653.2	13.48	0	0	0	0	0	0
CL_E	Clarence Lagoon E		No	Ft	50.7	1.09	0	0	0	0	0	0
CL_W	Clarence Lagoon W		No	L	159.22	3.21	0	0	0	0	0	0
HER_E	Herschel Island E		Yes	Mr	526.91	11.32	28	23	82.14	9	32.14	2.5
HER_N	Herschel Island N		Yes	Mr	840.39	17.3	22	15	68.18	17	77.27	1.3
HER_S	Herschel Island S		Yes	Mr	585.22	12.49	31	18	58.06	20	64.52	2.5
HER_W	Herschel Island W		Yes	Mr	270.93	5.47	18	15	83.33	7	38.89	3.3
KaP_SE	Kay Point SE		Yes	Mr	1179.3	24.18	74	50	67.57	35	47.3	3.1
KaPS	Kay Point spit		Yes	mb	42.93	1.44	0	0	0	0	0	0
KB	Komakuk Beach		No	L	654.8	13.53	0	0	0	0	0	0
KBW1	Komakuk Beach W1		No	L	91.49	1.84	0	0	0	0	0	0
KBW2	Komakuk Beach W2		No	L	399.82	8.13	0	0	0	0	0	0
KiP	King Point		Yes	L	50.54	1.1	0	0	0	0	0	0
KiP_NW	King Point NW		Yes	Mm	159.59	3.31	6	4	66.67	1	16.67	1.8
KiP_SE	King Point SE		Yes	L	188.07	3.78	12	9	75	3	25	3.2
KiPL	King Point lagoon		Yes	mb	110.1	2.49	0	0	0	0	0	0
MRF	Malcolm River fan		No	Ff	442.78	8.88	0	0	0	0	0	0
MRF_bi	Malcolm River fan with b		No	Ff	1410.88	28.36	0	0	0	0	0	0
PhB	Phillips Bay		Yes	L	449.36	9.68	5	3	60	2	40	0.5
PhB_NW	Phillips Bay NW		Yes	Mm	130.07	2.61	7	5	71.43	1	14.29	2.7
PhB_W	Phillips Bay W		Yes	mb	257.96	5.24	0	0	0	0	0	0
RB_E	Roland Bay E		Yes	L	110.02	2.24	4	3	75	0	0	1.8
RB_NW	Roland Bay NW		Yes	L	140.72	2.83	0	0	0	0	0	0
RB_W	Roland Bay W		Yes	Mm	141.23	2.86	10	8	80	0	0	3.5
SaP	Sabine Point		Yes	Mm	120.36	2.41	7	5	71.43	2	28.57	2.9
SaP_E	Sabine Point E		Yes	L	123.26	2.48	4	2	50	3	75	1.6
SaP_W	Sabine Point W		Yes	L	133.77	2.68	2	2	100	2	100	0.7
ShP_W	Shingle Point W		Yes	Mm	450.258	9.03	38	33	86.84	9	11.84	4.2
StP	Stokes Point		Yes	mb	242.73	5.03	0	0	0	0	0	0
StP_SE	Stokes Point SE		Yes	L	196.56	3.96	4	1	25	1	25	1
StP_W	Stokes Point W		Yes	Mm	141.09	2.86	12	5	41.67	6	50	4.2
WhC	Whale Cove		Yes	mb	133.41	2.71	0	0	0	0	0	0
WhC_E	Whale Cove E		Yes	Mm	40.59	0.83	2	1	50	0	0	2.4
WhC_W	Whale Cove W		Yes	Gp	182.97	3.82	0	0	0	0	0	0
WoP_E	Workboat Passage E		Yes	Gp	497.85	10.32	0	0	0	0	0	0
WoP_W	Workboat Passage W		Yes	Mm	235.27	5.03	1	1	100	1	100	0.2

Name	Segment	Segment_name	Total area of	Coverage_R1	Spit	E50-11	E70-11	CH	S500	Azimuth_RT	AL	PIV
Information	Segment	Segment_name	Area_RTS	Coverage_R1	Spit	E50-11	E70-11	CH	S500	Azimuth_RT	AL	PIV
Unit			(ha)	(%)		(m/yr-1)	(m/yr-1)	(m)	(*)	(*)	(cm)	(%)
Source	Rampton, 19	Rampton, 1982	This study	This study	This study	This study	This study	This study	This study	This study	Couture, 201	Couture, 201
BRD	Babbage River Delta		0	0	1	-0.9	-0.6	0.5	0		150	27.5
CL_E	Clarence Lagoon E		0	0	0	-0.9	-1.1	1.81	1.7		100	2
CL_W	Clarence Lagoon W		0	0	1	-1.6	-1.3	2.06	1.65		50	58.09
HER_E	Herschel Island E		68.37	12.9752179	0	-0.8	-0.8	16.17	11.4	144	45	55.52
HER_N	Herschel Island N		11.77	1.40050517	0	-0.7	-0.7	27.63	18.41	45	69	50.2
HER_S	Herschel Island S		8.19	1.39866698	0	-1	-1	7.06	7.94	225	50	62.67
HER_W	Herschel Island W		35.17	12.9804792	0	-0.8	-0.8	17.88	12.88	305	60	51.33
KaP_SE	Kay Point SE		149.45	12.6730173	0	-0.1	-0.2	12.53	15.56	55	37	38.22
KaPS	Kay Point spit		0	0	0	-1.2	-1.3	5.3	0		80	1.11
KB	Komakuk Beach		0	0	0	-1.3	-1.4	5.87	3	3	39	57.71
KBW1	Komakuk Beach W1		0	0	0	-1.6	-1.8	5.41	3.48	1	50	66.37
KBW2	Komakuk Beach W2		0	0	0	-1.1	-1.5	6.49	2.87		50	52.29
KiP	King Point		0	0	0	-0.6	0.4	6.29	4.34	26	34	52.1
KiP_NW	King Point NW		26.03	16.3126772	0	-0.2	-0.3	17.24	21.96	42	50	47.53
KiP_SE	King Point SE		17.61	9.36371915	0	-1.1	-1.2	5.38	5.37	29	42	73.58
KiPL	King Point lagoon		0	0	1	-0.3	0.6	6.31	12.05		80	2
MRF	Malcolm River fan		0	0	1	-0.8	-0.5	2.63	2.27		100	0
MRF_bi	Malcolm River fan with be		0	0	1	-0.2	-0.2	0.68	0.99		100	0
PhB	Phillips Bay		2.97	0.66144679	0	-0.6	-0.7	2.56	1.77	10	50	47.18
PhB_NW	Phillips Bay NW		16.72	12.8548092	0	-0.4	-0.3	7.69	7.48	48	83	61.82
PhB_W	Phillips Bay W		0	0	1	-0.5	-0.7	0.61	1.55		80	2
RB_E	Roland Bay E		4.56	4.14719387	0	-0.8	-0.8	4.64	4.1	32	35	53.78
RB_NW	Roland Bay NW		0	0	0	-0.3	-0.4	4.07	3.67		31	65.24
RB_W	Roland Bay W		14.96	10.5926138	0	-0.5	-0.5	4.56	4.49	45	50	51.5
SaP	Sabine Point		8.36	6.94371569	0	-0.8	-0.9	15.78	10.1	28	50	59.65
SaP_E	Sabine Point E		3.75	3.04234951	0	-0.4	-0.2	12.72	8.61	30	50	38.17
SaP_W	Sabine Point W		0.07	0.05232862	0	-0.7	-0.5	14.52	8.59	26	50	30.38
ShP_W	Shingle Point W		24.58	5.45998872	0	-0.2	-0.2	11.25	10.1	34	50	46.2
StP	Stokes Point		0	0	1	-3.6	-4.4	3.44	8.16	45	80	5.79
StP_SE	Stokes Point SE		1.24	0.63085063	0	0.4	0.3	9.01	5.7	46	28	55.59
StP_W	Stokes Point W		2.38	1.68853321	0	-0.9	-0.9	10.9	5.7	35	35	53.15
WhC	Whale Cove		0	0	1	-0.5	-0.4	0.7	1.7		80	2
WhC_E	Whale Cove E		5.52	13.5994087	0	-0.2	-0.5	3.59	4.59	52	52	53.28
WhC_W	Whale Cove W		0	0	1	-1	-1.2	1.75	2.25		32	57.35
WoP_E	Workboat Passage E		0	0	1	-0.4	-0.4	2.14	2.39		38	39.59
WoP_W	Workboat Passage W		0.12	0.05100523	0	-0.5	-0.5	5.36	6.16	350	34	54.87

Name	Segment	Segment_name	PEI	Depth to the	Depth to the	DMI	Wt	Ws	e	PI	WI	MI
Information	Segment	Segment_name	PEI	Dm	Dbm	DMI	Wt	Ws	e	PI	WI	MI
Unit			(%)	(m)	(m)	(m)	(m)	(m)		(%)	(%)	(%)
Source	Rampton, 19	Rampton, 1982	Couture, 201	Couture, 202	Couture, 202							
BRD	Babbage River Delta		0	0	0	0	0	0	0.54	100	0	0
CL_E	Clarence Lagoon E		0	0	0	0	0	1.7	18	0.36	100	0
CL_W	Clarence Lagoon W		22.88	1	3	2	1.7	16	0.44	39.21	13.12	47.66
HER_E	Herschel Island E		12.98	2.5	11.5	9	2.1	12	0.47	49.57	7.88	42.55
HER_N	Herschel Island N		2.15	2.5	8.5	6	2.1	12	0.47	82.82	3.56	13.62
HER_S	Herschel Island S		34.98	0	0	0	2.1	12	0.41	77.79	22.21	0
HER_W	Herschel Island W		4.45	10	16	6	2.1	12	0.47	80.2	3.73	16.07
KaP_SE	Kay Point SE		0	10	12	2	2.3	12	0.41	77.27	8.78	13.95
KaPS	Kay Point spit		0	0	0	0	0	0	0.36	100	0	0
KB	Komakuk Beach		22.16	0	0	0	1.7	16	0.44	85.69	14.31	0
KBW1	Komakuk Beach W1		38.49	2	3.5	1	1.7	16	0.44	39.08	12.01	48.91
KBW2	Komakuk Beach W2		11.83	0	0	0	1.7	16	0.44	86.25	13.75	0
KiP	King Point		0	0	0	0	2.3	12	0.52	72.41	27.59	0
KiP_NW	King Point NW		0	10	15	5	2.3	12	0.47	73.67	5.29	21.04
KiP_SE	King Point SE		43	7	11.5	4	2.3	9	0.52	36.39	15.2	48.42
KiPL	King Point lagoon		0	0	0	0	0	0	0.36	100	0	0
MRF	Malcolm River fan		0	0	0	0	1.7	14.5	0.52	0	0	0
MRF_bi	Malcolm River fan with be		0	0	0	0	1.7	18	0.33	0	0	0
PhB	Phillips Bay		0	0	0	0	1.7	16	0.46	87.57	12.43	0
PhB_NW	Phillips Bay NW		32.62	3	6	3	2.3	12	0.42	59.14	13.56	27.3
PhB_W	Phillips Bay W		0	0	0	0	0	0	0.36	100	0	0
RB_E	Roland Bay E		0.75	0	0	0	1.7	16	0.51	95.28	4.72	0
RB_NW	Roland Bay NW		10.04	0	0	0	2.3	15	0.6	81.98	18.02	0
RB_W	Roland Bay W		0	3	5	2	2.3	12	0.52	75.98	10.28	13.74
SaP	Sabine Point		20.05	7	14	7	1.5	12	0.48	69.25	2.29	28.46
SaP_E	Sabine Point E		0	2	6	4	1.7	12	0.47	63.45	3.9	32.65
SaP_W	Sabine Point W		0	0	0	0	1.7	12	0.47	95.1	4.9	0
ShP_W	Shingle Point W		0	1	6	5	2.3	12	0.44	68.07	8.38	23.55
StP	Stokes Point		0	0	0	0	0	0	0.36	100	0	0
StP_SE	Stokes Point SE		17	0	0	0	1.7	8	0.45	86.29	13.71	0
StP_W	Stokes Point W		0	5	7	2	2.3	12	0.53	78.11	8.61	13.28
WhC	Whale Cove		0	0	0	0	0	0	0.36	100	0	0
WhC_E	Whale Cove E		15.35	1.5	3.5	2	2.3	12	0.43	33.02	28.2	38.78
WhC_W	Whale Cove W		16.68	0	0	0	2.3	20	0.47	86.2	13.8	0
WoP_E	Workboat Passage E		1.62	0	0	0	2.3	12	0.37	63	37	0
WoP_W	Workboat Passage W		26.48	0	0	0	2	7.5	0.37	60.36	39.64	0

Table S2: Terrain characteristics. The table includes all geographic information for the coastal segment along the Yukon Coast.

	Name of the coastal segment on which the RTS occur	Geologic unit on which the RTS occur	Aerial surface of the RTS	Stage of development of the RTS	Initiated after 1972	Lobe width	Orientation of the RTS	Mean elevation within the RTS floor	Slope within the RTS
RTS_ID	Segment_name	Geolunit	Area_ha	Type	Initiation	Coastal_le	Azimuth	Z_MEAN	S200RTS
			ha			m	°	m (a.s.l.)	°
1	Herschel Island E	Mr	0.11	active	YES	13.5	135	17.05	11.36
2	Herschel Island E	Mr	0.1	active	YES	21.47	135	18.37	12.59
10	Herschel Island E	Mr	0.09	active	YES	17	135	11.45	12.94
14	Herschel Island E	Mr	0.13	active	YES	22.8	180	16.39	11.67
17	Herschel Island E	Mr	0.18	active	YES	3.65	182.75	20.43	9.52
18	Herschel Island N	Mr	0.19	active	YES	10.3	180	24.07	16.74
22	Herschel Island S	Mr	0.18	active	YES	44.75	214.54	5.71	14.65
26	Herschel Island N	Mr	1.24	active	YES	21	98.07	32.82	17.93
30	Herschel Island N	Mr	0.57	active	YES	12.48	58.1	30.63	15.08
31	Herschel Island N	Mr	0.07	active	YES	24.95	60	12.78	25.5
33	Herschel Island N	Mr	0.09	active	YES	0	45	29.87	19.48
34	Herschel Island N	Mr	0.1	active	YES	0	35	29.86	21.09
37	Herschel Island N	Mr	0.11	active	YES	0	35	37.45	12.59
48	Herschel Island W	Mr	0.29	active	YES	27.24	293.08	15.63	22.06
49	Herschel Island W	Mr	0.53	active	YES	5.98	293.08	15.17	28.69
50	Herschel Island S	Mr	0.07	active	YES	14.97	240	6.43	13.69
51	Herschel Island S	Mr	0.09	active	YES	40.02	270	2.41	3.87
52	Herschel Island S	Mr	0.07	active	YES	93.92	249.28	4.65	6.93
71	Kay Point SE	Mr	1.29	active	YES	1023.92	76.34	37.38	14.3
72	Kay Point SE	Mr	0.52	active	YES	19.15	56	29.06	18.86
80	Kay Point SE	Mr	0.11	active	YES	49.93	60.68	4.85	9.99
81	Kay Point SE	Mr	0.03	active	YES	11.91	45	2.95	14.77
87	Kay Point SE	Mr	0.06	active	YES	23.6	35	4.75	5.27
91	Kay Point SE	Mr	0.15	active	YES	25.37	51.58	14.68	24.63
92	Kay Point SE	Mr	0.04	active	YES	12.42	45	9.06	30.76
93	Kay Point SE	Mr	0.08	active	YES	13.89	35	16.49	26.6
94	Kay Point SE	Mr	1.04	active	YES	27.41	53.87	33.35	12.16
95	Kay Point SE	Mr	0.1	active	YES	27.41	56.01	13.19	21.96
100	Kay Point SE	Mr	0.06	active	YES	26.1	35	6.45	14.75
102	Kay Point SE	Mr	0.14	active	YES	18.03	51.76	17.7	18.06
103	Kay Point SE	Mr	1.14	active	YES	20.48	49.7	27.29	16.28
104	Kay Point SE	Mr	0.84	active	YES	52.43	33.61	32.02	17.89
107	King Point NW	Mm	0.05	active	YES	515.26	43.71	14.11	30.25
117	King Point SE	L	0.29	active	YES	58.63	35	10.18	21.23
120	Sabine Point	Mm	0.06	active	YES	14.63	25.07	8.6	17.03
123	Sabine Point E	L	0.44	active	YES	33.98	33.53	10.72	12.21
129	Shingle Point W	Mm	0.06	active	YES	14.43	31.63	11.97	15.94
130	Shingle Point W	Mm	0.14	active	YES	53.54	29.2	8.86	19.37
132	Shingle Point W	Mm	0.14	active	YES	28.43	35	14.2	13.69
149	Shingle Point W	Mm	0.02	active	YES	12.36	45	8.31	24.28
150	Shingle Point W	Mm	0.05	active	YES	18.23	10	9.28	16.62
159	Shingle Point W	Mm	0.11	active	YES	19.44	45.78	15.32	26.07
160	Shingle Point W	Mm	0.24	active	YES	81.16	41.82	8.3	19.33
162	Shingle Point W	Mm	0.04	active	YES	3.07	25	14.61	20.29
163	Shingle Point W	Mm	0.06	active	YES	16.17	43.95	7.2	20.65
165	Sabine Point W	L	0.05	active	YES	0	25.82	18.2	20.01
166	Sabine Point W	L	0.02	active	YES	0	25.82	19.42	23.52
167	Phillips Bay	L	0.18	active	YES	0	332.79	6.48	8.39
169	Herschel Island N	Mr	1.49	active	YES	10.64	168.82	39.74	7.95
174	Herschel Island W	Mr	0.08	active	YES	29.25	315	8.22	23.99
175	Herschel Island W	Mr	0.07	active	YES	18.14	330	5.06	19.38
179	Herschel Island E	Mr	0.11	active	YES	47.51	135	7.72	24.37

	Name of the coastal segment on which the RTS occur	Geologic unit on which the RTS occur	Aerial surface of the RTS	Stage of development of the RTS	Initiated after 1972	Lobe width	Orientation of the RTS	Mean elevation within the RTS floor	Slope within the RTS
RTS_ID	Segment_name	Geolunit	Area_ha ha	Type	Initiation	Coastal_le m	Azimuth °	Z_MEAN m (a.s.l.)	S200RTS °
184	Kay Point SE	Mr	0.04	active	YES	22.39	35	12.41	26.86
196	Kay Point SE	Mr	0.02	active	YES	19.08	45	3.77	7.6
197	Stokes Point W	Mm	0.04	active	YES	28.36	35.27	6.67	19.79
198	Stokes Point W	Mm	0.01	active	YES	3.88	35	5.17	26.39
200	Herschel Island W	Mr	0.08	active	YES	0	315	17.21	21.56
201	Herschel Island W	Mr	0.22	active	YES	28.99	293.08	14.28	28.1
202	Herschel Island N	Mr	1.1	active	YES	0	1.9	36.2	24.31
203	Herschel Island N	Mr	0.14	active	YES	0	360	40.98	24.08
206	Herschel Island S	Mr	0.05	active	YES	93.92	260	2.75	8.51
223	Herschel Island S	Mr	0.12	active	YES	21.42	252.03	6.39	15.9
232	Herschel Island S	Mr	0.43	active	YES	100.39	291.51	4.51	10.97
235	Herschel Island S	Mr	0.04	active	YES	39.16	155.11	0.48	11.09
236	Herschel Island S	Mr	0.02	active	YES	14.15	135	1.02	12.84
238	Herschel Island E	Mr	0.13	stable	YES	22.8	180	15.42	19.65
239	Herschel Island N	Mr	0.68	stable	YES	156.67	175	5.25	12.14
240	Herschel Island N	Mr	1.93	stable	YES	21	98.07	37.22	13.27
241	Herschel Island N	Mr	0.21	stable	YES	0	35	37.39	13.03
242	Herschel Island N	Mr	0.89	stable	YES	12.48	58.1	31.87	16.4
243	Herschel Island N	Mr	0.68	stable	YES	82.24	46.09	23.3	27.86
246	Herschel Island W	Mr	1.1	stable	YES	27.24	293.08	17.11	16.61
247	Herschel Island S	Mr	0.15	stable	YES	14.97	225	8.78	19.65
248	Herschel Island S	Mr	0.35	stable	YES	66.45	260	3.58	14.87
249	Herschel Island S	Mr	0.27	stable	YES	24.14	230	0.79	12.86
250	Herschel Island S	Mr	0.47	stable	YES	93.92	249.28	6.27	9.35
251	Herschel Island S	Mr	0.23	stable	YES	26.87	175	8.15	10.26
252	Herschel Island S	Mr	0.25	stable	YES	40.01	191.44	8.04	13.09
253	Herschel Island S	Mr	0.27	stable	YES	56.93	225	7.1	12.25
254	Herschel Island S	Mr	0.05	stable	YES	17.66	215	5.01	13.28
255	Herschel Island S	Mr	0.67	stable	YES	179.03	226.2	4.95	13.18
257	Herschel Island S	Mr	1.18	stable	YES	72.05	210.96	6.87	8.94
259	Herschel Island N	Mr	0.07	stable	YES	0	7.49	37.61	20.93
260	Herschel Island N	Mr	0.08	stable	YES	0	10	39.85	15.38
273	Herschel Island E	Mr	0.03	active	YES	490.2	140	0	0
275	Workboat Passage W	Mm	0.12	active	YES	0	350	0	0
292	Herschel Island S	Mr	0.45	stable	YES	66.25	260	0	0
298	Stokes Point W	Mm	0.47	stable	YES	93.88	41.3	13.39	9.77
303	Kay Point SE	Mr	6.73	stable	YES	392.92	71.32	28.31	15
305	Kay Point SE	Mr	0.73	stable	YES	93.78	61.43	11.14	14.53
310	Phillips Bay	L	1.08	stable	YES	282.92	332.69	3.73	11.89
311	Sabine Point E	L	0.1	stable	YES	0	20	15.33	16.98
312	Sabine Point	Mm	1.13	stable	YES	136.13	27.72	16.02	15.11
319	King Point SE	L	0.16	stable	YES	41.05	20.11	5.84	14.74
325	Kay Point SE	Mr	1.75	stable	YES	1.68	30.03	42.4	12.02
326	Kay Point SE	Mr	1.08	stable	YES	0	29.09	47.84	12.17
327	Kay Point SE	Mr	2.34	stable	YES	129.29	31.31	18.27	11.02
328	Kay Point SE	Mr	3.58	stable	YES	106.65	31.16	22.19	12.8
335	Herschel Island E	Mr	0.24	stable	YES	0	135	27.01	8.28
337	Stokes Point W	Mm	0.17	stable	YES	0	35.53	13.9	13.74
338	Stokes Point W	Mm	0.1	stable	YES	33.85	32.67	9.81	23.54
340	Sabine Point E	L	1.43	stable	YES	46.03	27.02	18.8	11.16
341	King Point SE	L	3.54	stable	YES	431.56	20.64	8.22	11.67
342	Kay Point SE	Mr	2.25	stable	YES	205.19	34.26	13.57	12.09

	Name of the coastal segment on which the RTS occur	Geologic unit on which the RTS occur	Aerial surface of the RTS	Stage of development of the RTS	Initiated after 1972	Lobe width	Orientation of the RTS	Mean elevation within the RTS floor	Slope within the RTS
RTS_ID	Segment_name	Geolunit	Area_ha ha	Type	Initiation	Coastal_le m	Azimuth °	Z_MEAN m (a.s.l.)	S200RTS °
343	Kay Point SE	Mr	5.55	stable	YES	391.04	34.24	18.84	12.01
345	Kay Point SE	Mr	16.72	stable	YES	963.07	44.28	19.44	9.62
346	Kay Point SE	Mr	14.77	stable	YES	849.39	64.64	14.49	8.5
347	Phillips Bay NW	Mm	0.12	stable	YES	33.05	45	4.29	6.73
348	Stokes Point SE	L	0.89	stable	YES	28.47	44.08	5.33	12.63
349	Stokes Point W	Mm	0.24	stable	YES	29.91	38.32	10.1	11.44
354	Kay Point SE	Mr	0.76	stable	YES	142.06	46.7	5.77	10.59
364	Kay Point SE	Mr	3.39	stable	YES	212.38	52.5	24.91	18.32
365	Kay Point SE	Mr	1.55	stable	YES	208.12	38.1	11.52	12.16
426	Kay Point SE	Mr	0.13	active	YES	41.77	45	29.36	10.4
427	Kay Point SE	Mr	0.18	active	YES	61.48	45	23.98	9.08
428	Kay Point SE	Mr	0.04	active	YES	21.05	45	17.63	6.32
429	Kay Point SE	Mr	0.18	active	YES	80.17	45	16.08	6.08
430	Kay Point SE	Mr	0.07	active	YES	20.37	45	20.81	7.7
443	Kay Point SE	Mr	0.07	stable	YES	42.68	45	0	7.5
9	Herschel Island E	Mr	20.82	active	active	677.33	129.29	21.01	8.94
11	Herschel Island E	Mr	0.21	active	active	44.65	149.05	8.02	17.23
12	Herschel Island E	Mr	0.54	active	active	75.74	156.84	9.96	15.3
13	Herschel Island E	Mr	2.07	active	active	154.41	162.57	9.32	7.33
15	Herschel Island E	Mr	4.78	active	active	201.6	1.21	24.04	9.6
16	Herschel Island E	Mr	5.94	active	active	201.6	176.1	24.58	9.52
19	Herschel Island S	Mr	0.41	active	active	35.45	218.8	6.45	8.19
21	Herschel Island S	Mr	0.07	active	active	30.38	225	6.25	7.21
24	Herschel Island S	Mr	0.11	active	active	44.66	155.81	3.55	11
25	Herschel Island S	Mr	0.11	active	active	54.78	135	2.08	11.49
35	Herschel Island N	Mr	0.18	active	active	13.76	25.52	17.82	20.84
36	Herschel Island N	Mr	3	active	active	339.45	13.51	25.79	25.62
39	Herschel Island W	Mr	4.83	active	active	390.8	316.72	26.77	17.91
40	Herschel Island W	Mr	8.25	active	active	366.24	314.32	28.25	13.81
41	Herschel Island W	Mr	8.36	active	active	458.59	309.39	15.66	15.72
45	Herschel Island W	Mr	0.31	active	active	30.64	315	5.04	11
46	Herschel Island W	Mr	1.7	active	active	66.97	296.31	11.4	13.39
47	Herschel Island W	Mr	0.89	active	active	4.02	291.51	20.64	20.31
53	Roland Bay W	Mm	6.64	active	active	716.65	47.98	9.63	9.41
57	Roland Bay E	L	1.33	active	active	393.98	33.03	5.72	9.87
59	Stokes Point W	Mm	0.21	active	active	54.73	35.38	11.06	10.47
60	Stokes Point W	Mm	0.05	active	active	54.73	34.33	8.66	20.05
61	Stokes Point W	Mm	0.33	active	active	74.35	33.18	11.77	10.98
64	Kay Point SE	Mr	0.06	active	active	29.3	63.41	3.13	12.97
65	Kay Point SE	Mr	0.17	active	active	56.72	59.82	10.94	12.82
66	Kay Point SE	Mr	0.04	active	active	29.64	35	7.14	13.78
67	Kay Point SE	Mr	0.08	active	active	29.64	66.11	10.74	14.41
68	Kay Point SE	Mr	0.07	active	active	44.26	66.29	9.47	15.2
98	Phillips Bay NW	Mm	0.31	active	active	39.97	49.88	10.36	10.47
99	Phillips Bay NW	Mm	0.3	active	active	56.72	48.78	6.59	10.37
101	Kay Point SE	Mr	0.21	active	active	34.63	51.76	11.84	16.86
106	King Point NW	Mm	0.83	active	active	9.81	40.14	17.26	8.7
110	King Point SE	L	0.56	active	active	104.66	27.77	3.02	3.65
118	Sabine Point	Mm	3.98	active	active	408.79	27.8	22.47	17.48
119	Sabine Point	Mm	0.09	active	active	32.3	28.12	9.34	23.93
128	Shingle Point W	Mm	0.05	active	active	9.44	35	10.95	14.56
135	Shingle Point W	Mm	0.19	active	active	53.39	25.78	11.91	26.3

	Name of the coastal segment on which the RTS occur	Geologic unit on which the RTS occur	Aerial surface of the RTS	Stage of development of the RTS	Initiated after 1972	Lobe width	Orientation of the RTS	Mean elevation within the RTS floor	Slope within the RTS
RTS_ID	Segment_name	Geolunit	Area_ha ha	Type	Initiation	Coastal_le m	Azimuth °	Z_MEAN m (a.s.l.)	S200RTS °
136	Shingle Point W	Mm	0.22	active	active	40.26	30.41	14.73	22.86
137	Shingle Point W	Mm	0.14	active	active	13.71	35	17.81	25.16
148	Shingle Point W	Mm	0.09	active	active	6	28.79	20.42	22.21
151	Shingle Point W	Mm	0.04	active	active	18.43	360	7.22	21.97
152	Shingle Point W	Mm	0.12	active	active	20.93	26.72	15.24	21.1
153	Shingle Point W	Mm	0.16	active	active	33.24	28.98	16.45	26.41
154	Shingle Point W	Mm	0.15	active	active	25	10	18.37	24.82
155	Shingle Point W	Mm	0.17	active	active	28.33	10	18.73	25.86
156	Shingle Point W	Mm	0.16	active	active	37.9	28.57	17.3	28.5
157	Shingle Point W	Mm	0.1	active	active	14.16	35	22.72	26.74
158	Shingle Point W	Mm	0.29	active	active	28.71	39.28	12.28	17.4
161	Shingle Point W	Mm	0.06	active	active	12.75	39.56	12.07	21.19
172	Herschel Island W	Mr	1.96	active	active	297.59	312.83	14.75	23.75
180	Herschel Island E	Mr	0.37	active	active	111.25	154.7	11.21	21.17
182	Herschel Island N	Mr	0.07	active	active	13.76	45	19.72	23.15
183	Herschel Island N	Mr	0.28	active	active	2.91	26.88	23.32	28.97
186	Shingle Point W	Mm	0.1	active	active	20.39	33.43	10.39	24.31
189	Roland Bay E	L	0.12	active	active	393.98	26.81	2.69	9.49
192	Herschel Island W	Mr	0.23	active	active	5.64	311.68	21.21	17.84
193	Herschel Island E	Mr	0.94	active	active	45.76	180	21.33	12.15
194	Herschel Island S	Mr	0.05	active	active	14.6	270	4.98	14
205	Herschel Island N	Mr	0.41	active	active	2.83	45	30.5	16.75
207	Herschel Island E	Mr	0.09	active	active	22.79	185	15.96	21.51
208	Herschel Island E	Mr	0.4	active	active	14.01	180	23.77	12.7
211	Phillips Bay NW	Mm	0.29	active	active	26.16	45.65	8.55	10.68
214	Sabine Point E	L	1.78	active	active	36.41	32.43	25.48	12.37
218	Roland Bay W	Mm	0.34	active	active	86.69	46.31	5.44	8.04
224	Kay Point SE	Mr	0.76	active	active	56.72	63.61	11.03	14.31
225	Whale Cove E	Mm	2.56	active	active	254.11	52.36	8.86	7.72
227	Phillips Bay NW	Mm	0.34	active	active	30.6	47.31	9.93	9.54
234	Herschel Island S	Mr	0.36	active	active	110.51	270	5.5	10
237	Herschel Island S	Mr	0.26	active	active	33	220	9.83	10.95
244	Herschel Island W	Mr	2.2	stable	active	66.97	296.31	26.66	20.47
245	Herschel Island W	Mr	0.62	stable	active	4.02	292.2	34.97	10.25
258	Herschel Island S	Mr	0.87	stable	active	35.45	218.8	7.27	13.85
261	Whale Cove E	Mm	2.96	stable	active	254.11	52.82	10.19	9.2
297	Roland Bay E	L	4.57	stable	active	393.98	32.02	12.22	10.17
299	Phillips Bay NW	Mm	14.66	stable	active	39.97	48.44	15.6	10.05
318	Sabine Point	Mm	6.86	stable	active	408.79	27.9	21.91	14.87
323	King Point SE	L	13.62	stable	active	104.66	28.09	9.88	10.01
324	King Point NW	Mm	9.8	stable	active	9.81	43.92	19.14	13.37
332	Herschel Island E	Mr	1.9	stable	active	44.65	149.05	15.21	7.82
333	Herschel Island E	Mr	12.37	stable	active	75.74	161.09	26.63	10.07
334	Herschel Island E	Mr	2.2	stable	active	22.79	184.82	17.79	18.69
350	Roland Bay W	Mm	4.28	stable	active	716.65	48.01	7.44	12.88
351	Stokes Point W	Mm	0.52	stable	active	74.35	32.43	17.7	8
352	Stokes Point W	Mm	0.16	stable	active	54.73	34.33	14.8	12.5
353	Kay Point SE	Mr	0.25	stable	active	56.72	59.82	18.08	13.88
358	Stokes Point W	Mm	0.41	stable	active	0	35.06	18.26	8.67
366	Kay Point SE	Mr	0.75	stable	active	56.72	66.22	17.96	11.08
4	Herschel Island E	Mr	7.36	active	stable	423.39	115.47	10.25	6.5
5	Herschel Island E	Mr	1.43	active	stable	131.52	114.9	18.84	8.08

	Name of the coastal segment on which the RTS occur	Geologic unit on which the RTS occur	Aerial surface of the RTS	Stage of development of the RTS	Initiated after 1972	Lobe width	Orientation of the RTS	Mean elevation within the RTS floor	Slope within the RTS
RTS_ID	Segment_name	Geolunit	Area_ha ha	Type	Initiation	Coastal_le m	Azimuth °	Z_MEAN m (a.s.l.)	S200RTS °
6	Herschel Island E	Mr	0.1	active	stable	26	135	5.44	9.32
7	Herschel Island E	Mr	0.24	active	stable	10.82	122.68	22.38	14.71
8	Herschel Island E	Mr	1.24	active	stable	74.73	124.87	20.49	11.31
23	Herschel Island S	Mr	0.09	active	stable	24.74	240	6.63	7.75
44	Herschel Island W	Mr	5.67	active	stable	20.52	301.81	14.11	12.05
54	Roland Bay W	Mm	0.06	active	stable	22.07	35	4.99	7.57
55	Roland Bay W	Mm	0.23	active	stable	67.74	45	5.81	10.69
56	Roland Bay W	Mm	0.02	active	stable	11.85	45	2.82	17.16
58	Roland Bay E	L	0.11	active	stable	50.37	32.1	5.53	19.5
62	Kay Point SE	Mr	0.14	active	stable	26.96	45	5.77	14.11
63	Kay Point SE	Mr	0.04	active	stable	26.96	59.2	3.71	16.08
69	Kay Point SE	Mr	0.36	active	stable	49.61	65.63	18	17.31
70	Kay Point SE	Mr	0.07	active	stable	59.65	45	4.3	15.94
73	Kay Point SE	Mr	0.93	active	stable	0	74	34.24	10.39
74	Kay Point SE	Mr	0.14	active	stable	6.07	71.36	22.1	17.72
75	Kay Point SE	Mr	0.09	active	stable	12.59	69.63	15.23	25.96
76	Kay Point SE	Mr	5.11	active	stable	307.81	74.78	23.2	19.42
78	Kay Point SE	Mr	0.09	active	stable	31.08	90	7.97	25.91
79	Kay Point SE	Mr	0.27	active	stable	543.28	71.18	24.78	9.81
82	Kay Point SE	Mr	0.05	active	stable	11.91	45	3.96	17.57
83	Kay Point SE	Mr	0.32	active	stable	20.92	55.58	5.52	11.93
84	Kay Point SE	Mr	0.03	active	stable	63.88	35	3.6	7.51
85	Kay Point SE	Mr	0.07	active	stable	14.58	35	4.74	15.47
86	Kay Point SE	Mr	0.85	active	stable	137.29	58.52	4.68	8.13
88	Kay Point SE	Mr	0.06	active	stable	18.64	45	11.58	14.41
89	Kay Point SE	Mr	0.04	active	stable	0	45	18.48	14.74
90	Kay Point SE	Mr	0.15	active	stable	12.23	51.76	15.79	17.15
96	Phillips Bay	L	0.31	active	stable	64.23	0.7	5.85	7.02
97	Phillips Bay	L	0.11	active	stable	342.2	10	8.44	9.2
105	Kay Point SE	Mr	0.1	active	stable	1.59	31.39	30.52	24.94
108	King Point NW	Mm	0.93	active	stable	122.11	47.74	5.71	8.37
111	King Point SE	L	0.09	active	stable	38.81	31.61	3.16	7.41
112	King Point SE	L	0.18	active	stable	67.2	23.95	2.77	7.61
113	King Point SE	L	0.03	active	stable	1109.25	45	1.11	3.96
114	King Point SE	L	0.03	active	stable	24.2	35	1.19	5.06
115	King Point SE	L	0.2	active	stable	36.01	36.29	2.95	7.47
121	Sabine Point	Mm	0.17	active	stable	77.48	23.28	4.23	20.82
122	Sabine Point	Mm	0.13	active	stable	77.48	35	6.57	15.05
124	Shingle Point W	Mm	1.91	active	stable	137.28	25.15	21.3	10.81
125	Shingle Point W	Mm	0.52	active	stable	34.42	36.03	17.94	19.18
126	Shingle Point W	Mm	0.44	active	stable	42.11	39.62	12.82	5.17
127	Shingle Point W	Mm	0.43	active	stable	44.06	40.68	21.51	24.11
131	Shingle Point W	Mm	0.11	active	stable	20.57	27.06	14.03	7
133	Shingle Point W	Mm	0.06	active	stable	6.17	35	15.4	18.09
134	Shingle Point W	Mm	0.04	active	stable	0	35	16.58	7.6
164	Shingle Point W	Mm	0.02	active	stable	258.72	34.63	2.17	29.08
185	Shingle Point W	Mm	0.06	active	stable	29.28	35	3.51	21.25
187	King Point SE	L	0.3	active	stable	99.34	26.03	3.05	7.92
188	King Point SE	L	0.24	active	stable	99.34	29.68	2.49	7.12
212	Kay Point SE	Mr	1.04	active	stable	59.65	68.52	20.12	9.51
213	King Point NW	Mm	2.61	active	stable	10.98	29.47	38.74	13.71
215	Stokes Point SE	L	0.13	active	stable	0	45.64	8.27	15.28

	Name of the coastal segment on which the RTS occur	Geologic unit on which the RTS occur	Aerial surface of the RTS	Stage of development of the RTS	Initiated after 1972	Lobe width	Orientation of the RTS	Mean elevation within the RTS floor	Slope within the RTS
RTS_ID	Segment_name	Geolunit	Area_ha ha	Type	Initiation	Coastal_le m	Azimuth °	Z_MEAN m (a.s.l.)	S200RTS °
216	Roland Bay W	Mm	0.07	active	stable	630.19	47.27	4.83	10.12
217	Roland Bay W	Mm	0.07	active	stable	630.19	43.67	3.37	13.45
219	Roland Bay W	Mm	0.16	active	stable	47.31	45	5.07	8.13
222	Herschel Island E	Mr	7.52	active	stable	1.59	123.75	41.96	9.54
226	Phillips Bay NW	Mm	1.66	active	stable	161.51	52.51	10.85	8.85
229	Kay Point SE	Mr	0.1	active	stable	31.1	59.72	7.2	24.12
230	Kay Point SE	Mr	0.6	active	stable	1023.92	58.55	21.94	14.9
233	Herschel Island S	Mr	0.45	active	stable	103.83	258.66	5.63	9.37
256	Herschel Island S	Mr	0.6	stable	stable	12.85	219.8	6.46	5.46
296	Roland Bay W	Mm	4.03	stable	stable	22.07	45.78	8.43	10.22
300	Kay Point SE	Mr	17.58	stable	stable	49.61	63.61	22.26	13.19
301	Kay Point SE	Mr	19.94	stable	stable	19.15	67.23	28.43	15.24
302	Kay Point SE	Mr	6.65	stable	stable	31.08	74.22	26.91	16.44
304	Kay Point SE	Mr	9.12	stable	stable	543.28	69.45	22.04	13.99
306	Kay Point SE	Mr	8.78	stable	stable	11.91	57.47	29.04	12.27
308	Kay Point SE	Mr	3.73	stable	stable	18.64	50.66	27.88	13.26
309	Phillips Bay	L	1.89	stable	stable	64.23	0.7	6.66	12.75
313	Shingle Point W	Mm	5.93	stable	stable	6.17	23.55	21.51	12.6
314	Shingle Point W	Mm	0.76	stable	stable	20.57	26.74	18.43	20.12
315	Shingle Point W	Mm	3.13	stable	stable	34.42	39.18	15.47	21.19
316	Shingle Point W	Mm	3.31	stable	stable	29.28	33.88	15.68	13.75
317	Shingle Point W	Mm	8.13	stable	stable	137.28	27.62	25.47	13.94
355	King Point NW	Mm	13.62	stable	stable	10.98	29.47	32.31	23.08
357	Kay Point SE	Mr	6.63	stable	stable	12.59	72.45	22.13	17.84
361	Stokes Point SE	L	0.04	stable	stable	0	45.64	7.6	16.46
362	Stokes Point SE	L	0.18	stable	stable	0	51.68	6.87	13.92
363	Kay Point SE	Mr	7.99	stable	stable	27.67	72.07	35	14.54

Table S3: Metadata for the 21 aerial photographs.

Region	Date acquired	Roll Number	Photo Number	Spectral Range	Focal length	Picture size [inch]	Scale	dpi scanned	Pixel resolution (digital)	Average LiDAR height [m]	total RMS	RMS ²	Total project RMS	Ground resolution [mm]	Estimated line pairs	LOA (operator error)	Uncertainty of shoreline position (for DSAS)	DOA to 2011
Stokes Point	9/20/1971	A22013	14	Black&White	153.39	9x9	25,000	1200	0.53				12.78	1250	20	5	13.8	0.35
Shingle Bay	9/9/1971	A22014	91	Black&White	154.085	9x9	15,000	1200	0.32					750	20	5		
Shingle Bay	9/9/1971	A22014	93	Black&White	154.085	9x9	15,000	1200	0.32					750	20	5		
East of Backhouse - Nunakluk spit	7/8/1972	A22879	3	Black&White	152.51	9x9	60,000	2000	0.76	10	2.27	5.15		3000	20	5		
Backhouse River - east	7/8/1972	A22879	99	Black&White	152.51	9x9	60,000	2000	0.76	10	2.08	4.33		3000	20	5		
Deep Creek - King Point	7/8/1972	A22879	105	Black&White	152.51	9x9	60,000	2032	0.75	10	1.4	1.96		3000	20	5		
Internat. border - Clarence	7/9/1972	A22881	20	Black&White	152.51	9x9	60,000	2000	0.76	8	0.97	0.94		3000	20	5		
Clarence - Backhouse River	7/9/1972	A22881	111	Black&White	152.51	9x9	60,000	2032	0.75	7	2.83	8.01		3000	20	5		
Nunakluk Spit	7/9/1972	A22881	112	Black&White	152.51	9x9	60,000	2000	0.76					3000	20	5		
Nunakluk Spit	7/9/1972	A22881	117	Black&White	152.51	9x9	60,000	2032	0.75	3	6.29	39.56		3000	20	5		
Nunakluk Spit	7/9/1972	A22881	163	Black&White	152.51	9x9	60,000	2032	0.75	2	5.25	27.56		3000	20	5		
Nunakluk Spit	7/9/1972	A22881	166	Black&White	152.51	9x9	60,000	2032	0.75					3000	20	5		
Firth River delta	7/9/1972	A22881	167	Black&White	152.51	9x9	60,000	2032	0.75	2	2.92	8.53		3000	20	5		
Deep Creek	7/9/1972	A22882	18	Black&White	152.51	9x9	60,000	2032	0.75	30	2.63	6.92		3000	20	5		
Babbage River	7/9/1972	A22882	20	Black&White	152.51	9x9	60,000	2032	0.75	30	1.98	3.92		3000	20	5		
Difficult Creek - Avadlek Spit	7/31/1972	A22974	207	Black&White	152.51	9x9	60,000	2032	0.75	3	2.63	6.92		3000	20	5		
WBP-Whale Bay	7/31/1972	A22974	215	Black&White	152.51	9x9	60,000	2032	0.75	5	1.47	2.16		3000	20	5		
WBP-Whale Bay	7/31/1972	A22974	216	Black&White	152.51	9x9	60,000	2032	0.75	5	2.12	4.49		3000	20	5		
Whale Bay - Stokes Point	8/14/1972	A22975	20	Black&White	152.51	9x9	60,000	2032	0.75	11	1.56	2.43		3000	20	5		
Stokes Point	8/14/1972	A22975	29	Black&White	152.51	9x9	60,000	2032	0.75	11	3.28	10.76		3000	20	5		
Phillips Bay - Kay Point	8/13/1972	A22975	55	Black&White	152.51	9x9	60,000	2032	0.75	30	1.92	3.69		3000	20	5		
Phillips Bay - Kay Point	8/14/1972	A22975	56	Black&White	152.51	9x9	60,000	2032	0.75	30	1.99	3.96		3000	20	5		
Shingle Point	8/14/1972	A22975	144	Black&White	152.51	9x9	60,000	2032	0.75	23	2.95	8.70		3000	20	5		
Sabine Point - Shingle Point	8/14/1972	A22975	154	Black&White	152.51	9x9	60,000	2032	0.75	26	2.7	7.29		3000	20	5		
King Point - Sabine Point	7/7/1976	A24501	190	Black&White	152.51	9x9	60,000	2032	0.75	23	2.45	6.00		3000	20	5		

Abbreviations and Nomenclature

Notation	Meaning	SI-Unit
%	percent; a number or ratio as a fraction of 100	
‰	per mille; a number or ratio as a fraction of 1000	
cm	Centimetre	1×10^{-2} m
°C	Degree Celsius	°C
a	Latin: annus; year	
AC	Accumulation	
ACD	Arctic Coastal Dynamics	
AL	Active Layer depth	m
AMAP	Arctic Monitoring and Assessment Programme	
BOR	Border section	
BORs	Border short GPS section	
BP	Before Present (before 1950)	
CH	Cliff height	m
CH ₄	Methane	
Chpt.	Chapter	
Ci	Change index	
CL	Coastal Length	m
CLA	Clarence Lagoon section	
CLAs	Clarence Lagoon short GPS section	
CO ₂	Carbon dioxide	
CSRS-PPP	Canadian Spatial Reference System- Precise Point Positioning	
C/N ratio	Carbon/Nitrogen ratio	
DEM	Digital Elevation Model	
DEW line station	Distant Early Warning line station	
DGPS	Differential Global Positioning System	
Dbm	Depth to the bottom of massive ice	m
Dm	Depth to the top of massive ice	m
DMI	Thickness of the massive ice (Dbm-Dm)	m
DOA	Loss of accuracy due to digitizing process	
DSAS	Digital Shoreline Analysis System	
E	East	
e	Soil porosity	
E50-11	Erosion rate between 1952 and 2011	m a^{-1}
E70-11	Erosion rate between 1972 and 2011	m a^{-1}
E _{GR}	Ground resolution	m
EPR	End Point Rate	m a^{-1}
et al.	Latin:et alii; and others	
ER	Erosion	
F	Annual Flux of SOC or sediment	kg a^{-1}
g	Gram	1×10^{-3} kg
GCP	Ground Control Point	
h	Thickness of a soil layer	m
ha	Hectare	10^4 m ²
i.e.	Latin: id est; that is	
IBA	Important Bird Area	
INAC	Indigenous and Northern Affairs Canada	
IPCC	Intergovernmental Panel on Climate Change	
kg	Kilogram	1 kg
KAY	Kay Point section	
KNG	King Point section	
KNGs	King Point short GPS section	

KOM	Komakuk Beach section	
KOMs	Komakuk Beach GPS section	
LiDAR	Light Detection and Ranging	
LOA	Loss of Accuracy	m
M	Total Mass of material per soil column	kg
m	Metre	m
m ²	Square metre	m ²
m ³	Cubic metre	m ³
M _c	Mass of SOC in a soil column	kg
MIS	Marine isotope stage	
mm	Millimetre	1×10 ⁻³ m
Mi	Massive Ice	
M _s	Mass of mineral sediment in a soil column	kg
n	Number of samples	
N	Nitrogen; North	
NT	Northwest Territories	
NRCan	Natural Resources Canada	
NUN	Nunaluk Spit section	
NUNs	Nunaluk Spit GPS section	
NW	North West	
Pg	Petagram	1×10 ¹² kg
PEI	Percentage of excess ice	
PI	Pore Ice	
PIV	Percentage of ice volume	
RCP	Representative Concentration Pathways (for IPCC scenarios)	
RMS	Root Mean Squared Error	
RTS	Retrogressive Thaw Slump	
S1	Conservative shoreline projection scenario	
S2	Dynamic shoreline projection scenario	
S500	Slope 500m inland	
SE	South East	
SHI	Shingle Point section	
S_MEAN	Mean slope of the slump floor	
SOC	Soil Organic Carbon	
STO	Stokes Point section	
Δ t	Temporal residual between two measurements	a
TC	Total Carbon	kg
TerrOC	Terrigenous Organic Carbon	kg
Tg	Teragram	1×10 ⁹ kg
TN	Total Nitrogen	kg
TOC	Total Organic Carbon	kg
TP	Tie Point	
U	Uncertainty in shoreline position	m
UNESCO	United Nations Educational, Scientific and Cultural Organization	
U.S.	United States	
vol%	per cent by volume	
W	West	
WBP	Workboat Passage section	
WHB	Whale Bay section	
WI	Wedge Ice	
W _s	Mean ice wedge spacing	m
W _t	Mean ice wedge width	m
yr	year	
Z_MEAN	Mean elevation above sea level	m
%wt	Percent by weight	
δ ¹³ C	Stable carbon isotope ratio	
δ ¹³ C _{org}	Stable soil organic carbon isotope ratio	
ρ _b	Dry bulk density	kg m ⁻³
ρ _i	Bulk density of ice	kg m ⁻³

Acknowledgements

So far, my PhD has been one of the most exciting and intense adventures in my life. Never before have I received so many opportunities to learn on so many scales simultaneously. I owe the opportunity for this unique life experience to **Hugues Lantuit**, who was willing to take the responsibility for my supervision. Thank you for your trust, motivation, and scientific guidance during the course of my research. I appreciate it very much!

Naturally, without funding, I would not have been able to do my PhD either. I express my deep gratitude to the **German Federal Environmental Foundation (Deutsche Bundesstiftung Umwelt)** for three years of financial support. **Mrs. Schlegel-Starmann**, I thank you for the assistance you provided me throughout my stipend. I also thank the **Alfred Wegener Institute** in Potsdam very much for hosting me, as well as for financial support and those unforgettable excursions to the western Canadian Arctic.

Gavin Manson, you acted as a very important scientific advisor throughout my entire PhD project, too. I would like to thank you for all the scientific discussions we shared, the time you sacrificed for me, the energy you invested in helping me improve my English, as well as your warm hospitality each time I was in Dartmouth.

My PhD committee consisted of **Hugues Lantuit, Paul Overduin, Frank Günther** and **Guido Grosse**. Our meetings were a critical component of my PhD and helped me stay on track and keep going. Thank you all for being part of that. **Paul Overduin**, our scientific discussions were always very inspiring and intellectually stimulating. I thank you for the time and effort you dedicated to improving my work.

Nicole Couture, Ashley Piskor and **Richard Gordon**, working together with you was a great pleasure for me. Thank you very much for our excellent collaboration.

I would like to also thank **Claudia Hanfland** and **Claudia Sprengel** for making **POLMAR** such a great graduate school. Thank you for your support and advice throughout the entire process – you are doing a great and important job! I learned very much in the POLMAR courses and am glad to have gotten the chance to take advantage of such a high quality graduate school. The same applies for the **Potsdam Graduate School (PoGS)**. I enjoyed my involvement with PoGS very much and am still a bit sad that the Junior Teaching Professionals Program is over!

Diana Otto from the AWI library division in Potsdam did an excellent job in organizing countless old papers, books and even movies for me. Thank you very much!

Boris Radosavljevic, you helped me a lot, especially during the first few months of my PhD. I enjoy discussing coastal science with you and am so grateful for your unwavering support and availability. Thank you for sharing your expertise and becoming such a good friend!

Justine Ramage, I would like to thank you as a colleague for our interesting and joyful discussions, as well as, all the GIS battles we fought and won together. As a friend, thank you for always being there for me and for sharing your positive energy and motivation with me.

I would also like to thank **Stefanie Weege, Samuel Stettner, Caroline Coch** and the rest of the **COPER group**, as well as **Josefine Lenz** and **Boris Biskaborn** for their friendship and support, as well as the sweet distraction they brought into my PhD life. Without you, my PhD time would not have been nearly as enjoyable as it was!

Furthermore, I would like to thank the 2014 and 2015 expedition teams, especially **George Tanski, Samuel Stettner** and **Justine Ramage** for their help and for making field life fun! Knowing that we can count on each other no matter what is very valuable and this contributed to the wonderful time I had in the Arctic.

In addition, I am in debt to my personal GIS-quiz team, consisting of **Ingmar Nitze, Matthias Fuchs** and **Sebastian Labor**. Thank you for your help and advice!

Leonie Sander and **Karoline MeBenzehl**, you were my best friends before I started my PhD and are my best friends today. Thank you for bearing with me, as well as for all your on-the-phone support and distractions!

I particularly would like to thank my **parents, Anna** and **Dariusz**, as well as my **brother Philip**, for your support by showing so much interest in my work. Having you behind my back is very important for me. My parents deserve even more gratitude for taking me to the same three beaches at the Polish Baltic Sea for my entire childhood and teenage years. I suppose that the absence of distractions helped me focus on the really important things!

Mama, Tata i Fio, pragnę Wam podziękować z całego serca za wasze wsparcie. Za to, że przez całe moje studia i doktorat okazywaliście zaciekawienie moją nauką i za to, że nigdy nie wątpiliście w to, że to co robię ma znaczenie!

Chris, there are not enough words in the World to describe how much I thank you for all that you have done for me! You supported me relentlessly, motivated me and kept me away from work whenever I needed it. Without you by my side, I would not have been able to fill these pages the way I did – Thank you a million times!

Eidesstattliche Erklärung

Hiermit versichere ich, dass ich die vorliegende Arbeit selbstständig verfasst und keine anderen als die angegebenen Quellen und Hilfsmittel verwendet habe.

Ich habe diese kumulative Dissertation am Alfred-Wegener-Institut Helmholtz Zentrum für Polar und Meeresforschung in Potsdam erarbeitet und in englischer Sprache angefertigt. Diese Dissertation wird erstmalig und ausschließlich an der Universität Potsdam eingereicht.

Die dem Promotionsverfahren zugrundeliegende Promotionsordnung vom 18.09.2013 ist mir bekannt.

Potsdam, den 28. September 2017



Anna M. Irrgang